WL TR-64-123

WL
TR
64-123

RESEARCH, LABORATORY TESTING AND THEORETICAL STUDIES SUPPORTING AFWL TREES PROGRAM

by

W. W. Grannemann
Harold Southward
William J. Byatt, et al.

TECHNICAL REPORT NO. WL TR-64-123

Research and Technology Division
AIR FORCE WEAPONS LABORATORY
Air Force Systems Command
Kirtland Air Force Base
New Mexico

January 1965

Research and Technology Division
AIR FORCE WEAPONS LABORATORY
Air Force Systems Command
Kirtland Air Force Base
New Mexico

WL TR-64-123

RESEARCH, LABORATORY TESTING AND THEORETICAL STUDIES SUPPORTING AFWL TREES PROGRAM

by

W. W. Grannemann

Harold Southward

William J. Byatt, et al.

FOREWORD

This report was prepared by the University of New Mexico Bureau of Engineering Research under Contract AF 29(601)-5976, Modification No. S.A. #2(65-87). The work was funded under Project 8812, ARPA Order No. 307-62, and Project 5710, DASA WEB No. 16.015.

The research was performed from April 13, 1963 to August 17, 1964. The report was submitted December 3, 1964. AFWL Project Officer was Lt John L. Mullis, WLDA-1.

Principal investigator for the contract was Dr. W. W. Grannemann. Other investigators were Dr. Harold D. Southward, Dr. William J. Byatt, Dr. Llewellyn Boatwright, Harold Cates, Goebel Davis, Arthur Golubiewski, and LeRoy Meyer.

The authors wish to acknowledge the assistance of TSgt F. W. Fisher, Alc A. H. Hoffland, and Alc P. L. Kowieski in operating the flash X-ray system.

This technical report has been reviewed and is approved.

John L. Mullis
JOHN L. MULLIS
Lt USAF
Project Officer

John W. Talley
JOHN W. TALLEY
Lt Colonel USAF
Chief, Nuclear Applications Branch

R. A. House
R. A. HOUSE
Colonel USAF
Chief, Development Division

ABSTRACT

Hall effect semiconductor devices and titanium dioxide diodes have been found to be highly resistant to transient X-ray pulses. Transient X-ray radiation effects on air surrounding resistive elements as a function of pressure were measured and a theory developed for the effects. Continuous X-ray spectrums have been calculated from X-ray transmission data in the energy range from 180 kilovolts to 600 kilovolts and this method has proved to be satisfactory for outputs of both the flash X-ray and the DC X-ray machines in this energy range. In addition, basic radiation effects measurements were made on dielectric materials using the Hall effect and magnetoresistance measurements in a steady state gamma flux. Hall effect magnetoresistance effects were observed in polystyrene, polyethylene, and other dielectric materials. A Schering Bridge method was used to determine the changes of capacitance of components during flash X-ray exposure. (This bridge is much less responsive to conductance changes than to capacitance changes.) And a Monte Carlo code has been written which describes time-dependent photon transport within finite pieces of material. The energy of the ejected electrons is recorded and photon histories are traced.

This page intentionally left blank.

TABLE OF CONTENTS

SECTION IV

SECTION V

SECTION VI

SECTION VII

SECTION VIII

APPENDIX I

APPENDIX II

APPENDIX III

APPENDIX IV

APPENDIX V

LIST OF FIGURES

LIST OF TABLES

This page intentionally left blank.

SECTION I

TRANSIENT GAMMA RADIATION EFFECTS ON RESISTIVE AND INSULATING MATERIALS

By W. J. Byatt and Harold Cates

1. Introduction

When a pulse of photons is incident on materials, electrons are generated within and around the sample by photoelectric, Compton, and pair-production interactions. The electrons then move so as to produce transient effects which may be observed as changes in conductivity, current, voltage, or charge.

Experimental findings of the effects of transient gamma irradiation of materials are oftentimes analyzed from a somewhat empirical point of view. For example, if a transient current-time curve resulting from irradiation of a sample is given, the technique used by many investigators in analyzing such data goes roughly in the following way: The system response,[1] exclusive of the component under irradiation, is calculated or determined experimentally and subtracted from the data. The remaining current is then plotted versus time and the curve is drawn to fit the data. Often, it develops that a series of exponentials will fit the data and the results are then interpreted in terms of a trapping model having the observed time constants.

The following report has a number of purposes. First, a number of papers on transient radiation effects within resistive and dielectric materials will be reviewed. Then, the results of some experiments which have been performed on resistors will be presented. A set of relations which can be used to predict the observed time-dependent behavior of transient voltage, current, conductivity and charge behavior within resistive and insulating materials will be developed, and how the relations can be used

---

[1] i.e., the response of such things as coaxial cable to gamma pulses, or the measuring system response time.

to analyze not only data of this experiment but data of other workers in the field will be shown.

Before embarking on the above program, it is convenient to discuss some basic ideas. It is known, for example, that the conductivity of a gas which is slightly ionized is given by

$$\sigma(t) = \frac{n_e(t)q^2\bar{\tau}}{m_e} \qquad (1)$$

where $n_e(t)$ is the number density of electrons of charge q and mass m_e, and $\bar{\tau}$ is a suitably averaged relaxation of recombination time. Now, under certain conditions, an expression of the form of (1) holds in metals and semiconductors. It is possible to write, for an n-type semiconductor,

$$\sigma_n(t) = \frac{n_e(t)q^2\bar{\tau}}{m_n^*} \qquad (2)$$

with $n_e(t)$ the time dependent behavior of n-type impurities of charge q and effective (scalar) mass m_n^*. For p-type materials,

$$\sigma_p(t) = \frac{p(t)q^2\bar{\tau}}{m_h^*} \qquad (3)$$

where p(t) is the concentration of holes of charge q and effective scalar mass m_h^*. The total conductivity can then be expressed as

$$\sigma = q\left[n\mu_n + p\mu_h\right] \qquad (4)$$

with the mobilities defined by, for example, $\mu = q\bar{\tau}/m^*$. The existence of a number density, $n_e(t)$, of electrons gives rise to the possibility that if the electrons move, a charge density proportional to

$$\rho(t) = -qn_e(t) \qquad (5)$$

will be transported. Finally, a current density will flow if a charge is transported. It will be given by either

$$j(t) = -qn_e(t)\bar{v} \tag{6}$$

or by solution of the equation

$$\frac{d\rho}{dt} + \nabla \cdot (j) = 0 \tag{7}$$

It is, therefore, obvious that a knowledge of the time-dependent behavior of free electrons is of importance in determining the transient behavior of materials under gamma irradiation.

2. <u>Development of Equations</u>

Once again the expression for the conductivity (1) should be considered; it is

$$\sigma(t) = \frac{n_e(t)q^2\bar{\tau}}{m_e}$$

The concentration of free electrons, $n_e(t)$, after a gamma ray pulse has passed over the sample under test, will decrease due to recombination of the electrons with, for example, ions and traps. One can write that

$$n_e(t + \Delta t) = n_e(t) - p_{abs}(\Delta t)\, n_e(t) \tag{8}$$

which states that the number density (or concentration) of free electrons decreases in time if there is no source for generation of electrons. The factor which governs the decrease is called $p_{abs}(\Delta t)$ in the relation given by (8), and is the probability that in a time Δt a free electron will disappear. For simplicity, it is assumed that

$$p_{abs}(\Delta t) = \lambda \Delta t \tag{9}$$

with λ a constant. On passing to the limit $\Delta t \rightarrow 0$, equation (8) becomes

$$\frac{dn_e}{dt} = -\lambda n_e \tag{10}$$

If the pulse of gamma radiation ceases at time $t = t_o$, at which time $n_e(t) = n_e(t_o)$, the solution to (10) is

$$n_e(t) = n_e(t_o)q^{-\lambda t} \quad (t \geq t_o) \tag{11}$$

According to (1) the conductivity-time curve, after the gamma ray intensity has gone to zero, should, if assumption (9) is valid, have the general form

$$\sigma(t) = \sigma(t_o)q^{-\lambda t} \quad (t \geq t_o) \tag{12}$$

It is of interest to generalize assumption (9). If there are several time constants λ_i^{-1} with relative weights a_i, a generalization of (12) is

$$\sigma(t) = \sigma(t_o) \sum_i a_i e^{-\lambda_i t} \qquad (t \geq t_o) \tag{13}$$

If both a_i and λ_i depend continuously on i, then

$$\sigma(t) = \sigma(t_o) \int_{-\infty}^{\infty} a(i) e^{-\lambda(i)t} di \tag{14}$$

One can generalize further. If

$$P_{abs} (\Delta t) = \lambda(t) \Delta t, \tag{15}$$

then the counterpart of equation (11) is

$$n_e(t) = n_e(t_o)e^{-\int_{t_o}^{t} \lambda(\xi)\, d\xi} \tag{16}$$

The generalizations of equation (13), (14) and (15) then follow naturally.

One could just as well have been deriving equations for the current density or the charge density according to equations (5) and (6) which are equivalent. What is important is a knowledge of $n_e(t)$, the electron concentration. During this discussion it is assumed that the gamma pulse is square as shown in Figure 1.

The above relations hold only for $t \geq t_o$, with t_o the time at which the gamma pulse amplitude goes to zero. It is easy to remedy this shortcoming by including the effect of the generation of electrons during the time that the pulse sweeps over the component. Restricting attention to the time behavior of $n_e(t)$, one writes

$$n_e(t + \Delta t) = n_e(t) - n_e^{abs} + n_e^{gen} \tag{17}$$

The last two terms in (17) are the number of electrons absorbed and the number generated per unit volume in a time Δt. For the number absorbed in a time Δt, it is postulated that

$$n_e^{abs} = n_e(t)\ p^{abs}(\Delta t) \tag{18}$$

stating that the number absorbed in the time interval $(t,\ t + \Delta t)$ is equal to the number present at time t multiplied by the probability that absorption will occur in time Δt. The quantity $p^{abs}(\Delta t)$ is proportional to the time interval Δt, with the constant of proportionality being the concentration of absorbing

centers of various kinds and their cross sections. For the latter

$$K = \sum_i N_i^{abs} \sigma_i \tag{19}$$

Then equation (18) becomes

$$n_e^{abs} = n_e(t) \, K \, \Delta t \tag{20}$$

The number of electrons generated in a time Δt is a function of the time-dependent incident gamma ray intensity, the number of electrons available for generation, and the cross section for the interaction of a gamma ray with a bound electron. The above means that

$$n_e^{gen} = \mu \, f\left[\gamma \; (t)\right] \Delta t, \tag{21}$$

where the quantity μ is proportional to the product of the number of electrons available for generation with the cross section for the interaction.

When (20) and (21) are substituted into (17) and the limit $\Delta t \to 0$ is taken, the result is

$$\frac{dn_e}{dt} + K \, n_e(t) = \mu f\left[\gamma(t)\right] \tag{22}$$

Equation (22) can be integrated between two instants of time, t_o and t. If, at t_o, $n_e(t) = n_e(t_o)$, the solution to (22) is

$$n_e(t) = n_e(t_o) e^{-K(t-t_o)} + \mu \int_{t_o}^{t} f\left[\gamma(\tau)\right] e^{-K(t-\tau)} \, d\tau \tag{23}$$

It will be observed that if t_o is the time at which the gamma pulse amplitude goes to zero, then the second term of (23)

goes to zero and (23) is identical with (11). The generalizations following equation (11) then hold for equation (23). The expressions for the current density, charge density, and conductivity become

$$j(t) = j(t_o)e^{-K_j(t-t_o)} + \mu_j \int_{t_o}^{t} f_j[\gamma(\tau)]e^{-K_j(t-\tau)} d\tau \qquad (24)$$

$$q(t) = q(t_o)e^{-K_q(t-t_o)} + \mu_q \int_{t_o}^{t} f_q[\gamma(\tau)]e^{-K_q(t-\tau)} d\tau \qquad (25)$$

and

$$\sigma(t) = \sigma(t_o)e^{-K_\sigma(t-t_o)} + \mu_\sigma \int_{t_o}^{t} f_\sigma[\gamma(\tau)]e^{-K_\sigma(t-\tau)} d\tau \qquad (26)$$

If the zero reference level of current density, charge density and conductivity is taken just prior to radiation, and if $t_o = 0$, then the build up of the number of free electrons as the pulse passes over is given by

$$n_e(t) = \mu \int_0^t f[\gamma(\tau)]e^{-K(t-\tau)} d\tau \qquad 0 \le t \le t_1 \qquad (27)$$

For a square radiation pulse of duration t_1 seconds, such that

$$f[\gamma(\xi)] = A \text{ in } 0 \le \xi \le t_1$$

$$n_e(t) = \frac{\mu A}{K}(1 - e^{-Kt})$$

At $t = t_1$,

$$n_e(t_1) = \frac{\mu A}{K}(1 - e^{-Kt_1}). \qquad (28)$$

If, in (23), t_o is now set equal to t_1,

$$n_e(t) = n_e(t_1)e^{-K(t - t_1)} \qquad t \geq t_1 \qquad (29)$$

On the basis of the very simple model chosen, Figure 1 gives, schematically, the time-dependent behavior of the number of free electrons. The assumed pulse shape is also shown. From equations (24), (25) and (26), the behavior of the current and charge densities, together with the conductivity can be found if equations such as (1), (5) and (6) are used to determine the constants of proportionality between $n_e(t)$ and the quantity being computed. The equations developed in this section will be used to analyze the data of this experiment as well as the data of other workers in the field.

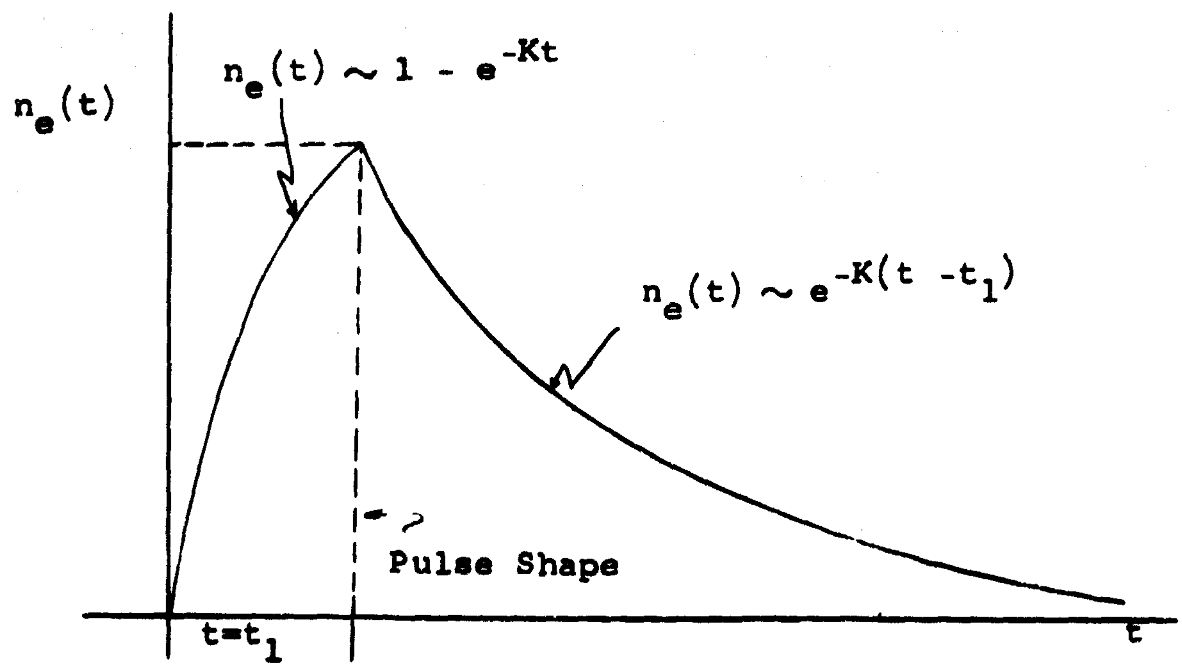

Figure 1. Illustrating the Behavior of the Number of Free Electrons per Unit Volume Under the Influence of an External Rectangular Pulse of Duration t_1 Seconds

3. Review of Previous Work on Resistive and Insulating Materials.

Several papers will be reviewed in this section. The literature in transient radiation effects is now so enormous that a word about the papers reviewed is in order. In part 4 of this section the results of the experiments will be discussed. The papers reviewed there discuss, in general, experimental results which may be compared to the present experiments. This fact has influenced the selection of papers.

Selections:

(a) Transient Radiation Effects in Electronic Materials (Reference 1)

The object of the above report written by D. B. Ebeoglu et al. is to determine the mechanisms of pulsed radiation effects in electronic materials. The sources of radiation are a KEWB water boiler reactor and a 600 kev flash X-ray unit. Only findings from the latter source of radiation shall be reviewed.

In pulsed radiation studies, air ionization effects and cable effects give rise to spurious signals. A large part of the report is devoted to a discussion of methods for coping with the above mentioned effects. It is to be noted that Ebeoglu et al. maintain that under flash X-ray pulses, the use of epoxy coatings is not so effective in reducing air ionization effects as is the use of a vacuum. On irradiating polyethylene at various pressures, it was observed that the air ionization effect increased until the pressure within the test chamber was about 200 μ and then it began to decrease. The decrease continued until a pressure of about 10 μ was reached, after which there was no noticeable change (See Table IV of Reference 1). The magnitudes of radiation-induced signals are in the ratio of 12:8 5:5 for atmospheric, epoxy-coated, and vacuum cases respectively.

The width of the pulse of X-rays is about .1 μ second, while the decay of induced conductivity was of the order of 1 μ second. The author asserts that it is reasonably certain that

the observed decay time is indeed characteristic of the polyethylene since care was taken to reduce the time constant of the measuring circuits to a magnitude significantly less than 1 μ second. It was necessary to eliminate all cable conductor to shield capacitance in the measuring circuits. This was done by using the cables as wires with the center conductor carrying the signal and the shield being left unconnected. With such an arrangement, resistors of values up to 100 KΩ were used as test components. Above such a value, the circuit time constant became large enough to dominate.

The authors conclude that the experiments performed on polyethylene with both the KEWB reactor and the flash X-ray unit point to the excitation of trapped carriers.

In the above report, large numbers of photographs are presented of the time dependent behavior of samples under irradiation. These are displayed together with the irradiation pulse shapes. No effort was made to fit the curves. The general form of the observed signals is, however, as shown in Figure 1. of this report.

(b) Some Effects of Pulsed Radiation of Electronic Components-III, (Reference 2)

The above report presents the results of tests conducted at the Godiva Reactor at Los Alamos in January, 1959. Only the results found on exposing resistors to the reactor pulse will be discussed herein. With the test circuit used by the IBM group, the change in the resistance under test is given by

$$\Delta R = \frac{E\Delta I}{I(I+\Delta I)} \tag{30}$$

where

ΔR = the resistance change,

E = the applied voltage

I = the original current through the test resistor,

ΔI = the change in current through the test resistor.

It is pointed out that the resistance varies inversely as the flux during the reactor pulse and is, therefore, time dependent. The authors present ΔR_{peak} in tabular form. They also point out that changes in resistance can be attributed not to the resistor itself, but to the creation of a shunt leakage path about the resistor due to air ionization. In Table I, Table B1 of the IBM report under discussion is reproduced. From Table I the percentage change in resistance as a function of dose rate can be plotted, with the result shown in Figure 2. The lower values of resistance have not been included since the $\Delta R/R$ values are less than 1% in general. From the data of Figure 2, it is clear that the ionization shunt leakage path becomes increasingly important as the rated value of the resistor under test increases. It will, therefore, be noted that if circuits can be designed having low values of pure resistive elements, at least the changes in resistance values will be small; i.e., the circuits will be more radiation resistant.

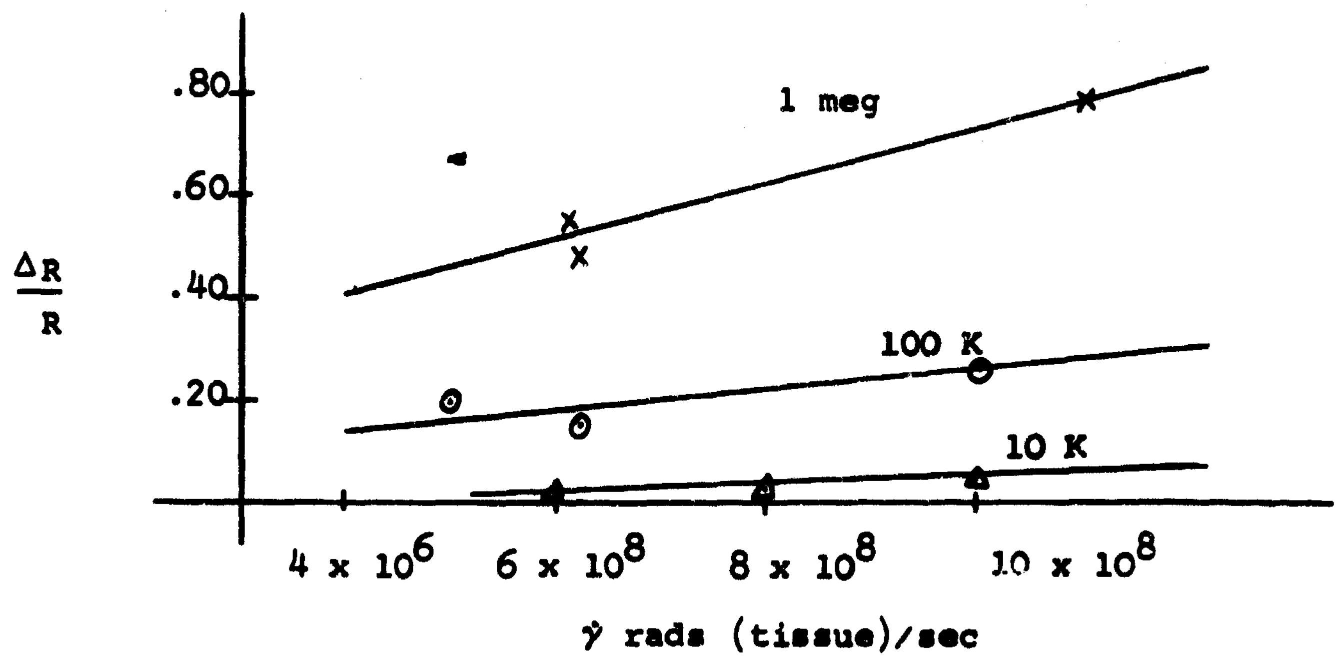

Figure 2. Percentage Change in Resistance as a Function of Dose Rate

Table I Observed Change in Resistance at Maximum Flux (Taken from IBM Rept. 59-816-916, Jan., 1959)

Resistance Type	Original Resistance (Ohms)	ΔR (Ohms)	Maximum Gamma Ray Dose Rate (Rads (Tissue)/sec)
Allen Bradley Carbon Composition 2-Watt	1.0240×10^7	8.89×10^6	13×10^6
	1.0553×10^6	7.90×10^5	11×10^6
	1.0222×10^6	4.92×10^5	6.4×10^6
	1.0508×10^6	5.47×10^5	6.2×10^6
	1.0463×10^5	2.59×10^4	10×10^6
	1.0079×10^5	1.985×10^4	5×10^6
	1.0017×10^5	1.55×10^4	6.5×10^6
	1.0228×10^4	2.14×10^2	6.4×10^6
	1.0107×10^4	4.89×10^2	10×10^6
	1.0234×10^4	2.66×10^2	8.1×10^6
	1.0236×10^3		8.8×10^6
	9.9882×10^2	3.54	4.5×10^6
	1.0291×10^3		16.0×10^6
	1.0244×10^3	8.99	8.1×10^6
	1.0228×10^3	12.63	14×10^6
	1.0215×10^2	.103	14×10^6
	1.0359×10^2	.024	6.5×10^6
	1.0170×10^2	.053	4.5×10^6

(c) <u>Transient Radiation Effects on Electronic Parts</u> (Reference 3)

The main purpose of the above mentioned report is to present experimental data on radiation-induced effects in coaxial cable. In particular, the radiation induced conductivity in RG-58 cable having a solid polyethylene dielectric is found to vary approximately as the .55 power of the dose rate in the range of dose rates from .36 to 7×10^4 rads/sec. For a given dose rate, the conductivity is independent of voltage applied to the cable in the range $-300 \le V \le 300$ volts. Secondary electron emission is constant over a measured dose rate of from .37 to 10^8 rads/sec. The conclusion is that gamma photoconductivity is important at low dose rates, while secondary emission is important at high dose rates.

(d) <u>Transient Radiation Effects on Electronic Parts</u> (Reference 4)

A relatively complete discussion of transient radiation effects in a Mylar capacitor is given. The analysis is presented in terms of the equivalent circuit shown in Figure 3.

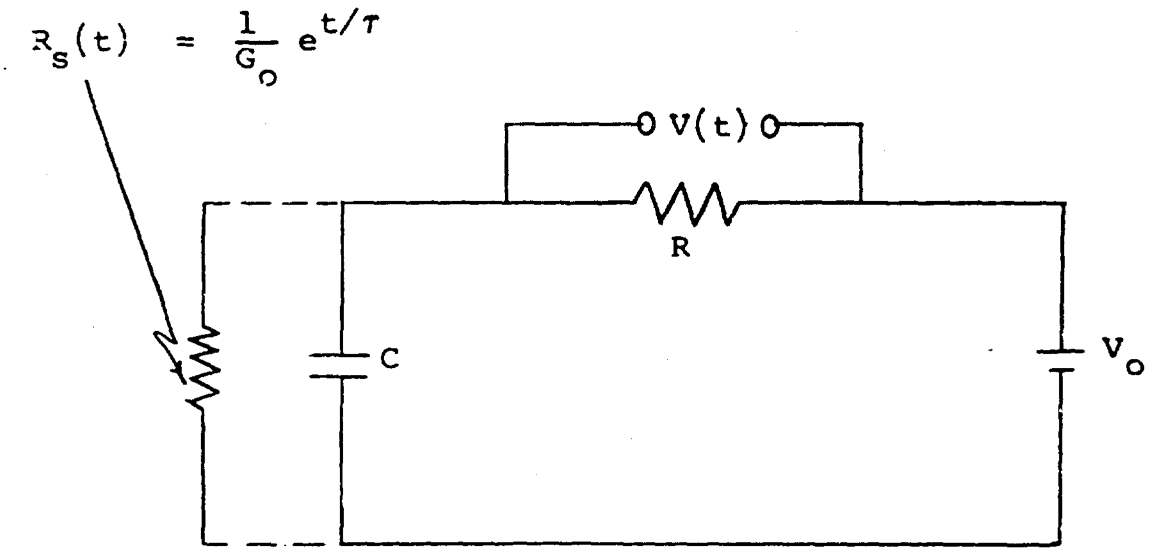

Figure 3. Equivalent Circuit for a Capacitor under Irradiation

The quantity $R_s(t)$ is a time-dependent shunt resistance induced by the incident radiation. The quantity R is a series resistance representing the parallel combination of 1 megohm resistor in series with the power supply and the 1 megohm input impedance of the measuring amplifier. The induced conductivity across the capacitor C is shown schematically in Figure 4 together with the radiation pulse.

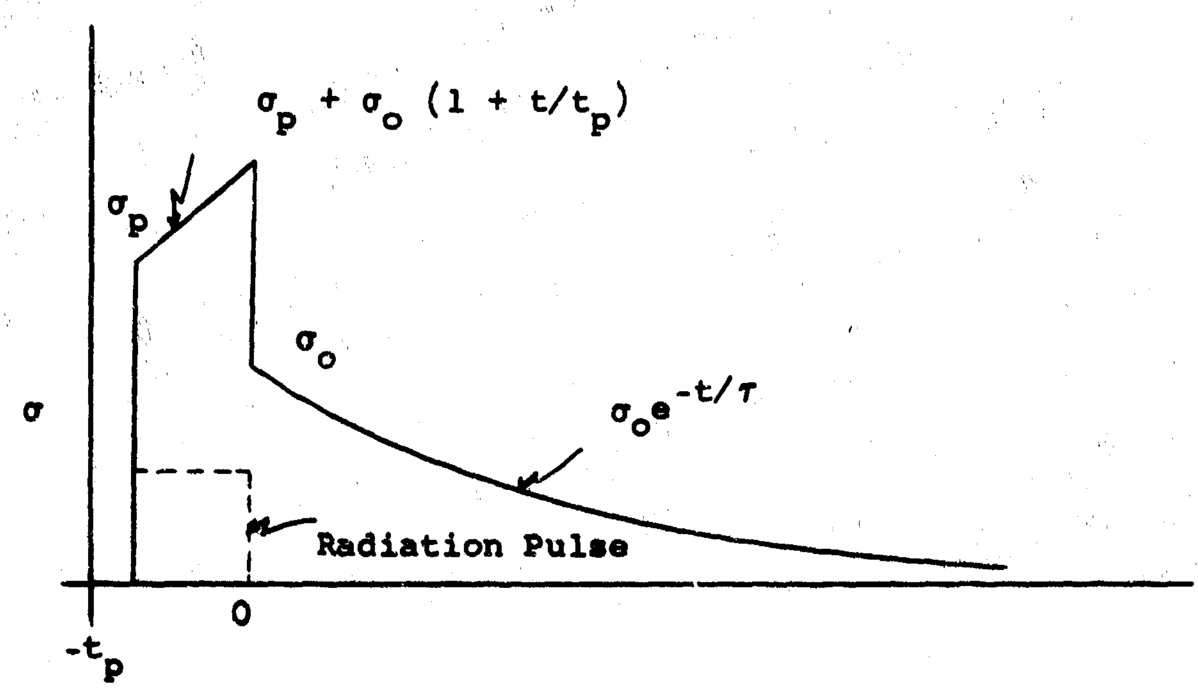

Figure 4. Induced Conductivity-Time Curve in a Capacitor due to the Radiation Pulse Shown.

Rather than following the analysis of the authors of the report under discussion Figure 4 will be discussed on the basis of an equation developed in part 2 of this report. Consider, therefore, equation (26) for the conductivity. It is

$$\sigma(t) = \sigma(t_o)e^{-K_\sigma(t-t_o)} + \mu_\sigma \int_{t_o}^{t} f_\sigma[\gamma(\tau)]e^{-K_\sigma(t-\tau)}\,d\tau$$

In order for (26) to conform with the data of Figure 4, it is convenient to set $t_o = -|t_p|$, and to take the range of t to be $-|t_p| \geq t \geq \infty$. Experimentally it is found that $\sigma(t_o) = \sigma(-|t_p|) = \sigma_p$, an initial condition. Further, since $\gamma(\tau)$ exists only in the interval $-|t_p| \leq t \leq 0$, equation (26) becomes

$$\sigma(t) = \sigma_p e^{-K_\sigma(t+|t_p|)} + \mu_\sigma \int_{-|t_p|}^{t} f_\sigma\left[\gamma(\tau)\right] e^{-K_\sigma(t-\tau)} d\tau \quad (-|t_p| \leq t \leq 0) \qquad (31)$$

and

$$\sigma(t) = \sigma_p e^{-K_\sigma(t + |t_p|)} \qquad t \geq 0 \qquad (32)$$

The most primitive assumption regarding $f_\sigma\left[\gamma(\tau)\right]$ is that it is constant in $-|t_p| \leq t \leq 0$. With such an assumption,

$$\sigma(t) = \sigma_p e^{-K_\sigma(t+|t_p|} + \frac{\mu_\sigma A}{K_\sigma}\left[1-e^{-K_\sigma(t+|t_p|)}\right] - |t_p| \leq t \leq 0 \qquad (33)$$

and

$$\sigma(t) = \sigma_p e^{-K_\sigma(t + |t_p|)} \qquad t > 0 \qquad (34)$$

In the above relation, A is the constant amplitude of $f_\sigma\left[\gamma(\tau)\right]$ in $-|t_p| \leq t \leq 0$.

It will be observed that as $t = 0$ is approached from the negative side,

$$\sigma(t) \rightarrow \sigma_p e^{-K_\sigma |t_p|} + \frac{\mu_\sigma A}{K_\sigma}(1 - e^{-K_\sigma |t_p|}) \qquad (35)$$

while as $t \to 0$ from the positive side,

$$\sigma(t) \to \sigma_p e^{-K_\sigma |t_p|} \qquad (36)$$

From these two forms, it is seen that the observed discontinuity in $\sigma(t)$ at $t = 0$ is predicted. While it would be of some interest to find the values of the parameters K_σ and $\mu_\sigma A/K_\sigma$ which sould permit a fit of the data in the report under discussion, it is not possible since no absolute magnitudes are given.

(e)

1) "Gamma-Ray Photoconductivity Decay in Organic Dielectric Materials." (Reference 5)

2) "Measured Behavior of Gamma-Ray Photoconductivity in Organic Dielectrics." (Reference 6)

3) "Gamma-Ray and Neutron-Induced Conductivity in Insulating Materials." (Reference 7)

The above three papers, by staff members of the Sandia Corporation of Albuquerque, New Mexico, represent some of the more definitive work done in the area of transient radiation effects. The papers discuss the transient gamma ray response of a variety of materials, including polyethylene, polypropylene polyisolretylene, Mylar, Teflon, cellulose acetate, reconstituted mica, tantalum oxide, and polyvinylchloride. In all of the quoted materials the authors find that the response of the materials to gamma radiation can be split into three regions which they call A, B, and C. The three regions are shown in Figure 5. It will, first of all, be noted that the logarithm of the conductivity is plotted versus time in Figure 5. In region A, Harrison et al. find that the conductivity-time curve varies as

$$\sigma - \sigma_o = A(1 - e^{-t/t_o}) \qquad (37)$$

where σ_o is the dark conductivity and τ_o is a function of the dose rate. Specifically, it is found that τ_o can be determined from a knowledge of dose rate by writing

$$\tau_o = K_o \dot{\gamma}^{-\mu} \tag{38}$$

where K_o and μ are determined empirically.

In region B equilibrium is reached, at which time generation of carriers is in equilibrium with recombination. In region B,

$$\sigma - \sigma_o = A_\gamma \dot{\gamma}^{\zeta} \tag{39}$$

with A_γ and ζ constants to be determined empirically.

In region C it is found that

$$\sigma = \sigma_{eq} \sum_{i=1}^{n} K_i e^{-t/\tau_i} \tag{40}$$

with

$$\sigma_{eq} = \sigma_o + A_\gamma \dot{\gamma}^{\zeta} \tag{41}$$

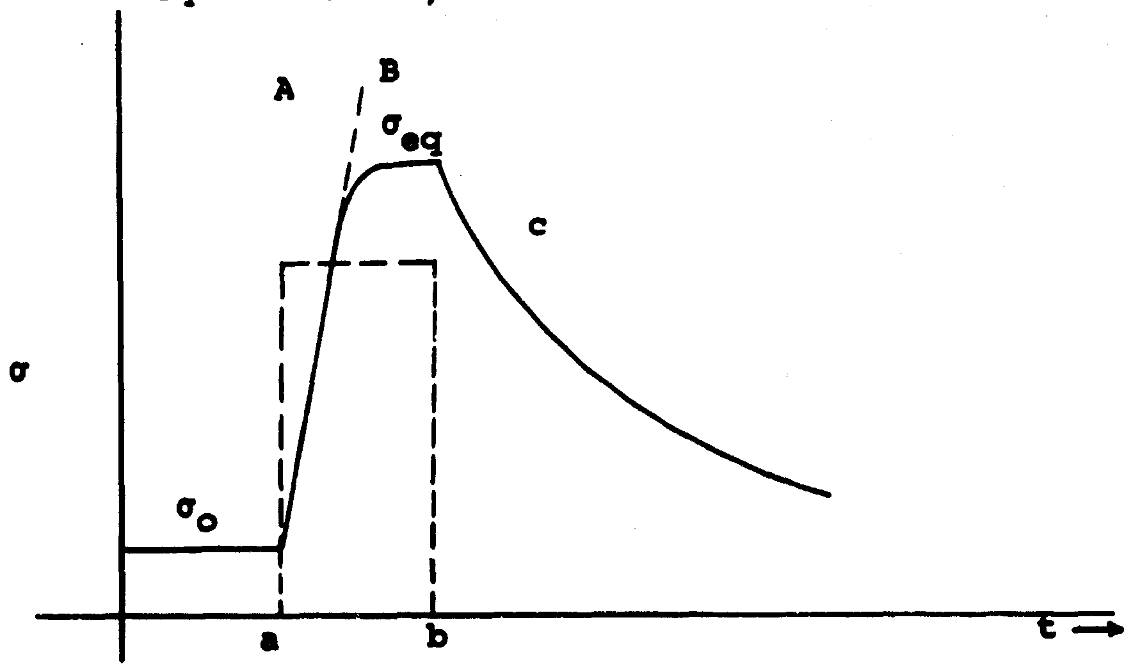

Figure 5. The Conductivity-Time Behavior for the Gamma Pulse Shown.

It will be observed that equation (37) is of the form of equation (28), while equation (40) is identical with (13). The fact that region B exists in the experiments of Harrison et al, is due to the time duration of the pulse. It is of the order, in many of their experiments, of 10 seconds. This means that the generation of carriers by the external source can come to equilibrium with the recombination of carriers within the material. In the experiments which we shall discuss in part 4, the pulse duration is of the order of 2×10^{-7} second, and equilibrium cannot be established.

4. Experimental Work

A Fexitron flash X-ray unit capable of delivering a .2 μ sec. pulse at accelerating voltages up to 600 kev provided the gamma ray source in the experiments to be described. The gamma ray pulse is collimated by a 1 inch hole cut in about 1/2 an inch of lead. A Consolidated Vacuum Corporation vacuum unit with a glass bell jar of average wall thickness of about 1/4 inch is placed inside a screen room. The bottom plate of the vacuum chamber has openings for a number of electrical leads. Lead shielded coaxial cable runs from connections made outside the bell jar through 2 inches of lead block shielding to a Tektronix 1121 A amplifier. The outer shields of the coaxial cable used in the test circuit are grounded. A coaxial cable runs from the output of the 1121 A amplifier to a 551 Tektronix oxcilloscope with a type CA plug-in unit. The cable mentioned above provides a matched impedance from the output of the 1121 A to the oscilloscope input. Figure 6 is a schematic diagram of the circuit used for testing the components. Figure 7 is a drawing of the vacuum system. The 1121 A amplifier and the remainder of the circuitry as shown in Figure 6 are enclosed in a lead brick shield to the right of the vacuum system.

Certain tests made to determine whether there was any discernible pickup as the flash X-ray unit was pulsed when no

test component was in place across the two contact posts shown in Figure 7 are mentioned before describing the experiments themselves. An 18 volt potential difference, supplied by the power supply indicated in Figure 6 was placed across the binding posts. If air ionization effects were important, if secondary electron emission from the glass walls were a problem, or if spurious signals were generated within the cables, some effect would be observed. None was seen. When a resistor was placed between the binding posts and a 2 inch lead block was placed inside the bell jar so as to interrupt the photon beam, no effect was seen. When the lead block was removed, there was a voltage pulse observed on the oscilloscope. Finally, when a bare wire was inserted between the binding posts and the X-ray unit was pulsed, there was no detectable signal at the levels at which we were operating. On the basis of the above results, it can be assumed that spurious signals due to secondary electron emission from the bell jar wall, cable effects, and the like are not a factor in these experiments.

One final comment should be made before the results to date are briefly described. Far more thorough analyses of the data will be given in the theses of H. T. Cates and L. C. Meyer of the University of New Mexico.

Resistors

Allen Bradley carbon composition, solid core resistors have been tested with rated values of 1 megohm, 1 watt, and 1 megohm 1/4 watt. The tests have been run with the flash X-ray tube operating at 400 kev with an anode to test sample distance of 8 1/4 inches. At this distance, the dose rate is approximately 10^6 roentgens per second. Since the pulse duration is $.2 \times 10^{-6}$ second, a total dose of approximately .2 roentgen was delivered by the tube at the position of the sample. Clearly, the .2 roentgen is not absorbed dose. The vacuum system was operated such that exposures to the X-ray pulse took place at pressures between atmospheric and 10 microns.

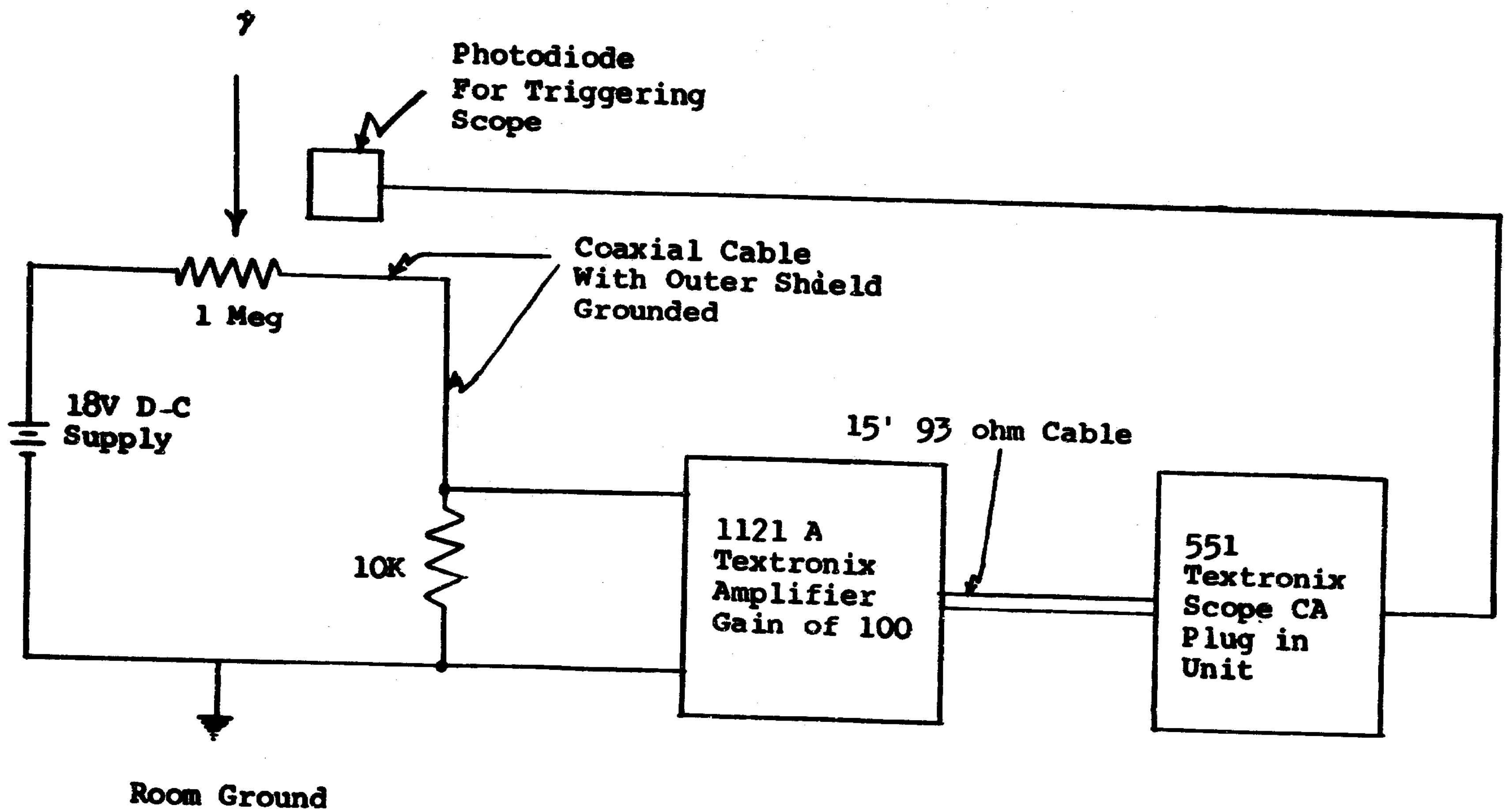

Figure 6. Schematic Diagram of Test Circuit

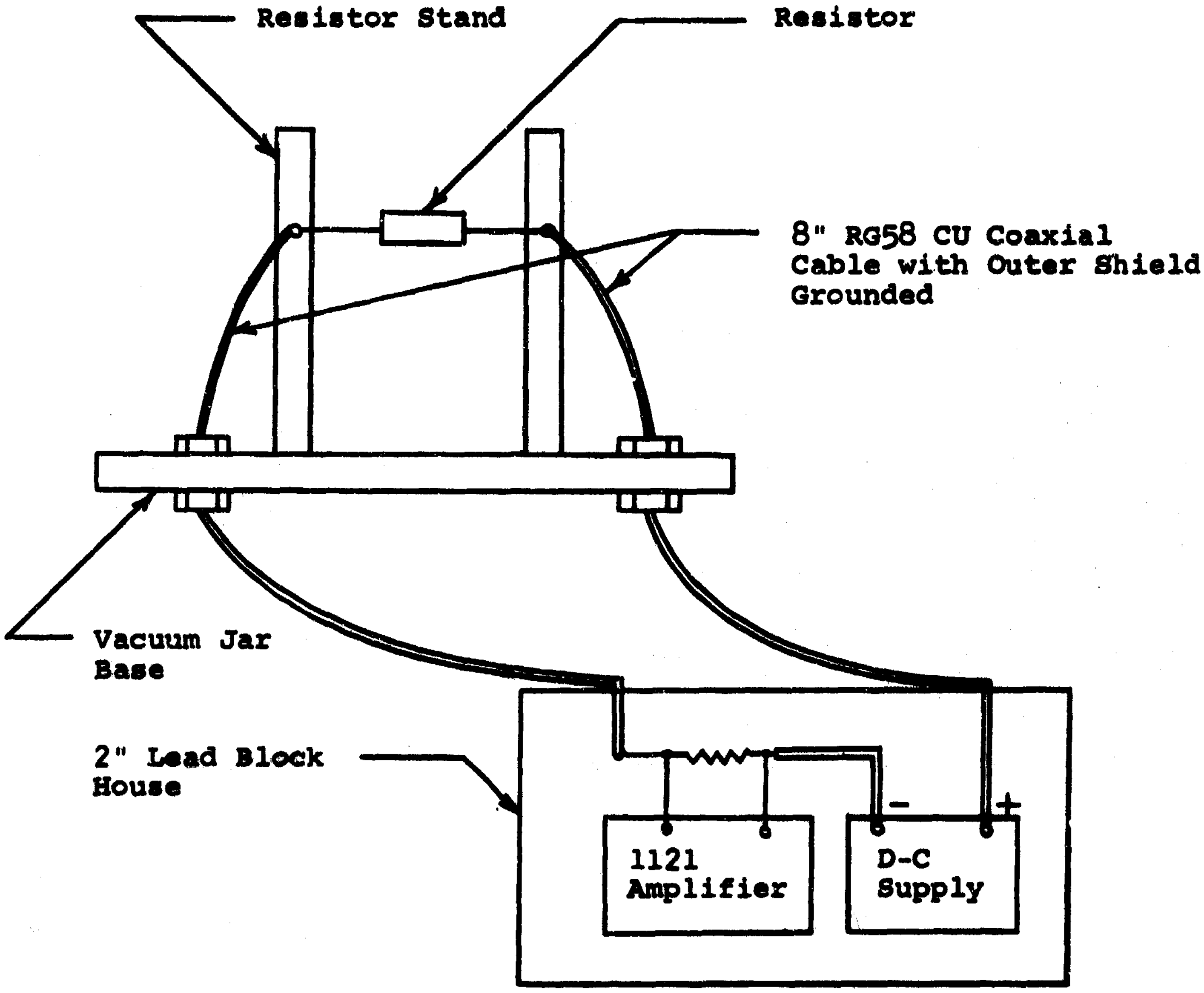

Figure 7. Vacuum System

A variety of exposures was taken. In some, both the leads and the resistor itself were not potted. In some experiments only one lead was potted, and in others both leads were potted. Finally, not only were the leads potted, but the body of the resistor was also potted.

The experimental findings are presented in a series of figures. In Figure 8 the magnitude of the peak voltage developed across the 10 K viewing resistor for 1 megohm resistors of 1/4 watt, 1 watt, and 2 watt power ratings is plotted. From the figure, it is seen that the peak amplitude of the voltage is inversely proportional to the pressure from atmospheric to about 150 mm. As the pressure is further lowered, the amplitude of the voltage finally becomes independent of pressure changes. In previously reported tests of the kind discussed here, the same general shape of curve was seen. The detailed behavior of the peak voltage versus pressure as discussed by Ebeoglu et al. (Reference 1) is somewhat different. The fact that the present tests were at about 5000 ft. (the altitude of Albuquerque) equivalent pressure and at low humidity can account for the difference. In Figure 9 there is plotted $\frac{\Delta R}{R_o}$ as a function of R_o, the original resistance, at one dose rate. It is seen that as the value of R_o is increased, the percentage change in the resistance increases. This result can be explained from the equation for the time-dependent resistance

$$R(t) = \frac{R_o R_s(t)}{R_o + R_s(t)} \tag{42}$$

where $R_s(t)$ is the shunt air leakage resistance. Thus a greater percentage change in total resistance would be expected for a higher value of resistance. This result is in keeping with the IBM results shown in Table I.

In Figure 10, the value of ΔV as a function of the tube accelerating potential (or dose rate when the conversion is made)

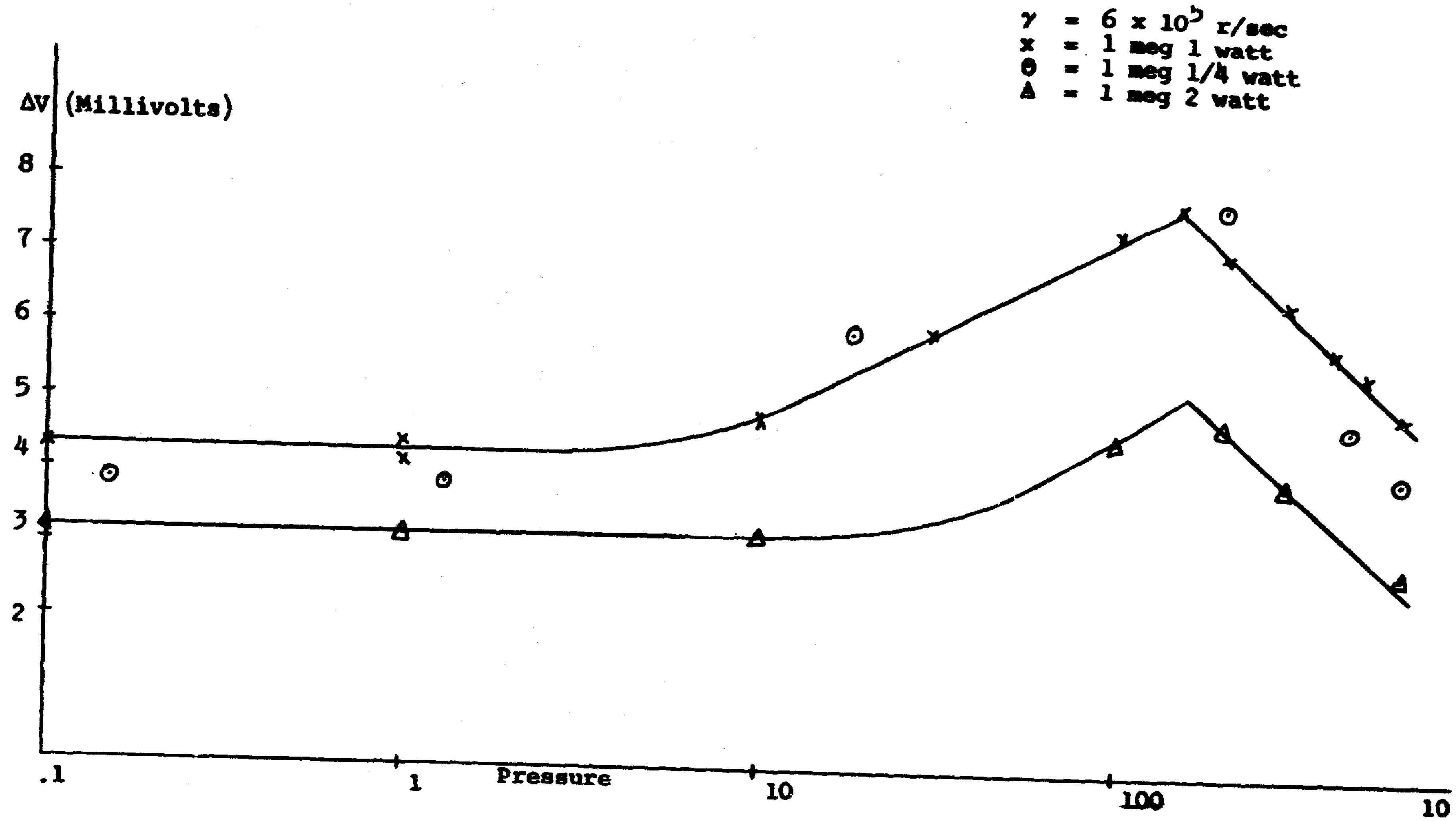

Figure 8. Maximum Change in Transient Voltage as a Function of the Log of Pressures

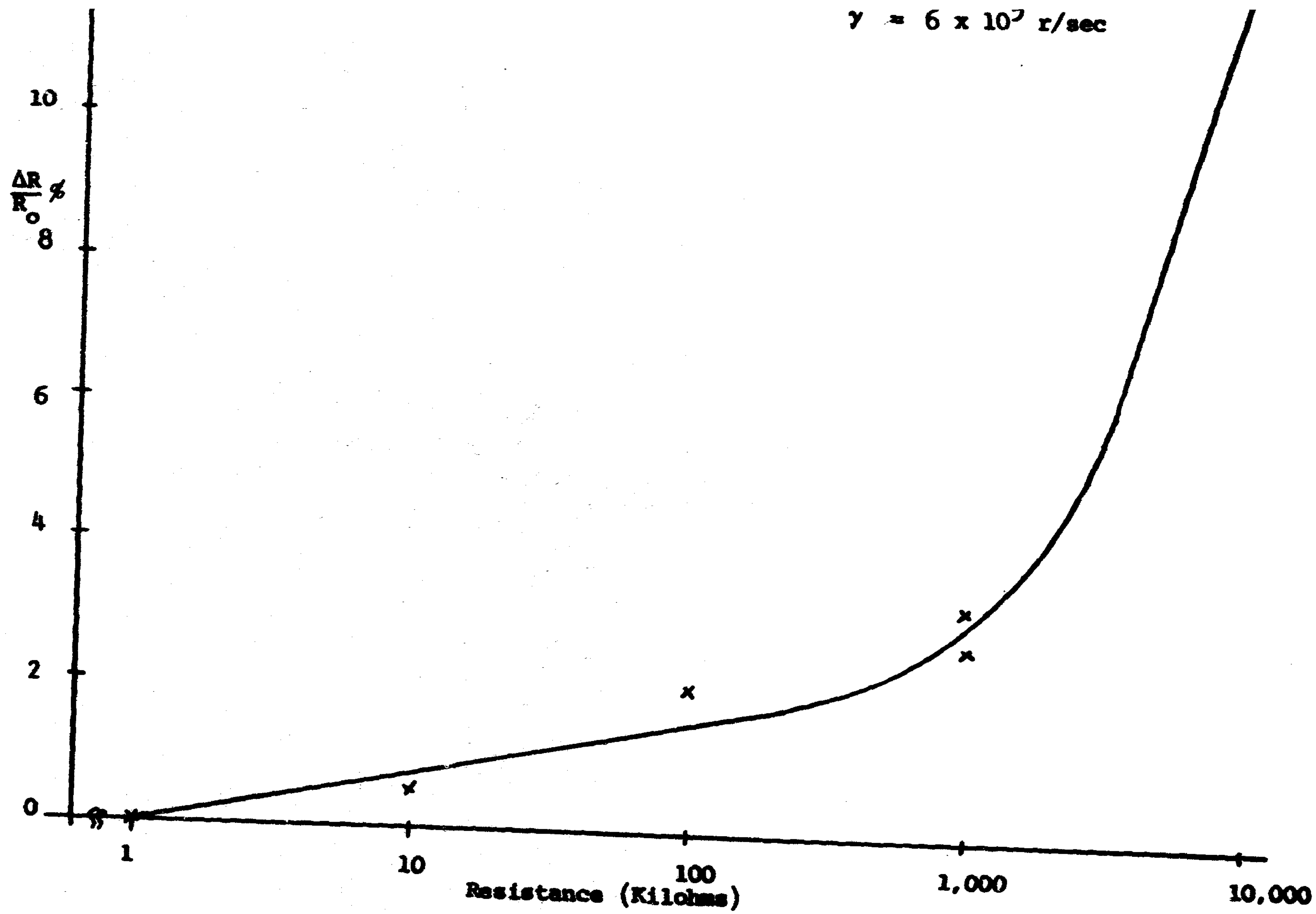

Figure 9. $\frac{\Delta R}{R_o}$ as a Function of R_o, the Original Resistance, at One Dose Rate

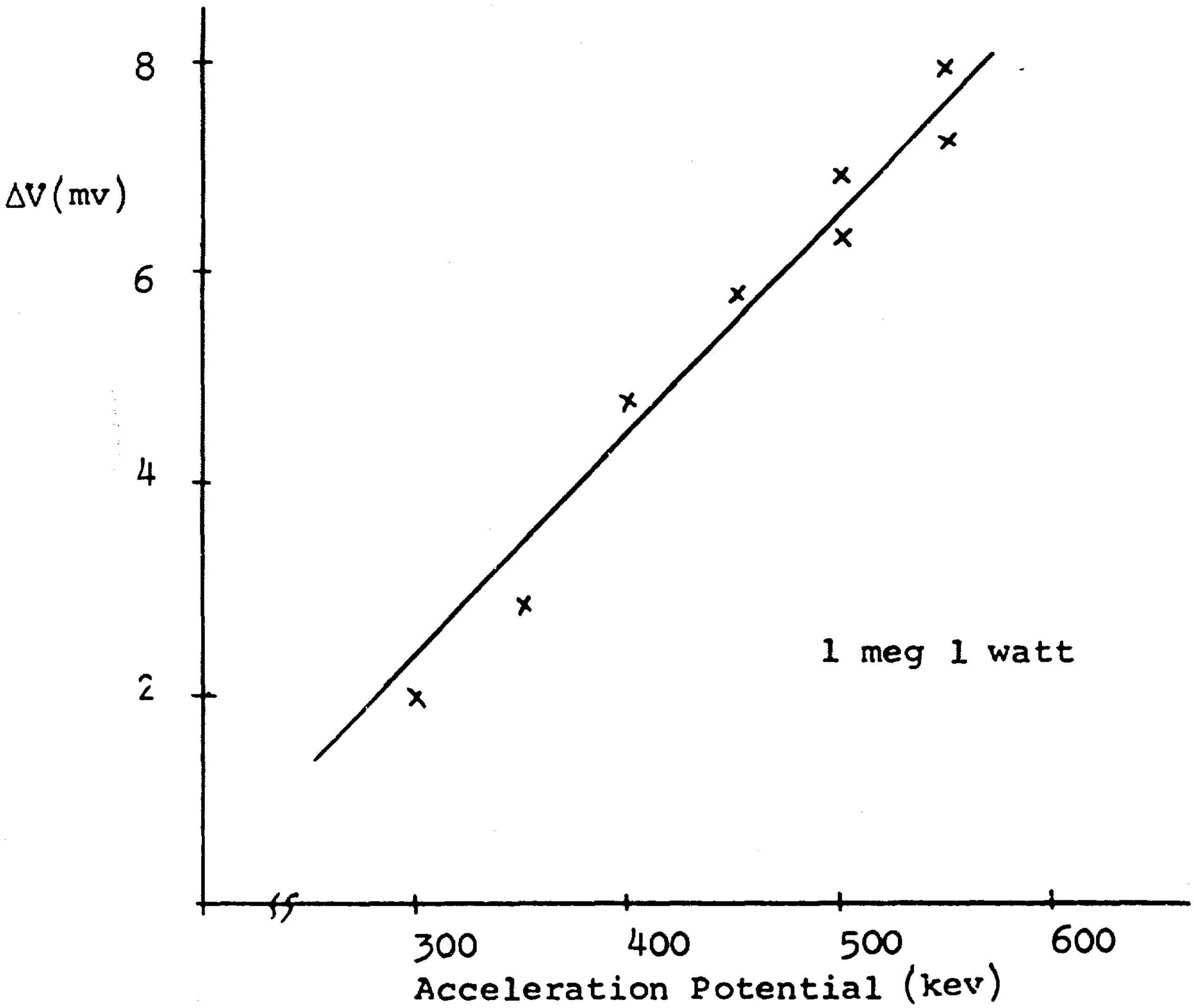

Figure 10. Maximum Transient Voltage as a Function of Accelerating Potential

is given for a 1 ohm, 1 watt resistor. The results from Figure 10 have been plotted again in Figure 11 as ΔR versus dose rate. As previously reported in the TREES Handbook (Reference 8) a model for radiation effects observed in resistors postulates a shunt leakage path given by

$$R_s(t) = \frac{A}{\dot{\gamma}(t)} \qquad (43)$$

and a replacement current equal to

$$i(t) = B\dot{\gamma} \qquad (44)$$

where $\dot{\gamma}(t)$ is the dose rate in r/sec, A is a constant having units of ohm-r/sec, and B is a constant having units of amp-sec/r.

The values for A and B calculated from these experiments at atmospheric pressure (630 mm Hg) for an unpotted Allen Bradley 1 meg, 1 watt, carbon composition resistor are the following:

$$A = 2.1 \times 10^{13}$$
$$B = 7.8 \times 10^{-13} \text{ amp-sec/r.} \qquad (45$$

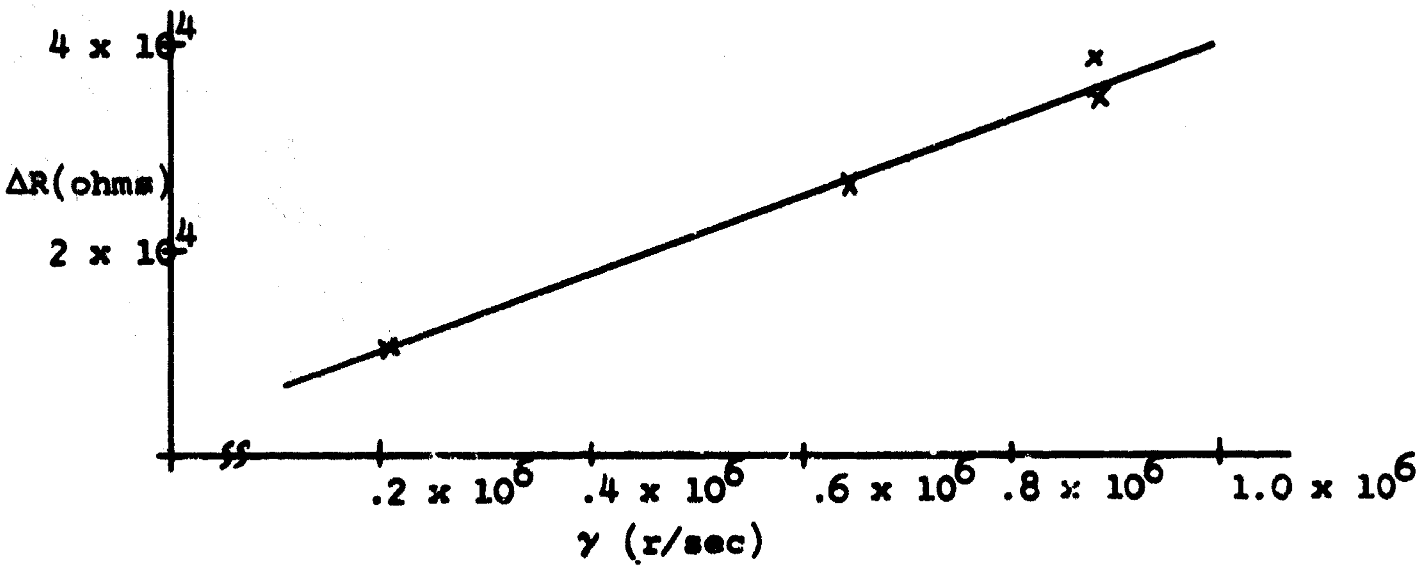

Figure 11. Maximum Change in Resistance as a Function of Dose Rates

These values are in the range of those reported in the TREES Handbook. Figure 12 shows the relative effects of an unpotted resistor at atmospheric pressure, an unpotted resistor at a low pressure, and an epoxy-coated resistor at atmospheric pressure. Ebeoglu et al. maintain that evacuating the test chamber reduces the transient effect on resistors more than potting them. The results of these experiments are contrary to their findings. However, it has been found that when different thicknesses of epoxy coating on the resistor are irradiated, the one with the heavier coating gave the smaller transient effect. It is possible that Ebeoglu et al. had thin epoxy coatings. A comparison of potting the resistor leads and potting the resistor and its leads was made and there was not any noticeable difference in the transient pulse.

For 1 roentgen per hour source of photons of energy of the order of .5 mev the gamma ray energy flux is about 5×10^5 mev/cm^2-sec. The number flux of photons is twice this: namely, $N_\gamma = 10^6$ mev/cm^2-sec. The dose rate delivered by the flash X-ray unit is about 10^6 roentgens per second. Therefore, for the source, $N_\gamma = 3600 \times 10^{12}$ γ's/cm^2-sec or

$$N_\gamma \approx 3.6 \times 10^{15} \ \gamma\text{'s/cm}^2\text{-sec} \qquad (46)$$

This number flux of photons, when multiplied by the total Klein-Nishina cross section for the generation of electrons, will yield the probability per unit time that a single electron is generated. On denoting the probability density by p(t), the order of magnitude estimate is obtained:

$$\begin{aligned} p(t) &= 3.6 \times 10^{15} \times .6 \times 10^{-24} \text{ sec}^{-1} \\ &= 2.16 \times 10^{-9} \text{ sec}^{-1} \end{aligned} \qquad (47)$$

Since the gamma pulse duration is of the order of $.2 \times 10^{-6}$ second the total probability that an electron is generated is given approximately by

$$\rho = p(t)\Delta t = .4 \times 10^{-15} \qquad (48)$$

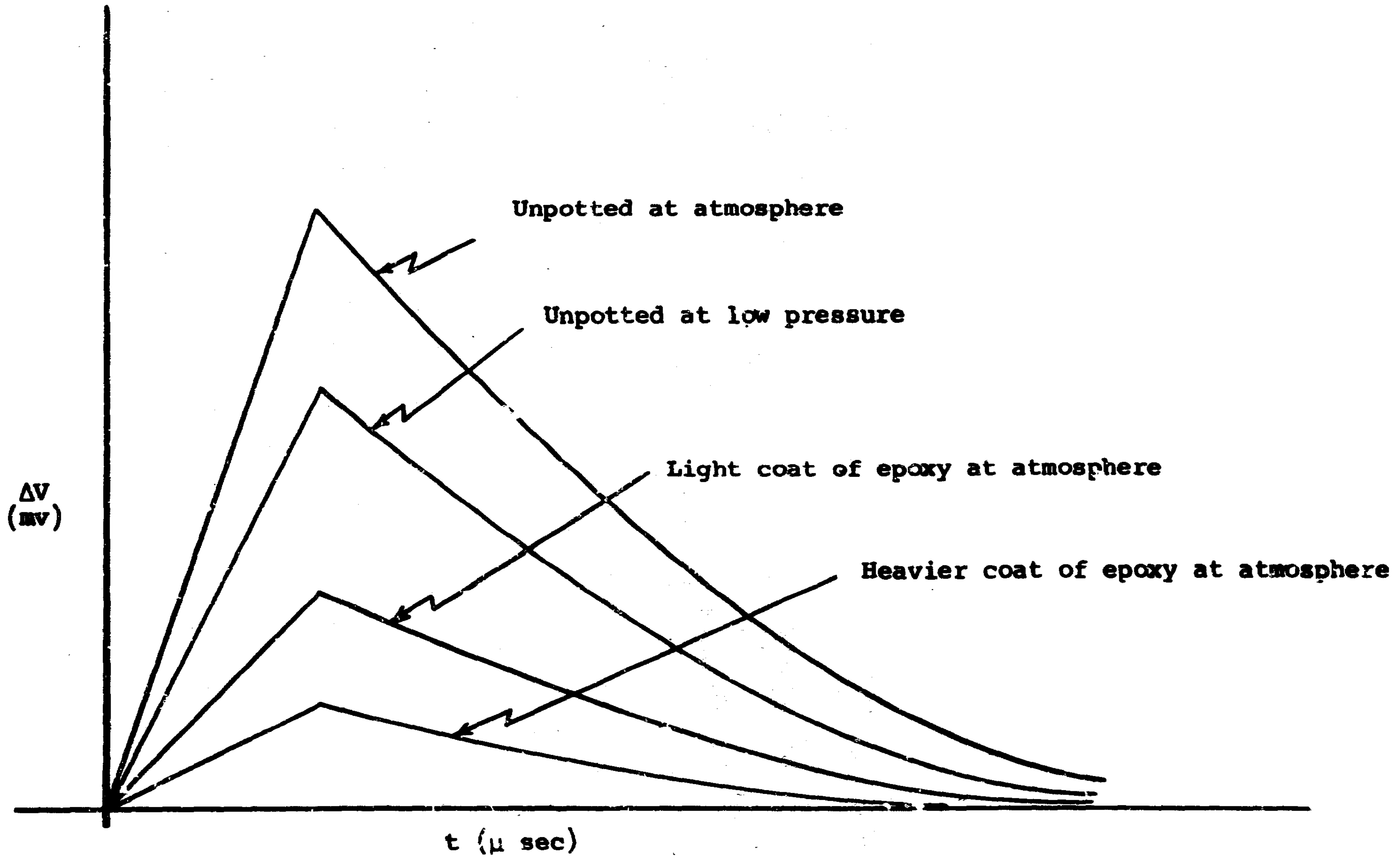

Figure 12. Maximum Change in Transient Voltage as a Function of Pressure or Potting

Then the number of electrons generated per cubic centimeter is the number available times the probability of generation. At atmospheric pressure the number of electrons per cubic centimeter is of the order of

$$N_e \approx 4 \times 10^{20} \text{ cm}^{-3} \tag{49}$$

The number of free electrons generated in the gas for the pulse length will be

$$N_e^f = \rho N_e \approx 10^5 \text{cm}^{-3} \tag{50}$$

The conductivity of an ionized gas can be calculated from

$$\sigma = \frac{q^2 N_e^f \tau}{M} \tag{51}$$

M = mass ion
τ = relaxation time

when τ is known. At atmospheric pressure the dominant process leading to the recombination of free electrons is the attachment of the electrons to oxygen molecules. The time constant for the process is given by

$$\tau^{-1} = \lambda N_{O_2}^2 \tag{52}$$

where $\lambda \sim 2 \times 10^{-30} \text{cm}^6/\text{sec}$ and $N_{O_2}^2$ is the square of the number density of air molecules. The calculated value of τ is of the order of

$$\tau \approx .2 \times 10^{-7} \text{ seconds.} \tag{53}$$

Now σ can be calculated. Its magnitude, with $M_e^f \approx 10^5 cm^{-3}$, $q^2 \approx 23 \times 10^{-20} (esu)^2$, $\tau \approx .2 \times 10^{-7}$ second, and $m_e \approx 9.11 \times 10^{-27}$ gms becomes, on converting from $(\text{statohm-cms})^{-1}$ to $(\text{ohm-cms})^{-1}$, is

$$\sigma \approx 10^{-6} \ (\text{ohm-cms})^{-1} \tag{54}$$

Since the shunt resistance will be inversely proportional to the conductivity, one should expect to find a peak value of R_s (the shunt resistance) of the order of 10^6 ohms if ℓ/A, the length to area ratio, is of the order of unity. Calculations confirm that the value of the shunt resistance in these experiments is, indeed, of the order of 1 megohm.

The peak voltage developed across the 10 KΩ viewing resistor in these experiments is about 5×10^{-3} volts. The current flowing through the viewing resistor is, therefore, of the order of a cm^2, the current density will be of the order of

$$j \approx 5 \times 10^{-7} \ \text{amperes/cm}^2 \tag{55}$$

It is of interest to compute the expected velocity of the electrons within the gas if it is assumed that a current density of the same order of magnitude as that given above flows from the gas across the boundaries of the irradiated resistor. Thus,

$$j(n_e^f q)^{-1} = v \tag{56}$$

with $j \approx 5 \times 10^{-7}$ amperes/cm^2, $n_e^f \approx 10^5 cm^{-3}$, and $q = 1.6 \times 10^{-19}$ amps-sec

$$v \approx 10^7 \ \text{cm/sec.} \tag{57}$$

Now this velocity is what one would expect if the electrons had come into thermal equilibrium with molecules within the gas. It is certainly not typical of electron drift velocities within a conductor or resistor. These are of the order of a few cm/sec. We may interpret the findings as providing further evidence for the fact that the transient effects observed in irradiating resistors are wholly due to effects within the gaseous medium surrounding the sample under test.

This discussion on experimental findings will be concluded by examining the behavior of the time decay of the voltage pulse observed on irradiating resistors. If the attachment of electrons to oxygen molecules is the dominant process over most of the pressure range in which we have conducted experiments, it would be possible to correlate the theoretical predictions of time constants with the experimentally observed ones. Figure 13 is a plot of the theoretical time constants found by evaluating

$$\tau^{-1} = \lambda N_{O_2}^2 \qquad (58)$$

with

$$N_{O_2} = \frac{6.023 \times 10^{23}}{2.24 \times 10^4} (.2) \frac{p}{p_o} \qquad (59)$$

The number of molecules in 22.4 liters of air is just 6.023×10^{23}. The factor .2 accounts for the fact that only one fifth of the total number (approximately) are oxygen molecules. Finally, since the number will decrease with pressure, the factor p/p_o is the ratio of pressure p to atmospheric pressure p_o.

Superimposed on the theoretical curve of Figure 13 are experimental points. The agreement between theory and experiment in the range of pressures between 1 and 10 mms of Hg is within the uncertainties of plotting the oscilloscope traces. Above

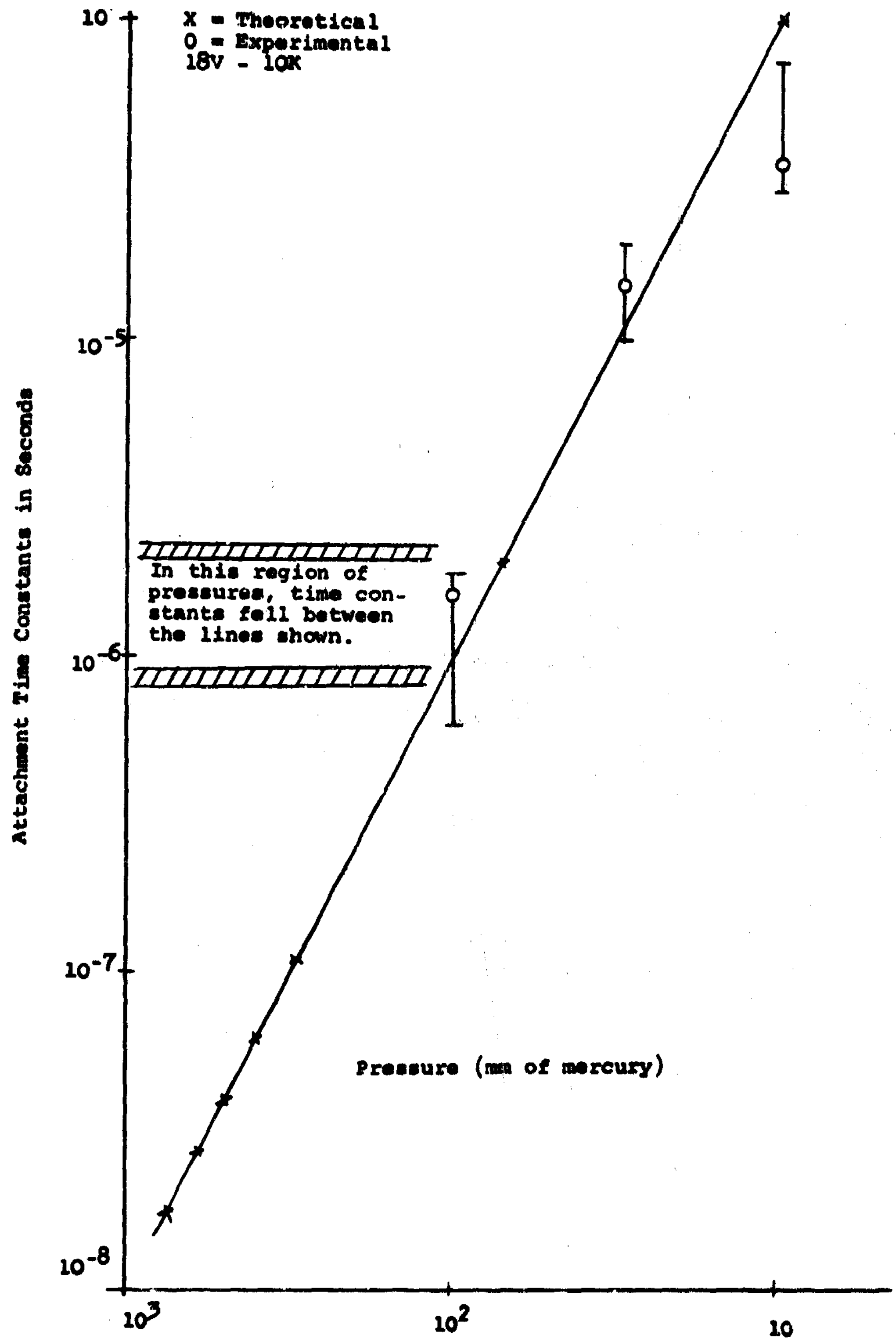

Figure 13. Attachment Time as a Function of Pressure

100 mms of Hg time constants were found to be of the order of 2×10^{-6} seconds to pressures of 630 mms of Hg. It is felt that such a time constant is characteristic of these circuits and not of the decay processes in the gas. Attempts were made to lower the time constant of the circuit of Figure 6 by replacing the 10 KΩ viewing resistor with a 1 KΩ viewing resistor. Severe noise problems resulted, and, as a consequence, the construction of a screen room about the capacitor bank of the flash X-ray unit has been recommended. Below pressures of 10 mms of Hg the time constant of the decay begins to drop towards values of a few microseconds once again. Since radiative recombination may be the dominant process at such low pressures, and since the constant for such a process is of the order of 10^{-7} sec, it is expected that a drop in the value of the time constant should occur and that it should be masked by the circuit time constant.

5. Conclusions

Experiments have been performed which involved irradiating carbon composition resistors with the Kirtland Air Force Base flash X-ray unit. From these experiments the following information has been found:

1) The magnitude of the transient voltage observed on an oscilloscope is a function of pressure. The voltage increases until a pressure of about 150 mms of Hg is reached, and then it decreases until a pressure of 1 mm of Hg is reached. The magnitude then remains constant.

2) The time constants of the voltage decay agree, within experimental error, with a model which maintains that the dominant process in a gas leading to disappearance of free electrons is the attachment of free electrons to oxygen molecules over the pressure range from 10 to 100 mms Hg. Above 100 mms of Hg, time constants of voltage decay are of the order of a few microseconds, these being characteristic of the measuring circuit.

3) A theory had been developed in which the time-dependent behavior of the number of free electrons plays a dominant role. The theory has been used to calculate the peak conductivity, current density, and pulse shapes of the present work, as well as that of other investigators. The agreement is good.

4) It has been found that the value of resistance changes as a function of dose rate and the percentage change in rated resistance value depends critically on the original value of the resistance. Such work confirms earlier findings which are also discussed in this report.

5) Potting of resistors leads to a decrease of air ionization effects, and it has been found that potting of the leads only has a major effect in reducing the magnitude of the observed transients. This suggests that heavier coatings cause a further reduction.

6) One may conclude, as has been done earlier by other workers, that transient resistance changes under gamma irradiation are entirely due to air ionization effects. No bulk effect was observed. In order to minimize air ionization effects, it is important that circuits be designed having as low an impedance as possible for the job they are designed to do.

SECTION II

TRANSIENT RADIATION EFFECTS ON HALL DEVICES

By W. W. Grannemann, Harold Cates and LeRoy Meyer

1. Introduction

A complete discussion of the transient radiation effects on Hall devices is given in AFWL TDR-64-38, June 1964. Any application of the Hall device in a nuclear environment would require a knowledge of the transient radiation effect on them. Therefore, experiments and calculations were performed to determine the gamma radiation effects on both thin film and bulk type devices. The results of this work will make it possible to separate the gamma radiation effects from the EM and circuit effects. A few applications of Hall devices include the following: magnetic flux meters, compasses, magnetometers, clip-on DC ammeters, computor elements, modulators, amplifiers, variable attenuators, frequency multiplexing, and DC to AC conversion.

The commercial devices used were the Ohio Semiconductor Halltrons, and the Beckman thin-film Hallefex voltage generators. These are the indium antimonide (Halltron HS-51 and Hallefex 351) and/or indium arsenide (Halltron HS-31 and Hallefex 350) devices. Also some InSb Hall devices were made in the University of New Mexico laboratory with special non-inductive leads.

The gamma radiation sources that were used are the AFWL 600 KV flash X-ray and the White Sands gamma Linac.

2. Theory

a. Gamma and Electron Irradiation of Hall Device Materials

The effects discussed here apply primarily to InSb, but much of the same phenomena apply to other semiconductor materials.

The effects studied are primarily those caused by gamma radiation, although electrons have been used with Linac experiments.

Under the heading of TREES (transient radiation effects on electronic systems), there are several effects that may be important, depending on the environment and instrumentation. These are ionizing effects, sudden creation of permanent defects, and the sudden rise of temperature. In many cases these effects are small and there is difficulty in separating them from cable effects and noises. While these small effects are unimportant as far as transient radiation effects on electronic circuits are concerned, it is desirable to understand them and see them clearly enough in experiments so that predictions can be made as to their effects in higher dose rate environments.

The excess electrons and holes temporarily created in a semiconductor by exposure to ionizing radiation enhance the conductivity and Hall constant of the media. The conductivity and Hall constant are a function of the majority carriers. In addition to this current in the volume of the device, there may be an additional current component from surface conduction, or conduction to some other elements of an encapsulating or supporting structure. The degree to which these excess carriers affect the operation of the device will depend on the function of the device. An estimate of the magnitude of the radiation-generated current can be obtained for a device by knowing the geometry and electrical characteristics.

At normal temperatures the generation and recombination processes constantly occur due to the influence of thermal energy. A state of equilibrium is maintained by these processes as determined by Fermi-Dirac statistics. This distribution is independent of the manner in which carriers are either generated or recombined.

The change in carrier density in a semiconductor, δn, can be estimated from the known radiation dose rate, the efficiency of the material in producing carriers (.36 to .72 ev/pair for InSb), and the carrier recombination rate for the material. If the

radiation pulse is short compared to carrier lifetime, τ, the total number of excess carriers at the end is proportional to the radiation dose. If the carrier lifetime is much shorter than the radiation pulse, the excess carrier density (δn) at any time during the pulse is

$$\delta n = \delta n_t t \tag{60}$$

where t is the time duration of the radiation pulse, and δn_t is obtained from the continuity equation as follows:

$$\begin{Bmatrix}\text{time rate of}\\ \text{increase of}\\ \text{conduction}\\ \text{electrons}\end{Bmatrix} = \begin{Bmatrix}\text{rate of}\\ \text{generation}\\ \text{of conduction}\\ \text{electrons}\end{Bmatrix} - \begin{Bmatrix}\text{rate of re-}\\ \text{combination}\\ \text{of electron-}\\ \text{ion pairs}\end{Bmatrix} \tag{61}$$

$$\delta n_t = g - R$$

The generation rate g can be estimated if the energy of the radiation beam and the absorption coefficient for the material are known. The energy absorbed is given by the expression

$$\Sigma_{abs}\,(\text{ev}) = \gamma_a \frac{\text{cm}^2}{\text{gram}} \cdot I_o \frac{\text{ergs}}{\text{cm}^2} \cdot \frac{\text{gram}}{\text{device}} \cdot \frac{10^7\,\text{ev}}{1.9\times10^{-9}\,\text{ergs}} \tag{62}$$

where

γ_a = absorption coefficient

I_o = energy of gamma beam

The energy lost per electron ionized in any material can be approximated as 2 to 4 times the ionization potential of the material (Reference 9). This ionization potential in solid-state materials is interpreted to be the forbidden energy gap, which is 0.18 ev for InSb. The ionizing efficiency for InSb is then about 0.36 to 0.72 ev per electron-ion pair. The processes

involved are the Compton scattering events and photoelectric events. All the calculations were made using the numbers which gave the maximum radiation effect. In this case .36 is used and the number of carriers produced is then

$$n_s = \frac{\text{energy absorbed (ev)}}{0.36 \text{ ev/electron-ion pair}} \tag{63}$$

If a square wave radiation pulse of duration t, is assumed, the generation rate g of conduction electrons is given by

$$g = \frac{n_s}{t} \tag{64}$$

An equation similar to equation (61) can be applied to holes. The excess conductivity can be shown to be

$$\delta\sigma = q(\mu_n \delta n + \mu_p \delta p) \tag{65}$$

where

μ_n = electron mobility
μ_p = hole mobility
δ_p = excess number of holes

Equation (65) reduces to

$$\delta\sigma = \delta n q \mu_n \tag{66}$$

for n-type material where $n >> p$ and $\mu_n >> \mu_p$

For steady state, $R = g$, and the steady-state concentration increment is

$$\delta n = g\tau \tag{67}$$

where

τ = mean lifetime of the carriers.

Equation (67) corresponds to equation (3), page F-2, of the TREES Handbook where it is given in the form

$$n - n_o = g\tau \qquad (68)$$

where

$n - n_o = \delta_n$ in this report.

The equation given in the TREES Handbook for g is

$$g = K\dot{\gamma} \qquad (69)$$

where

K = the energy-dependent generation constant [electron-hole pairs per erg g^{-1}(c)]

$\dot{\gamma}$ = the gamma exposure rate (ergs g^{-1}(c) sec^{-1})

Since the constant K is not known for this material and energy, the above derivation was needed to arrive at a generation rate g.

These empirical equations look nice mathematically, but are not always applicable unless all the constants are known.

$\tau = 50 \times 10^{-9}$ sec for InSb, and thus equation (67) would apply for InSb when calculating the change in carrier density.

For build-up,

$$\delta n = g\tau\left[1 - \exp\left(-\frac{t}{\tau}\right)\right] \qquad (70)$$

And for decay,

$$\delta n = g\tau \exp\left(-\frac{t}{\tau}\right) \qquad (71)$$

where

t = time in seconds

b. <u>Effects on Hall Voltage Output</u>

Since current is related to voltage, the increase in the number of carriers calculated by equation (67) will cause a change in conductivity of the material $\delta\sigma$ by the following relation

$$\delta\sigma = q\delta n\mu_n \tag{72}$$

Since current is related to the voltage, V, across the device by the relation

$$i = \sigma V w d/\ell \tag{73}$$

where

w = width of device
d = depth
ℓ = length

the change in current through the device will then be

$$\delta i = \delta\sigma V w d/\ell \tag{74}$$

The change in Hall voltage output, δV_h, may be calculated for three different modes of operation, if it is assumed that the conventional Hall voltage equation holds under the radiation conditions. This relationship is given by

$$V_h = \frac{R_h BI}{d} \tag{75}$$

where

R_h = Hall coefficient (cm^3/coul)
B = Magnetic field (grams)
I = Current lines (amperes)
d = Material thickness (cm)

The three cases considered are for the Hall device operated with the bias circuit as

1. a constant voltage source
2. a constant current source
3. a constant power source

(1) Constant Voltage Source

This circuit arrangement is shown in Figure 14.

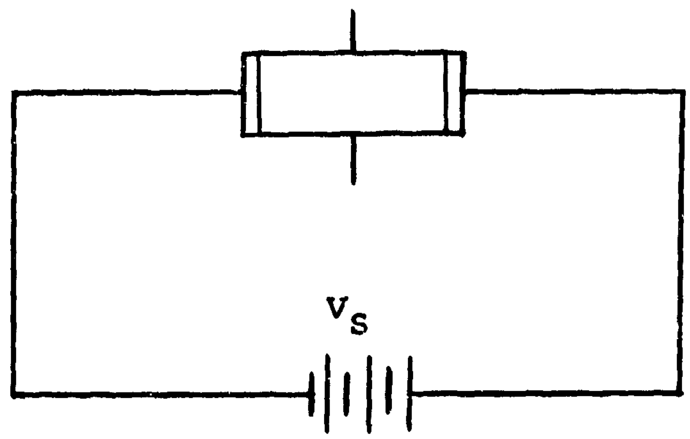

Figure 14. Constant Voltage Source Bias Circuit

By using the relations for the Hall coefficient and current density in the Hall voltage equation, one gets the following results:

$$R_h = \frac{1}{nq} \tag{76}$$

where

n = number of conduction electrons

q = charge of an electron

and

$$\frac{I}{wd} = \frac{qn\,\mu V_s}{\ell}$$

$$I' = qn\,\mu\,\frac{wd}{\ell}\,V_s \qquad (77)$$

where

μ = mobility

V_s = source voltage

d, w, and ℓ = dimensions of sample

Then

$$V_h = \frac{R_h BI}{d} \qquad (78)$$

$$V_h = \frac{B\mu w}{\ell}\,V_s \qquad (79)$$

Equation (79) indicates that for a constant voltage source the Hall voltage should remain constant during a radiation pulse, since B, μ, V_s and the device's dimensions are not a function of the radiation energy absorbed.

(2) Constant Current Source

The constant current source has a large output impedance compared to the Hall device input impedance. This circuit arrangement (Figure 15) keeps the current through the device constant. Then using equations (75) and (76) one may obtain

$$V_h = \frac{BI}{nqd} \qquad (80)$$

The current in the Hall voltage equation will be a constant. Then if n changes by an amount δn, a quantity δV_h, the change in Hall voltage is defined by

$$V_h + \delta V_h = \frac{K_1}{n + \delta n} \qquad (81)$$

where

$$K_1 = \frac{BI}{qd}$$

so that

$$\delta V_h = \frac{K_1}{n + \delta n} - \frac{K_1}{n} \qquad (82)$$

(3) Constant Power Source

If energy is supplied to the Hall device at a constant rate, the result that Hall voltage is a function of $\frac{1}{\sqrt{n}}$ is obtained in the following manner. The power equation is

$$P = I^2 R \qquad (83)$$

The resistance, R, can be expressed in terms of the resistivity and dimensions of the device by

$$R = \frac{\rho \ell}{wd} \qquad (84)$$

Then

$$I = \left[\frac{Pwd}{\rho \ell}\right]^{1/2} \qquad (85)$$

Next, using equation (84) and the following relations for R_h and ρ in the Hall voltage equation one may obtain

$$R_h = \mu\rho, \quad \text{and } \rho = \frac{1}{nq\mu} \qquad (86)$$

$$V_h = \left(\frac{\mu}{n}\right)^{1/2} B\left(\frac{Pw}{q\ell d}\right)^{1/2} \qquad (87)$$

$$V_h = \frac{K_2}{\sqrt{n}} \quad \text{when } K_2 = B\left(\frac{P\mu w}{q\ell d}\right)^{1/2} \qquad (88)$$

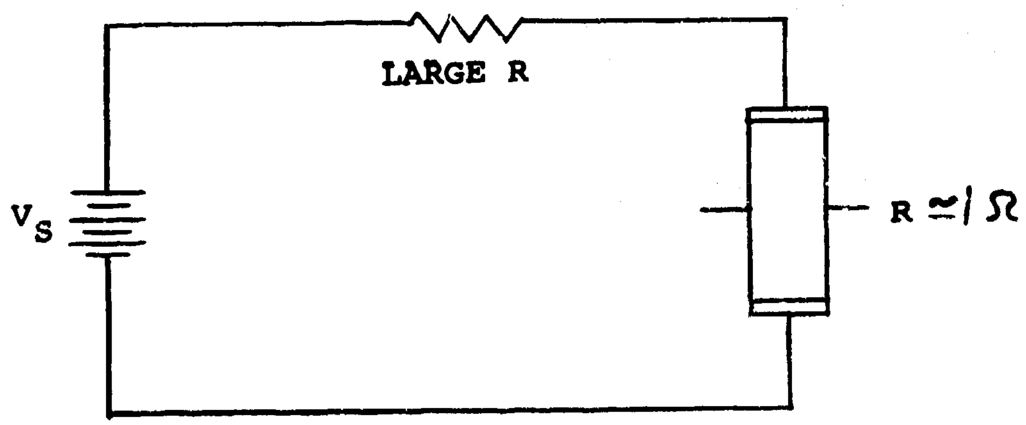

Figure 15. Constant Current Source Bias Circuit

If n changes by an amount δn, the change in Hall voltage, δV_h, will be given by

$$V_h + \delta V_h = \frac{K_2}{\sqrt{n + \delta n}} - \frac{K_2}{\sqrt{n}} \tag{89}$$

so that

$$\delta V_h = \frac{K_2}{\sqrt{n + \delta n}} - \frac{K_2}{\sqrt{n}} \tag{90}$$

Equations (82) and (90) indicate that the Hall voltage should decrease when n-type material is irradiated by gamma rays.

c. Theoretical Results

In the AFWL TDR-64-38 the constant current case is taken and the change in Hall voltage calculated, for a typical operating condition, always assuming the worst case, for various radiation dose rates. The results were that there was no significant change in Hall voltage for dose rates up to 10^9 r/sec. An n-type Indium Antimonide bulk type device was used in the calculations.

At a dose rate of greater than 10^9 r/sec both holes and electrons had to be taken into account (which involves a much more complicated expression), and a transient radiation effect was predicted.

The thin film devices have even less calculated transient radiation effect than the bulk type device because they have less material in which to abosrb energy. This does not eliminate the possibility of having a transient radiation effect due to lead arrangements or other inherent error effects in Hall devices. There are a number of causes of Hall voltage errors which would have to be investigated for a particular application. These are: 1) loops in lead arrangements which are necessary in making contact to the material, but could cause errors when measuring changing magnetic fields; 2) displacement voltage

which is due to misalignment of Hall voltage leads; 3) r-f pick-up; 4) air ionization; and/or 5) cable effects.

3. Experiment

In the 600 KV flash X-ray experiments no transient radiation effects were observed when the constant current circuit configuration was used. Also there was no change in Hall voltage when the constant voltage circuit was used. The dose rates were 10^6 r/sec.

It was found that the bulk type device had an upper cut-off frequency of around 150 KC. To be sure that the transient radiation effect was not being lost due to band width limitations, the White Sands Gamma Linac was used. It had a gamma pulse width of 10 microseconds. No change in Hall voltage was observed for dose rates up to 10^6 r/sec using either constant current or constant voltage circuits.

4. Conclusions

The Hall devices were found, by experiments with the flash X-ray and gamma Linac, to be radiation resistant for dose rates up to 10^6 r/sec. Theoretical calculations indicate a radiation resistance up to at least 10^9 r/sec. These results were obtained using the constant current circuit configuration. Theoretical calculations for the constant voltage circuits indicate no change in Hall voltage for n-type material. At dose rates above 10^9 both holes and electrons become involved and the Hall voltage equation becomes more complicated. A transient radiation effect is predicted at the higher dose rates. Higher dose rate machines are needed to check the theory at the higher dose rates.

This page intentionally left blank.

SECTION III

THE FABRICATION AND IRRADIATION OF TITANIUM DIOXIDE DIODES

By James Woodward and W. W. Grannemann

1. Introduction

Probably the biggest need in the transient radiation effects program is for a highly radiation resistant diode and transistor which exhibit both desirable electrical characteristics and resistance to transient radiation and steady state radiation. Titanium dioxide diodes have some interesting possibilities in this respect. Recent research at the University of New Mexico indicates that titanium dioxide diodes are highly radiation resistant to permanent type damage. The study in this section was instigated to provide some information on the transient radiation properties of titanium dioxide diodes.

Titanium dioxide diodes are not presently commercially available. So this section covers the fabrication of the devices, a mathematical approximation of the transient radiation effects, and the results of irradiating the devices with the flash X-ray.

2. Fabrication of Titanium Dioxide Diodes

Titanium dioxide diodes can be fabricated by several different methods in the laboratory. Three of the most practical and successful methods are listed below:

1) Titanium Dioxide on Titanium Base Using Forced Steam One-Step Process (Reference 10).

Heated titanium will readily coat with a semiconducting titanium dioxide film when steam is passed over the sample. As the oxide is formed some reduction takes place by the surplus hydrogen, causing oxygen vacancies in the oxide film. The final result is an n-type semiconductor film which gives diode action to impressed voltages.

2) Titanium Dioxide on Titanium Base Using a Two-Step Heating Process (Reference 11).

In this method an oxide film is formed by heating the

titanium sample in oxygen. This is followed by reduction in a hydrogen atmosphere creating the n-type titanium dioxide film on the titanium sample.

3) Rutile Point Contact Diode (Reference 12).

In this method of manufacture crystal rutile is heated in a hydrogen atmosphere causing oxygen vacancies in a surface layer of n-type semiconductor. The sample is cleaved to expose a clean surface which is secured to a copper stud, and a point contact is applied to the titanium dioxide semiconductor.

a. Diode Manufacture

It has been determined that the one-step, steam reduction process gives the most reliable and repeatable results. This is most probably due to the fact that reduction of the titanium dioxide film takes place continuously during the film coating process, thereby providing a nearly homogeneous distribution of oxygen vacancies. The other two processes are basically surface processes; hence the reduction can be considered to be more concentrated near the surface. Diodes made by these methods are not consistent in characteristics and are more prone to aging (Reference 13). Because of the aging factor, the titanium dioxide diodes were fabricated using the one-step steam process.

Chemically pure samples of titanium .5 x 5 x .016 inch in size were prepared from sheet Ti-55A (this is chemically pure titanium). A copper lead was attached to one .5 x .5 inch surface by brazing with a helium shielded arc. Attaching the copper ohmic lead to the pure metal in this manner prior to coating the sample with the oxide film was considered more advantageous than attempting this step later on in the manufacturing process. The alternative was to completely coat the sample with an oxide film and then scrape away part of the film so that an ohmic contact could be made to the pure titanium. This alternative procedure risks heat and mechanical damage to the semiconductor film; therefore, it was not attempted.

The pure titanium samples with copper leads attached were then polished to provide a smooth surface on which to coat the oxide film. This is considered an important step as rough surfaces were found to readily cause shorting through the semiconductor film.

Oxide films were coated on the samples by placing them within a 1 1/2 inch quartz tube which had been inserted in an electric furnace. A constant flow of superheated steam was passed through the quartz tube and over the samples at all times while the samples were at elevated temperatures. The equipment used required approximately 8 to 10 minutes to bring the samples to temperatures in the vicinity of 700°C.

A variety of temperatures and time periods for depositing the film was investigated. Temperatures below 650°C for periods up to 1 hour, in general, produced oxide films which readily shorted out under applied voltages. Satisfactory results were obtained by keeping the samples in an atmosphere of 750°C for approximately 30 minutes while passing superheated steam over them. It is, however, estimated that longer exposures of about 3 hours would have produced satisfactory results at temperatures in the 650°C range.

Oxide films obtained in this manner had a black-blue-gray coloring which could not be readily scraped off. The film is estimated to be 10^{-3} cm thick.

Leads to be applied to the semiconductor surface were prepared from thin copper sheet. The strips of sheet copper were bent so that an area of about 1/8 x 1/16 inch was placed flat against the oxide film; the strips were fastened with conducting epoxy. The conducting cement required a 20 minute temperature cure at 200°F. This did not cause any noticeable change in the diode characteristics.

b. <u>Typical Characteristics of the Manufactured Diodes</u>

Titanium dioxide diodes fabricated by the above method exhibit characteristics which compare favorably with the older types of germanium diodes (Reference 14). The manufactured diodes had

consistently similar characteristic curves. The voltage versus current for a typical diode is shown in Figure 16. When voltages were first applied across the diodes most of them showed an initial characteristic curve of less slope than that shown in Figure 16. After 5 or 10 seconds the slope tended to increase and stabilize, never again returning to the curve initially observed. This is believed to be the "healing effect" frequently discussed in literature about diode characteristics. Also observable was a slight hysteresis effect when voltages were rapidly swept across the diode (Reference 15). The reason for this phenomenon was not immediately clear, but further investigation of this characteristic was not attempted.

c. Additional Preparation for Testing of the Samples

The completed diodes were cast in a resin sealant to protect the diode from mechanical damage during subsequent handling. Without potting the diode in this manner it was difficult to attach cable leads for further testing without twisting off the semiconductor surface contact lead as the sample was moved about or stored. The resin sealant also served to isolate the semiconductor film from the atmosphere and reduced the possibility of aging or contamination from atmospheric impurities (Reference 16).

Additional resin sealant was poured around the diode after test cable leads were attached. The quantity of resin sealant poured was large enough to effectively reduce or eliminate ionization effects across the diode leads when the diode was irradiated. The sealant completely enclosed the diode as well as the soldered connections to standard shielded cable used at irradiation testing facilities.

3. Computation of Radiation Effects Upon Titanium Dioxide Diodes

It must from the beginning be pointed out than any computation of a transient current in a semiconductor material can only be as accurate as the physical constants and crystal parameters used. It is beyond the scope of this report to determine the

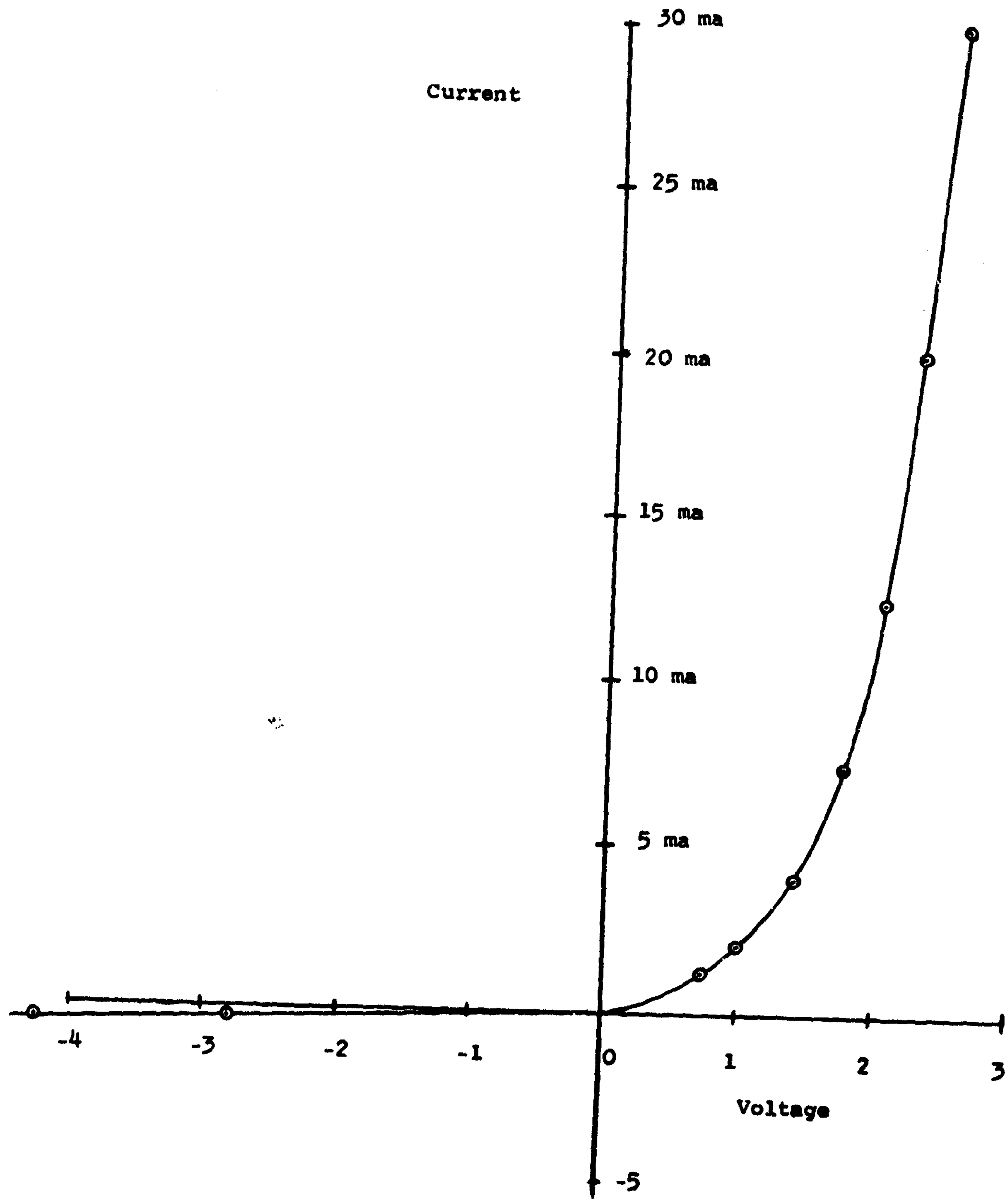

Figure 16. Typical Characteristic (Current Versus Voltage) Curve of Fabricated Titanium Dioxide Diodes

exact values of the ionization energy, electron mobility, etc. of the fabricated crystal. Instead, reasonable values for these and other constants have been selected from the literature to give as near as possible the correct order of magnitude. Other assumptions as to the nature of the crystal doping, the hole current, the diffusion current, etc. also detract from the accuracy of these calculations.

At best, the computations which follow can be considered a crude approximation of what actually takes place in the TiO_2 semiconductor crystal when exposed to a pulse of radiation. The general method as well as the computations may, however, serve as a starting point for the laboratory investigation of radiation effects.

The Air Force Weapons Laboratory flash X-ray facility at Kirtland Air Force Base was used to radiate the manufactured titanium dioxide diodes. Computation of radiation effects upon the diode must of necessity start with consideration of the range and limitation of the flash X-ray system. X-ray tube location, shielding, and instrumentation considerations dictated that the sample to be radiated should be placed 6 inches from the X-ray tube. Data available at the facility for dose and dose rate at the 6 inch location are shown in Table II for the 300 KV to 500 KV range. The dose, designated I_o, is given in erg/cm^2, and the dose rate, I_o/sec, is given in erg/cm^2 sec.

After consideration of tube life and waiting periods between pulses (7-10 minutes for cooling after a 400 KV burst) it was decided that 400 KV operation would best satisfy the test requirements. Computations to follow, therefore, are based upon a dose (I_o) of $.9 \times 10^{-15}$ erg/cm^2.

Brewster lists values for the mass absorption coefficient for titanium dioxide crystal (rutile) (Reference 10). The coefficients, designated W, associated with various wavelengths are shown in Table III.

Table II. Dose and Dose Rate at
6 Inches From X-Ray Tube

	I_o erg/cm^2 x 10^{-15}	I_o/sec erg/cm^2 - sec x 10^8
300 KV	0.60	0.30
400 KV	0.90	0.45
500 KV	1.80	0.90

Table III. Mass Absorption Coefficients of Rutile

Wavelength (λ) in Angstrom Units	.01	0.1	1	2
W in cm^2/gm	.0543	.1790	38.71	250.4

X-ray wavelength (λ) is given by the expression $\frac{hc}{E}$ where h is Planck's constant, c the speed of light, and E the energy. For 400 KV,

$$\lambda = .031 \text{ A}^o$$

Graphical interpolation on log paper of the values in the above chart gives W = .075 cm^2/g for .031 A^o.

The total absorbed energy, E_{abs}, in the titanium dioxide semiconductor is given by the expression

$$E_{abs} = WI_og \tag{91}$$

where W is the mass absorption coefficient, I_o the dose, and g the mass of the semiconductor. The thickness of the semiconductor is taken as 10^{-3} cm and the total area of the semiconductor surface as 3.22 cm^2, giving a volume of 3.22 x 10^{-3} cm^3 and a mass of 13.8 x 10^{-3} grams. (The density of rutile is 4.28

g/cm^3) (Reference 17).

$$E_{abs} = 5.83 \times 10^7 \text{ ev} \tag{92}$$

For gamma irradiations of this frequency range almost all of the absorbed energy of the incident gamma rays upon the semiconductor material is converted into free electron production and motion by photoelectric effect and Compton events. The energy lost per ionization in any material can be approximated as 2 to 4 times the ionization potential of the material. This approximation is commonly found in the literature.

This ionization potential in semiconductors is interpreted to be the forbidden energy gap which is 3.05 ev for rutile TiO_2 (Reference 17). This value can be taken to be a close approximation for the semiconductor material in a back biased diode. The energy lost per electron produced is therefore taken to be approximately 6.10 ev.

The number of electrons (N) produced is computed by the expression

$$N = \frac{E_{abs}}{6.10 \text{ ev}} = .957 \times 10^7 \text{ electrons} \tag{93}$$

If a square wave radiation pulse of .2 microsecond duration is assumed, the rate g(t) of generation of conduction electrons is given by

$$g(t) = \frac{N}{t} = 4.78 \times 10^{13} \text{ electrons/sec} \tag{94}$$

where

t = time

The mobility of electrons (μ_n) in reduced rutile at room temperature is believed to be less than 10 cm^2/volt-sec.

Current flow in the reduced titanium dioxide semiconductor material is known to be purely electronic (Reference 18). X-ray irradiation produces additional electrons for conduction. Hole current is non-existent or at best negligible.

The electron mobility (μ_n) is related to the diffusion constant D_n by the Einstein relationship (Reference 19).

$$\mu_n = \frac{q}{kT} D_n \tag{95}$$

where at $300^\circ K$, $\frac{kT}{q} = .026$ volt

Therefore,

$$D_n \leq \; = \; 0.26 \ cm^2/sec$$

The transient current flow through the back biased diode will be caused by the excess electrons generated by the incident radiation. The diffusion current occurs whenever there is a density gradient of carriers (∇n). This current is related to the density gradient of electrons by the expression,

$$i_n = q \, D_n \, \nabla n \tag{96}$$

In the case of a thin film, the density gradient can be considered equal to n/ℓ, where n is the concentration of charge carriers and ℓ is the thickness of the semiconductor film. Then,

$$i_n = q \, D_n \, \frac{n}{\ell} \tag{97}$$

The concentration of charge carriers at any time t is a function of both the generation g(t) and the current flow, so that

$$n = \frac{g(t) - \int \frac{i_n}{q} dt - \text{number of electrons which recombine}}{} \tag{98}$$

If it is assumed that the electrons recombining with ions are negligible, the i_n computed is a "maximized" value greater than what should be found experimentally. For the time period of the radiation pulse,

$$i_n = \frac{q \, D_n}{\ell(\text{VoI})} \left[g(t)t - \int \frac{i_n}{q} dt \right] \tag{99}$$

and for $t > .2 \times 10^{-6}$ sec, when electron generation has ceased

$$i_n = \frac{q\ D_n}{\ell\ (\mathrm{Vol})}\left[-\int \frac{i_n}{q}\,dt\right] \tag{100}$$

By substituting values,

$$i_n = .618\ t - 8.07 \cdot 10^4 \int i_n\,dt \qquad (t < .2 \times 10^{-6}\ \mathrm{sec}) \tag{101}$$

and solving for i_n,

$$i_n \leq 7.65 \cdot 10^{-5}\left[1 - \exp(-8.07 \times 10^5 t)\right]\ (t < .2 \times 10^{-6}\ \mathrm{sec}) \tag{102}$$

at $t = .2 \times 10^{-6}$ when the radiation pulse ends,

$$i_n \leq 7.65 \cdot 10^{-5}\left[1 - \exp(-.1614)\right] = .000113\ \mathrm{ma} \tag{103}$$

The current as a function of time after the radiation pulse has passed is

$$i_n \leq 1.13 \cdot 10^{-7} \exp(-8.07 \times 10^5\ t) \quad (t > .2 \cdot 10^{-6}\ \mathrm{sec}) \tag{104}$$

A graph of the transient current rise and fall as expressed by the two equations above is plotted graphically in Figure 17 along with the radiation square pulse.

The computations above do not take into consideration electron-ion recombination, surface effects, and trapping effects. A detailed numerical analysis of these three effects must start with a thorough study of the doped semiconductor crystal, measurement and calculation of the various crystal parameters, and selection of a suitable semiconductor model.

Ths Schottky model (Reference 20) appears best for our particular diode. This model pictures a metal in contact with a uniform semiconductor.

The fabrication process for our titanium dioxide diode, whereby a semiconductor film is deposited upon pure titanium,

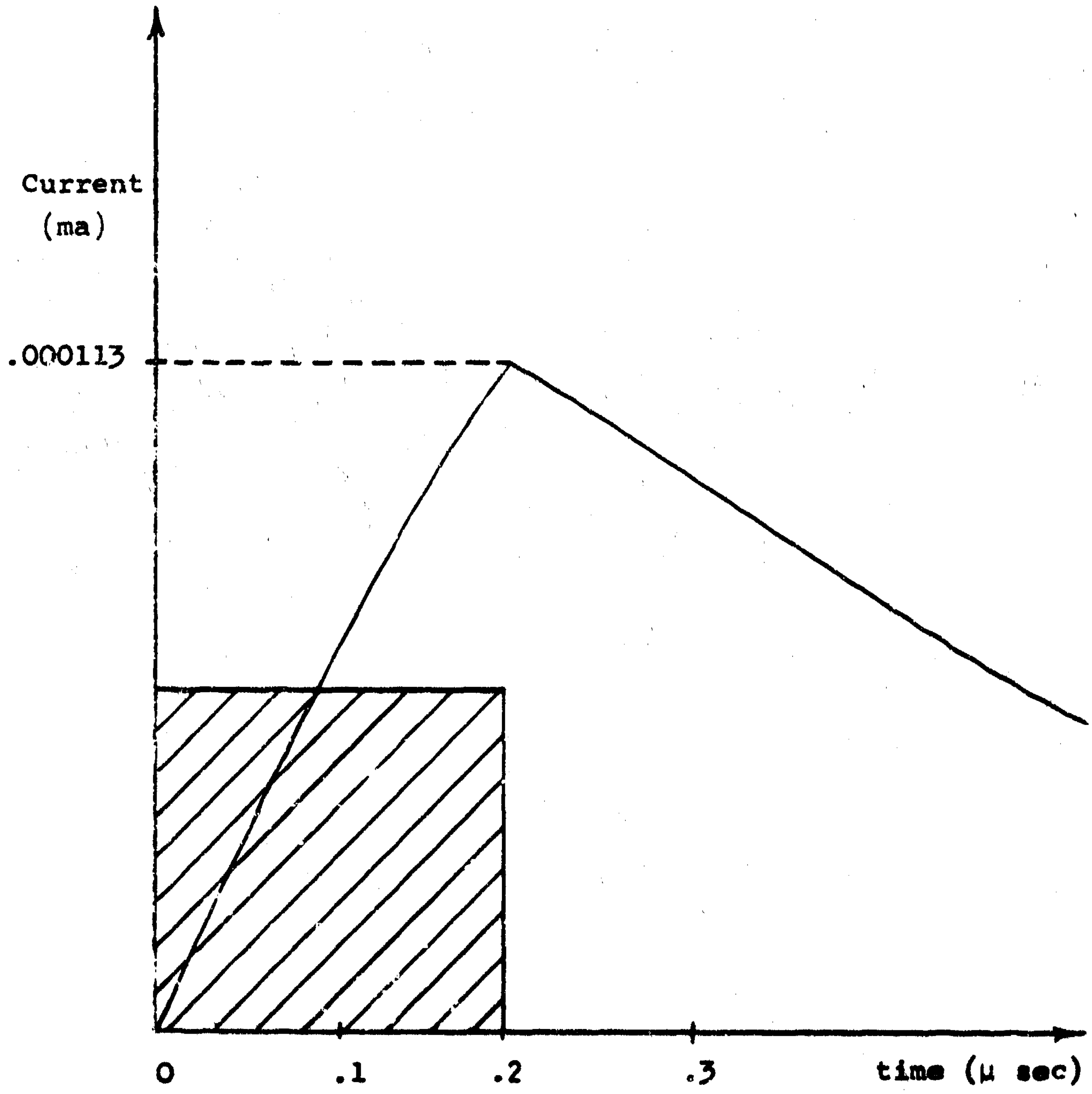

Figure 17. Ideal Transient Current Rise and Fall (With Superimposed Ideal Square Radiation Pulse)

produces an n-type semiconductor. Reduction by steam, causing oxygen vacancies, takes place continuously throughout the period that the film is deposited. The vacancies are assumed to be uniformly distributed throughout the crystal. This type crystal lends itself to the Schottky model.

If further analysis reveals the existence of some sort of surface layer between the titanium metal and the semiconductor, consideration should be given to the Bethe model (Reference 21). This model takes into consideration an insulating layer of a specified thickness between the metal and a uniform semiconductor.

Consideration of the electron-ion recombination phenomenon surface effects, and the trapping phenomenon as discussed above would modify the transient pulse so far computed and shown in Figure 17.

Electron-ion recombination will reduce the number of electrons available for the diffusion current and, therefore, will reduce to some extent the peak value of the transient pulse. Thermal release of charge carriers from the trapping centers will cause a slower decay of the transient current peak.

The transient current pulse shown in Figure 17, therefore, displays two important limits for the expected transient pulse. The peak value expected to be found experimentally should not exceed the peak value shown, and the time constant for the rise and fall of the transient pulse should not be less than that computed and shown in Figure 17.

4. Laboratory Investigation of Transient Effects

a. Instrumentation

Within the screen room are 3 Tektronix type-551 oscilloscopes with type L and type CA plug-in units for recording test results. These also have Polaroid camera attachments. Polaroid film with a film speed of 10,000 ASA is normally used.

A bank of power supplies is available for instrumentation. It includes a Lambda regulated power supply transistorized small voltage/current supply and various dry and wet cell batteries.

RG-58 C/U cable with appropriate connecting and matching hardware is normally used for device circuitry and instrumentation.

b. Radiation Test Set Up

It was considered desirable to establish test circuitry which would provide information about both the voltage across the diode and the current flow through the diode during the radiation pulse and afterward until steady state conditions were again obtained. This meant displaying current versus time and voltage versus time on the scopes where the pulse width was $.2 \times 10^{-6}$ second. The Tektronix scopes, type 551, have this capability with the results permanently obtained for permanent record by Polaroid camera. Care, however, must be taken to provide a circuitry which is accurately responsive during time periods of such short duration.

The first circuitry investigated included a circuit loop with diode, power supply, and current sensing resistor in series. Display probes from the scopes were connected across the current viewing resistor and the diode itself (see Figure 18). All leads were coaxial cable with the copper shielding grounded.

It was soon found that the extensive footage of cable and the interaction of two display connections were causing oscillations or "ringing" which obscured any valid test results.

Efforts then were made to reduce the cable footage and examine only the transient current through the viewing resistor. It was also noted that excessive noise and oscillation occurred when the diodes were forward biased and exposed to radiation pulses. For this reason, and the fact that the back biased condition is of more interest in radiation effects studies, it was decided to conduct all tests at a back bias value of 6 volts.

The final configuration used consisted of the basic circuit loop but with a Tektronix 1121 amplifier close to the test sample (see Figure 19). This arrangement eliminated the long cables, and the system proved to have adequate time response. A Rutherford pulse generator was used to thoroughly check out the system and to determine that the frequency response of the circuit was within the time limits of our measurements.

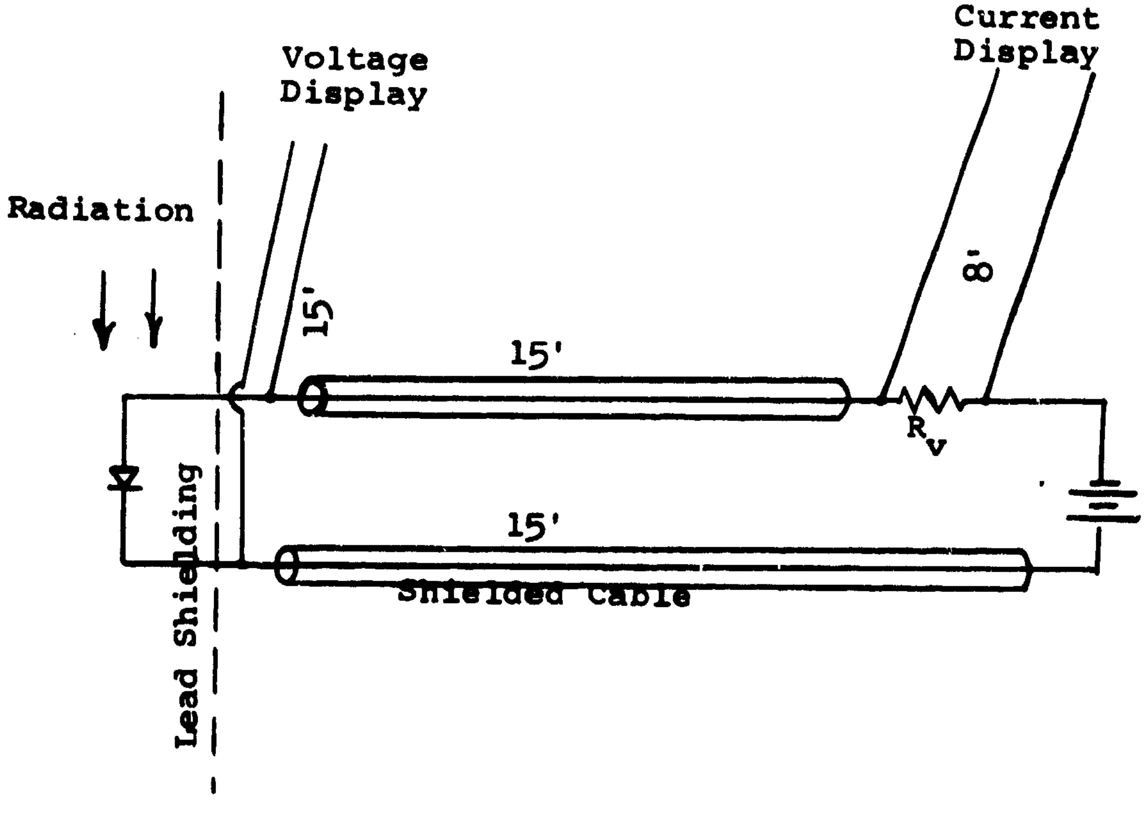

Figure 18. Trial Circuitry for Examination
of Transient Current and Voltage

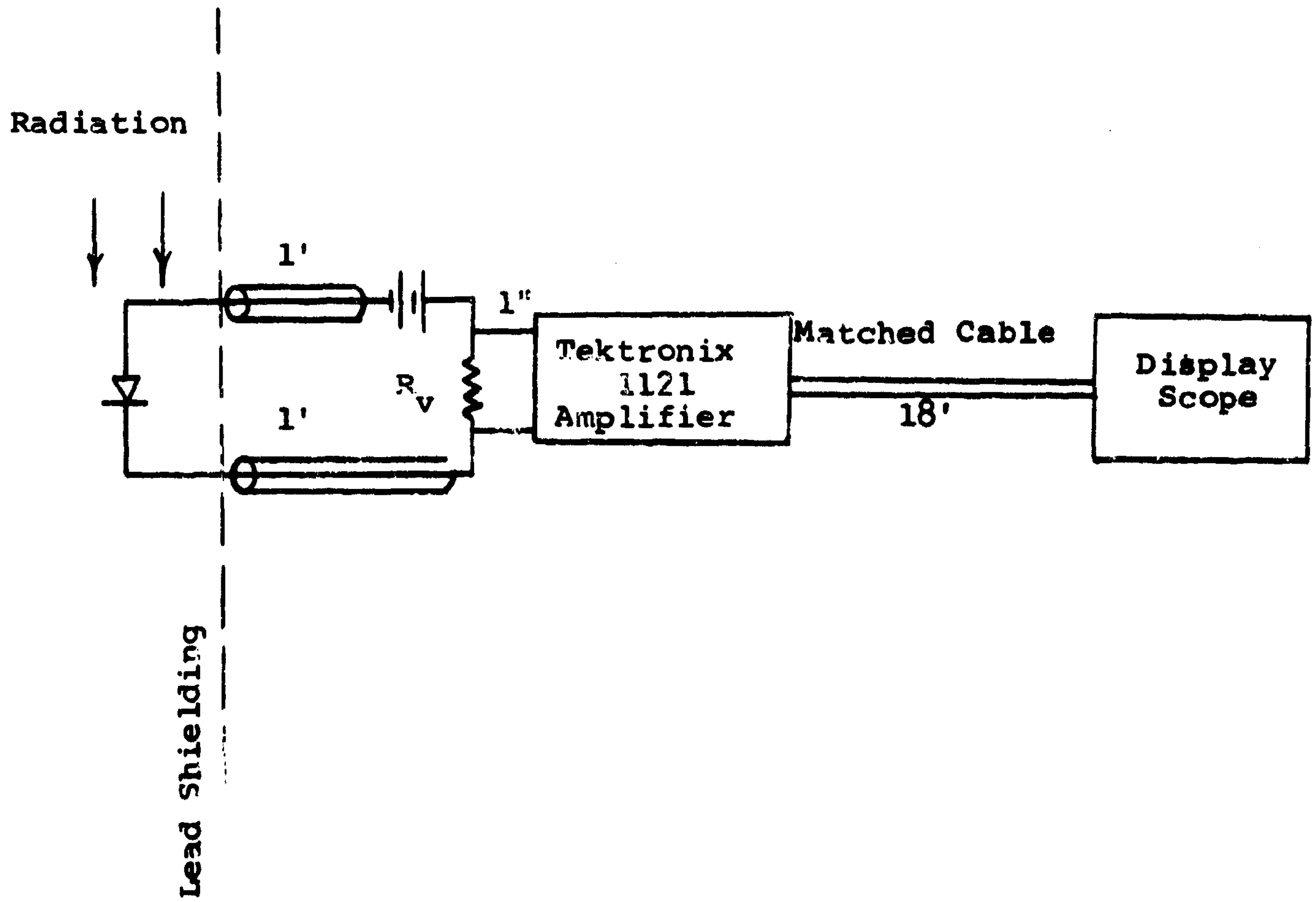

Figure 19. Final Circuitry for Testing of Diodes

Additional shielding of the power supply and the Tektronix 1121 amplifier was accomplished by using lead blocks and a lead sheet. Only the diode itself and less than 1 inch of the connecting leads were exposed to the direct radiation.

An additional check of the test circuitry was made under radiation conditions by comparing the results obtained from the irradiated diode with the results obtained from the same diode after it had been lowered 1 inch out of the direct radiation beam. In all cases the transient radiation effects upon the lowered diode were either undetectable or negligible in comparison with the effects observed on the diode in the radiation beam. It was concluded that all results by the irradiated diodes can be attributed only to the diode and its short leads exposed to radiation. Pickup elsewhere in the circuit directly or indirectly caused by the radiation pulse is therefore considered negligible.

c. Potting of Diodes

A commercial diode with a characteristic curve similar to the fabricated titanium dioxide diodes was irradiated under various environments. When it was irradiated at atmospheric pressure without any potting, a maximum transient current excursion of .010 ma was observed. The same diode in a partial vacuum (10 microns) had a maximum excursion of .008 ma. When encased in resin epoxy (3/4 inch diameter cylinder) the maximum excursion was reduced to .004 ma (see Figure 20). It is believed that this variation in results is caused by ionization around the diode leads providing a secondary path for current around the diode during the radiation burst.

Some potting material was used in fabricating the titanium dioxide diodes and could not be removed without structurally damaging the diode. It, therefore, appeared invalid to compare a partially potted titanium dioxide diode with commercially unpotted diodes. It was determined best to "pot" all diodes in an identical 3/4 inch cylinder of potting epoxy. In this manner a valid comparison could be achieved and at the same time ionization effects of all samples would be reduced under similar environments.

d. Noise Levels

The Tektronix oscilloscopes used to display the transient current have a variable gain control for the vertical or current axis. By changing the gain it is possible to determine a noise level for each sample and circuit combination. The noise level observed on the oscilloscopes is a subject presently being investigated at the TREES laboratory; however, investigation and analysis so far have not revealed any way of reducing the noise level with the present electronic equipment, screen room, and flash X-ray machine.

The noise level, therefore, is an inherent limitation of the flash X-ray system and its instrumentation. Experimental results otherwise obtainable are obscured by noise if the magnitude of the results is at or below the noise level.

e. The Radiation Pulse

The shape of the radiation pulse can be measured and recorded on an oscilloscope having a Polaroid camera attachment. The shape may vary from pulse to pulse and may be adjusted to some extent by changing various machine parameters prior to pulsing the X-ray machine. Although the radiation pulse is not a square wave in form, its concentrated form and short time duration make the approximation of a square wave for computation purposes a reasonable one.

f. Irradiation of Diode Samples

Irradiation of a commercial diode (1N459) produced the transient current pulse shown in Figure 20-c. The maximum transient current value is .004 ma. The time required for the diode to return to steady state conditions is of the order of 5 microseconds. Maximum amplitude was achieved at 1 microsecond. The reason for the continued rise of the transient current after the pulse duration is not clear.

Since the above diode has a characteristic curve which matches that of the fabricated titanium dioxide diode, it was expected that results obtained by irradiating the titanium dioxide would be comparable to those obtained above.

With the same scope settings, circuitry, bias, etc. the

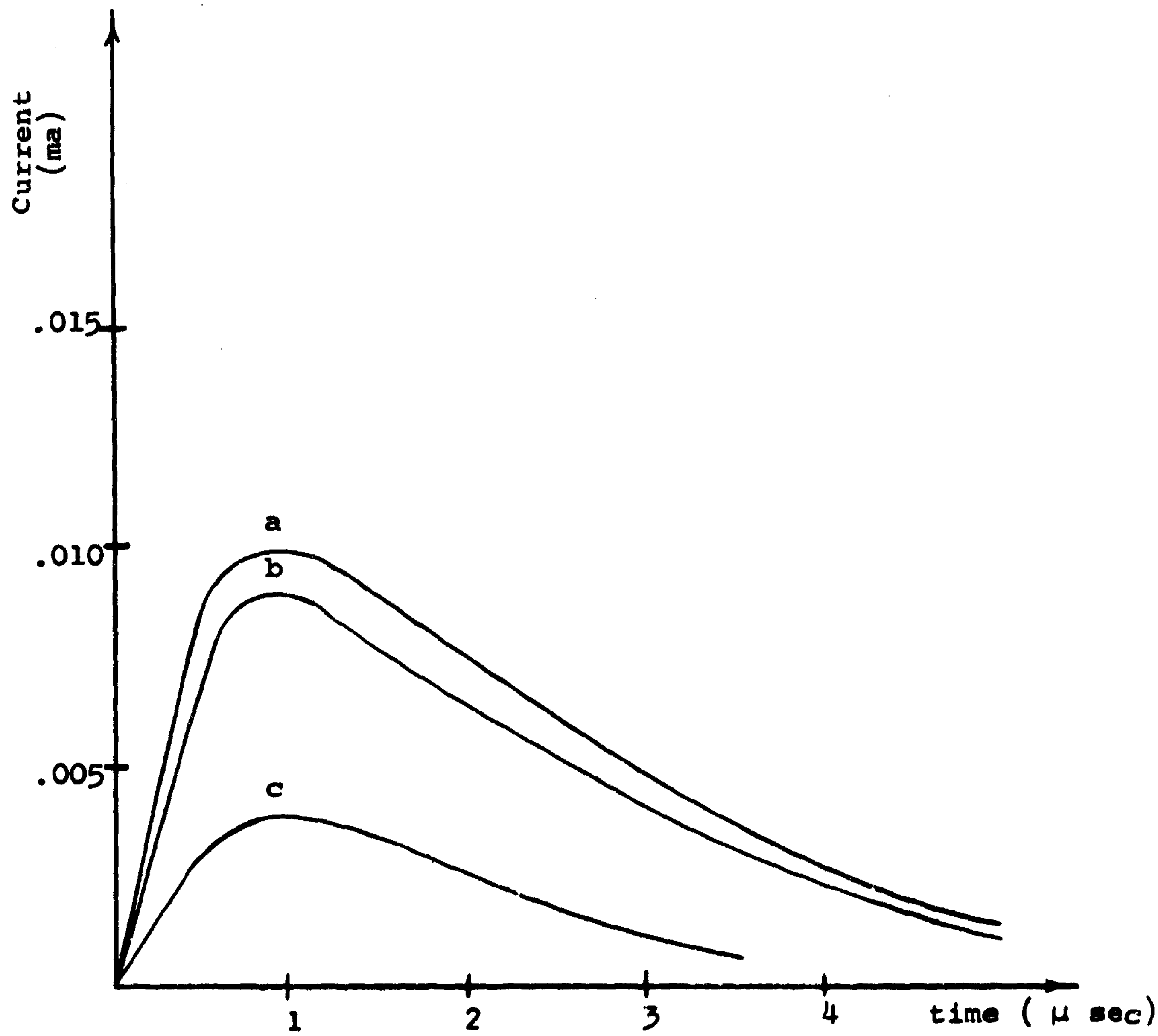

Figure 20. Commercial Diode (1N459) Transient Current (a-unpotted. b-in partial vacuum. c-potted in resin epoxy)

titanium dioxide diode was irradiated. No noticeable transient current was recorded. The gain was increased to the maximum allowable by the existing noise level. Irradiation at this setting again produced no detectable transient current. At no time did any of the noise oscillations exceed a value of .001 ma. Repeated irradiations had no apparent effect on the diodes, and results were consistently repeated.

To further substantiate the test circuitry and test comparison, it was decided to irradiate a variety of commonly used commercial diodes. The results of these tests are shown in Figures 21 through 23.

5. Conclusions and Recommendations

Irradiation of titanium dioxide diodes and other commercial diodes at the flash X-ray facility, Air Force Weapons Laboratory, revealed the following:

1) No permanent or semi-permanent effects were observed in any of the diodes tested. The components responded identically to successive bursts, and no change in the electrical characteristics was found subsequent to the irradiation.

2) Titanium dioxide diodes, when exposed to pulsed gamma radiation of .2 microsecond duration and an average dose rate of $.45 \times 10^{-8}$ erg/cm^2-sec., produced a transient current which was less than the noise level of the test circuitry and not detectable by the equipment used. At no time did the transient current and noise current combination exceed .001 ma. Other commercial diodes showed current excursions between .0025 and .625 ma for the same 400 KV radiation pulse.

3) If the electrical properties of titanium dioxide diodes can be improved through further development and the use of thinner films, it appears that these diodes will give a highly radiation resistant diode. It has been proven that the titanium dioxide diodes are much more resistant to radiation both of the transient and permanent damage type than similar germanium or silicon diodes.

4) It is recommended that the titanium dioxide diodes be further investigated under higher radiation intensities to

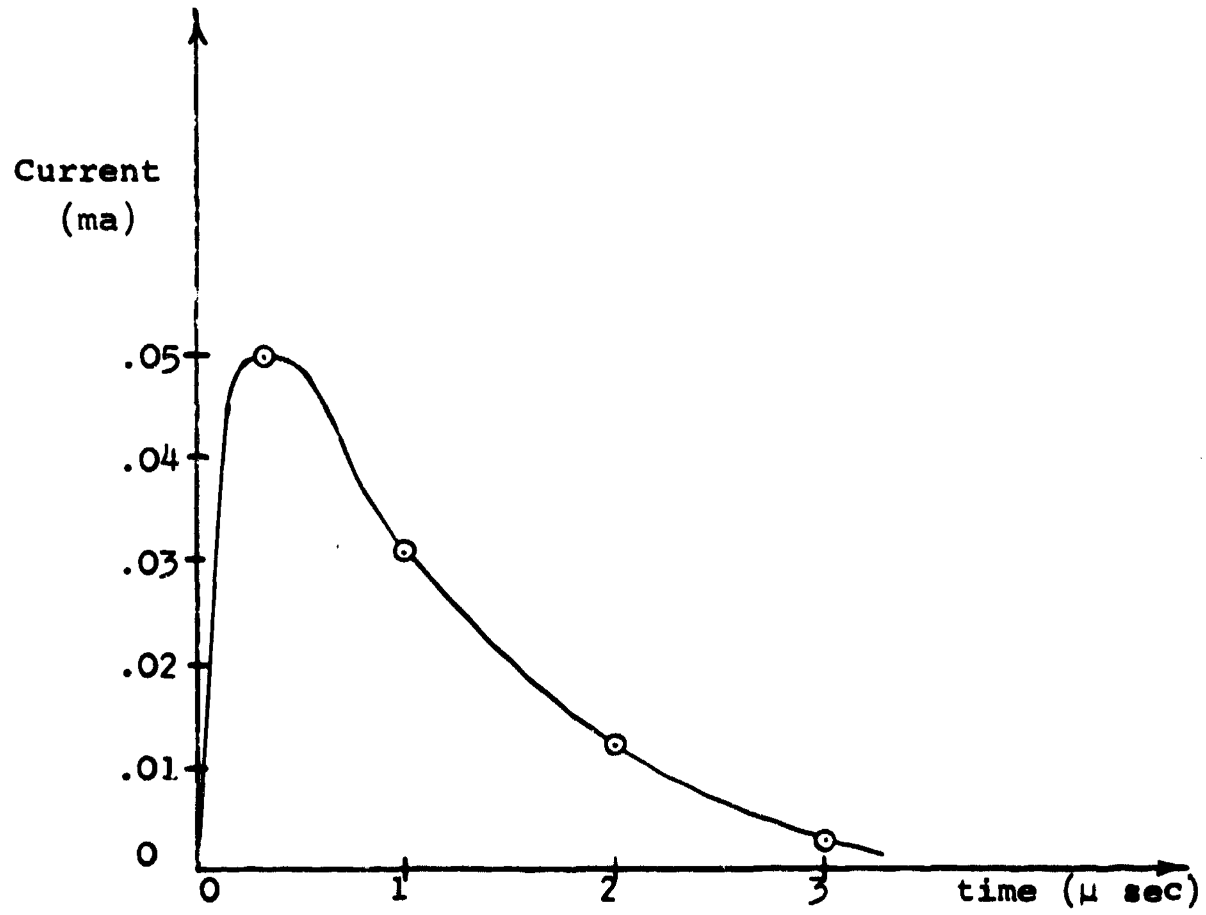

Figure 21. Transient Current Pulse 1N639 Diode

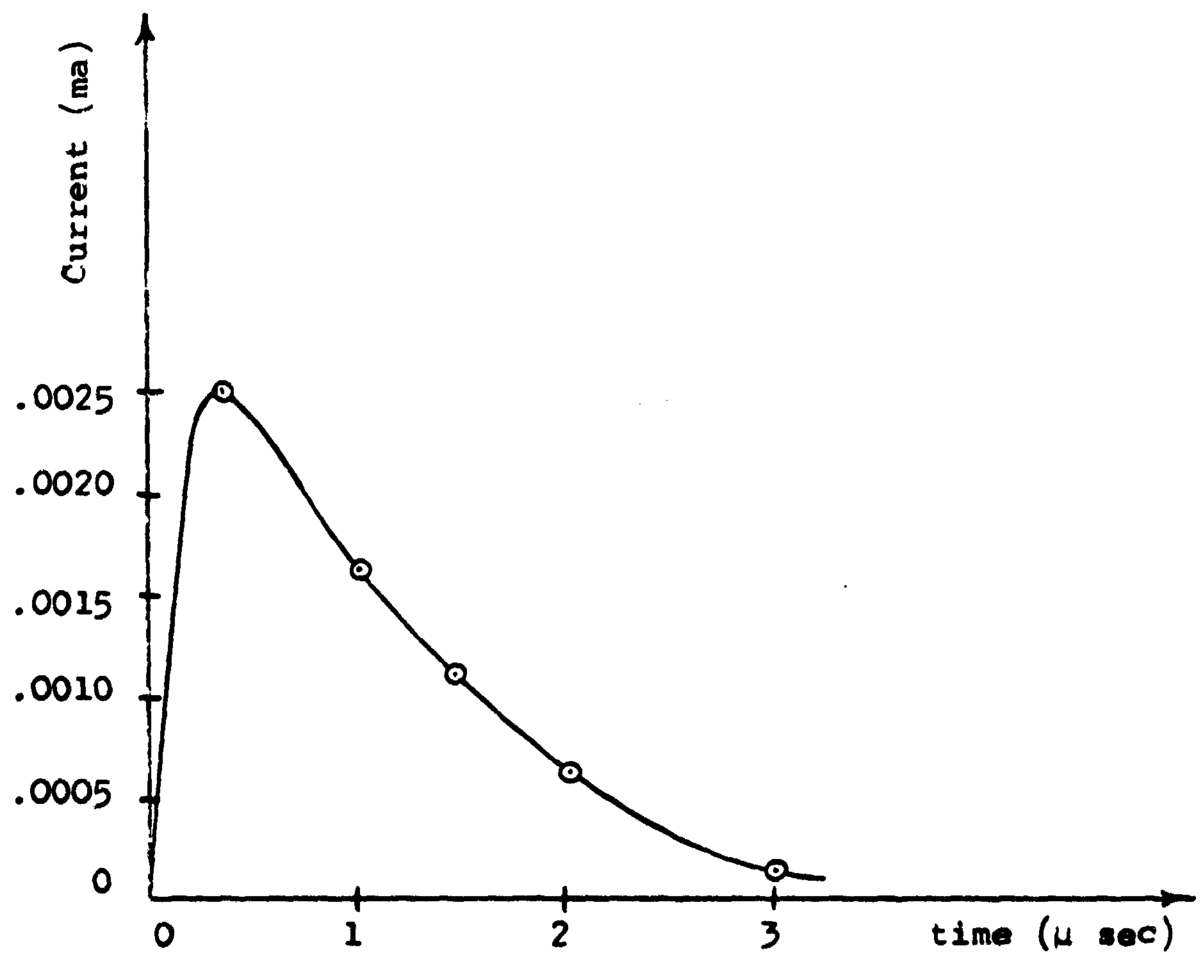

Figure 22. Transient Current Pulse Fairchild 300 Diode

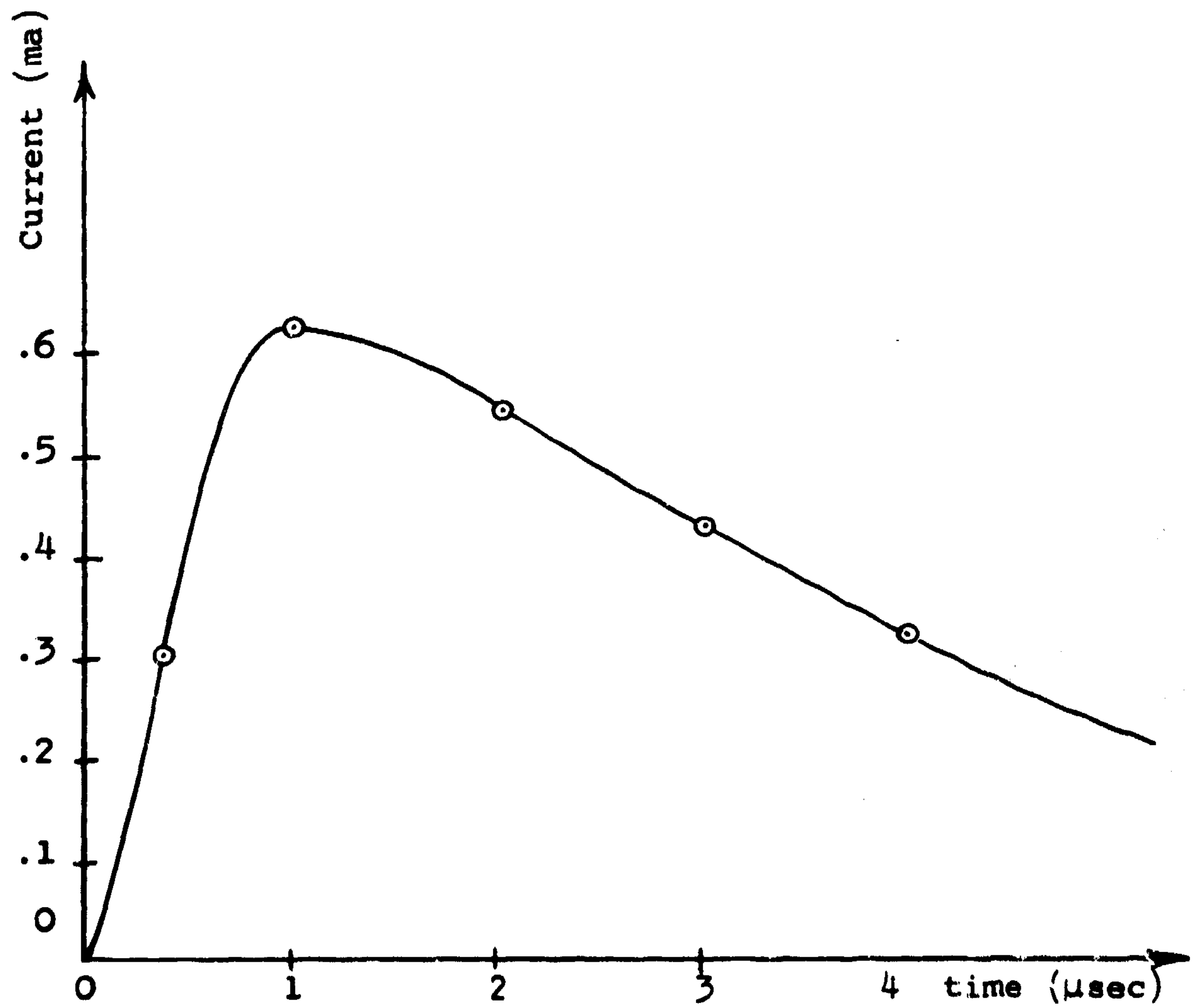

Figure 23. Transient Current Pulse 1N315 Diode

determine accurately the shape and extent of the transient current resulting from pulsed radiation. Further development for the improvement of the electrical characteristics of titanium dioxide diodes is also recommended.

This page intentionally left blank.

SECTION IV

MEASUREMENT OF THE CONTINUOUS SPECTRUM OF A FLASH X-RAY MACHINE

By Harold Southward

1. Introduction

A complete discussion of the technique used to measure the continuous spectrum of a flash X-ray machine is given in AFWL TDR-64-36, June, 1964, by H. D. Southward. The use of a curve of transmitted X-ray intensity versus attenuator thickness to calculate the spectrum of continuous X-rays was reported by L. Silberstein. Silberstein's experimental method consisted of measuring the intensity of a well-collimated beam of X-rays transmitted through various thicknesses of metal scattering material. Photographic film was used as the radiation detector. The transmission curve was fitted to an empirical formula, and the spectrum was calculated from a process which basically involved the inversion of a Laplace transformation. (Reference 22).

It is important to consider the following points when Silberstein's method is used: (1) The response of the radiation detector as a function of photon energy should be known; (2) The response of the radiation detector should be linear with the incident X-ray intensity for a given spectral distribution (i.e., it should not be dose rate dependent); (3) The absorption coefficient μ of the scattering material, which is a function of photon energy E, should be accurately known along with its derivative $d\mu/dE$; (4) An idealized geometry should be approximated so that only single scattering occurs within the scattering material; (5) Background radiation which arises principally from scattering of X-rays off the floor, ceiling, walls and surrounding objects should be avoided; (6) And finally, an empirical formula must be found which will fit the experimental data.

The method described herein uses a scintillation detector to measure the intensity of the X-ray beam transmitted through the scattering material, thereby eliminating the objections which tend to arise when film is used.

2. The Apparatus and Basic Data

Figure 24 shows a block diagram of the equipment used to obtain the transmission data. The detector consisted of a 2" x 2" NaI(Tℓ) Harshaw crystal mounted on a 2" type 114 ITT photodiode. The photodiode was chosen because of its relative insensitivity to variations in high voltage and because of its wide range of linearity. The signal and its time integral were recorded from an oscilloscope with a Polaroid camera. Figure 25 shows some typical data. The NaI(Tℓ) crystal did not follow the shape of the burst of X-rays because its 0.25 microsecond time constant was nearly the same as the 0.2 microsecond duration of the radiation. However, the NaI(Tℓ) crystal has the advantage of a higher sensitivity.

The X-ray machine output was monitored with detection apparatus similar to that shown in Figure 24 except that a Pilot "B" scintillator was used. A signal and its time integral are shown in Figure 26. The transmission data were normalized to the output of the monitor in order to correct for small variations of the output of the flash X-ray machine. The shape of the monitor signal was also helpful in determining whether the flash X-ray machine malfunctioned when it was fired, and formed a good basis for rejection of data. Typical transmission data are shown in Figures 27 and 28 along with their empirical curves for the X-ray machine operating at 400 and 500 kilovolts respectively. The data are represented by points and the empirical curve fitted to the data is represented by the smooth curve.

3. System Linearity

A simple function which approximates the shape of the Flash X-ray machine output is shown in Figure 29. If it is assumed that the radiation detecting system is a linear system,

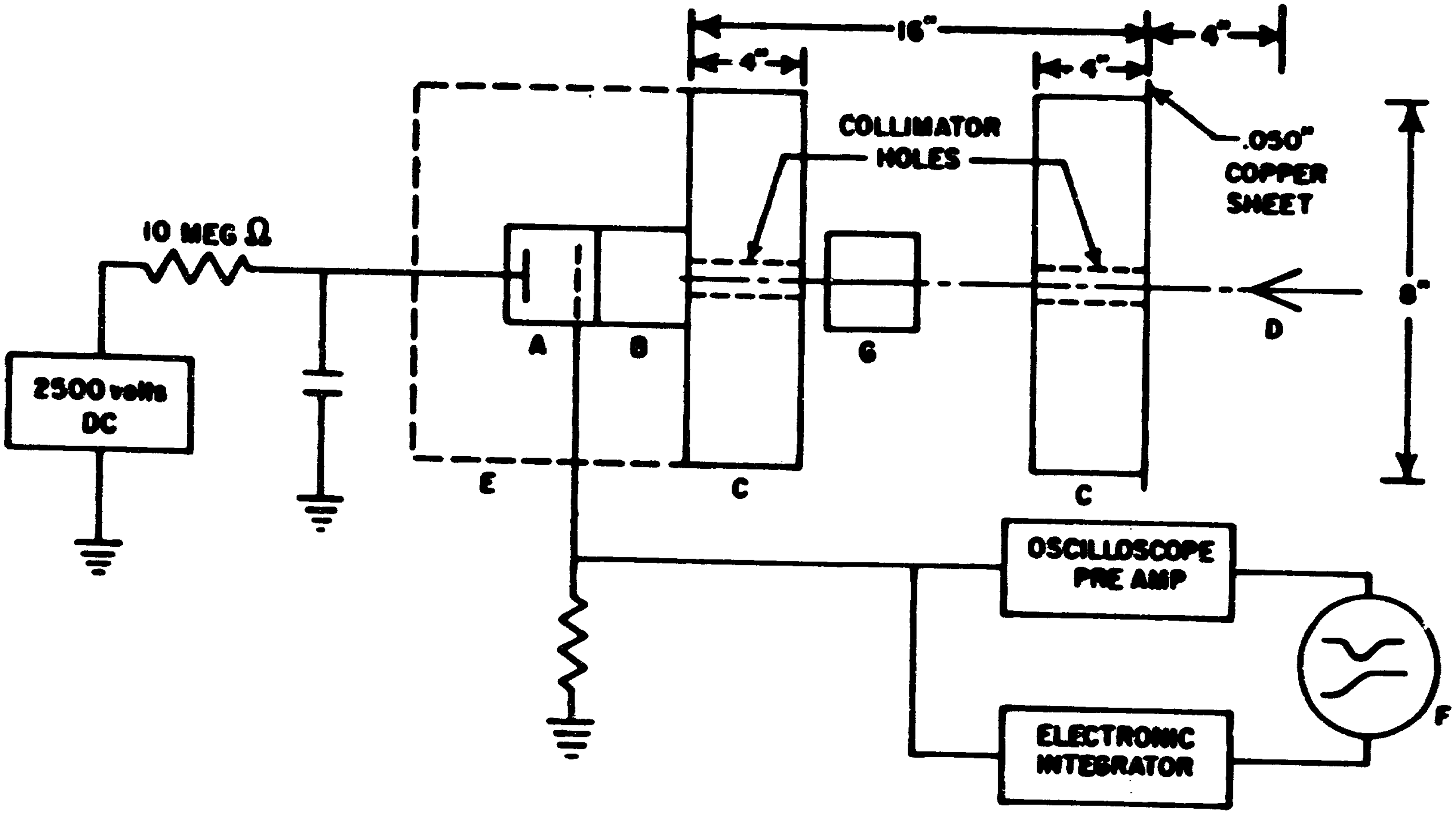

Figure 24. Schematic of Equipment Used in Obtaining Transmission Data With Flash X-Ray Pulses. (A) Type-114 Photodiode, (B) Harshaw 2" x 2" Cylindrical NaI(Tℓ) Crystal, (C) Brass Collimators, (D) X-Ray Target, (E) Lead Shield for Detector, (F) Tektronix Type-551 Oscilloscope, (G) Scattering Material

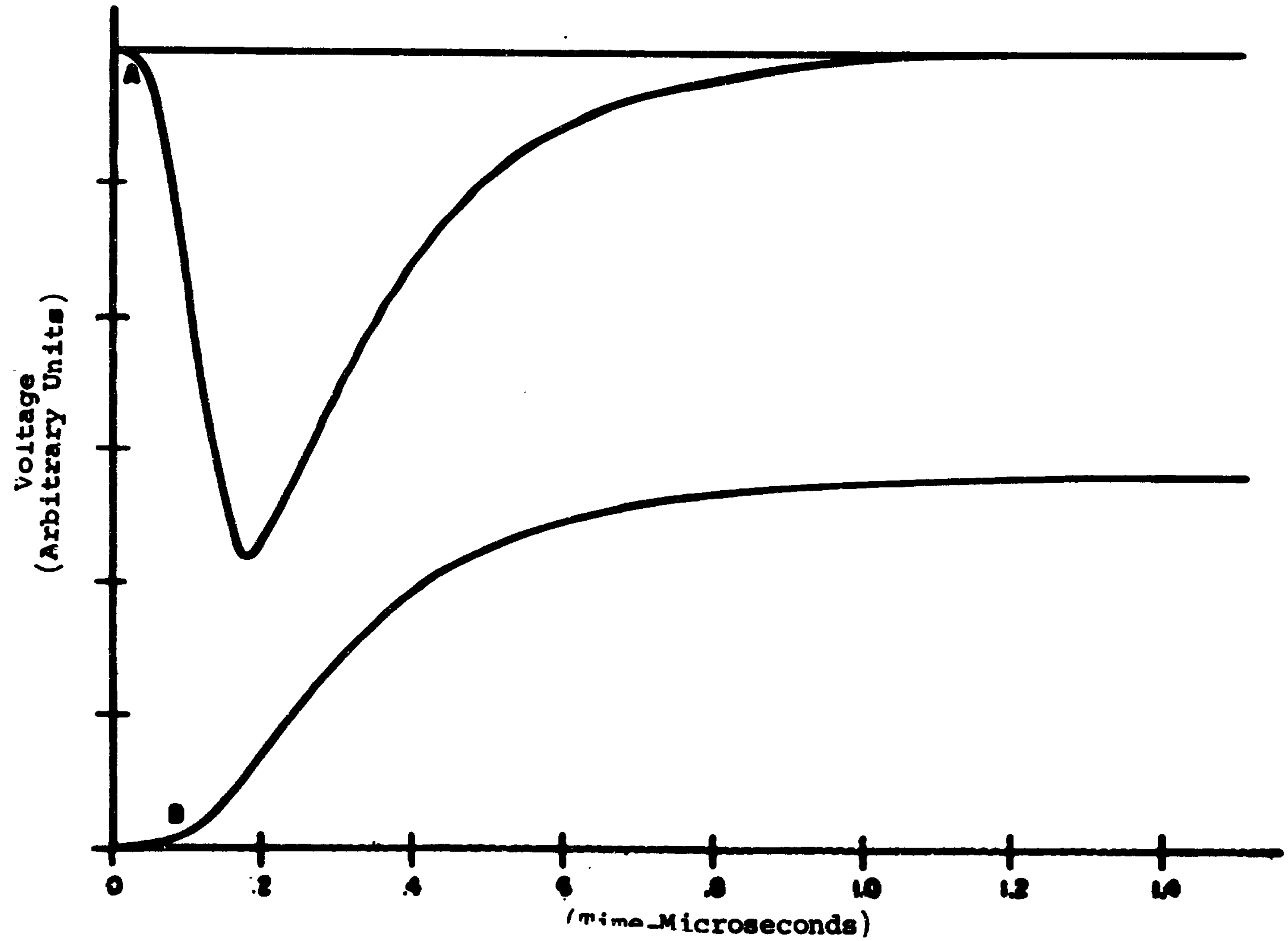

Figure 25. Representative Data Used in Determining the X-Ray Transmission Curves.
A. Upper Trace: Response of the NaI(Tl) Crystal to a Flash X-Ray Pulse.
B. Lower Trace: Time Integral of the Upper Trace

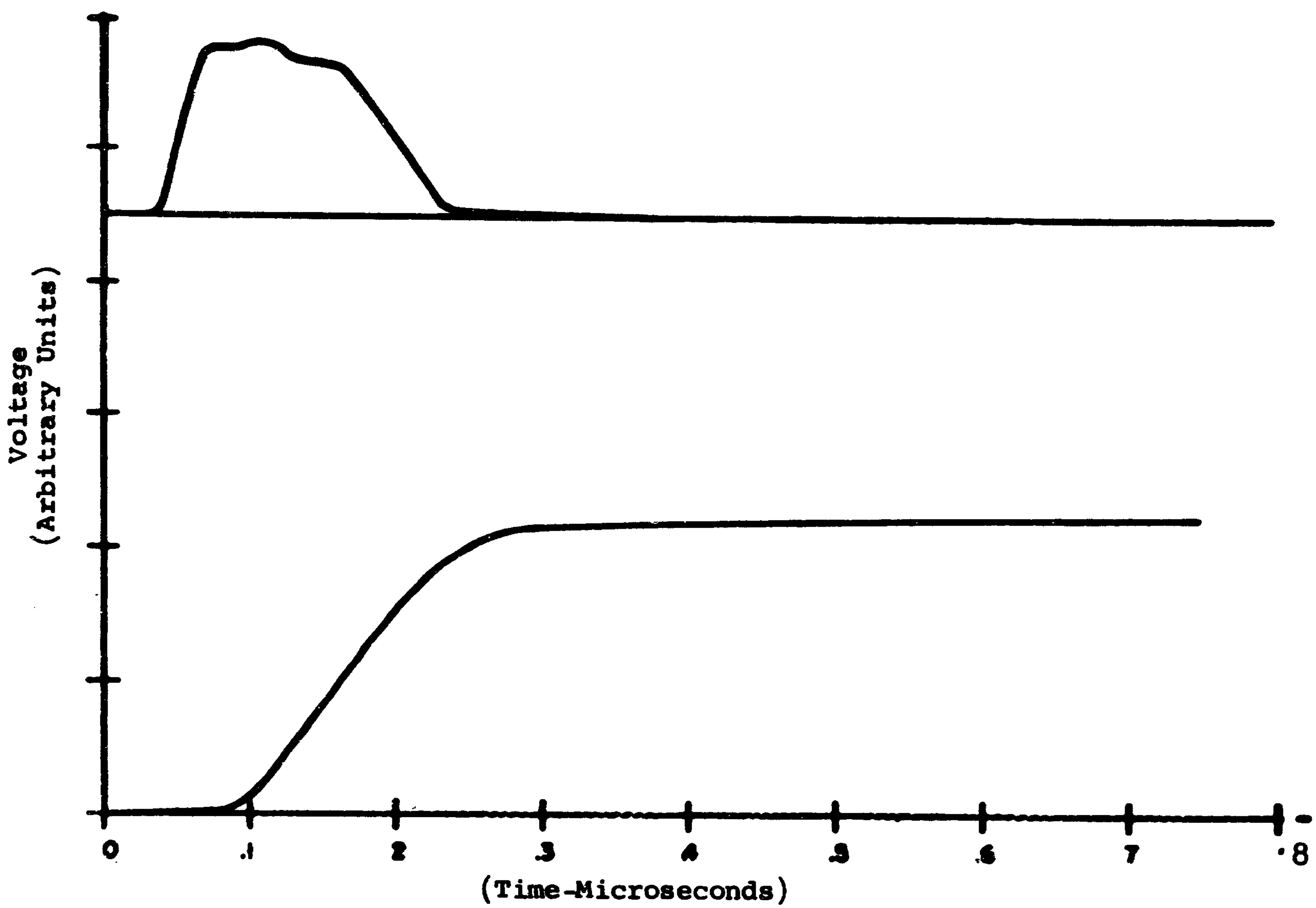

Figure 26. Representative Data Used for Monitoring the Output of the X-Ray Machine.
Upper Trace: Response of a Pilot "B" Plastic Scintillator to the Same Flash X-Ray Pulse as in Figure 25. This Response Follows the X-Ray Pulse Very Closely
Lower Trace: Time Integral of the Upper Trace

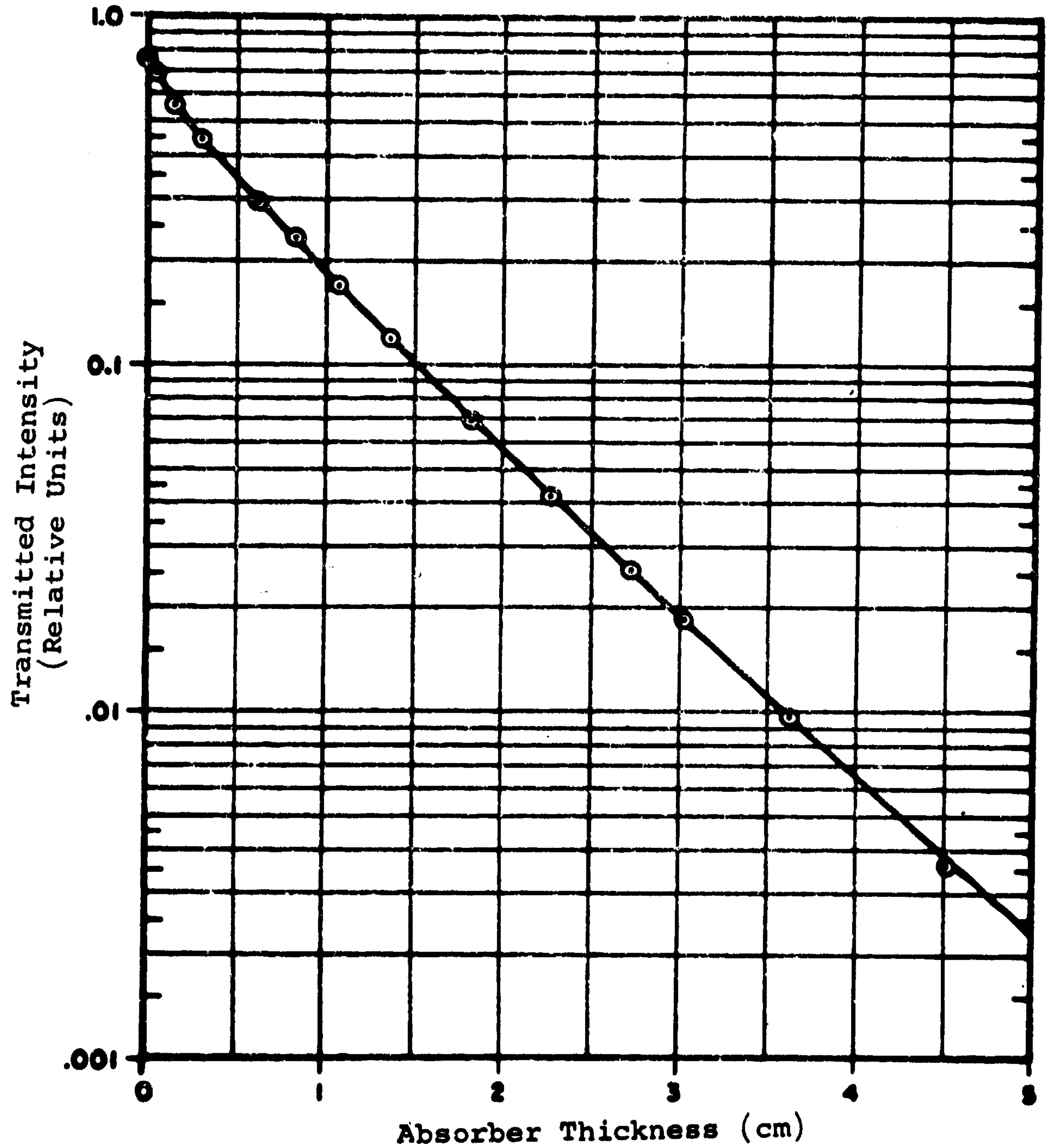

Figure 27. Transmitted Intensity of X-Rays Produced by a Flash X-Ray Machine at a Tube Potential of 400 kev

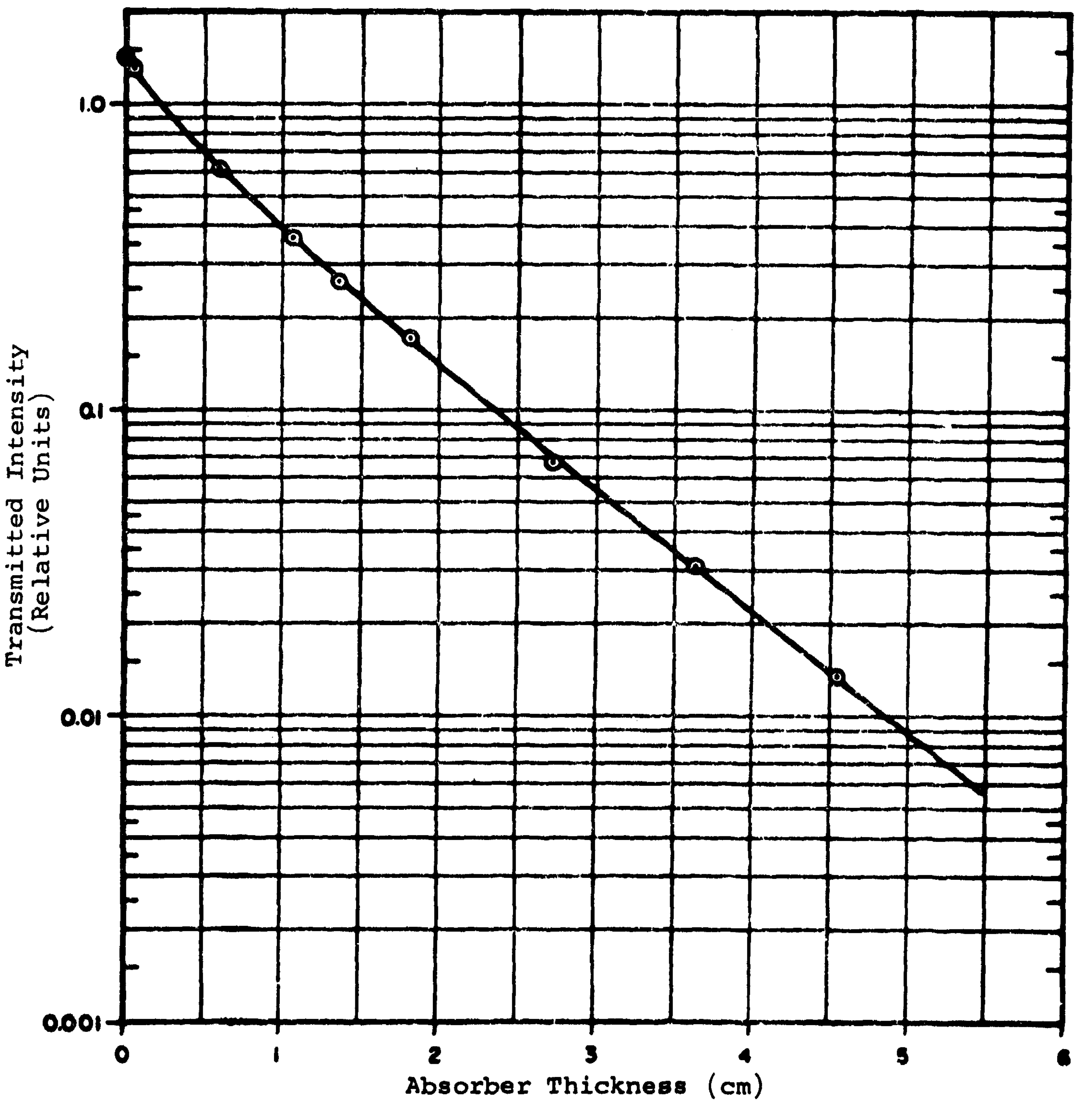

Figure 28. Transmitted Intensity of X-Rays Produced by a Flash X-Ray Machine at a Tube Potential of 500 kev

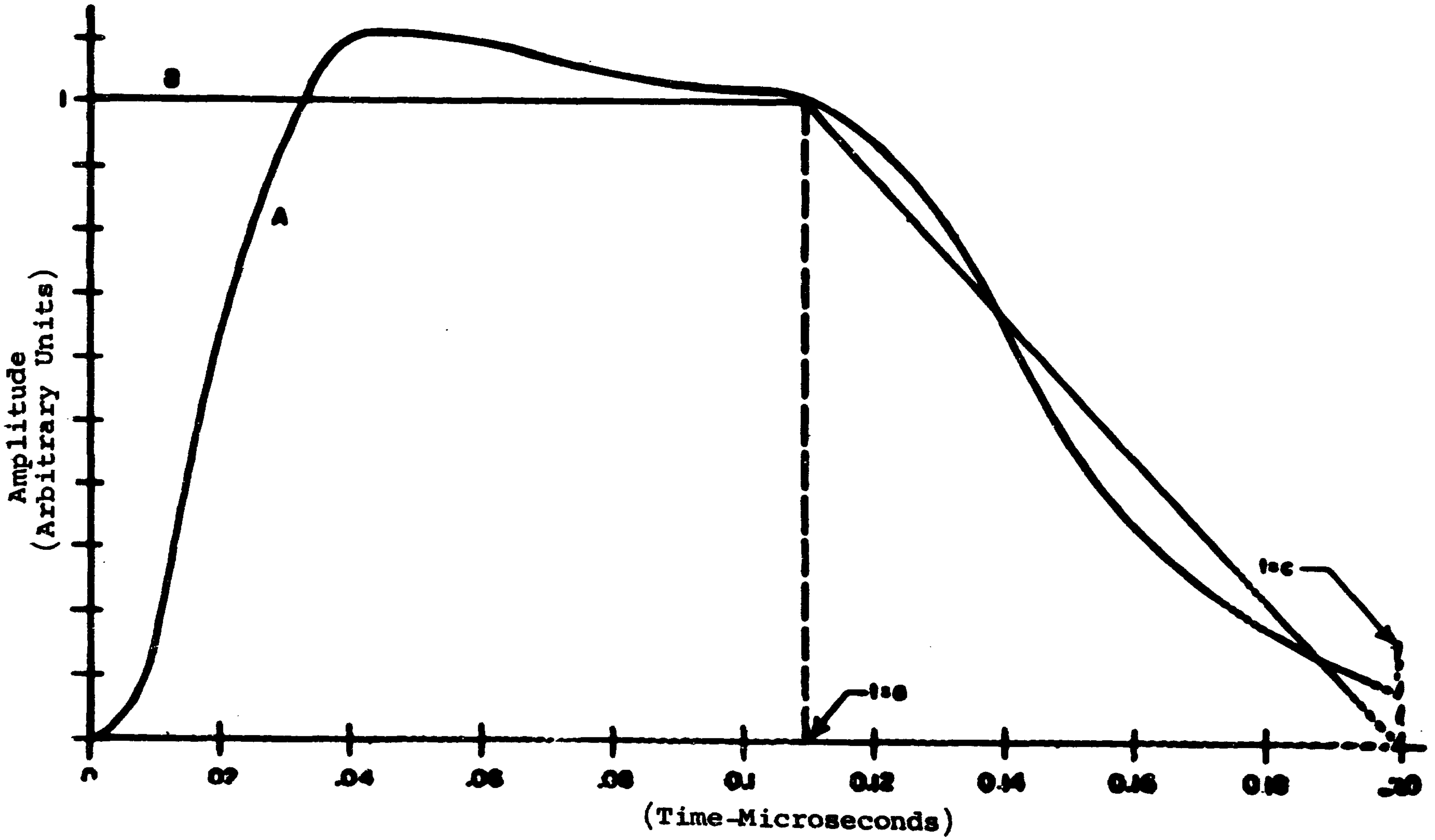

Figure 29. Approximation of a Typical X-Ray Pulse

The Output of the Flash X-Ray Unit as Measured by a Pilot "B" Scintillator on a Type-114 Photodiode. Line A is the Experimental Response. Line B is an Approximation to the Actual Response.

the response of this system to an idealized pulse is

$$R(t) = K \int_0^t F(\tau) e^{-\beta(t - \tau)} \, d\tau \qquad (105)$$

Here R(t) is the system response, K is the proportionality factor, $F(\tau)$ is the idealized input, and β is the time constant of the NaI(Tl) crystal. Figure 30 shows a comparison of the experimental response of the NaI crystal detector system with the theoretical response. One may conclude from this close agreement that the radiation detector system is linear. Strictly speaking, this conclusion is not completely true. However, the same results can be obtained only if the two measuring systems used contained the same nonlinearities. This is very unlikely due to the vast difference in the characteristics of the radiation detectors.

4. Calculation of the X-Ray Spectrum

Various techniques for calculating the X-ray spectrum from transmission data have been published (References 22, 23, 26 and 27). They all follow the general procedure given by Silberstein. The basic data form a transmission curve I (x), which is obtained experimentally by measuring the integrated intensity of the X-ray beam after it has passed through x cm. of copper. This curve was fitted to an empirical formula and the spectrum was calculated from a process which involved the inversion of a Laplace transformation. The following treatment is due to Greening (Reference 26):

$$I(x) = I_o e^{-Ax - B(\sqrt{x + d} - \sqrt{d})} \qquad (106)$$

Here A, B, and d are constants and I_o is the incident intensity of an X-ray beam upon the absorber. If $F(\lambda)$ is the intensity distribution of the X-ray beam per unit wavelength λ, then the transmitted intensity I(x) through a material having absorption

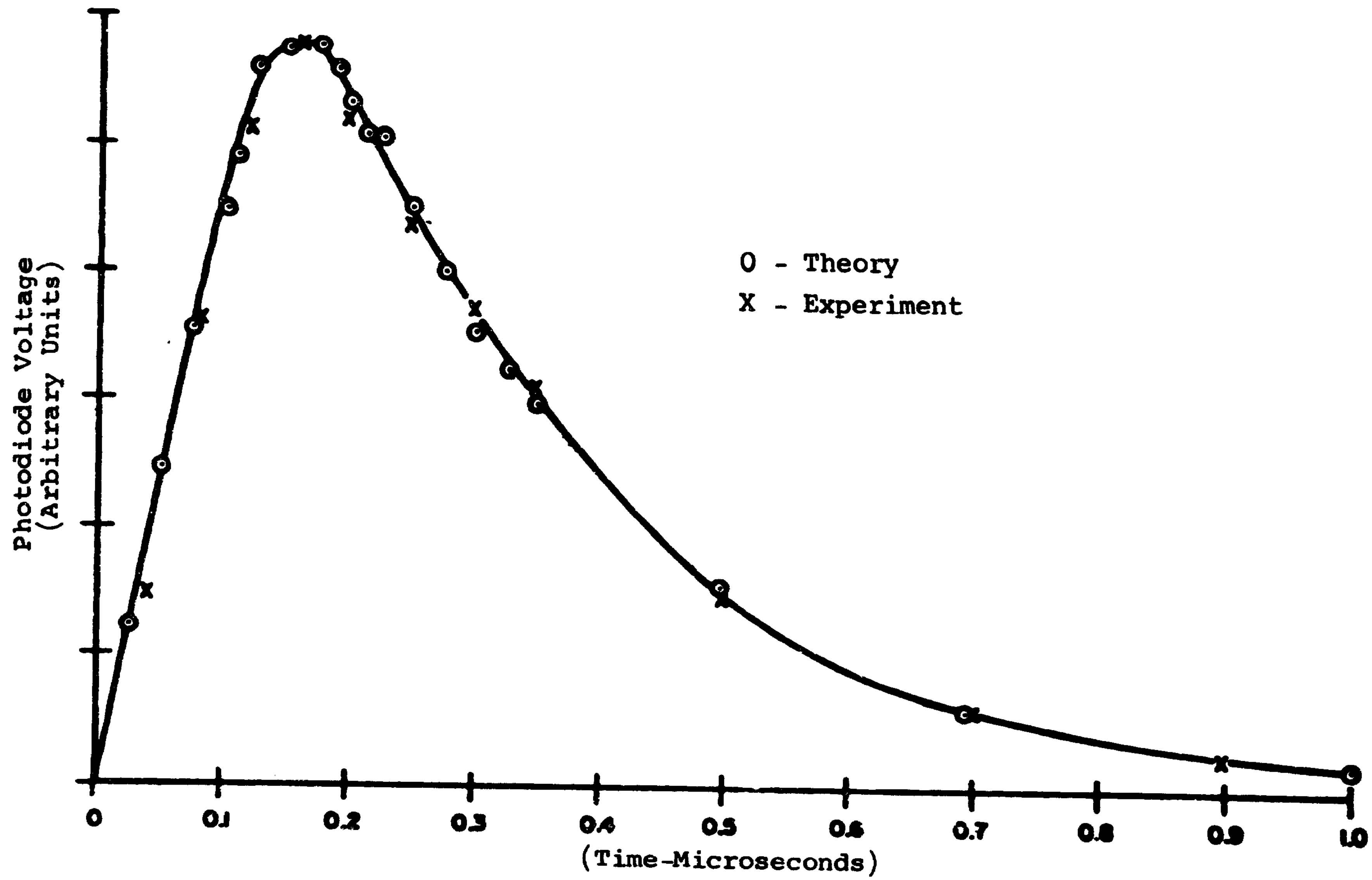

Figure 30. Comparison of the Experimental Response of an NaI(Tl) Crystal with its Theoretical Response. The Calculation is Based Upon the Idealized X-Ray Pulse Shown in Figure 29.

coefficients $\mu(x)$ is

$$I(x) = \int_{\lambda min}^{\infty} F(\lambda)e^{-\mu(\lambda)x}dx. \tag{107}$$

Here

$$\int_{\lambda min}^{\infty} F(\lambda)d\lambda = I_o \tag{108}$$

The minimum wavelength is determined by the relation

$$\lambda_{min} = \frac{hc}{E_{max}} \tag{109}$$

where h is Planck's constant, c is the velocity of light and E_{max} is the maximum photon energy in the X-ray spectrum. It is more convenient to use photon energies in calculations. By defining

$$\begin{aligned} \mu' &= \mu - \mu\ (\lambda_{min}) \\ &= \mu - A \end{aligned} \tag{110}$$

it can be shown that the validity of equation (110) by examining equation equation (106). If it is assumed that the absorption coefficient $\mu(E)$ is a monotone decreasing function of the photon energy E, then for large x, $I(x) \propto e^{-Ax}$. Hence, A can be found from a table of $\mu(E)$ if E_{max} is known.

Now one considers

$$\mu' = \mu'(\lambda) \tag{111}$$

It is possible to consider the intensity distribution as a distribution in μ', $\varphi(\mu')$.

$$f(\lambda)d\lambda = \varphi(\mu')\ d\mu' \tag{112}$$

Equation (107) then becomes

$$I(x) = \int_0^\infty e^{-\mu' x}\varphi(\mu')d\mu' \qquad (113)$$

which is a Laplace transformation. By using equation (105) for I(x) and inverting equation (113) it can be shown that the intensity distribution of the X-ray beam per unit photon energy is

$$\epsilon(E)I(E) = \frac{Be^{Ad + B\sqrt{d}}}{2\sqrt{\pi}} \cdot \frac{e^{-\frac{B^2}{4(\mu - A)}}}{(\mu - A)^{3/2}} e^{-\mu d} \frac{d\mu}{dE} . \qquad (114)$$

Here I(E) is taken as a relative distribution and $\epsilon(E)$ is the energy absorption efficiency of the detector used to measure I(x). The energy absorption efficiency of NaI crystal is shown in Figure (31), and is defined as the ratio of the photon energy absorbed in the crystal to the incident photon energy. This calculation was performed at Argonne National Laboratory using a Monte Carlo technique for a 1/4" diameter collimated beam of X-rays hitting the end face of a 2" x 2" cylindrical sodium iodide crystal (Reference 28).

A table of the mass absorption coefficient of copper and its derivative as a function of photon energy is given in Table IV. These values were derived from those given by Grodstein (Reference 29) using a formula of the form

$$\text{Log}_e\ \sigma(E) = A_o + \sum_{i=1}^{8} A_i E^i . \qquad (115)$$

It is necessary to evaluate the constants B and d in equation (114). This is equivalent to fitting the transmission data to equation (105). This may be done very simply by the method of Greening (Reference 26), by defining

$$y = -\left[\log_e \frac{I(x)}{I_o}\right] - Ax \qquad (116)$$

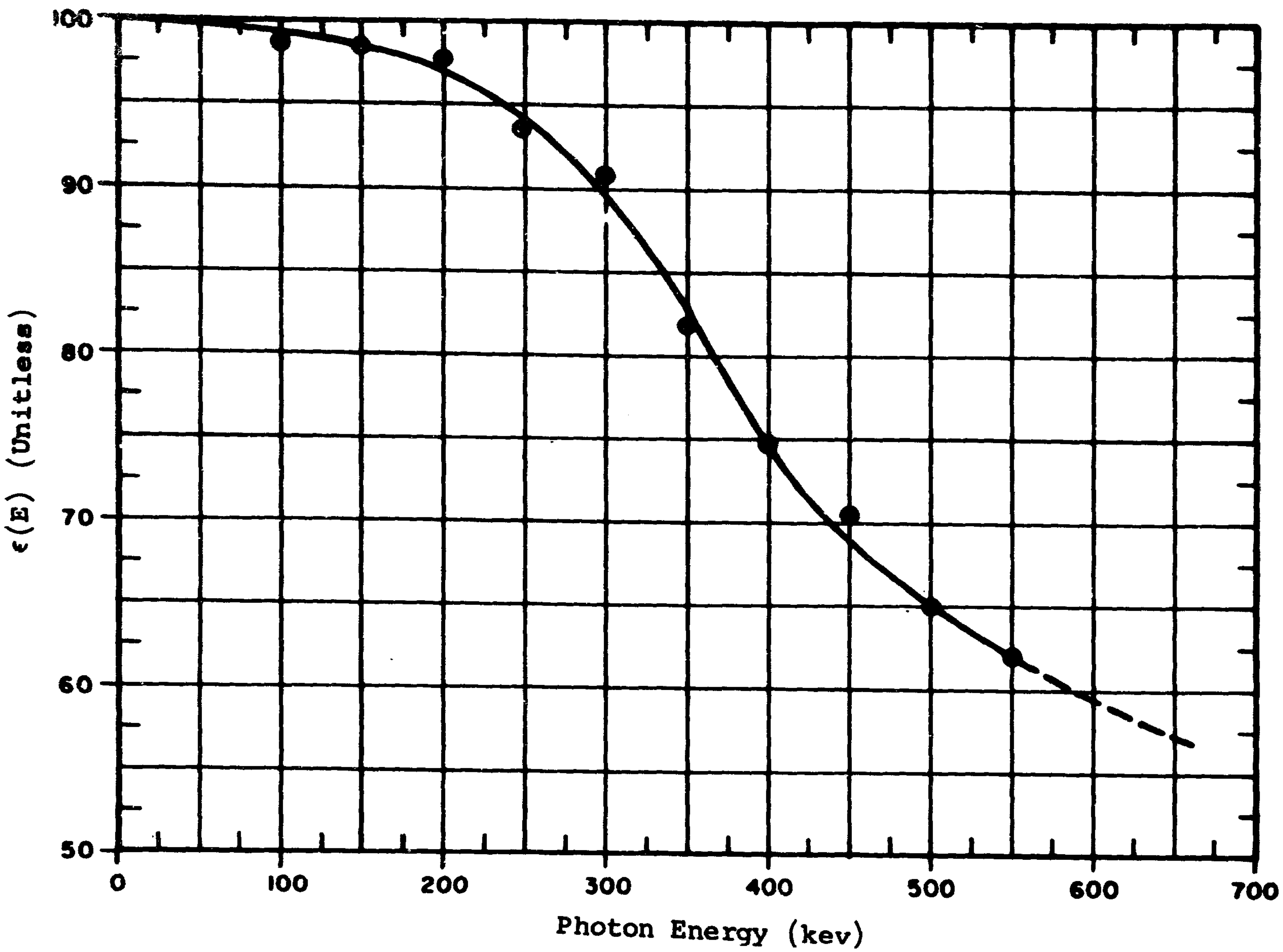

Figure 31. Energy Absorption Efficiency of a 2-Inch Diameter by 2-Inch Long NaI(Tℓ) Crystal for a 1/4 Inch Collimated Beam of X-Rays Incident Normal to a Circular Fact at the Center

Table IV Mass Absorption Coefficient, σ, and its Derivative $\frac{d\sigma}{dE}$ as a Function of Photon Energy, E, for Copper[2]

E(mev)	$\sigma(E)$ $\frac{cm^2}{gm}$	$\sigma(E)$ $\frac{cm^2}{gm}$ (from Ref. 29)	$\frac{d\sigma}{dE}$ $(\frac{cm^2}{gm\text{-}mev})$
.01500	76.37	76.8	19030
.02000	34.86	34.6	5772
.02500	18.64		2379
.03000	11.07	11.1	1154
.03500	7.101		623.5
.04000	4.837	4.83	364.4
.04500	3.457		226.5
.05000	2.572	2.56	147.9
.05500	1.978		100.7
.06000	1.565	1.58	70.93
.06500	1.269		51.49
.07000	1.051		38.35
.07500	0.8856		29.21
.08000	0.7585	0.762	22.69
.08500	0.6588		17.93
.09000	0.5792		14.39
.09500	0.5149		11.71
.10000	0.4622	0.461	9.642
.10500	0.4185		8.031
.11000	0.3819		6.756
.11500	0.3509		5.735
.12000	0.3245		4.910
.12500	0.3018		4.234
.13000	0.2822	(continued)	3.678

[2] These data have been calculated from a close fit of the data in Reference 29. Note that the data are questionable in the third significant figure. $\frac{d\sigma}{dE}$ is less accurate than $\sigma(E)$.

Table IV (cont'd)

E (mev)	$\sigma(E)\ \frac{cm^2}{gm}$	$\sigma(E)\ \frac{cm^2}{gm}$ (from Ref. 29)	$\frac{d\sigma}{dE}\ (\frac{cm^2}{gm\text{-}mev})$
.1350	0.2650		3.215
.1400	0.2500		2.826
.1450	0.2368		2.498
.1500	0.2250	0.222	2.220
.1550	0.2146		1.981
.1600	0.2052		1.776
.1650	0.1968		1.599
.1700	0.1892		1.445
.1750	0.1824		1.310
.1800	0.1761		1.192
.1850	0.1704		1.088
.1900	0.1652		0.9964
.1950	0.1605		0.9148
.2000	0.1561	0.156	0.8422
.2050	0.1521		0.7773
.2100	0.1483		0.7192
.2150	0.1449		0.6669
.2200	0.1417		0.6198
.2250	0.1387		0.5773
.2300	0.1359		0.5388
.2350	0.1333		0.5038
.2400	0.1308		0.4720
.2450	0.1286		0.4430
.2500	0.1264		0.4165
.2550	0.1244		0.3923
.2600	0.1225		0.3701
.2650	0.1207		0.3496
.2700	0.1190		0.3309
.2750	0.1174		0.3136
.2800	0.1159	(continued)	0.2976

E (mev)	$\sigma(E)\ \frac{cm^2}{gm}$	$\sigma(E)\ \frac{cm^2}{gm}$ (from Ref. 29)	$\frac{d\sigma}{dE}\ (\frac{cm^2}{gm\text{-}mev})$
.2850	0.1144		0.2829
.2900	0.1130		0.2692
.2950	0.1117		0.2566
.3000	0.1105	0.112	0.2448
.3050	0.1093		0.2339
.3100	0.1081		0.2238
.3150	0.1070		0.2143
.3200	0.1060		0.2055
.3250	0.1050		0.1973
.3300	0.1040		0.1897
.3350	0.1031		0.1825
.3400	0.1022		0.1758
.3450	0.1013		0.1695
.3500	0.1005		0.1636
.3550	0.09968		0.1580
.3600	0.09890		0.1528
.3650	0.09815		0.1480
.3700	0.09742		0.1433
.3750	0.09672		0.1390
.3800	0.09603		0.1349
.3850	0.09537		0.1311
.3900	0.09472		0.1274
.3950	0.09410		0.1240
.4000	0.09348	0.094	0.1207
.4050	0.09289		0.1176
.4100	0.09231		0.1147
.4150	0.09174		0.1120
.4200	0.09119		0.1093
.4250	0.09065		0.1068
.4300	0.09012		0.1045
.4350	0.08960		0.1022

(continued)

Table IV (cont'd)

E (mev)	$\sigma(E)\ \frac{cm^2}{gm}$	$\sigma(E)\ \frac{cm^2}{gm}$ (from Ref. 29)	$\frac{d\sigma}{dE}\ (\frac{cm^2}{gm\text{-}Mev})$
.4400	0.08910		0.1001
.4450	0.08860		0.09802
.4500	0.08812		0.09608
.4550	0.08764		0.09422
.4600	0.08717		0.09245
.4650	0.08672		0.09075
.4700	0.08627		0.08913
.4750	0.08583		0.08759
.4800	0.08539		0.08610
.4850	0.08496		0.08468
.4900	0.08454		0.08332
.4950	0.08413		0.08201
.5000	0.08372	0.0834	0.08075
.5050	0.08332		0.07954
.5100	0.08293		0.07838
.5150	0.08254		0.07726
.5200	0.08216		0.07618
.5250	0.08178		0.07514
.5300	0.08141		0.07404
.5350	0.08104		0.07317
.5400	0.08067		0.07223
.5450	0.08031		0.07133
.5500	0.07996		0.07045
.5550	0.07961		0.06960
.5600	0.07926		0.06877
.5650	0.07892		0.06797
.5700	0.07858		0.06720
.5750	0.07825		0.06644
.5800	0.07792	(continued)	0.06571

Table IV (cont'd)

E (mev)	$\sigma(E)\ \frac{cm^2}{gm}$	$\sigma(E)\ \frac{cm^2}{gm}$ (from Ref. 29)	$\frac{d\sigma}{dE}\ (\frac{cm^2}{gm\text{-}mev})$
.5850	0.07759		0.06500
.5900	0.07727		0.06430
.5950	0.07695		0.06362
.6000	0.07663	0.0760	0.07695
.6050	0.		0.07663

A plot of x/y versus y should be a straight line if no characteristic radiation is present in the X-ray beam. In practice, flash X-ray irradiation studies are conducted in a room shielded from electromagnetic radiation. The radiation was filtered by a 50 mil window of copper which removed most of the characteristic radiation from the X-ray beam. It can be shown that

$$B = \left[\frac{d}{dy}\left(\frac{x}{y}\right)\right]^{-1/2} \tag{117}$$

and

$$d = \frac{c^2}{4\frac{d}{dy}\left(\frac{x}{y}\right)} \tag{118}$$

Here c is defined as the intercept of the straight line on the x/y axis.

A typical x/y plot is shown in Figure 32. The first set of values determined by this method is generally satisfactory. The time-integrated intensity distributions of a flash X-ray machine operating at 400 and 500 kilovolts charging voltage are shown in Figures 33 and 34.

5. General Discussion

The method described for obtaining flash X-ray spectra is limited to situations in which the shape of the X-ray pulse is closely reproducible from shot to shot. Experience has shown that the intensity distribution changes with the shape of the X-ray pulse in time as shown in Figure 26.

This method, employing essentially the same apparatus, was also used for measurements on a high intensity continuous X-ray machine and found to be satisfactory.

In the inversion of equation (113) it is assumed that $\mu'(\lambda)$ is a single valued function of λ, the wavelength, so that the derived spectrum is unique. A study of a table of absorption coefficients for the various elements shows that this method is

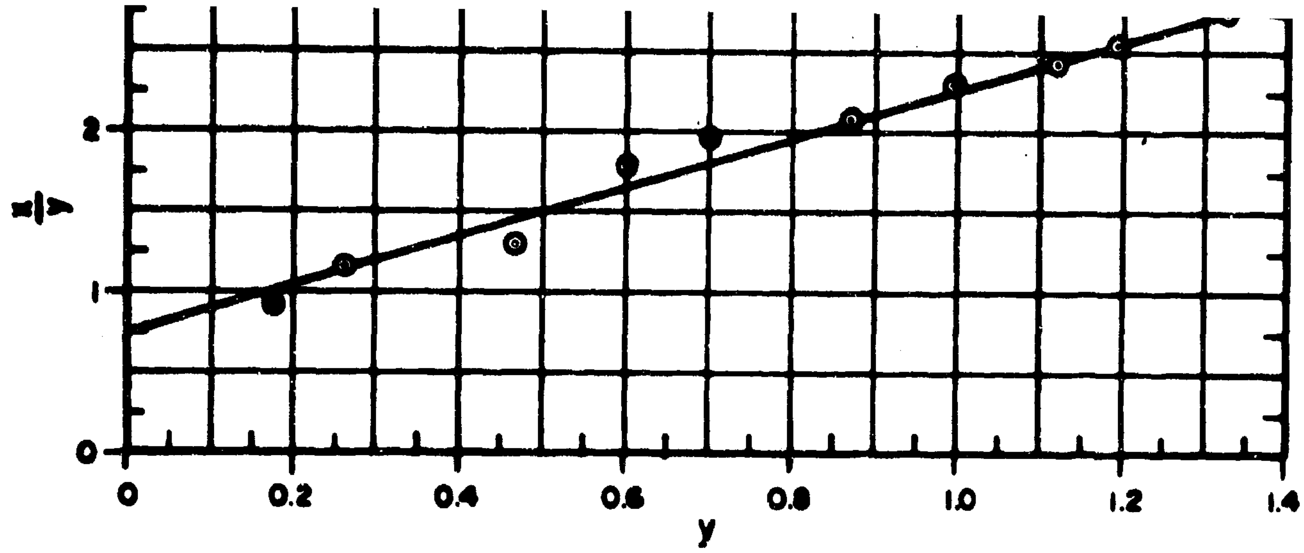

Figure 32. Plot of $\frac{x}{y}$ Versus y for 400-kev Flash X-Ray Data Used to Determine the Co-

Figure 32. Plot of $\frac{x}{y}$ Versus y for 400-kev Flash X-Ray Data Used to Determine the Coefficients B and d.

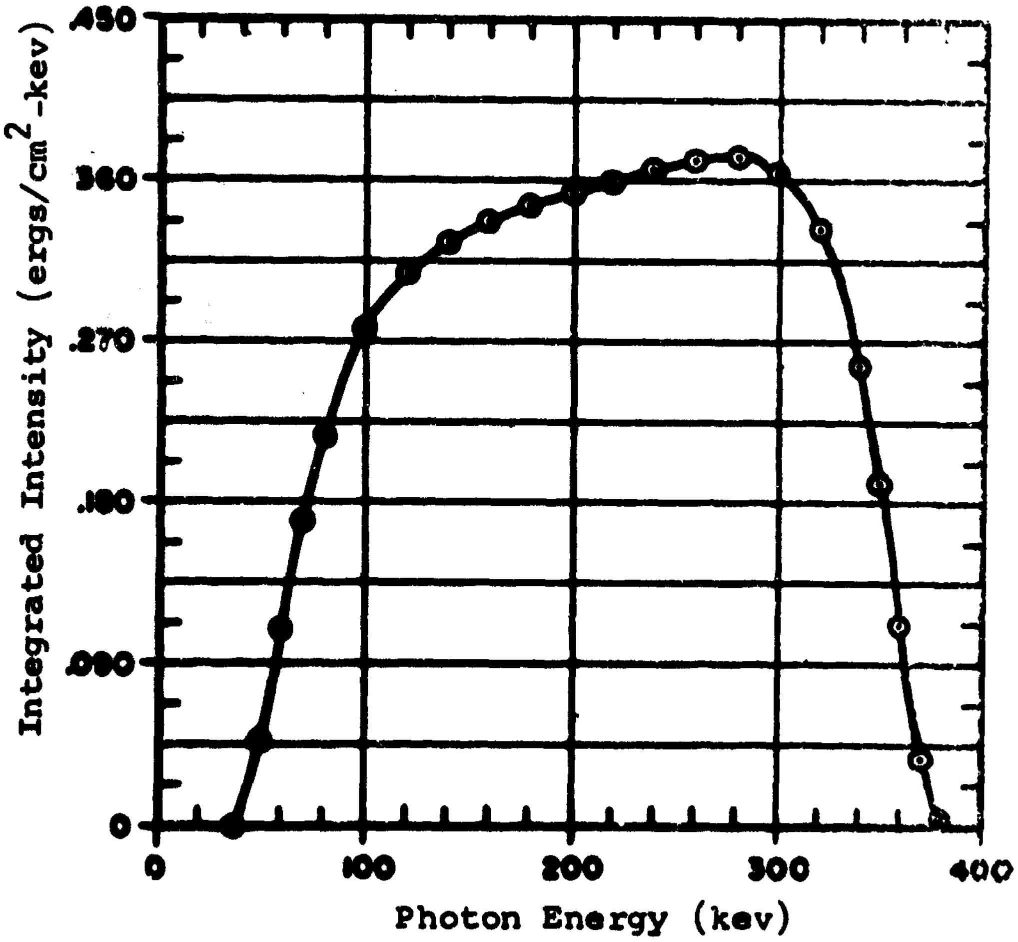

Figure 33. Time-Integrated Intensity Spectrum of 400-kev X-Ray Machine at 20 in. From the Target. The Total Energy was 90 ergs/cm^2 with the Geometry Shown in Figure 24. The X-Ray Beam was Filtered with .050 in. of Copper.

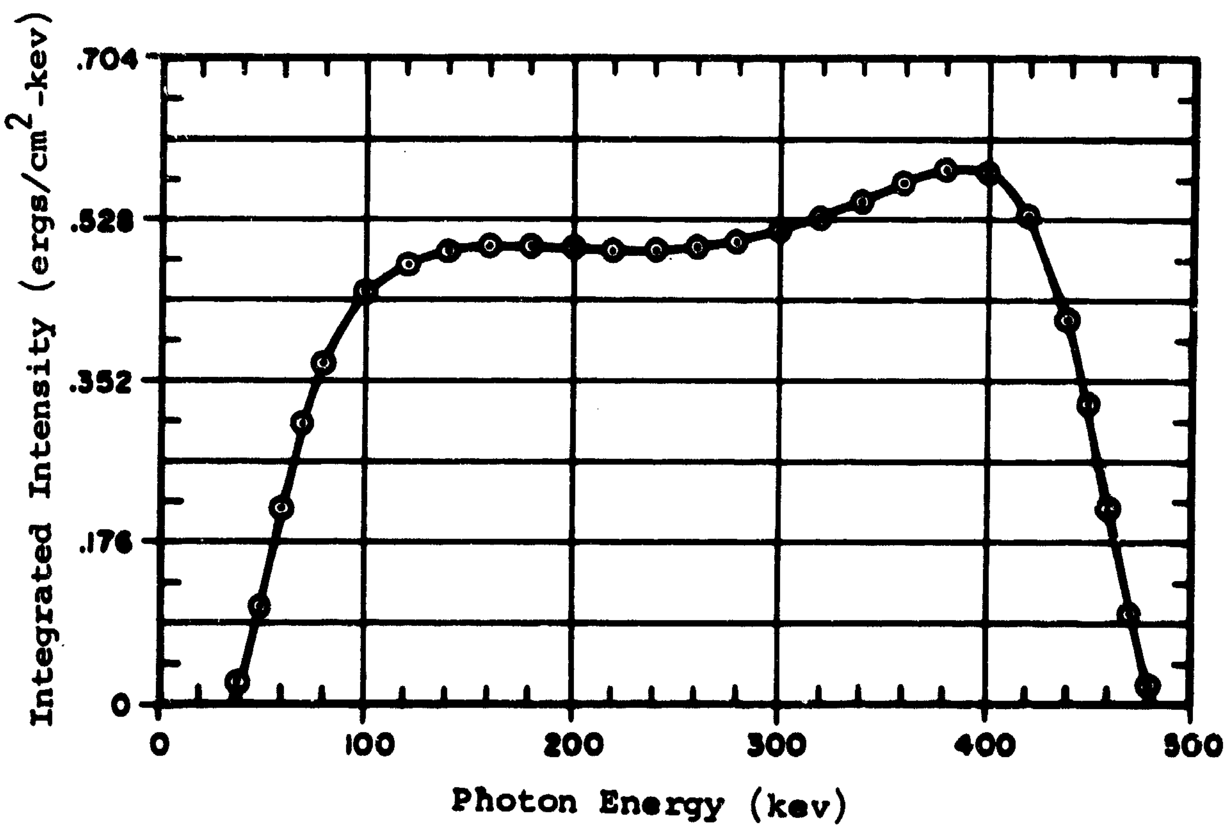

Figure 34. Time-Integrated Intensity Spectrum of 500-kv X-Rays Produced by a Flash X-Ray Machine at 20 Inches from the Target. The Total Energy was 192 ergs/cm^2. The X-Ray Beam was Filtered with .050 Inch of Copper.

limited to spectral measurements at energies below the point where pair production begins to dominate and cause $\mu(E)$ to increase with further increase of E. According to equation (114) the accuracy of computation is dependent on $d\mu/dE$. This derivative decreases in magnitude near the minimum in $\mu(E)$. The maximum photon energies contained in a distribution therefore determine the type of material used as an attenuator in the transmission method. The maximum photon energy to which the method may be applied depends upon the attenuator material and desired accuracy of the results.

A simplification of the technique to include radiation detectors sandwiched between successive absorbers is a possibility, but this does not conform to the idealized geometry described above. The problem of inversion of equation (113) is formidable if one tries to include a radiation build-up factor to correct for the deviation from the exponential attenuation law.

There may be occasion to calculate an intensity distribution as a function of the time during the X-ray flash. This could be accomplished by using a fast scintillator, such as plastic scintillator, as a primary radiation detector. Again, it will be necessary to know the energy absorption efficiency of this detector, $\epsilon(E)$, which may not be readily available. The measurement of a time-dependent spectrum will require a higher degree of reproducibility of the flash X-ray pulse than the measurement of a time-integrated spectrum.

Finally, if radiation intensity is required, it is possible to calibrate the NaI(Tℓ) detector against a radioactive standard or X-ray machine.

SECTION V

GAMMA RADIATION EFFECTS ON DIELECTRIC MATERIALS

By LeRoy Meyer and W. W. Grannemann

1. Introduction

Many studies have been made of the conductivity induced in dielectric materials by exposure to ionizing radiation. The problem is of interest because of the information obtained on the conductivity processes in dielectrics and on the application of dielectrics in a radiation environment. The first investigations were made by F. T. Farmer in 1942, and were followed with experiments by John F. Fowler, A. Rose, and many others. In these works the effects were treated in terms of conventional band theory (which uses the model of trapping and recombination levels in the forbidden gap to account for the observed effects). More recently the "hopping" model has been suggested as being more appropriate, the magnitude of the mobility being the determining factor as to which model is used (Reference 30).

The dielectric materials may be divided into two classes, organic and inorganic. The organics may be further broken down into crystalline and polymeric materials. The present work is concerned primarily with a study of the basic mechanisms of radiation induced conductivity (which will be referred to as RIC hereafter) in the polymer materials. The polymers were chosen for most of the experiments because they were more readily available, and their mechanisms of conduction are not yet completely understood.

Both transient and steady state experiments were performed. The basic mechanisms involved are the same when proper time constants and lifetime are taken into account. In many cases the steady state experiments are easier to perform and have fewer side effects to take into account.

The materials used were polyethylene, teflon, and mylar. Of these three mylar shows greater resistance to permanent damage

and has the advantage over the others of being available in film form (Reference 31). Also, it is a pure chemical compound of constant chemical composition. The other materials gave more variability in RIC. Teflon is probably the least radiation resistant, with properties similar to polyethylene. Polyethylene is the most extensively used insulator of the three; most cables have polyethylene insulation.

As will be shown, the RIC in polymeric materials is low, and special precautions are necessary in making measurements to eliminate the many side effects such as noise, cable effects, secondary emission, air effects, and circuit time constants.

The radiation sources used in the experiments were the Cs-137 gamma calibration source, the 250 KV, 15 MA DC X-ray machine, and the 600 KV, 2000 amp., 0.2 μsec flash X-ray machine. A range of dose rates was available from these three sources from about 50 r/hour to 10^6 r/sec.

The radiation effects observed in dielectrics are closely associated with the dielectric properties. These properties (thermal, structural, electrical, etc.) will be discussed at the beginning of this section where the ones most sensitive to radiation will be pointed out.

The Hall effect and magnetoresistance were investigated as a means of measuring the mobility of charge carriers in a dielectric. These mobilities had previously only been predicted. The Hall effect method was successfully used for measuring the mobilities in polyethylene when the material was under the irradiation of gamma rays. In connection with these experiments some of the theory of galvanomagnetic effects in intrinsic polymers is presented.

Experiments were also performed on various polymer materials to determine the effects of surface area, surface roughness, electrode material, and the direction of radiation relative to the sample on the RIC in the material. Photovoltaic effects were also observed. The long tails of RIC decay in polyethylene

were measured and related to the relaxation time of the material. The RIC in the air surrounding a dielectric sample was also investigated and found to vary with pressure and temperature.

2. The Properties of Dielectrics

a. Electrical Properties

The important electrical properties are: the dielectric constant, volume resistivity, surface resistivity, the dielectric strength, the dissipation factor, and the loss factor. Many of these electrical properties are difficult to measure under radiation environment for the resistivity may not be linear under all radiation conditions.

The dielectric constant (ϵ) can be shown to be related to the polarizabilities of the material arising from electronic, ionic and dipolar contributions.

The dielectric strength depends on the breakdown potential of the material, which varies with material thickness, temperature, surrounding media, gas and voids in the dielectric, chemical deterioration and radiation exposure.

Resistivity or conductivity is discussed in detail in a later section. The loss and dissipation factors were not observed in this study.

The properties of some of the dielectric materials used in this study are shown in Table V. Electrical breakdown is initiated by some action of electrons or ions at voids in the electrode-polymer interface and grows by an intermittent discharge mechanism. The breakdown path slowly meanders through the sample over a period of hours with little reference to the overall voltage gradient. It then usually terminates in the formation of a highly conductive path through the material (Reference 32). Under radiation environments the electrical breakdown may originate from the ionizing effect of radiation on the surface, chemical changes within the material, or internal heating due to gamma radiation. These reactions then lead to intrinsic electrical breakdown by electron avalanche, thermal breakdown from gamma heating, or electric discharge in cavities due to gas evolution from chemical impurities.

Table V. Properties of Some Dielectric Materials

	Resistivity $23^{o}C$ $\rho(\Omega\text{-cm})$	Dielectric Constant	Specific gravity (d_4^{20})	Dielectric Strength Volts/mil	Power Factor 10^6 cycles	Density g/cc
Polyethylene	1.6×10^{13}	2.3	.926 - .941	460	.0005	0.19 to .97
Teflon (tetra flouroethylene)	10^{15}	2.0 to 2.1	2.15	480	.0002 - .0005	
Mylar (polyethylene terephthalate)	2.5 x 10	3.0	1.38	4.17×10^3		
Air		1.00059		30.0		2.34×10^{-7} ($20^{o}C$ 760 mm. Hg)
TiO_2	2×10^5	100	1.05 - 1.08	500 - 700	.0001 - .0004	

b. <u>Structural Characteristics</u>

The structural parameters are difficult to interpret in terms of dielectric qualities. It appears that structures that are stable to heat are also stable to radiation.

The important properties are tension, compression, bending, shear, torsion, elastic strength, fracture strength, ductility, resilience, elongation, tensile strength, and Young's modulus. These will not be discussed further except for a few comments from the literature. For example, the failure of dielectrics is usually due to physical deterioration and to mechanical rather than electrical properties. They often provide good electrical insulation even though their mechanical properties are severely damaged by radiation.

c. <u>Chemical Changes in Polymers Due to Irradiation</u>

Chemical deterioration may lead to thermal decomposition and dielectric failure. An arc produces ozone, and its subsequent reaction with the dielectric causes chemical deteriorations. These are usually long term effects.

Typical chemical reactions are classified as molecular chain scission, cross-linking, and excitation (Reference 33). These processes are given below for polyethylene (which received a dose of about 10^9 ergs/gm C). The molecular chain scission is given by

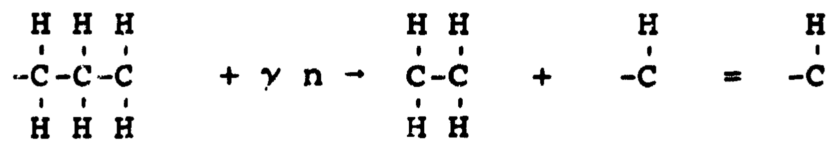

(119)

The molecular cross-linking reaction is given by

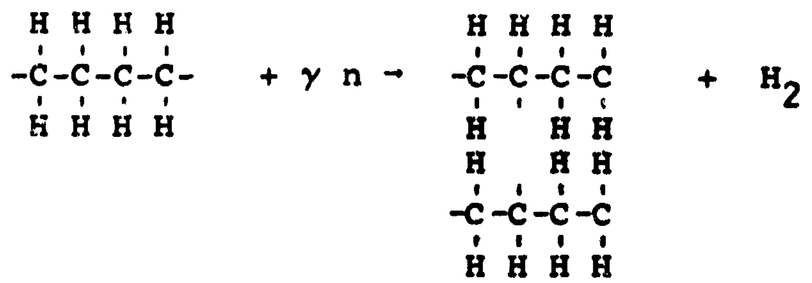

(120)

Each bond indicated by a dash is formed by a pair of electrons. The energy required to remove these electrons is of the order of 3 to 5 ev. However, one can remove adjacent hydrogen atoms and form a series of double bonds such as equation (119). As the number of double bonds increase the binding energy of these electrons decreases due to resonance phenomena.

One consequence of double bonds is that the material becomes colored. For a sequence of 3 double bonds absorption is in the ultraviolet; with 4, the material is yellow; for 8 and 9 it is red; and for 20 it is brown or black.

d. Thermal Properties

Although the resistivities are high, they do change with temperature in the same manner as in semiconductors. The equation for resistivity is

$$\rho = \rho_o \exp\left(+ \frac{E}{KT}\right) \tag{121}$$

where E is the activation energy.

The source of heat in dielectrics is the conduction currents from the free electrons present, and energy absorbed from the lag between charge and applied voltage in an alternating field. Heat is a function of electric field in both cases, as well as frequency in the second case. In some semiconducting polymers the ratio of thermal conductivity to electrical conductivity is much less than for ordinary semiconductors.

e. Optical Phenomena

The prominent optical phenomena is florescence, which is associated with electron-recombination processes. The optical efficiences reported in the literature are of the order of 1% to 10% depending on the material used.

f. Observed Effects when Insulators are Irradiated

The observed effects reported in the literature are: gas evolution from organics, discoloration, change in conductivity, embrittlement or softening, and change in mechanical properties. The effects are both transient and permanent.

The effects vary widely depending on composition, type of material (organic or inorganic), type of radiation, dose rate, total dose, environment, amount of material, and amount of energy absorbed. The effects caused by interaction of these factors can be extremely complex. Many of these are discussed in detail with experimental results in Section 6.

Two important applications of dielectric materials are in cables and capacitors. In cables the secondary emission signals are dominant over RIC for high dose rates. RIC is dominant at low dose rates (Reference 34). For capacitors in a gamma radiation environment, little or no change in the value of capacitance has been reported. This is what might be expected if one looks at the equation for capacitance

$$C = \frac{\epsilon A}{d} \tag{122}$$

when

ϵ = dielectric constant

A = area

d = plate separation distance

From equation (122) it is clear that any change in C would have to be due to a change in ϵ. The ϵ can be related to the polarizabilities of the material through the susceptance. The polarizability can be made up of three parts: electronic, ionic, and dipolar contributions. Any change in C would most likely come from a change in the dipolar polarization. A build-up of polarization has been reported in the literature and also observed in experiments performed on polyethylene. This build-up is small. Even when combined with the other polarizabilities the overall change in ϵ is quite small. Thus any noticeable change in C is not likely.

A more significant factor in the application of capacitors in a gamma radiation environment is the leakage conductivity. The leakage time constant (RC) is in the millisecond range for most circuits. R is the short circuit leakage resistance of the capacitor.

3. Theory

a. Phenomenon of Radiation Induced Conductivity in Dielectrics

There are two aspects to the phenomenon of RIC in dielectrics. The first consists of determining the nature of the charge carriers, how they form, how they recombine, and what their mobilities are. The second aspect is that once the properties are known one should be able to predict the behavior of the currents as a function of radiation intensity, applied voltage, properties of the material, and temperature. A summary of a few relevant experimental facts that determine the model to be used will be given first.

Experimental evidence has been obtained on molecular crystals which indicates that carriers are formed only on the surface of the crystal or at electrodes by excitons (Reference 30). A modified electron-band of solids has been used to explain the experimental transport properties. In this theory the intermolecular binding is weak, and the overlap is small, which leads to narrow energy bands and therefore implies small carrier mobilities.

The properties related to conduction of current in polymers is not nearly so well established. The mobilities are always low, and these materials are usually P-type. Also, there is no evidence that a band model is applicable to polymers. Any interpretation of experimental conductivity and activation energy of band model energy gaps is not yet justified, although it is often done in the literature. Only hole conduction and trapping effects have been observed in the pure materials.

The atoms in a polymer structure are held together by the weak forces of the covalent bonds. What is left is an environment of free electrons, ionized molecules, and free radicals. These are free to move about within the material and may recombine in various ways.

The phenomena that occur in organics that do not occur in inorganics are: changes in dielectric properties, increased sensitivity to environmental interactions, and gas evolution.

Because of covalent bonding between atoms most polymers exhibit dielectric properties. The conductivity of organic polymers is now known to range from 10^{4} to 10^{-21} mho/cm, a range of 10^{25}. They can thus be classed as semiconductors as well as insulators. Most of the polymers in the higher part of the conductivity range have filler materials added during the manufacturing process. They have future possibilities as semiconductors since one could make film, and mold shapes as components of semiconductor devices. There the most serious limitations would be high temperature tolerance.

There is remarkable agreement between different experimenters who have worked with commercial specimens of polymers (plastics). The currents and exponents that have been measured are found to give fair agreement. There seems to be some fundamental property of the basic molecular structure that is more important than the impurity content (Reference 35).

The semicrystalline polymer may be considered to be a mixture of crystallites and intervening amorphous regions. It may be regarded as a system of rigid particles (crystallites) dispersed in a rubbery medium with some type of periodicity. They are not crystalline in the sense that their molecules are periodically arranged in space, such as in an NaCl crystal, but rather that the polymer chains must be folded somewhat as shown in Figure 35, (Reference 36). The calculated dimenions of the

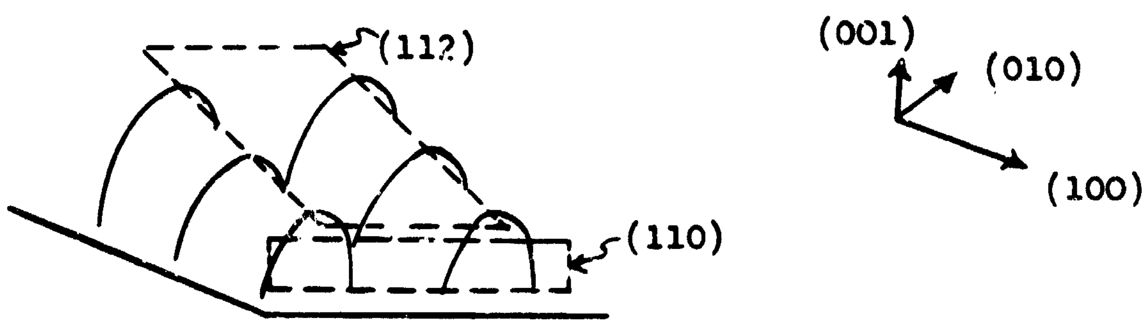

Figure 35. Folding of Polymer Chains in Laminar Crystals

crystallites were much less than the length of the polymer molecules. Thus, the fringed-micelle model of the structure of polymer crystals no longer holds (Reference 32). Also mentioned in this reference is the fact that electron microscope pictures have shown a screw axes of spiral growth; and electron diffraction patterns have shown that the chain axes of the molecules are normal to the large dimensions of the platelets. Therefore, while the molecules themselves are not periodic, the intramolecular arrays or chains in the material might be said to have a pseudo periodicity. A comparison can be made between the chainlike molecules and the elongated crystallites in a wire. They both try to align themselves parallel to the fiber axes.

The properties of the polymer are not unlike that of the complete relaxation of lattice periodicity: that is, the melting of a solid. When melting occurs, the mechanism of transport is not clear. One possibility is that the band model is replaced by the so-called "hopping" model. The term "hopping" has been given to carrier motion observed in certain ionic crystals whose electron-phonon coupling is determined by electrostatic interaction between the electrons and ions. In nonpolar crystals the electron-phonon coupling is determined by interactions between electrons and induced molecular dipoles and is much smaller. Neither the "hopping" model nor the band model is completely satisfactory. The magnitude of the mobility has been used to determine the applicability of the appropriate model. When the mobility is greater than 1 cm^2/v-sec, the band theory is more appropriate, and when the mobility is less than 1 cm^2/v-sec the "hopping" model is more suitable. In general, when the band model scattering free path is equal to or smaller than the lattice spacing, a "hopping" process is favored (Reference 30).

H. A. Pohl has shown that the conductivity in polymers is electronic and not ionic. He performed the following experiment:

Over a seven day period a sufficient current was passed through the polymer to electrolyze every carrier, hydrogen, or oxygen atom in it. The resistivity of the sample did not change during this period. It was concluded that electrolysis does not occur. The conductivity is not ionic and must be, most probably, electronic. That the conductivity is electronic in nature also follows from the measured ability to pass much more charge through a sample than it would store as a capacitor. Charge transport by ions, rotation of dipoles, or other chemical processes was ruled out for the same reason by G. T. Cheney et al, and they also observed that RIC is a linear function of voltage and does not depend on the electrode material (Reference 37).

It has thus been established beyond reasonable doubt that the polymers are electronic conductors and that they have an exponential temperature dependence. Mathematically the band theory equations describe the semiconductivities of polymers. Holes have greater mobilities than the electrons. This does not mean that these materials are intrinsic semiconductors in the sense of band theory, but, rather, that mathematically a good fit can be obtained using such equations. The application of band theory to materials of low mobility is questionable. In the light of these facts the problem of conductivity in dielectrics shall be examined. A model will be used in which it is assumed that the charge carriers behave as particles possessing characteristic diffusion constants and mobilities.

Experimentally a positive Hall coefficient has been obtained for polyethylene. This could arise in two ways: 1) an intrinsic material in which the mobility of the positive charge carriers is greater than the mobility of the negative carriers, and 2) an extrinsic material in which the number of positive charge carriers is greater than the number of negative carriers. This would require that the impurity concentration be greater than the host atom concentration, and is not practical. Assuming then that the material is intrinsic, one can calculate the concentration of

holes and electrons from equation (123) below, where the rest mass of the electron is used for m*.

$$n = p = \frac{2(2\pi m^* KT)^{3/2}}{h^3} e^{-E/KT} \qquad (123)$$

where

n = density of electrons
p = density of holes
m^* = effective mass
K = Boltzmann constant
T = temperature (degrees Kelvin)
h = Planck's constant
E = activation energy

The equation for conductivity in intrinsic material is given by

$$\sigma = |e| n \mu_h (1 + b) \qquad (124)$$

where

e = electronic charge
μ_h = hole mobility
b = μ_e/μ_h ratio of the electron mobility to hole mobility

Experimentally, E. E. Conrad et al. found that the conductivity of a dielectric in a radiation environment may be described by the equation

$$\sigma = \sigma_o + \sigma_i + K\dot{\gamma}\Delta \quad \text{(Reference 31)} \qquad (125)$$

where

σ_i = photoconductivity
σ_o = dark conductivity
$K\dot{\gamma}\Delta$ = gamma induced photoconductivity
K = constant or proportionality of the material
Δ = an exponent which is characteristic of the material and varies between 0.5 and 1.

The simple power relationship between σ and $\dot{\gamma}$ seems reliable as a means of predicting the behavior of dielectrics over a wide range of gamma flux. The relationship is empirical and does not lend itself to investigation of microscopic material properties, but the design engineer may use the relationship with reasonable confidence.

S. E. Harrison et al used equations similar to equation (125) to explain the three time intervals observed in RIC during a transient gamma pulse (Reference 38).

RIC is a function of dose rate as can be seen in Table VI. Most investigators used only a limited range of dose rates; therefore the following table is given for data collected from several sources on induced conductivity in mylar.

TABLE VI

INDUCED CONDUCTIVITY IN MYLAR

Source	Flux r/sec	Induced Conductivity $(\text{ohm-om})^{-1}$
Fowler	1.3×10^{-1}	6×10^{-20}
Conrad	1.1×10^{2}	1.1×10^{-16}
Conrad	3.5×10^{3}	5.7×10^{-15}
Day	6.5×10^{4}	1.5×10^{-13}
"	1.5×10^{5}	3.7×10^{-13}
"	3.3×10^{5}	9.7×10^{-13}
"	7.5×10^{5}	1.9×10^{-13}
"	3.8×10^{6}	1.1×10^{-11}

b. <u>Hall Effect in Polymers</u>

The Hall effect is one of the most valuable tools in the study of semiconducting materials. It could be equally valuable in the study of organic materials, except for the

difficulty that arises in organic materials because of the low mobilities. Mobilities have been reported for various organics that range from 10^{-6} cm^2/volt-sec to 10^2 cm^2/volt-sec.

For intrinsic material the following relations exist:

$$n = p = n_i \tag{126}$$

where

n = electron density

p = hole density

n_i = carrier density

The Hall coefficient can be shown to be

$$R_h = \frac{1}{n_i e} \frac{(1-b)}{(1+b)} \text{ cm}^3/\text{coul} \tag{127}$$

where

$$b = \frac{\text{mobility of electrons}}{\text{mobility of holes}}$$

$e = 1.6 \times 10^{-19}$ coul

The values of the mobility ratio, b, have been reported in the literature to range from 0.25 to 0.9, the mobility of holes being slightly higher than that of the electrons (Reference 30).

From equations (124) and (127) the relation between hole mobility, conductivity and the Hall coefficient can be obtained as

$$\mu_h = \frac{\sigma R_h}{1-b} \tag{128}$$

The Hall voltage for the conditions of constant voltage bias, and for intrinsic material, can be shown to be proportional to the difference in mobility as follows.

Consider the Hall voltage equation

$$V_h = \frac{R_h \ I \ B}{d} \tag{129}$$

where

I = bias current

B = magnetic field

d = thickness of material

For constant voltage bias this equation can be rewritten as

$$V_h = R_h \frac{V}{R} \frac{B}{d} \qquad (130)$$

where R is the resistance of the material to bias current. Remembering that R can be written in terms of σ by

$$R = \frac{L}{\sigma A} \qquad (131)$$

where

L = length of the sample

A = cross sectional area

and when equations (124) and (127) are substituted for σ and R_h the following equation is obtained.

$$V_h = (1-b)\, \mu_h \frac{VAB}{Ld} \qquad (132)$$

or

$$V_h = (\mu_n - \mu_e)K \qquad (133)$$

where K is a constant $= \frac{VAB}{Ld}$

Therefore the Hall voltage of an intrinsic material for the condition of constant voltage bias depends on the difference of mobilities.

The Hall voltage is very small and must be separated from the displacement voltage and magnetoresistance effects. For example, when a sample of polyethylene is placed in a magnetic

field and a bias current applied, the resulting small Hall voltage is difficult to read accurately even with a microvolt meter. However, when the experiment is performed under irradiation from a constant source of gamma rays the conductivity increases. Therefore, the current increases, and the Hall voltage, being proportional to current, also increases and can usually be read in the μ-volt range. If the assumption of having intrinsic material is correct, then according to equation (133) there is a change in the mobilities of the holes and electrons under radiation conditions.

One might ask what the true meaning is of a Hall voltage which is measured by a meter having 1 megohm impedance connected to a dielectric sample having an impedance of 10^{12} ohms. The meter would appear to be a short-circuit across the sample. In terms of a voltage source, the equivalent circuit would be as shown in Figure 36. If 10 μ V are read across a 10^6 ohm meter, a current

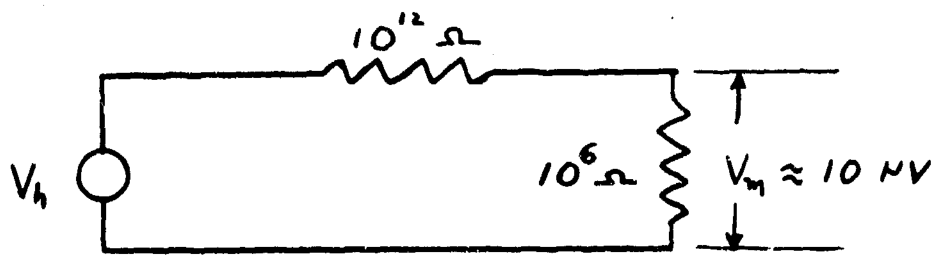

Figure 36. Equivalent Circuit for the Hall Effect in Polymers

of 10×10^{-12} ampere would have to be flowing. This would mean that a drop of 10 volts would occur across the 10^{12} ohms of sample. Therefore the true Hall voltage developed is 10 volts. Usually, in circuit theory where high impedance sources are used a constant

current source would be more appropriate. In this case one might say that he has a constant Hall current source of 10×10^{-12} amperes.

The Hall voltage always comes out to be positive as is discussed in part 6.a of this section which, according to equation (133), means that the hole mobility is greater than the electron mobility. This agrees with what has been reported in the literature on dielectric crystal samples.

c. Magnetoresistance Effect in Polymers

When a sample of polyethylene was placed in a gamma field of 190 r/hour and a magnetic field was suddenly turned on in a direction perpendicular to the direction of current flow through the material, a change in resistance was noted. This is called magnetoresistance. It is caused by a departure from the free electron model, because the electrical charge carriers do not all have the same velocity. The relative change of resistance, $\Delta\rho$, with the sample in a transverse magnetic field, is usually referred to the resistance of the sample in a zero magnetic field. This ratio yields the magnetoresistant coefficient and is given by the expression

$$\frac{\Delta\rho}{\rho_o} = AB^2 \qquad (134)$$

where

ρ_o = resistivity without the magnetic field
A = magnetoresistant coefficient
B = magnetic field
$\Delta\rho$ = change in resistivity when the magnetic field is turned on.

This equation holds for low magnetic fields. A similar formula, called Frank's formula, refers the change in resistivity to the resistivity when the magnetic field is on. It is given by

$$\frac{\Delta\rho}{\rho_m} = \frac{AB^2}{1 + CB^2} \qquad (135)$$

where C = a constant

Frank's formula holds for semiconductors where C is usually taken as equal to μ^2, which agrees with values calculated from the Hall effect. For polymers where the mobility of holes is only slightly greater than the mobility of electrons a more correct value of C might be

$$C = Q^2 b\, \mu_h^{\,2} \tag{136}$$

where

b = mobility ratio

Q = a dimensionless quantity which depends on the device dimensions and other factors not completely understood.

The relation between the Hall coefficient and the magnetoresistance can be shown to be

$$\frac{\Delta\rho}{\rho_o} = \frac{R_h^{\,2}}{\rho_o^{\,2}}\; Q^2\, B^2 \tag{137}$$

The expression for the magnetoresistance coefficient is then

$$A = \frac{R_h^{\,2}\, Q^2}{\rho_o^{\,2}} \tag{138}$$

which can be expressed in terms of the mobilities by using equations (124) and (127) and the relation $\rho = 1/\sigma$ as

$$A = Q^2\, \mu_h^{\,2}\, (1-b)^2 \tag{139}$$

Experimental magnetoresistance data would only yield information in terms of the mobility product and Q^2. If the Hall voltage data are combined with the magnetoresistance data the value of Q^2 can be obtained. It was about 2 for the samples used in this series of experiments.

4. Experimental Techniques

a. Steady State

Conductivity measurements on dielectric materials present two special problems. These are: 1) to measure low currents of order 10^{-12} amperes; and 2) to prevent electrical leakage in the sample and measuring apparatus. When the sample was cleaned with alcohol and not touched by hand before measurements were made, the leakage currents were not a problem. A millivac MV-07c DC micro-volt-ammeter was used for the direct measurement of currents as low as 10^{-12} amperes, and voltages as low as 10^{-6} volts.

Room temperature measurements of static conductivity may be misleading because of the low currents involved and the long time constant of change in the conductivity when the voltage is changed. Fowler gives the time constant as

$$\tau = 10^{-14} e^{E/KT} \tag{140}$$

where E is the average level for deep traps. If E is about 1 ev, τ will be 10,000 seconds at 20°C.

When sufficient time is allowed between readings the volt-ampere relation should be ohmic in both static and induced conductivity.

b. Transient Conductivity Measurements

The problem of observing transient effects in insulators is also a difficult one because the currents involved are of the order of microamperes or less. These currents are easily masked by the various side effects of the flash X-ray system. These side effects are: cable effects, air ionization, electrodes-geometry and material, circuit time constant, and RF interference of the flash X-ray machine.

(1) Cable effects

The radiation pulse produced in cables may be of the same order of magnitude and have decay characteristics the same as those produced in the dielectrics under test. All cables were shielded with 2" lead bricks up to the feed-through connectors

in the vacuum system (see Figure 37 and see Appendix II for details of the vacuum system). A short bare wire was used in the vacuum system for support and electrical connection to the sample. With this cable arrangement cable effects were negligible compared to the signal level of the dielectric.

(2) Air ionization

Air ionization around the sample provides a shunt current path on the order of one megohm. A vacuum system will reduce the air effect to a minimum during an experiment. Potting a dielectric sample as is done with other components to reduce air effects, is not practical. The air effects are discussed in detail in part 6.f.

(3) Electrodes

The electrodes consisted of 1/2" square copper plates between which the sample was held by pressure contact in a special holder as shown in Figure 38. Other types of electrodes were also used to determine whether they had any effect on the measurements. Some were painted on the sample with copper print paint and silver paint. Vapor coated indium was also used. They all gave similar results.

(4) Circuit time constant

The circuit used is shown in Figure 39. The measured rise time of the system was about 30 nanoseconds and the decay time was about 120 nanoseconds. Thus, the long tails which were observed can not be attributed to the circuit.

(5) RF interference

The double-walled screen room reduces the RF interference by about 120 db. This effectively reduces the RF noise from the flash X-ray system, but does not eliminate it. Another screen room around the flash X-ray system would be required to eliminate this source of error.

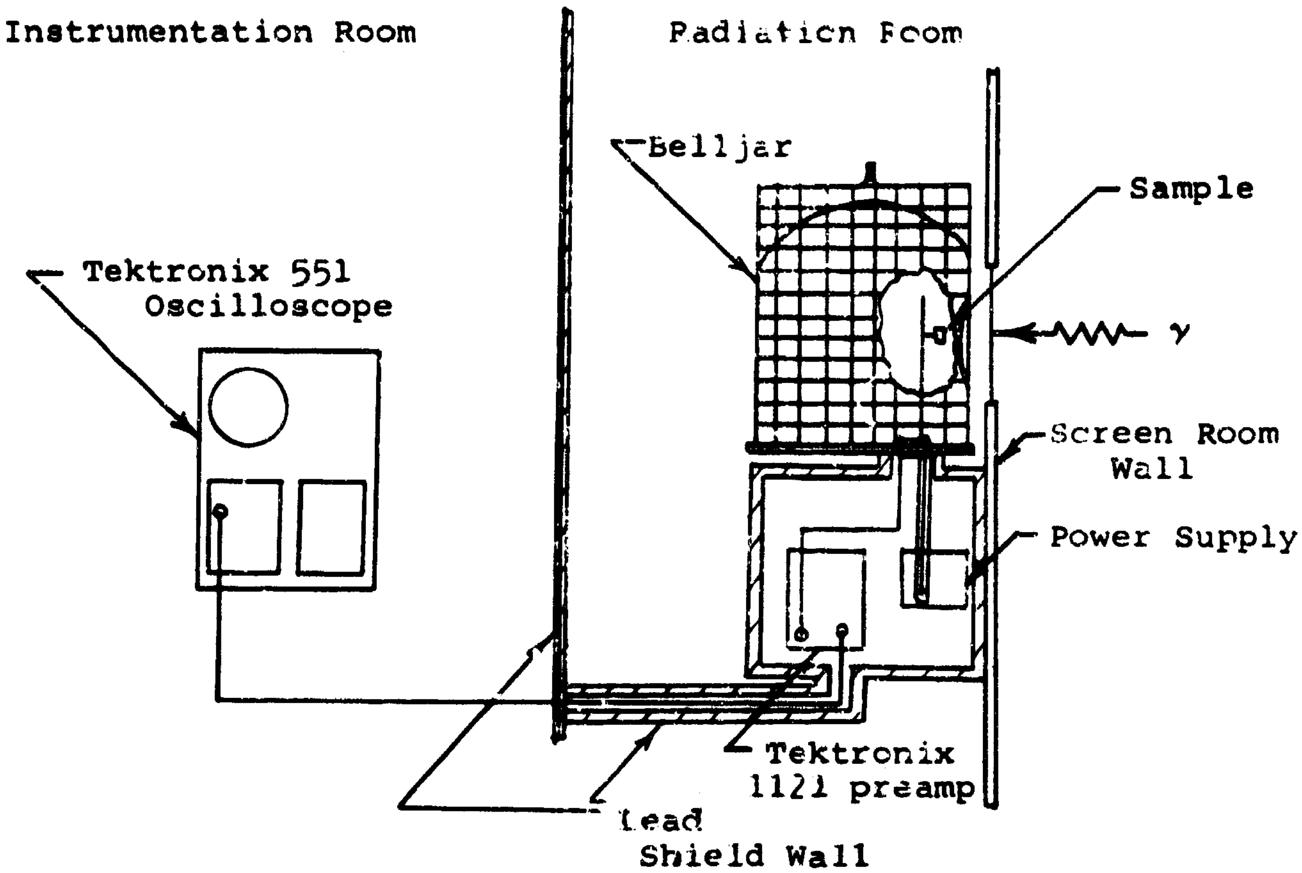

Figure 37. Arrangement of Vacuum System, Lead Shielding and Instrumentation in the Flash X-Ray Experiments

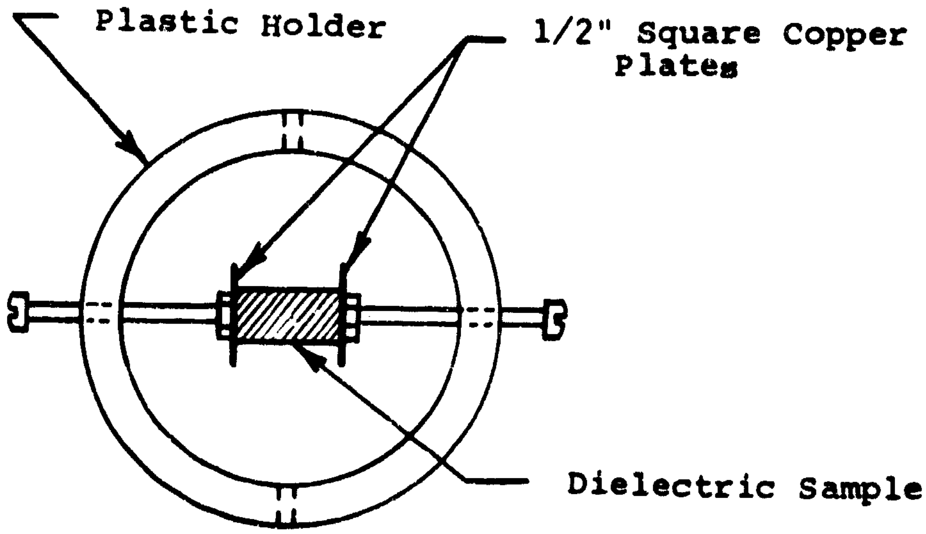

Figure 38. Sample Holder

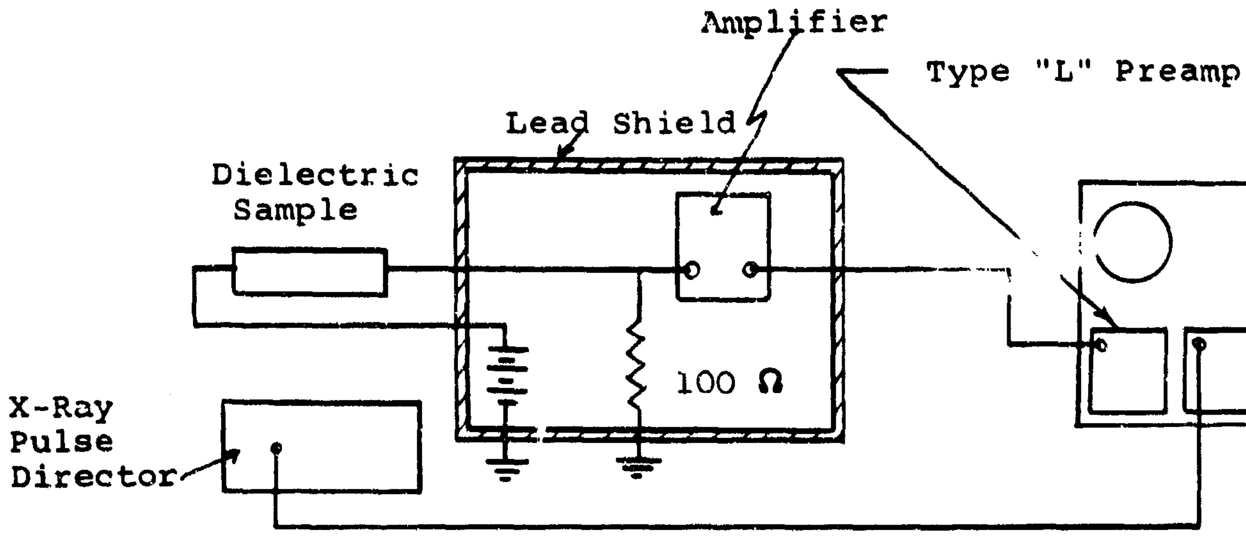

Figure 39. Circuit for Transient Conductivity Experiments

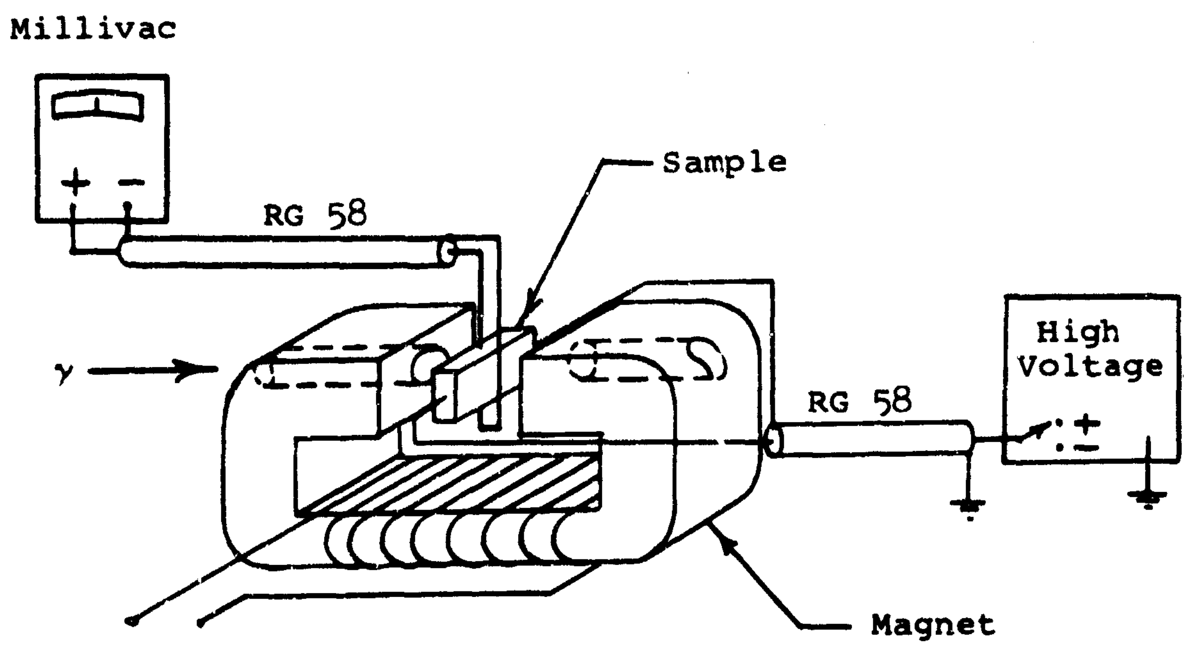

Figure 40. Hall Voltage Experimental Set-Up

5. Dosimetry

For practical application of the test data, the energy absorbed by the material or the energy to which it was exposed must be determined. The mechanisms of energy deposition are the photoelectric effect and Compton scattering. Most of the energy deposited is accounted for by the Compton scattering. To calculate the absorbed dose, knowledge of elemental structure of the sample, environment, sample dimensions, and absorption coefficients for each element present are required. This makes calculation of the absorbed dose in insulating materials extremely difficult because of the variety of complex molecular structures present. Thus, the use of an exposed dose usually is more practical than the mathematical and quantitative chemical analysis involved in calculating the amount of energy absorbed.

6. Experimental Results

a. Hall Effect Experiments

The experimental apparatus used for measuring the Hall voltage in polyethylene is shown in Figure 40. A Millivac microvoltmeter was used to read the voltage to an accuracy of $\pm$ 2 microvolts on the 10 microvolt scale.

The 1/8" x 1/4" x 1/2" polyethylene sample was mounted between two copper plates in the special holder as shown by Figure 38. The electromagnet had tapered poles with a hollow bolt holding the poles in place. The 1/2" hole through the poles served as a means of irradiating the sample with a collimated gamma beam from the Ce-137 source. The gamma dose rate at the location of the sample was 190 r/hour. The electromagnet was capable of being varied from zero to two kilogauss. The bias voltage source was variable from 0 to 3000 volts.

The bias current measured, with 3000 volts applied to the sample, was 2.8 μμamps. This was with no radiation or magnetic field applied. When the magnetic field was applied the current dropped to 2.4 μμamps due to a magnetoresistance effect.

When the radiation was turned on the bias currents increased to the 10^{-9} ampere range. The current would decrease by 20% to 40% when the magnet was turned on. The magnetoresistance effect on polymers will be discussed in part 6.b.

A large displacement voltage was measured at the Hall voltage probes. Cable and air effects also had to be accounted for. The voltage read at the Hall voltage terminal was positive (or negative, depending on the polarity of the biasing current) for both directions of the magnetic field. However it was larger in one direction than the other. The difference between these two readings always gave a positive Hall voltage. The manner in which the difference is obtained is important here because of the many side effects involved. If a series of Hall voltage readings is taken for different bias voltages with the magnetic field in the N-S direction and then with the magnetic field reversed, S-N direction the resulting averages will not be consistent because of meter drift and hysteresis effects in the sample. The magnetic field must be reversed for each bias current setting.

With a 3000 volt/inch bias on a polyethylene sample and no radiation applied, a Hall voltage of 4 μV was observed. This displacement voltage was 10 μV with no magnetic field and no radiation. When the radiation was turned on the displacement voltage increased to 235 μV with no magnetic field. When the magnetic field was turned on the displacement voltage dropped to 127 μV, due to the smaller current caused by the magnetoresistance effect. The Hall voltage was + 21 μV, which was an increase of a factor of 5 over the Hall voltage without radiation. This was at a radiation dose rate of 190 r/hour. At lower bias voltages the increase was less. This indicates that the mobilities are a function of the voltage applied as well as dose rate.

The Hall voltage data and conductivity data were used to calculate the mobilities of electrons and holes in polyethylene. By means of equation (123) one can calculate the number of carriers as a function of excitation energy. Table VII gives these values.

Table VII. The Number of Carriers n for Various Excitation Energies as Calculated Using Equation (5)

E (electron volts)	n (carrier density)
0.2	8.76×10^{21}
0.4	3.3×10^{18}
0.5	6.2×10^{16}
0.6	12.1×10^{14}
0.7	2.35×10^{13}
0.8	4.39×10^{11}
0.85	6.27×10^{10}
0.9	8.46×10^{9}
0.912	5.12×10^{9}
1.0	1.53×10^{8}
1.1	2.08×10^{6}
1.5	0.39×10^{6}

The Hall coefficient was obtained from the measured value of Hall voltage and equation (129). The mobility ratio, b, can be obtained by making use of equation (127) and a value of n from Table VII. It was found that only values of n for activation energies greater than 0.912 ev would fit the data for Hall voltage measurements. For energies greater than 1.1 ev, b became equal to 1, which indicates that electron and hole mobilities would be equal. Thus, the activation energy for the polyethylene used in the experiment was in the neighborhood of 1 ev. This value falls within the range of E given by Fowler of 0.4 ev to 1.5 ev for polyethylene.

By using the trap depths of 1 ev, the value for b, and the values for the mobilities of holes and electrons were calculated making use of equation (128). The results of measured and calculated values are combined in Table VIII for three different bias voltages.

b. Magnetoresistance Experiments

(1) Polyethylene

(a) Mobility calculations

From the magnetoresistance data on a .25" x .35" x .175" sample of polyethylene and equation (139) the values of $Q^2\mu_e\mu_h$ were calculated for several intensities on the sample. They are shown in Table IX.

Table VIII. Hall Voltage Data and Calculated Values of Mobilities for Polyethylene at 190 r/hour

Bias Voltage Volts/in	Bias Current $\times 10^{-12}$ amp	Hall Voltage 10^{-6} volts	Resistivity (ρ) $\times 10^{13}$ ohm cm	Hall (R_h) Coefficient $\times 10^9$
1500	120	+10	1.56	1.22
2000	145	+15	1.87	1.52
3000	175	+21	2.02	1.62

Bias Voltage Volts/in	Mobility Product ($\mu_e\mu_h$) $\frac{cm^4}{(v\text{-}sec)^2} \times 10^{-6}$	Mobility Ratio b	Electron (μ_e) Mobility $\frac{cm^2}{v\text{-}sec} \times 10^{-3}$	Hole (μ_h) Mobility $\frac{cm^2}{v\text{-}sec} \times 10^{-3}$
1500	1.02	0.923	0.97	1.05
2000	1.18	0.932	1.05	1.13
3000	1.71	0.94	1.27	1.35

The mobility product, $\mu_e\mu_h$, calculated from the Hall voltage data was greater than the $Q_2\mu_e\mu_h$ product by a factor of about 2

(see Table VIII). This would indicate the Q^2 constant was about 2 for polyethylene.

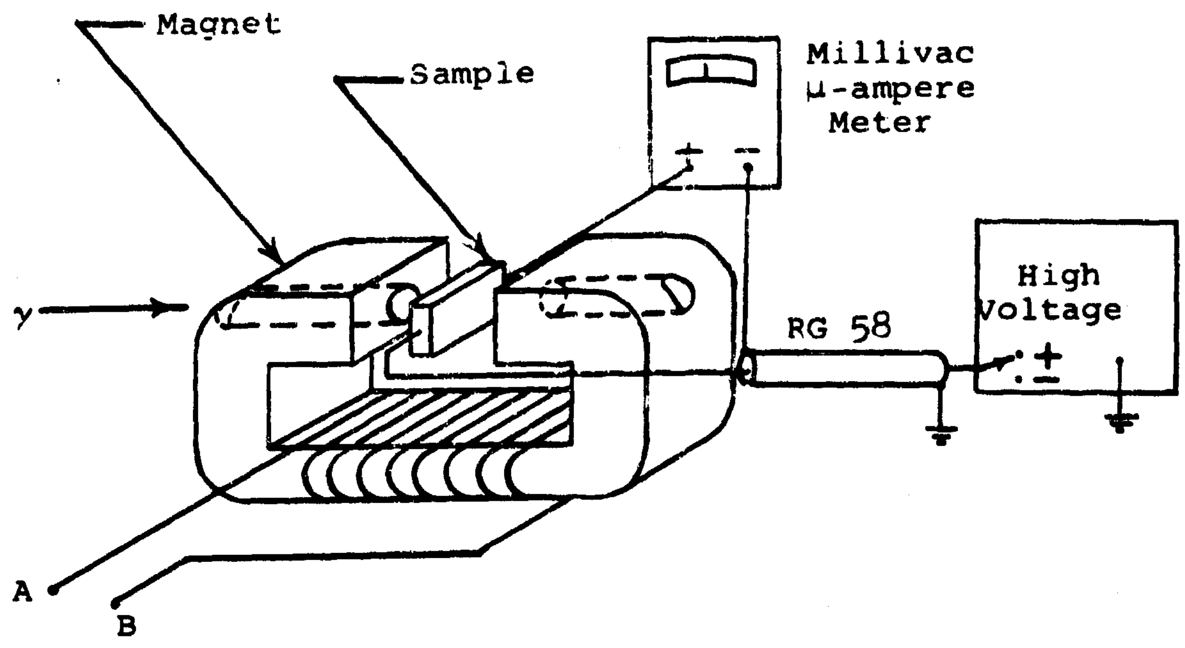

Figure 41. Magnetoresistance Experimental Set-Up

The curve of current versus voltage with the sample out of the radiation field is shown in Figure 42. The magnetoresistance effect is noted by the smaller current for the curve plotted from data with the magnetic field turned on.

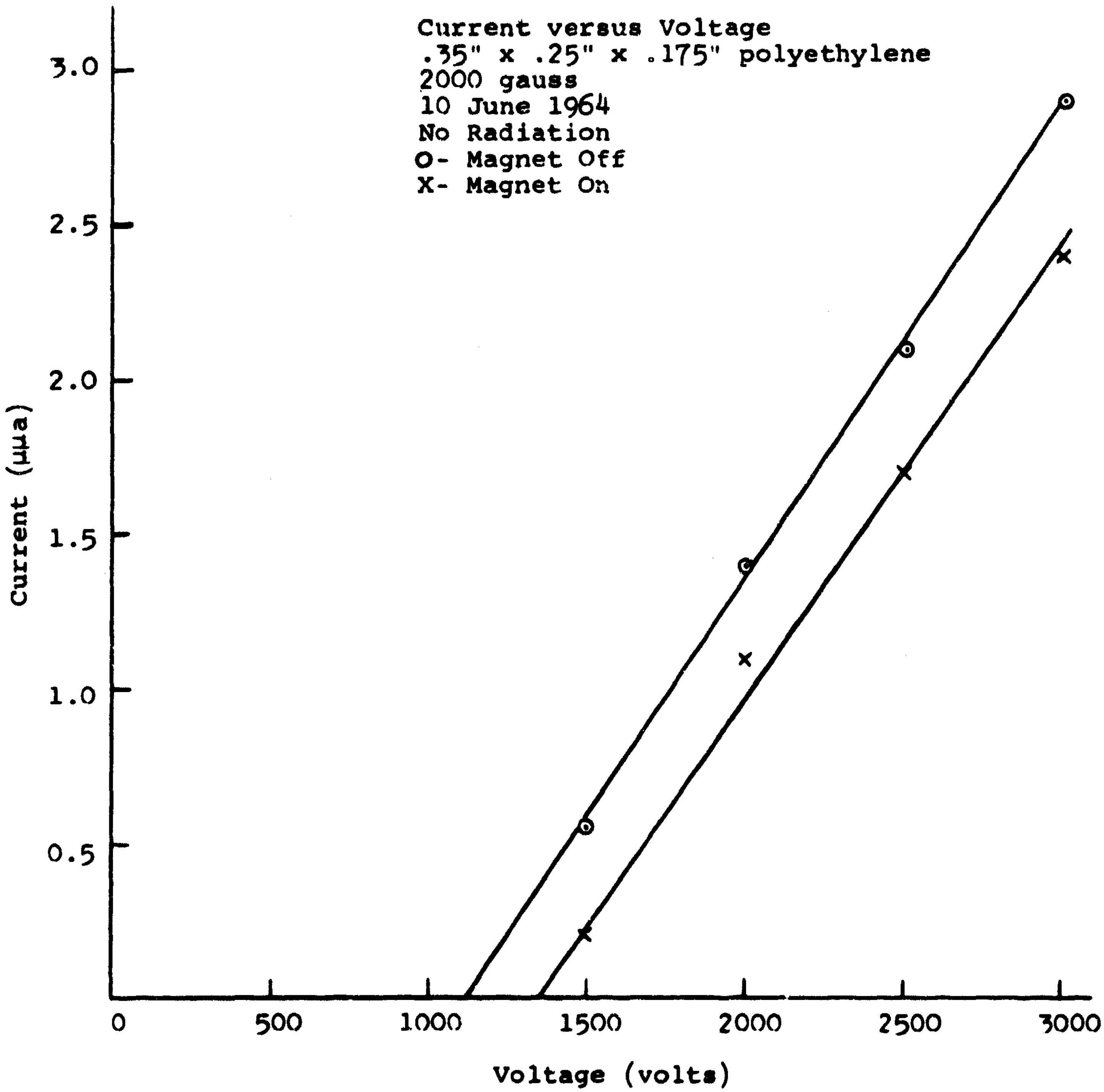

Figure 42. Curve of Current Versus Voltage for Polyethylene with no Radiation Applied

Table IX. Values of Resistivity and Mobility Product Obtained from Magnetoresistance Data on Polyethylene in a Radiation Environment of 190 r/hour Gamma Flux

Volts/in	$\rho_o \times 10^{12}$	$\rho_m \times 10^{12}$	$\frac{\Delta\rho}{\rho_o}$	$Q^2 \mu_e \mu_h \times 10^{-6}$
8600	6.58	20.2	2.07	0.518
7150	6.41	20.9	2.27	0.567
5730	5.69	18.72	2.29	0.572
4290	4.7	15.62	2.32	0.583
2860	3.32	11.73	2.53	0.635
1430	1.85	9.93	4.38	1.095

(b). Radiation Effects as a Function of Sample Orientation

A .35" x .25" x .175" sample of polyethylene was arbitrarily given x y z directions as shown in Figure 43. The bias current was flowing in the x-direction, and the sample was irradiated first from the y-direction and then from the z-direction. The results are shown in Figure 44. The two currents are almost identical with the indirect current caused by irradiating from the y-direction being slightly larger. This is explained on the basis of the energy absorbed in the y-direction being slightly greater than in the z-direction.

The sample was uniformly irradiated at atmospheric pressure. The dose rate was 190 r/hour.

(c) Radiation Effects as a Function of Surface Area

Three samples were prepared with the same cross sectional area and length, but different surface areas. They are shown in Figure 45 and the results are plotted in Figure 46. All three curves are within experimental error.

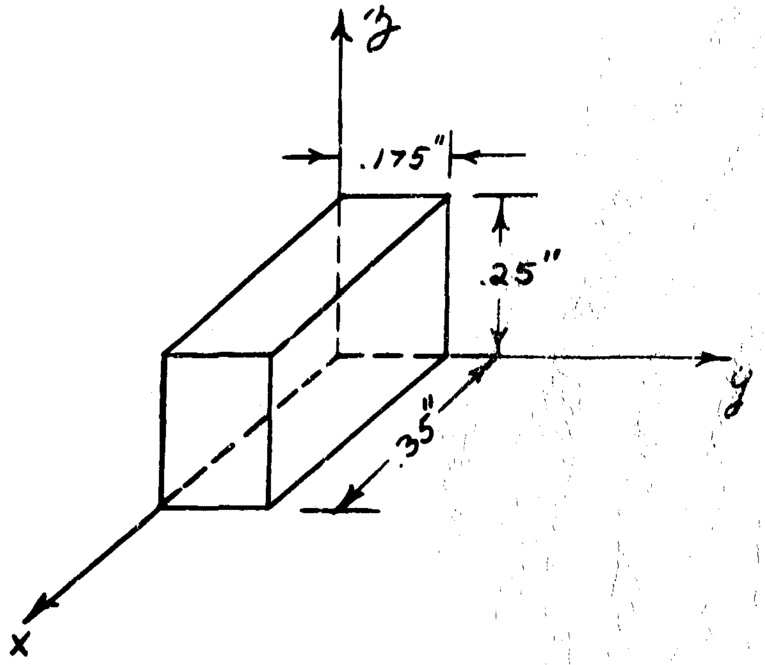

Figure 43. Sample Orientation

(d) Radiation Effects as a Function of Surface Roughness

Two samples of polyethylene were prepared with the same dimensions, but one had grooves cut in the surface in such a way that its actual surface area was doubled. They are designated smooth and rough surfaces and are shown in Figure 47; the effects were almost identical as can be seen in Figure 48.

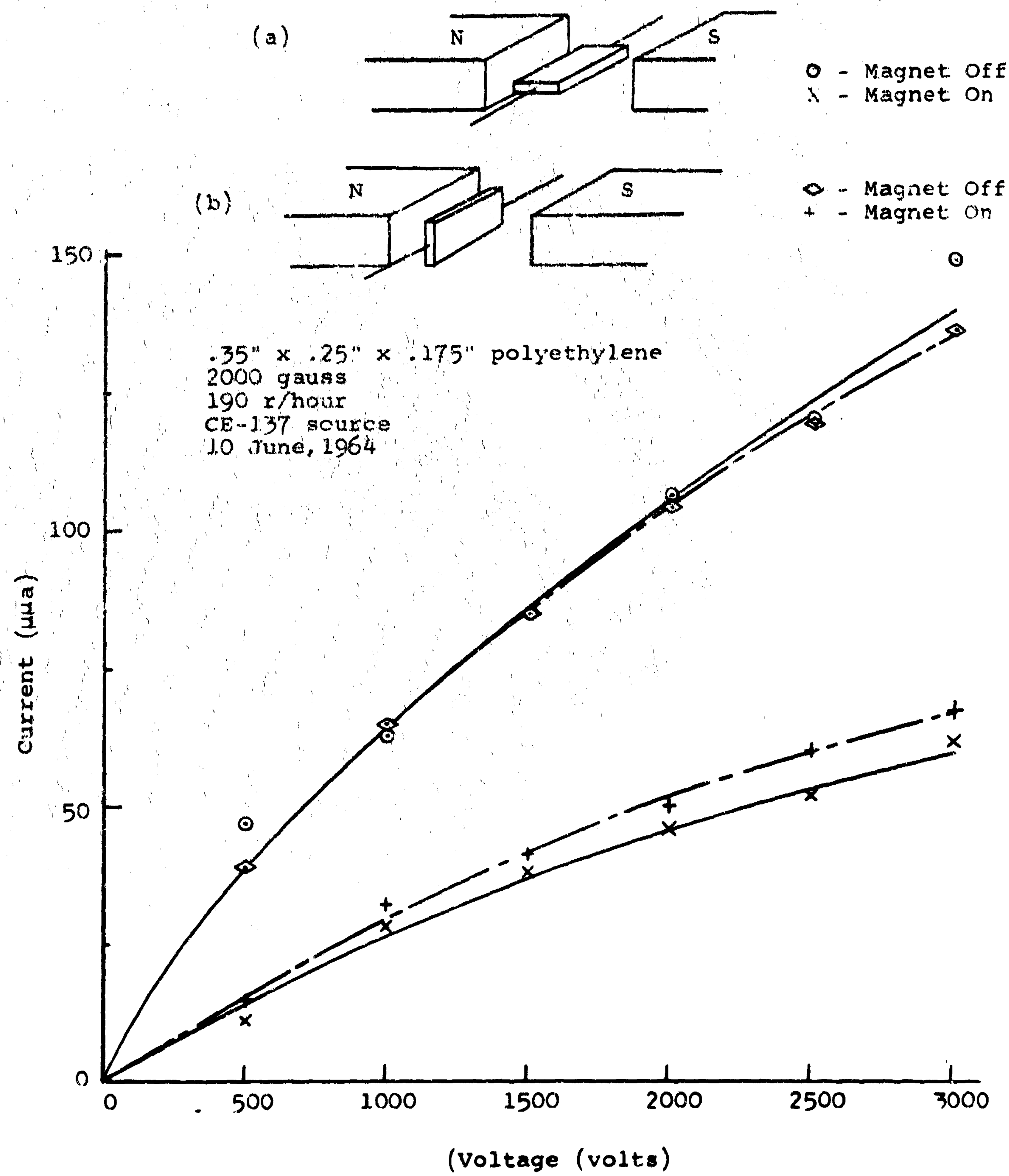

Figure 44. Curve of Current Versus Voltage for Polyethylene which Compares Results of Irradiation from two Different Directions

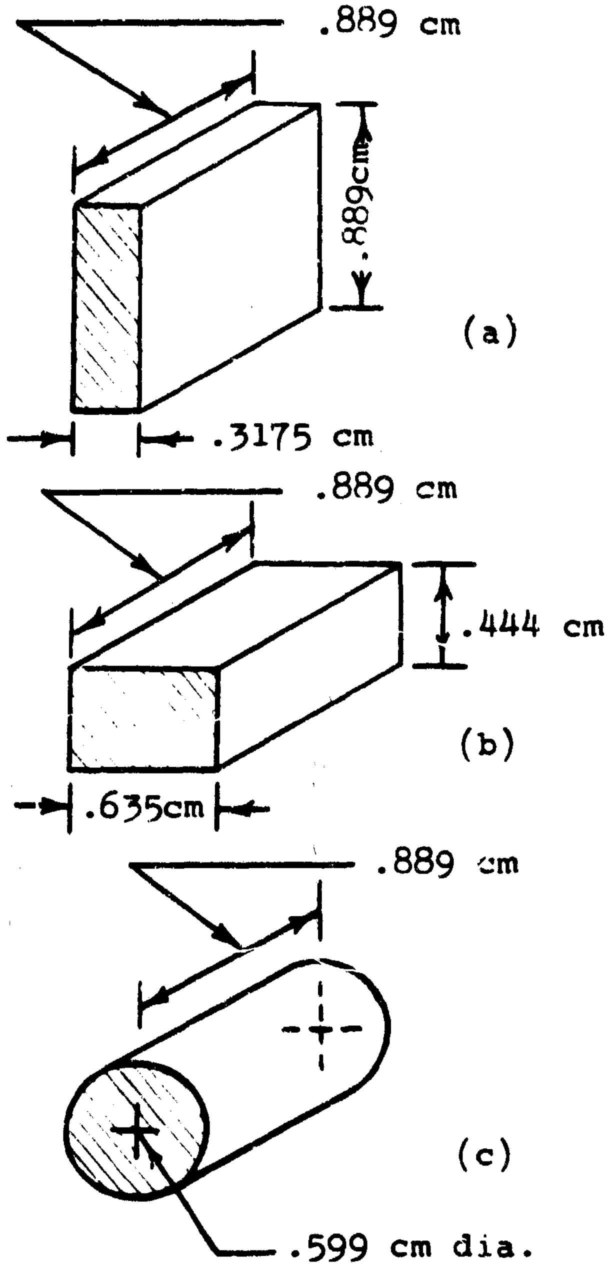

Surface Area = 2.14 cm^2
(not including ends)

Surface Area = 1.92 cm^2
(not including ends)

Surface Area = 1.67 cm^2
(not including ends)

Figure 45. Polyethylene Samples with Three Different Surface Areas, but the Same Volume and Cross Sectional Area

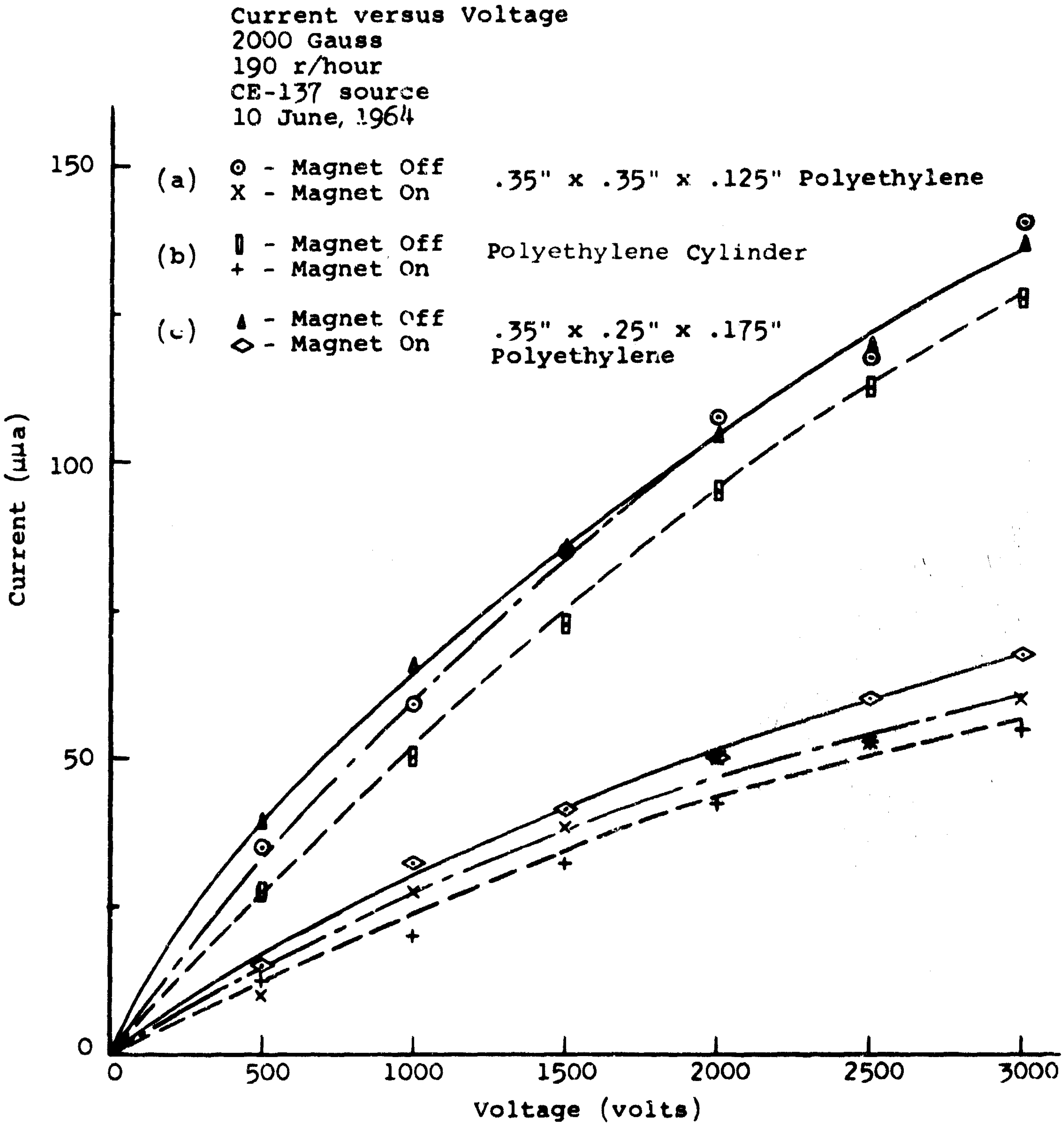

Figure 46. Plot of Current Versus Voltage for the Three Samples of Polyethylene having Different Surface Areas, but the same Volume

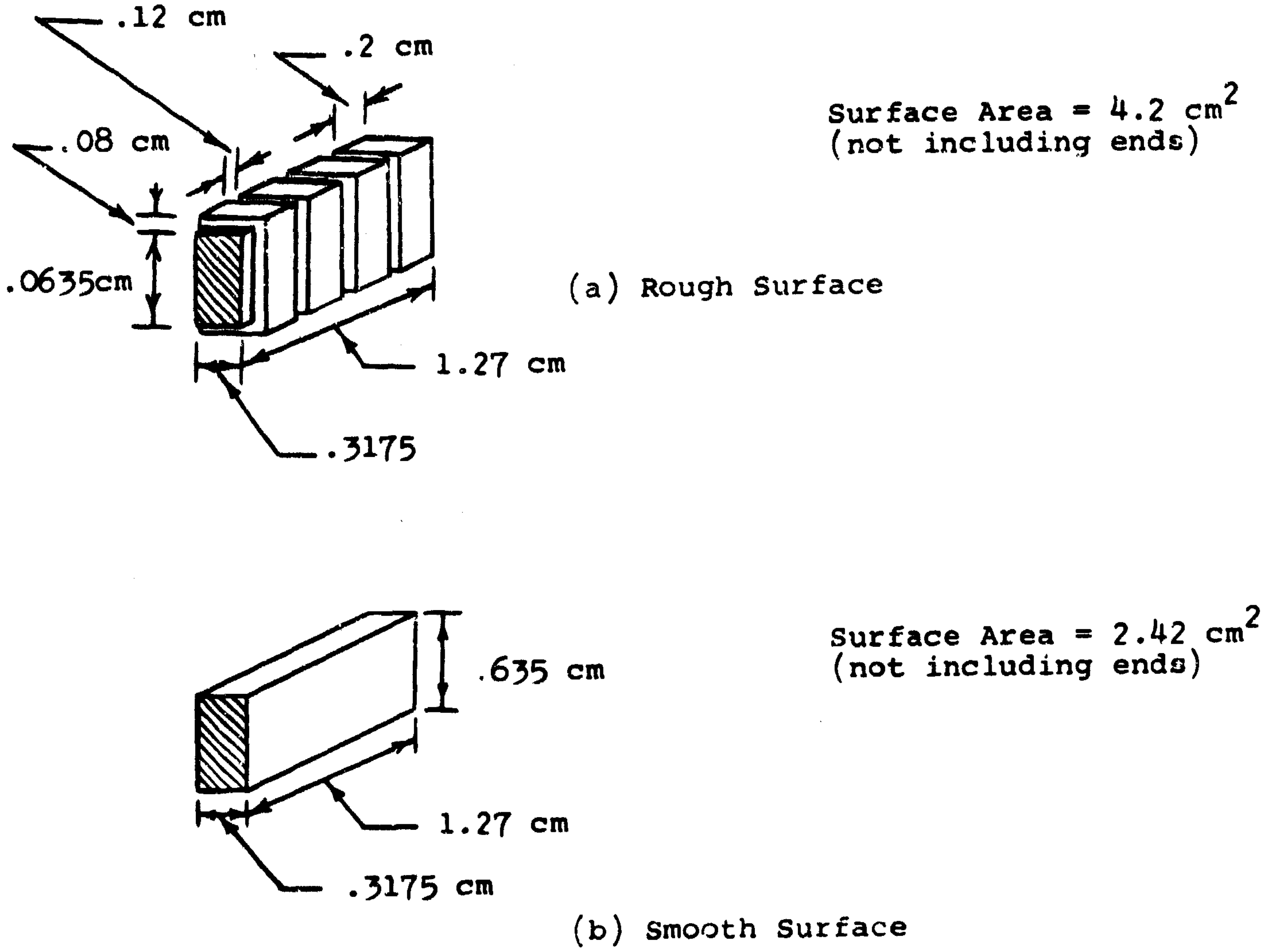

Figure 47. Smooth and Rough Surface Samples of Polyethylene

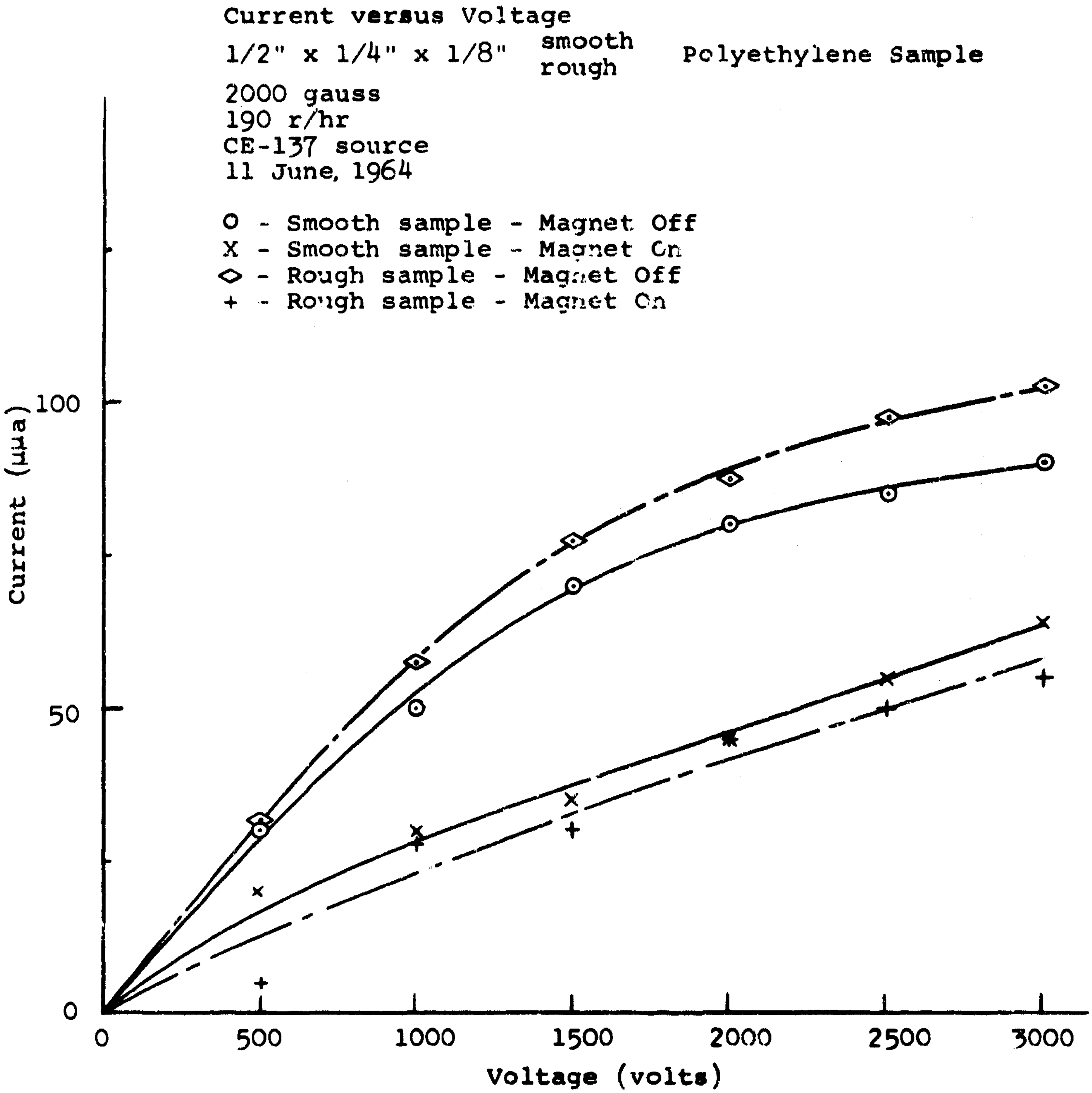

Figure 48. Curve of Current Versus Voltage which Compares the Smooth and Rough Surface Samples

(2) A 1/4" x 1/4" x 1/2" sample of teflon was irradiated using the Ce-137 source at a dose rate of 190 r/hr. The results of the data are tabulated in Table X. The resistivity of the sample with no radiation field was not calculated because the currents were less than 10^{-12} ampere. The published value of ρ is greater than 10^{15} (ohm cm)$^{-1}$.

From the magnetoresistance data the mobility product was obtained. No Hall voltage data was taken for teflon so b, μ_h, and Q^2 cannot be found; but if Q^2 is around 2, as was found for polyethylene, and b $\approx$ 1, the mobilities would be around 9 x 10^{-4} cm^2/v-sec. A curve of current versus voltage for teflon is shown in Figure 49.

Table X. Values of Resistivity and Mobility Product for Teflon Obtained from Magnetoresistance Data of Sample Being Irradiated at 190 r/hour Gamma Flux

V/inch	Resistivity (ohm-cm) $\rho_o(190\frac{R}{m})\times10^{12}$	Resistivity in Magnetic Field (ohm-cm) $\rho_m(\frac{190\frac{R}{m}}{2000G})\times10^{12}$	$Q^2\mu_e\mu_h\times10^{-7}$
6000	10.53	29.3	4.45
5000	10.19	28.4	4.47
4000	8.93	22.7	3.86
3000	6.9	15.87	3.25
2000	4.32	10.72	3.70
1000	2.04	5.89	4.73

(3) A 3/64 x 7/32 x 3/8" sample of TiO_2 was irradiated with the Ce-137 source with a dose rate of 190 r/hr. There was no observed change in conductivity. Next a magnetic field was applied perpendicular to the direction of current flow. There was no magnetoresistance effect observed in or out of the radiation beam.

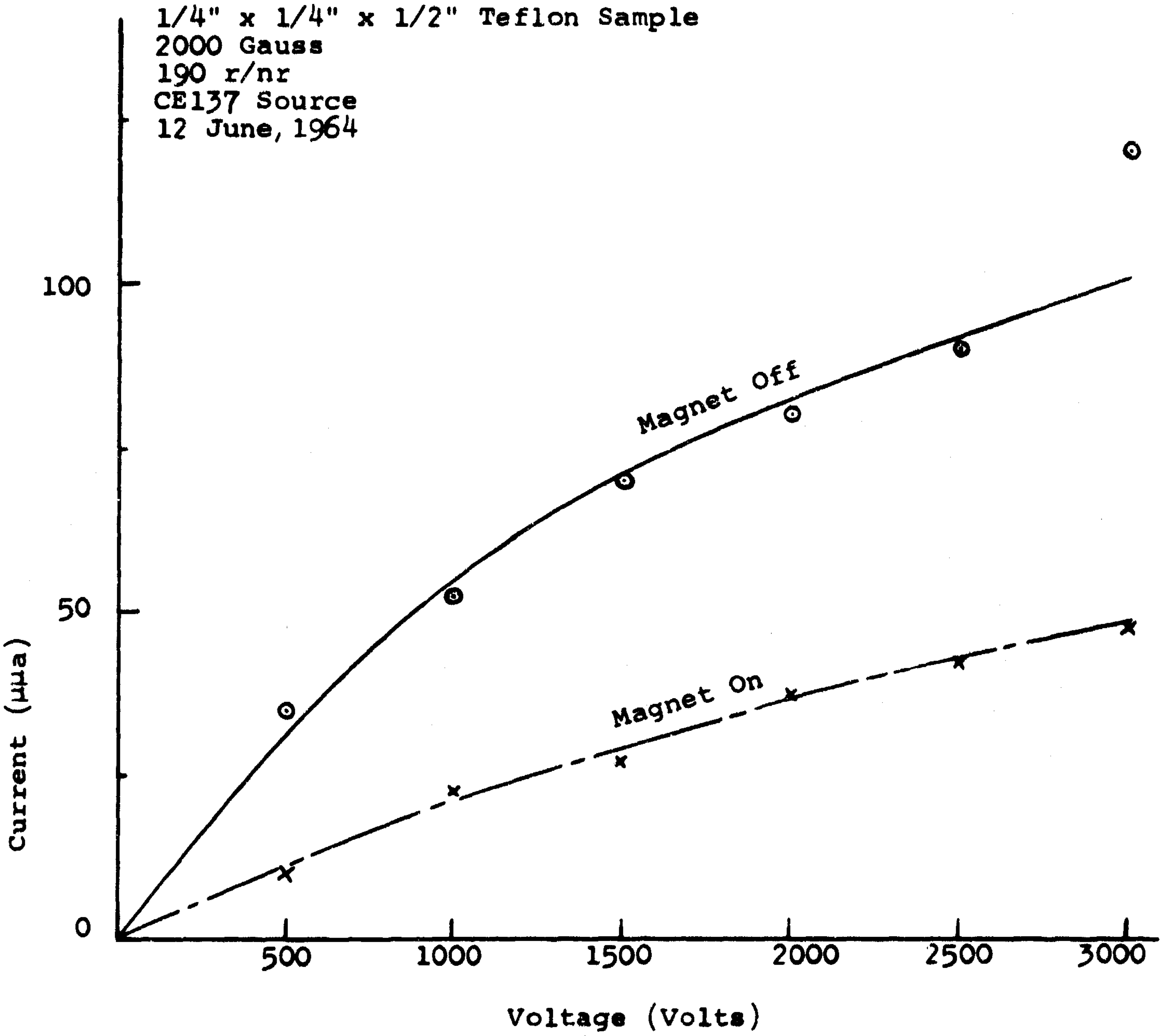

Figure 49. Curve of Current Versus Voltage for Teflon in a 190 r/hr Gamma Ray Environment

A plot of current versus voltage applied to the sample is shown in Figure 50. The calculated conductivity for this sample was 1.01 x 10^{-5} $(\text{ohm-cm})^{-1}$. The value given for conductivity (σ) in the American Institute of Physics Handbook, is $\sigma = 5 \times 10^{-6}$ $(\text{ohm-cm})^{-1}$. The purity of the material was not known in either case. The conductivities depend somewhat on the purity of crystalline materials.

c. Dose-Rate Dependence of Polyethylene

The dose-rate dependence for the polyethylene was found to be in the range given by other experimenters. The current dependence on dose rate is given by

$$i \propto R^{\Delta}$$

The exponent Δ was found to be 0.58 in the 50 to 200 r/hour range.

d. Photovoltaic Effects

When a sample of polyethylene is irradiated at one end with a collimated beam of γ-rays, a voltage appears across the sample. The circuit is shown in Figure 51; there is no applied voltage in the circuit. The polarity of the voltage pulse is always such that the irradiated part of the dielectric becomes negative. This effect was observed on three different sources: the Ce-137, the 200 KV DC X-ray machine, and the flash X-ray machine. This effect occurs because the material is non-uniformly excited with γ-rays. It is a well-known effect in high purity crystal materials using light excitation.

The photovoltaic equation in general is given by

$$V_{ph} = -\frac{KT}{e}\int_{\Delta n \Delta p}\left[\frac{\mu_h dP - \mu_n dn}{\mu_h P + \mu_n n}\right] \tag{141}$$

where

K = Boltzmann constant

e = Electronic charge

P = Hole density

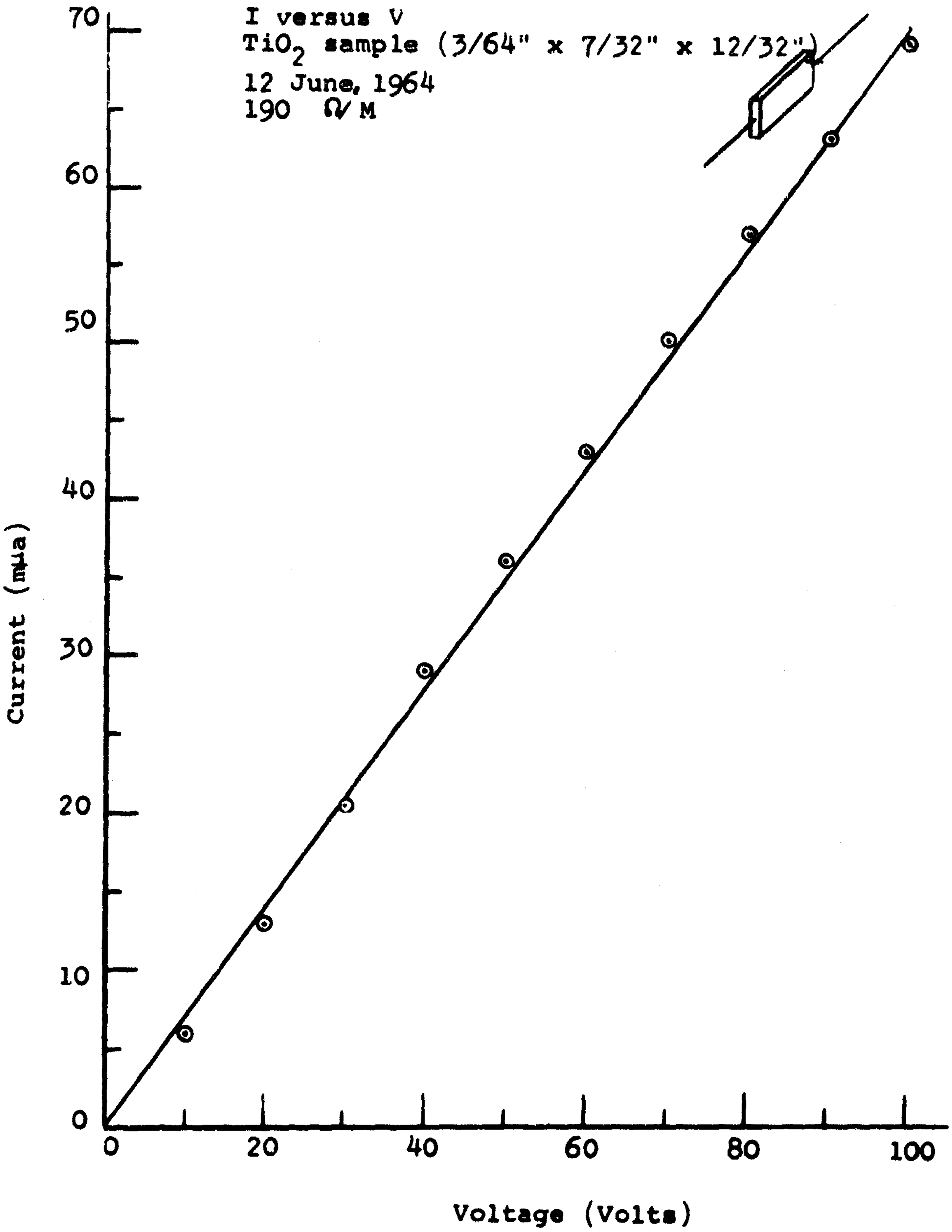

Figure 50. Plot of Current Versus Voltage for TiO_2

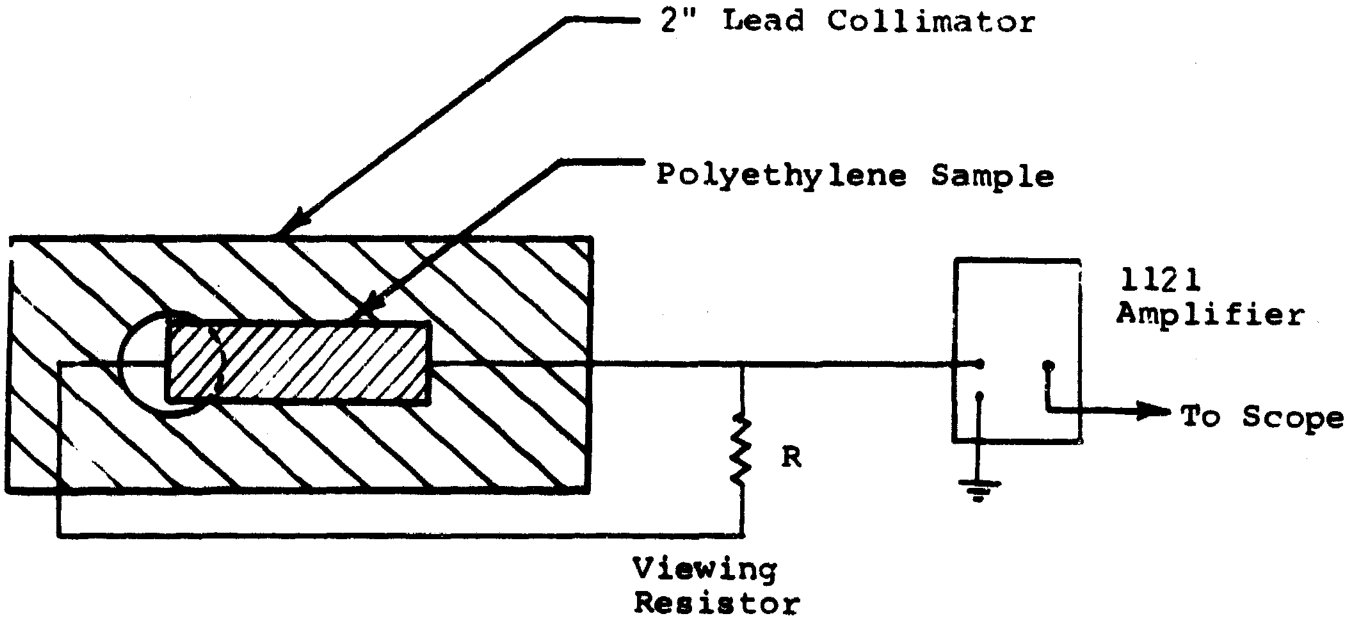

Figure 51. Photovoltaic Experimental Circuit

Since the distribution of carriers inside the sample is not known, this formula is not too helpful.

A 1/4" x 1/4" x 1/2" sample produced about 20 microvolts when one half of the sample was irradiated at the Ce-137 source with a dose rate of 190 r/hr. A similar experiment was performed on the 250 KV, 15 ma DC X-ray machine at a dose rate of 5 r/sec. The photovoltage was about 1 millivolt in this case. Corrections were made for cable pick-up in each case.

The same experiment on the flash X-ray at dose rates of 5×10^5 gave a peak pulse of about 1 mv. The flash X-ray beam was found to be nonuniform over the cone of radiation. At 20.35" from the X-ray target the beam was found to vary as shown in Table XI.

Table XI. Dose Measurements of the 400 KV Flash X-Ray Pulse at 20.35 Inches from Target and at Various Positions across the Beam

Position across beam	R Milli-roentgen	% of Center Value
Center	33	100
1" Off Center	29	88
2" Off Center	28	83
3" Off Center	10	28.7

A polyethylene disk 3 11/16" is diameter and 1" thick was irradiated in the flash X-ray. There was a 7/8" hole in the center as shown in Figure 52. Due to the nonuniformity of the X-ray beam there should be a photovoltage built up with the outer electrode becoming positive. This was observed when the

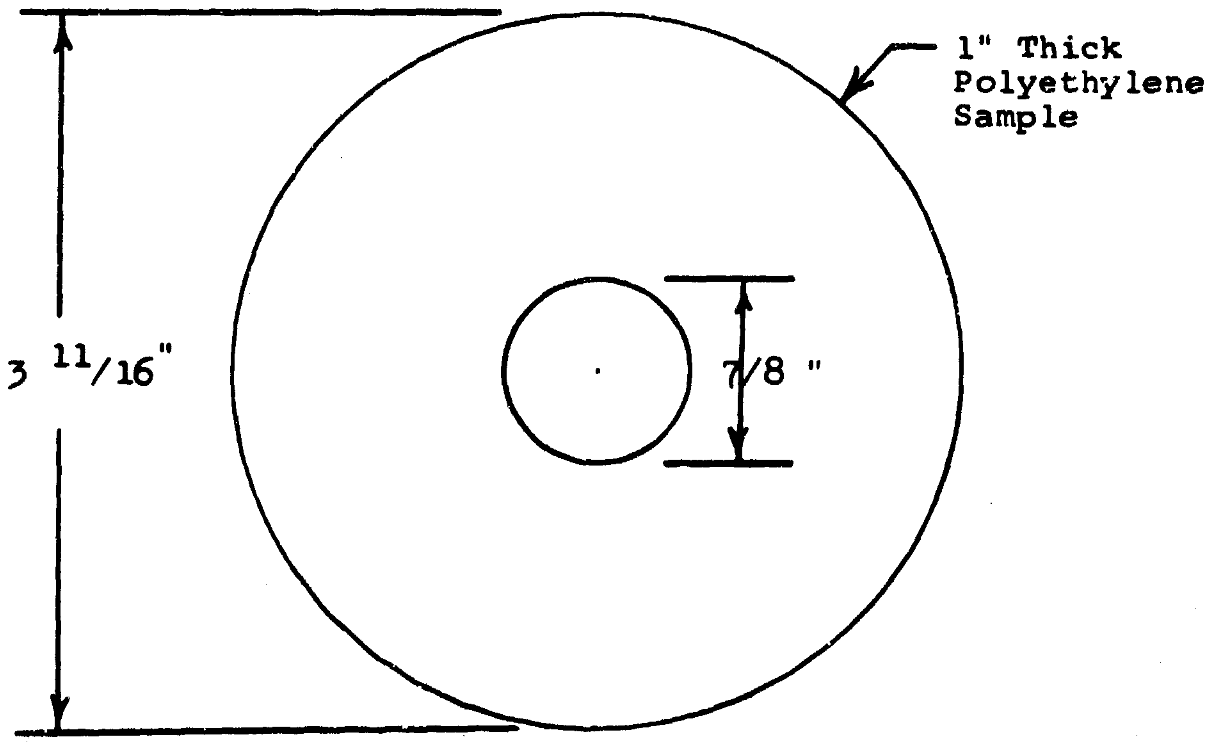

Figure 52. Polyethylene Disk

center was grounded and the outer electrode connected to a viewing resistor as shown in Figure 53(a). A 2 millivolt peak signal was observed on the first shot, with the peak signal getting larger with each successive shot. On shot 5 the peak pulse was 7.5 mv. When the outer electrode was grounded (Figure 53(b)) a small negative pulse was observed at the center electrode.

These results indicate there is a build-up of polarization in the sample. It had not been irradiated before. This build-up has been observed in cables by other investigators who have found that it continues until about a 1000 R total dose has been absorbed, after which no further increase is observed.

This photovoltage may explain the pulse observed by other investigators in experiments where they obtained a pulse with no applied voltage and the device received nonuniform irradiation.

e. Leakage Conductivity of a Parallel Plate Polyethylene Capacitor

In an experiment with a parallel plate capacitor arrangement (Figure 54) the capacitor was charged to 200 volts and then the battery removed. When irradiated uniformly with a 400 KV X-ray shot, the observed pulse had a very long decay time. This suggests that charge carriers are being released from traps. After several milliseconds the monitoring electronic system would not follow the pulse; the decaying current pulse is shown in Figure 55. The capacitor size was .35" x .25" x .175".

f. Air Ionization Effects in the Flash X-Ray Experiments

The Hall effect measurements were not successful in the flash X-ray experiments because of the many side effects masking the desired pulse. Also, the instrumentation problems were much greater with the transient measurements than in the steady state experiments. For the size of samples used the induced currents were calculated to be in the nanoampere range. The largest unwanted side effect was air ionization. Since this effect is observed in circuit experiments as well as experiments on components, it was studied in some detail. A high vacuum does not entirely eliminate the effect; it only reduces it.

(a)

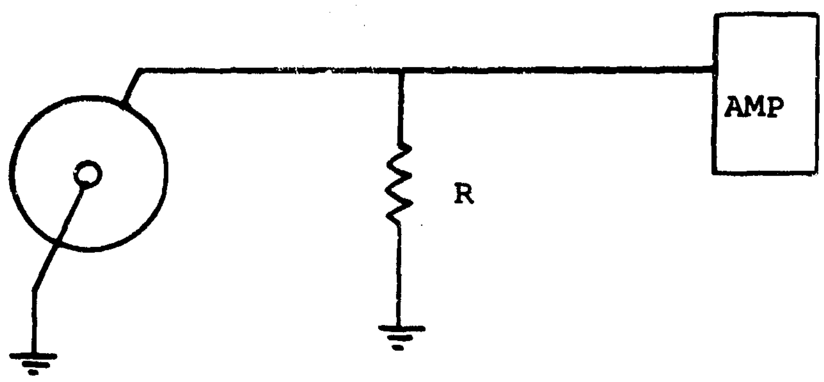

(Grounded Center Electrode)

(b)

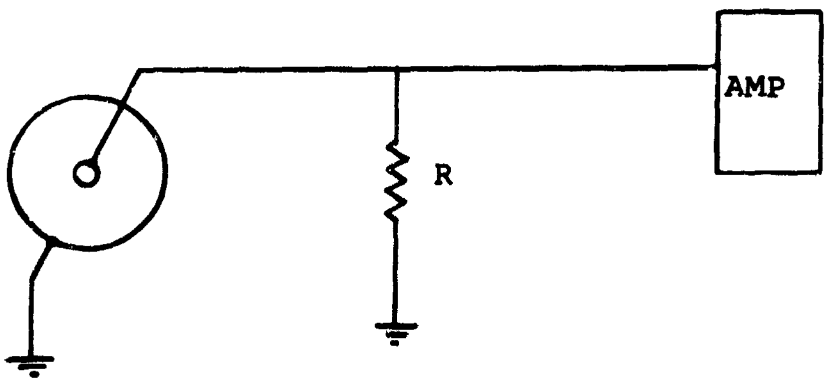

(Grounded Outside Electrode)

Figure 53. Photovoltaic Experiment Circuit
with Polyethylene Disk

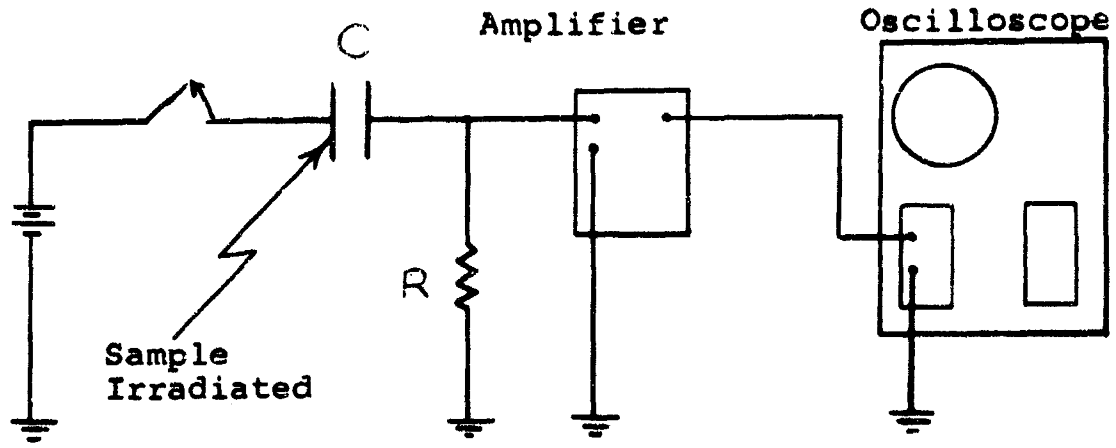

Figure 54. Circuit for Measuring the Leakage Conductivity of a Parallel Plate Capacitor

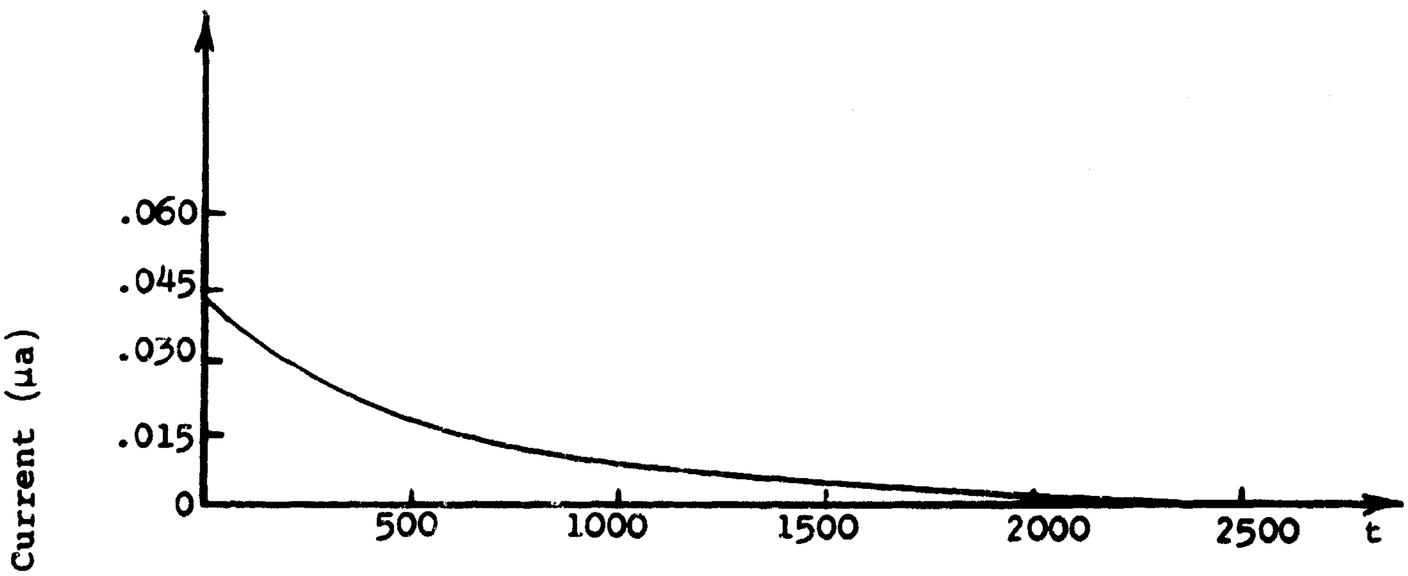

Figure 55. Parallel Plate Capacitor Leakage Current Decay Curve

A parallel plate capacitor was used with air as the dielectric. The separation of the plates was about what the distance between leads would be for circuit components. The circuit arrangement is shown in Figure 56. Here, two 1 centimeter square copper plates are separated a distance of 1 centimeter. They were irradiated by the 400 KV flash X-ray 0.2 μsec gamma pulse at various pressures inside a vacuum chamber. The results are shown in Figure 57. These pulses were traced from Polaroid pictures of the oxcilloscope traces and put on one plot for easier comparison at the different pressures. The initial time constant was a function of the measuring circuit and is approximately 2 microseconds. The long tails are observed between pressures of 200 mm Hg and about 1 mm Hg. They are explained by the "attachment time" of electrons to oxygen molecules in air. This phenomenon of the variation of attachment times of electrons to oxygen molecules in air as a function of pressure, and in a gamma radiation environment, is covered in detail in Section I of this report.

The creation of an electron-ion pair in air requires about 32 ev of energy. The absorption coefficient for air is 0.0157 cm^2/g for 400 KVP gamma rays. When calculations are carried out for currents resulting from the shunt leakage path due to air ionization across components, they are in the microampere range which agrees with the experimental results obtained. The general procedure for calculating the RIC in air is as follows: The energy of the gamma ray beam in ev/cm^2 is multiplied by the absorption coefficient of air. This yields the energy absorbed in air. Then energy absorbed is divided by 32 ev to get the electron-ion pairs created. Another approach was used in Section I of this report.

The ions created by the X-ray pulse do not gain much energy for the ratio $E/p < 10$, where E is the electric field across the plates and p is the pressure in mm Hg. For values of the ratio, E/p, greater than 10 the ions gain energy, which explains the

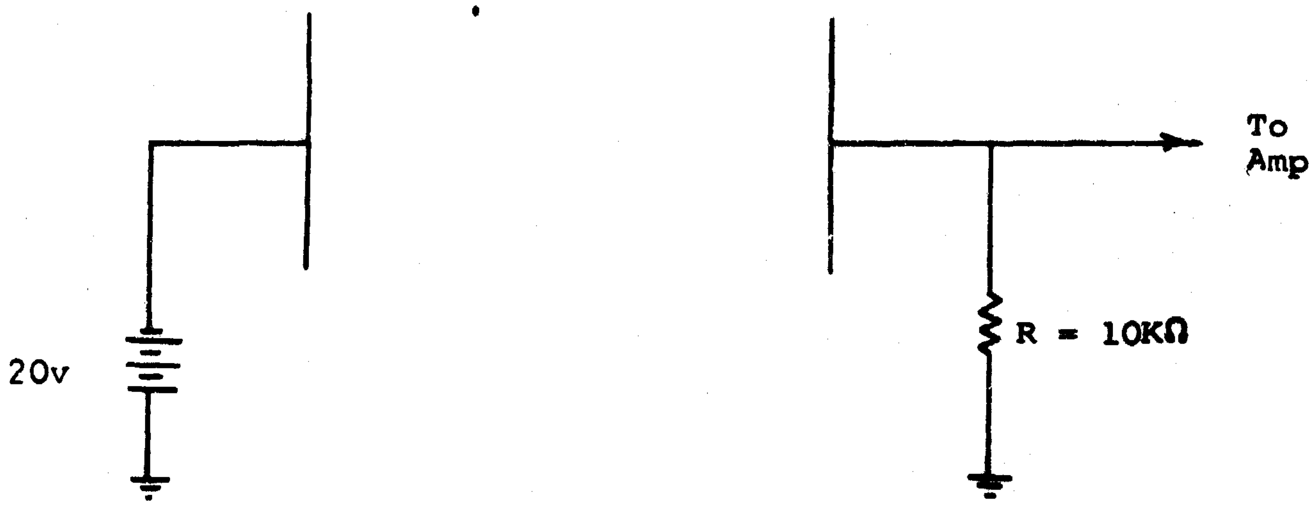

Figure 56. Circuit for Air Ionization
Effects Study

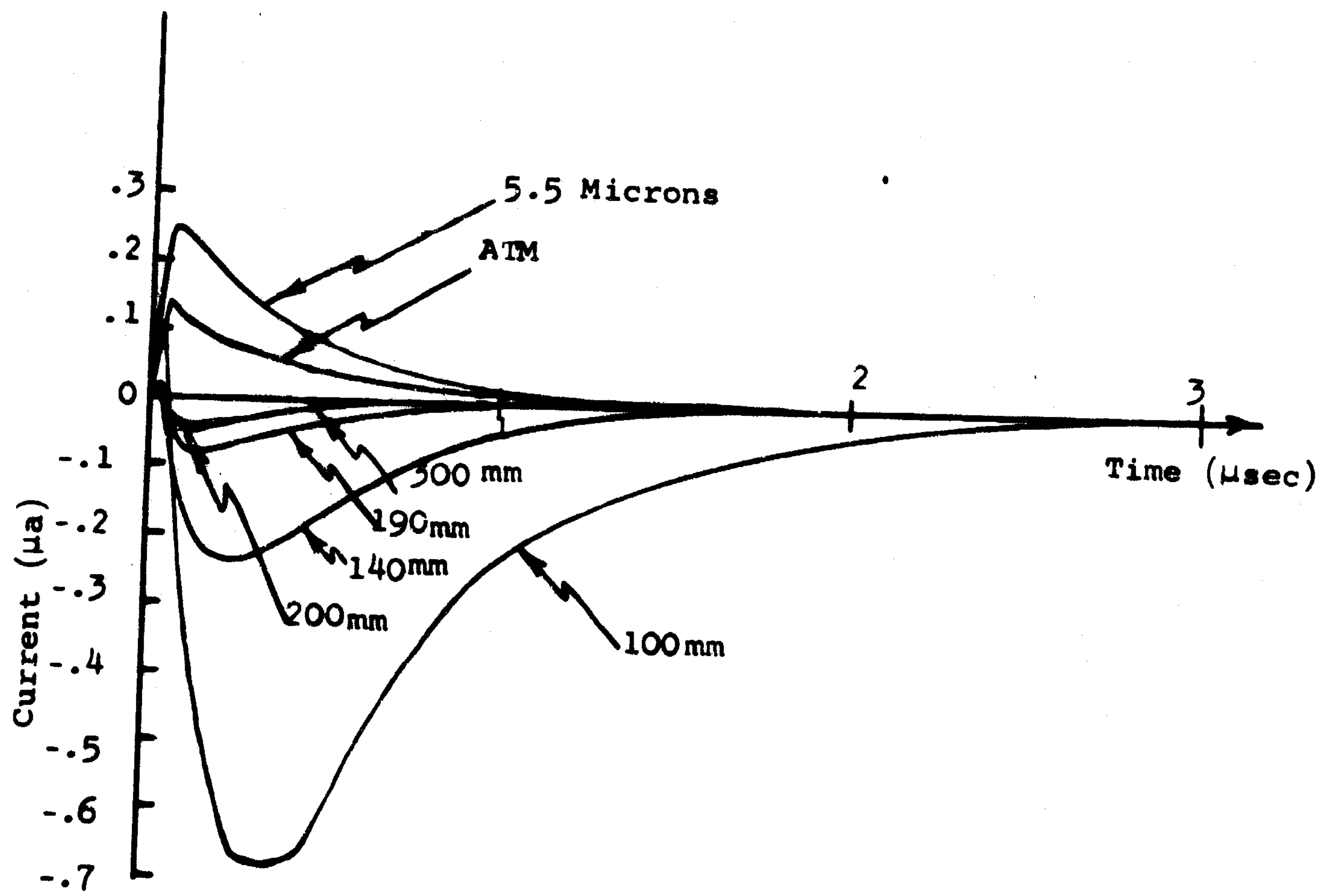

Figure 57. Observed Current Pulses for Parallel Plates with Air Dielectric at Various Pressures (10KΩ Viewing Resistor, 20v Bias Voltage)

fact that the tails get shorter when the potential gradient is increased. If the voltage pulses for pressures of 300 mm Hg to 100 mm Hg are observed (Figure 57), one sees that they first go positive and then negative. The initial positive pulse is due to injection current (i.e., electrons flowing from ground through the 10 K viewing resistor to replace those knocked off as secondary electrons from the plate). A space charge is set up between the two plates. When the electrons return to the plate due to the potential gradient and the fact that the electrons have not yet combined with oxygen molecules in the air, the pulse goes negative. At atmospheric pressure and pressures below 10 microns the pulse stays positive. This is because the attachment times of the electrons to oxygen molecules are much shorter at atmospheric pressure and the mean free path is much longer at low pressures.

When the polyethylene sample is placed between the plates similar pulses were observed. A 1/8" x 1/4" x 1/2" polyethylene sample was used. The observed induced current caused by the ionizing X-ray pulse can be explained as being entirely due to air ionization, secondary emission, circuit matching impedance and time constants, and space charge effects. This also appears to be true of other circuit components of similar size, such as resistors and, possibly, diodes and transistors. The temperature also has an effect on the pulse shape. At higher than room temperatures the pulse sometimes went positive again after being negative.

The negative-going pulse was not observed when a smaller viewing resistor (100 Ω) was used. With this 100 Ω viewing resistor the circuit time constant was much less than the observation time and the resulting pulses are shown in Figure 58. These curves were also traced from Polaroid pictures of the pulses and put on one plot for easier comparison. The long tails are again explained by the attachment time of electrons to oxygen molecules. The initial pulse follows the X-ray pulse and is a combination of currents from secondary emission replacement current, RIC, and space charge effects.

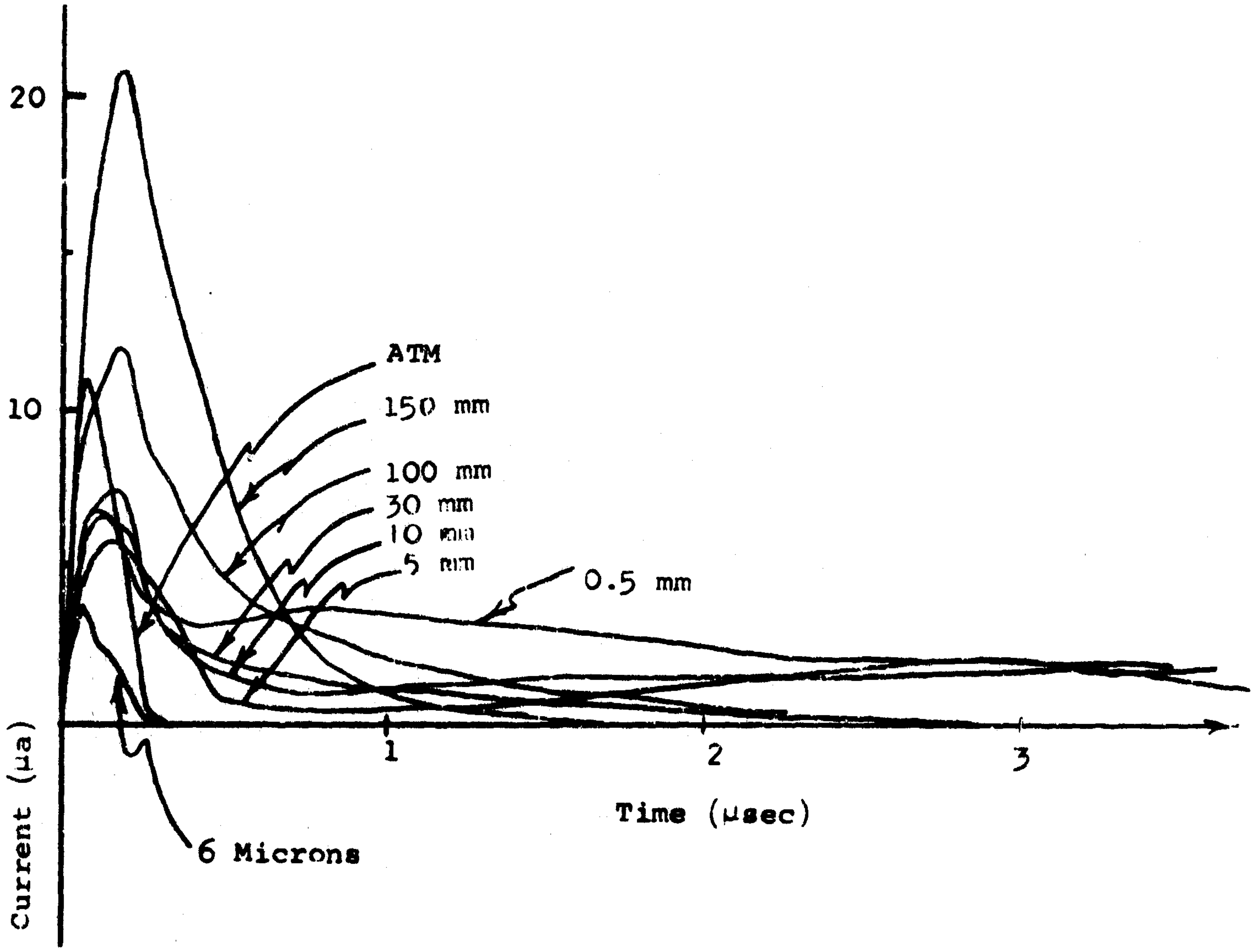

Figure 58. Air Ionization Effects Around a Polyethylene Sample at Various Pressures (100 Ω Viewing Resistor, 315 V Bias Voltage)

The peak current as a function of pressure is shown in Figure 59. This curve is for the polyethylene sample. The maximum air effect can be seen to occur around 150 mm Hg. This was the same point that was found for resistors by H. T. Cates.

An equivalent circuit of the parallel plate capacitor arrangement is shown in Figure 60.

For the size of the polyethylene sample used here the value of C was a few $\mu\mu$f and the leakage resistance through the material was of the order of 10^{12} ohms. The calculated induced current in the material was $\sim 10^{-9}$ ampere, which would not be observed on the viewing resistor of 100 ohms. The shunt air resistance is of the order of megohms.

The same two parallel plates were placed in the constant gamma radiation beam of the Ce-137 source. The currents observed due to air ionization as a function of voltage are shown in Figure 61. The lower curve was in a transverse magnetic field of 2000 gauss. Thus, there appears to be some magnetoresistance effect in air at these currents levels.

g. <u>Correlation of Flash X-Ray Experiments with the Ce-137 Gamma Source Experiments</u>

Two types of samples were prepared for irradiation in both the flash X-ray and the Ce-137 gamma source. These were thin film parallel plate capacitors made of .008 inch mylar film and 0.005 inch polyethylene film. However, the mylar samples had different electrode material. The samples' dimensions were such that the predicted currents under irradiation in the flash X-ray were in the microampere range. Microamperes could be read out with the instrumentation system used, but any current less than a microampere would produce signals near the noise level.

(1) Polyethylene Film Capacitor

The capacitor was made with a 2 inch wide strip of .005 inch polyethylene 16 inches long. A guard ring was made around the center electrode which was made of aluminum foil. The ground electrode was made of silver paint. The sample was bent

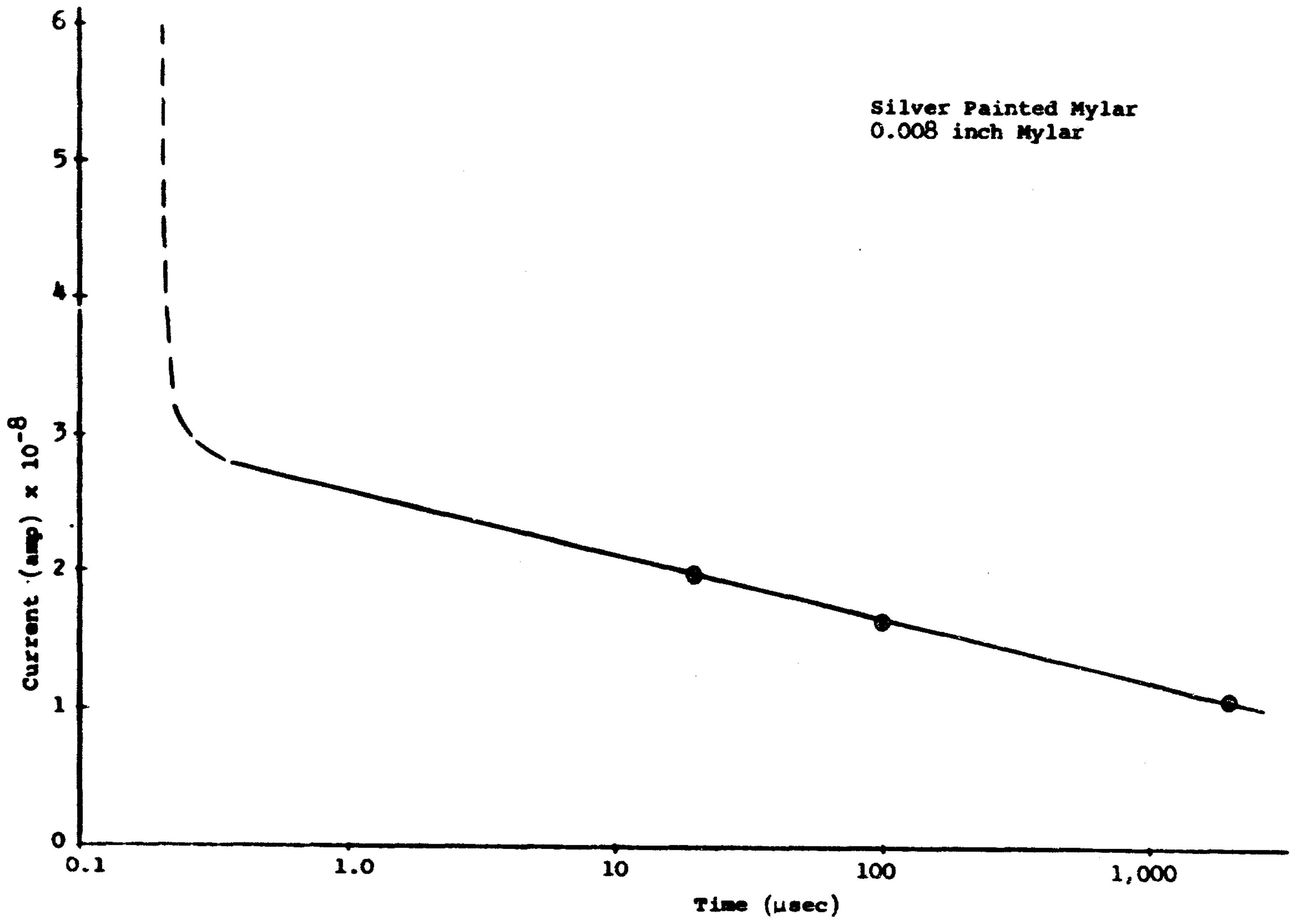

Figure 59. Peak Currents as a Function of Pressure

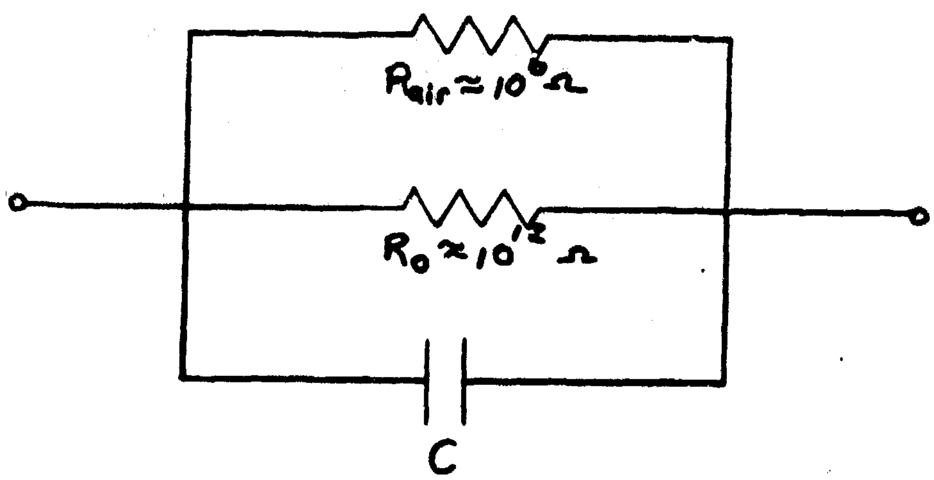

Figure 60. Equivalent Circuit for the Parallel Plate Capacitor in a Radiation Environment

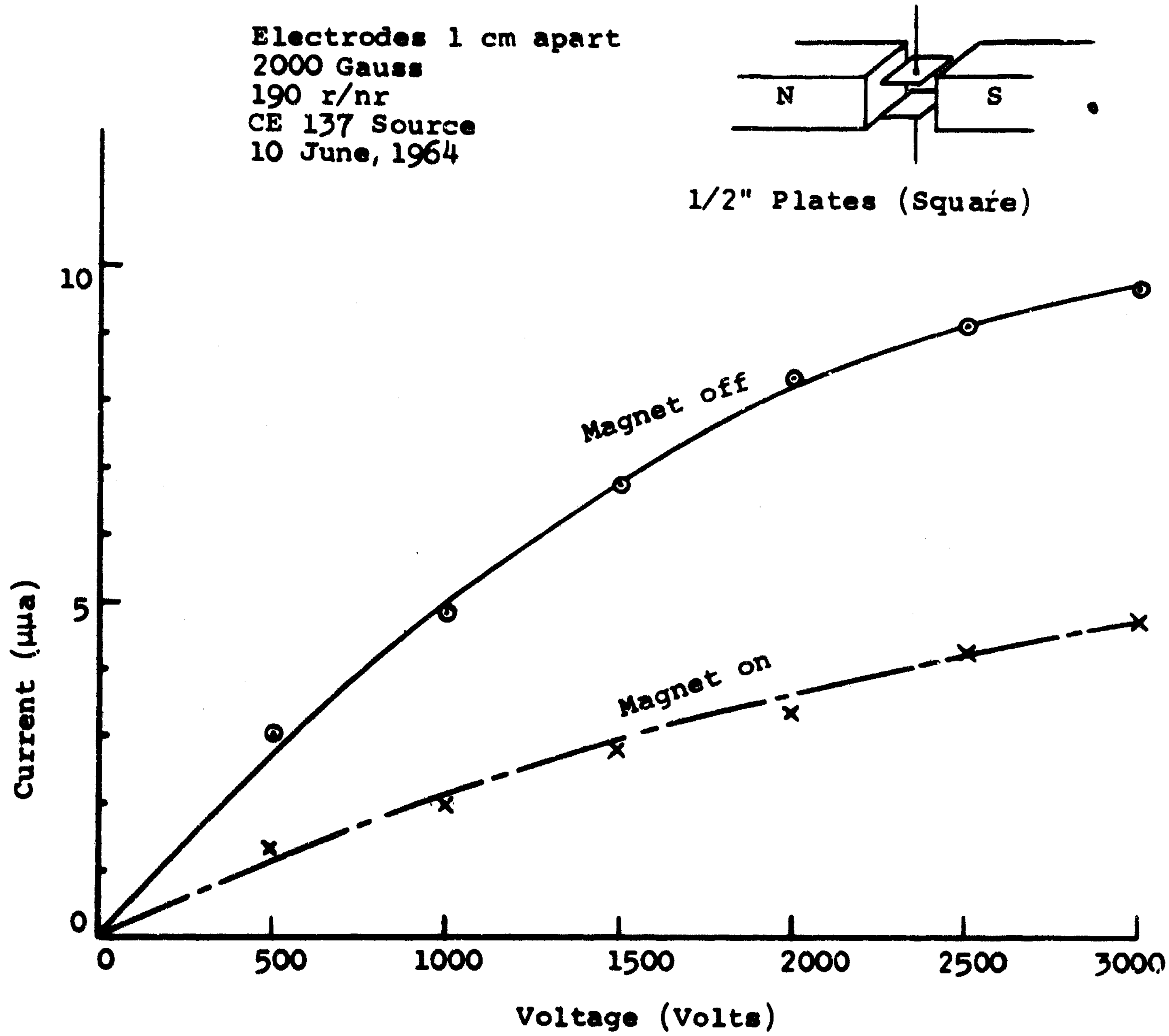

Figure 61. Air Ionization Effects - Steady State

in the form of an accordion bellows to reduce the exposure area in the flash X-ray beam. The results of the irradiation in the Ce-137 source are shown in Figure 62. The same sample was irradiated in the flash X-ray. The observed current pulse followed the shape of the X-ray pulse. The maximum value of current was 60 microamperes using a bias voltage of 22 1/2 volts. The guard ring voltage was 16 1/2 volts. The resistivity was calculated for the different dose rates and the results are shown in Table XII.

Table XII. Resistivities at Different Dose Rates for Film Polyethylene

Dose Rate	Resistivity (ohm-cm)
1.59×10^{-2} r/sec	2.7×10^{15}
2.78×10^{-2} r/sec	1.72×10^{15}
6.52×10^{-2} r/sec	1.33×10^{15}
1.5×10^{6} r/sec	3.05×10^{10}

(2) Mylar Film Capacitor

Two mylar parallel plate capacitors were built. One had indium evaporated electrodes and the other had silver painted electrodes. The film was 0.008 inch thick. The surface area was 24 square inches. The capacitors were constructed with a guard ring and positive electrode sandwiched between 2 pieces of dielectric. The ground electrodes were on the outside of the sandwich as shown in Figure 63.

The capacitance of this type of construction was less than that for the polyethylene capacitor. It was about 1000 μμ farads. The results of the Ce-137 experiments are shown in Figures 64 and 65. The sample with the indium evaporated contacts had about

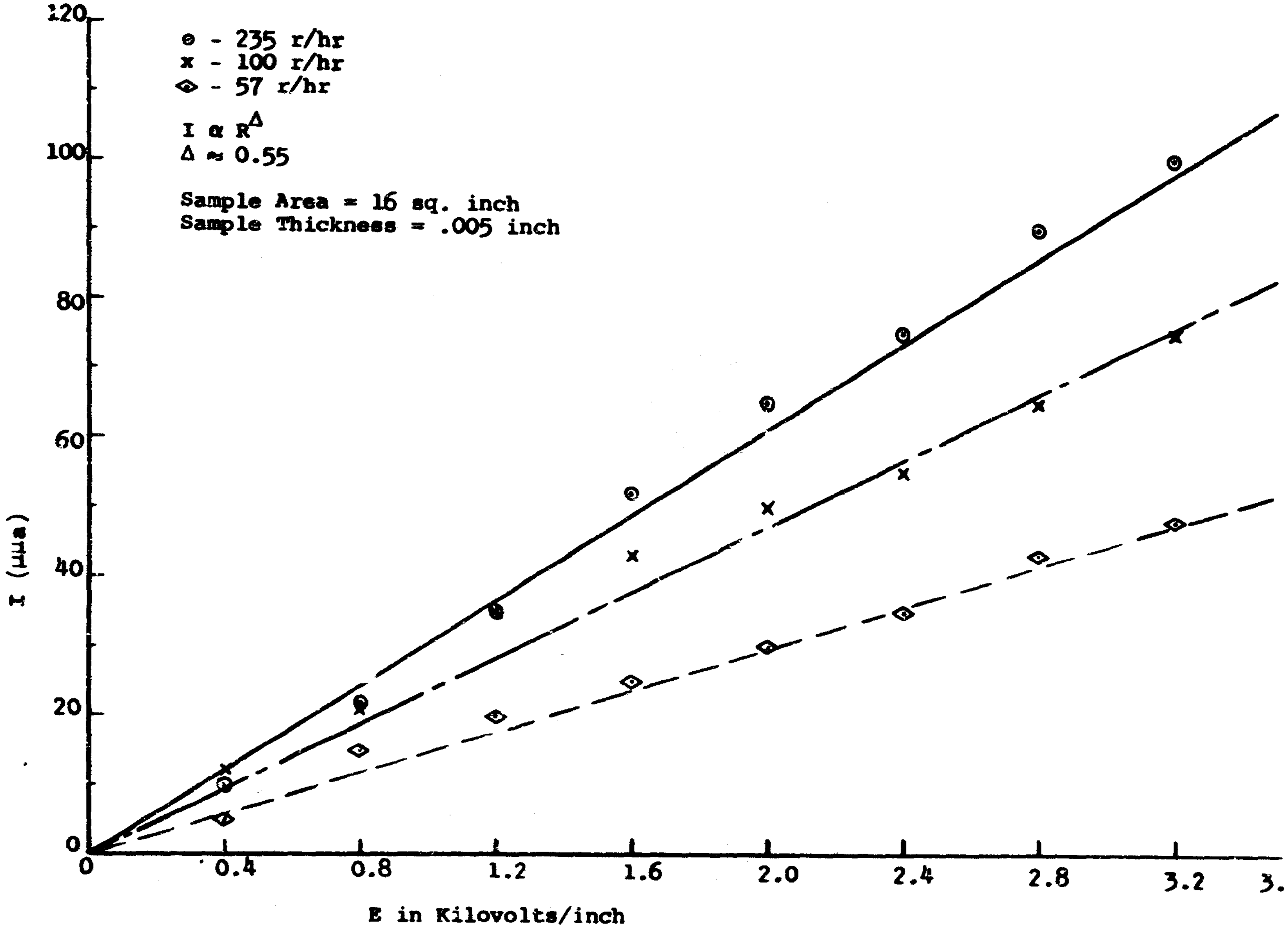

Figure 62. Current Versus Voltage for a Polyethylene Thin Film Capacitor

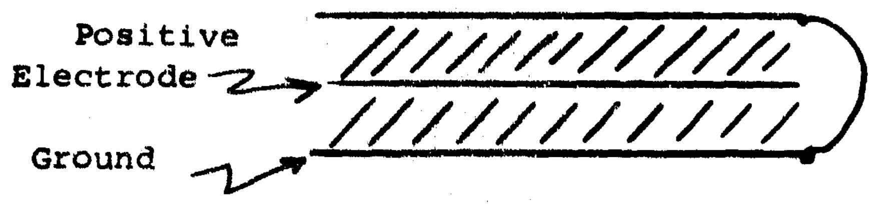

Figure 63. Mylar Film Capacitor

2 and 1/2 times less resistance than the one with the painted contacts. Table XIII shows the values of resistivity for mylar as measured at the various dose rates. These values are found to be in the range given in Table VI for conductivity, which is the reciprocal of resistivity.

Table XIII. Resistivity of Film Mylar at Various Dose Rates

Dose Rate r/sec	Resistivity ohm-cm
6.4×10^{-3}	4.87×10^{16}
1.4×10^{-2}	2.36×10^{16}
2.7×10^{-2}	9.26×10^{15}
4.3×10^{5}	2.28×10^{11}

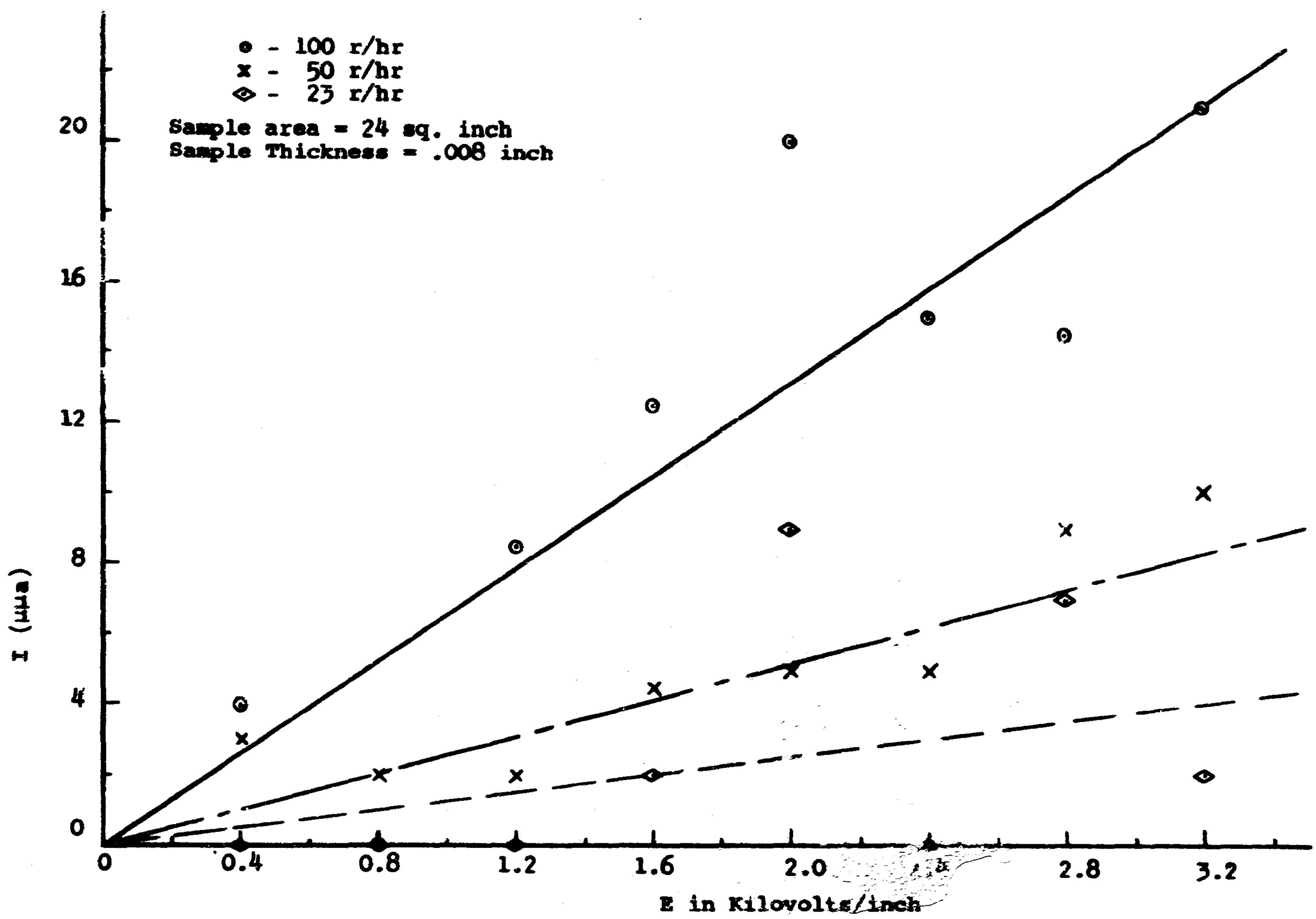

Figure 64. Current Versus Voltage for an Indium Electrode Film Parallel Plate Mylar Capacitor in a Gamma Radiation Environment

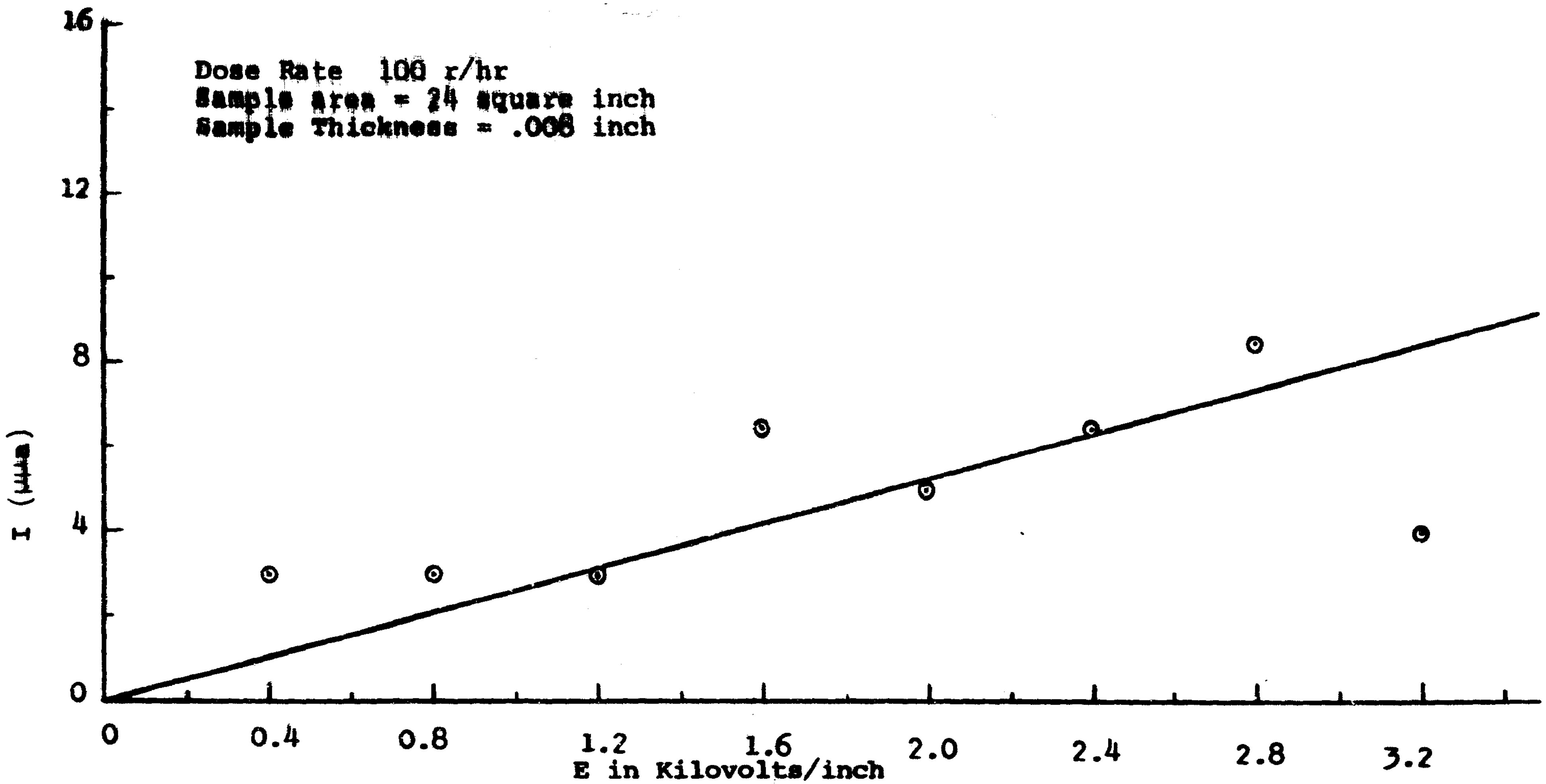

Figure 65. Current Versus Voltage for a Silver Electrode Film Parallel Plate Mylar Capacitor in a Gamma Radiation Environment

The currents were measured using a 10 ohm viewing resistor in the circuit of the flash X-ray experiments. The circuit is the same as that shown in Figure 56 except that the battery has a bypass capacitor for the AC pulse. The total charge generated by the X-ray pulse was also measured by using a 1 megohm viewing resistor. This made the circuit time constant long compared to the pulse time, and the change in voltage across the capacitor plates could be observed. The charge is then obtained from the equation

$$q = CV$$

This value of charge was then used to check the current values measured with a 10 ohm viewing resistor. They checked very well. The charge transferred across the capacitor in one 400 KV flash X-ray pulse at a dose rate of 4.3×10^5 r/sec was 11.9×10^{-14} coulomb.

The Ce -137 source experiments were performed at atmospheric pressure using the guard ring technique to eliminate surface currents. The flash X-ray experiments were performed both at atmospheric pressure and in a vacuum of about 10 microns. The currents were almost identical. The currents obtained in the vacuum were just slightly less. The difference in current readings was within experimental error.

The long tail of the RIC induced pulse was also observed for the silver painted mylar sample when irradiated with the flash X-ray. This tail is shown in Figure 66. This indicates trapping is involved in the process of returning to equilibrium after the X-ray pulse. It is of interest that this tail is of the same order of magnitude as that observed for the leakage conductivity of polyethylene in part 6.e. Figure 55.

7. Summary and Conclusions

Some of the characteristics of insulators have been reviewed to give a basic understanding of their relation to radiation effects. The largest bulk radiation effect observed was RIC

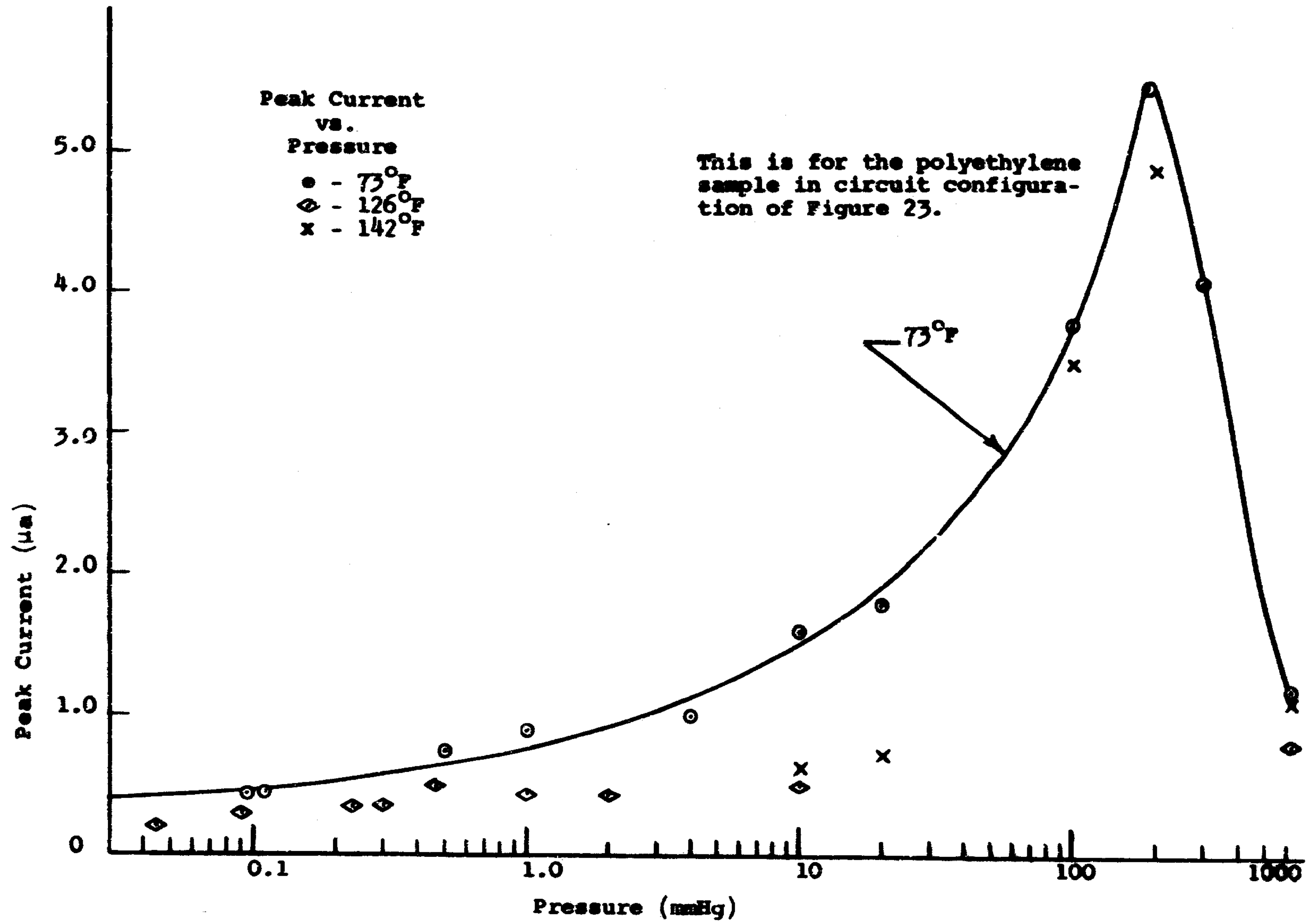

Figure 66. The Long Tail Observed in Mylar After the Flash X-Ray Pulse

(radiation induced conductivity). Air ionization is a significant effect around high impedance components in a circuit which is exposed to the air.

The Hall effect method and magnetoresistance method were developed to measure the mobility of polymeric materials. It was found to be around 10^{-3} $cm^2/v\text{-}sec$ for polyethylene and slightly less than this for mylar. The positive Hall coefficient observed indicates the charge carriers are holes. From a literature survey the conduction process was found to be electronic and not ionic.

The number of carriers produced was found to be directly proportional to the amount of radiation absorbed. The mechanism of charge transport in polymers is not yet completely understood, and a completely satisfactory model has not yet been established. It appears that some combination of the band model and "hopping" model might apply.

In order to predict the amount of RIC, the number of charge carriers must be known. This requires a knowledge of the material composition, absorption coefficients, density, geometry, and intensity, as well as the type of radiation. This is a complicated problem for any but the most simple geometry and controlled environment. This is why empirical equations have been resorted to. The difficulty in using these empirical equations is that all the constants must be known for the material and geometry.

The effect of different contact materials on dielectrics under irradiation was found to give some variation in RIC. Parallel plate capacitors made with evaporated indium electrodes had 2 1/2 times greater RIC than ones made with painted silver electrodes. There was no observed RIC in TiO_2 capacitors.

A photovoltaic effect is observed when materials are not uniformly irradiated.

The directional study indicated only a slight difference in RIC in a polyethylene sample when irradiated from different directions. These differences can be related to the amount of energy absorbed in the material.

The maximum air ionization effect was found to be at a pressure of 150 mm Hg. The RIC in air increased with decreasing pressure to about 150 mmHg and then decreased until the pressure was around 10 microns. It remained constant at pressures below 10 microns. This was in agreement with what has been found for resistors. Below 10 microns the RIC was about 1/3 that at atmospheric pressure.

A guard ring on the film capacitors was found to reduce the air ionization effect at atmospheric pressure to approximately that of 10 microns Hg.

This page intentionally left blank.

SECTION VI

ALTERNATING CURRENT BRIDGE METHODS IN TRANSIENT RADIATION EFFECTS STUDIES

By L. T. Boatwright

1. Introduction

Much effort and many ingenious instrumentation schemes have been pursued in transient radiation effects studies, the principle objective being the determination from various component responses exactly which of the several basic electrical properties are being affected (References 39 and 40). For example, in a capacitor, the electrical quantity C is quite dependent on the dielectric constant and conductivity of the insulating materials. Responses of active components, such as semiconductors, to transient radiation are more complex because charge carrier generation, carrier lifetime and mobility are drastically affected (Reference 8). It is well recognized that external air ionization (and internal, depending on the component) has an important effect on the operational performance of the part.

2. Experimental Work

As shown in Appendix III, a Schering bridge network for measuring capacitance is relatively insensitive to changes in conductivity. The relationship describing the magnitude of changes is

$$\frac{\delta C}{C} = \tan \theta \frac{\delta R}{R} \qquad (142)$$

where θ is defined as the loss angle (very small for high quality capacitors), and C and R are the effective capacitance and series loss resistance, respectively, of the test item. Thus, a change in conductivity as seen by the bridge is suppressed by the tan θ factor; whereas a capacitance change should be evidenced by bridge unbalance, the magnitude of which is controlled by relationships between the other bridge arms.

Experiments were conducted at the Air Force Weapons Laboratory TREES facility on a limited number of components including mica capacitors, resistors, general purpose diodes and miniature transistors. The facility utilizes a Fexitron X-ray system capable of delivering a 0.2 microsecond pulse up to 600 KVP. Radiation exposure rate utilized in the experiments described was approximately 0.65×10^6 r/sec. The component holding fixture was a general Radio Type 874 Q2 adapter which was connected to an older model, GR Type 916-A RF bridge by 3 feet of RG-58 cable. This is a substitution type bridge utilizing a modified Schering circuit and is rated from 3 to 50 megacycles. Signal source for the bridge was a GR Type 1330-A oscillator, set for maximum output at 20 megacycles ($\approx$9V). The bridge and oscillator were surrounded by lead shields ranging from 1/2 to 2 inches thick. Bridge output was recorded on a Type 555 Tektronix dual beam oscilloscope connected to the output of the Tektronix Type 1121 amplifier, which was in turn connected to the bridge by 15 feet of RG-8 coax cable. Sensitivity of this arrangement is limited by amplifier noise, typically about 50 microvolts. Inclusion of 3 feet of RG-58 cable in the bridge arm causes some balancing problems because of the added capacity.

Certain tests were made to determine pickup when the flash X-ray unit was pulsed. These included the RG-58 cable alone in the bridge circuit, with a shorted and open test fixture, with 2 inch lead blocks between test fixture and radiation source and gamma pulsing with and without the test items in place.

3. Test Results

Qualitative results only are reported since the bridge experiment was preliminary and further consideration must be given to calibration details, transient response of the recording system, and data analysis.

Figures 67 through 69 are responses of a 20 μμf disk capacitor, 50 μμf and 100 μμf mica capacitors respectively at room temperature. The lower trace is the output of the plastic scintillator-photo-diode X-ray monitor described in Reference 41, and

closely follows the actual shape of the gamma pulse. The middle trace is bridge output at null taken a few minutes before firing the pulser. The top trace is bridge output during irradiation and occurs at the same time as the lower pulse on the dual beam oscilloscope. The scope is triggered by the lower pulse.

Displacement of the upper trace during irradiation is not bridge unbalance, but can be attributed to a form of replacement current (Reference 8), although the possibility of external pickup cannot be completely ignored.

Figure 70 is the bridge output when a 1N604 Silicon Diode (rectifier) is pulsed. Initial displacement of the bridge output indicates the creation of excess charge carriers. The bridge unbalance after X-ray pulse termination indicates a change in effective capacitance because of redistribution of charge across the junction. This decays exponentially in about 10^{-3} second, which roughly corresponds to carrier recombination at a rate determined by the minority carrier lifetime (Reference 39).

Figures 71 and 72 are the collector-base junction responses from a miniature transistor, Type TO-51, manufactured by TRW Semiconductors, Inc. The response of Figure 71 is with the collector grounded, and of Figure 72 with the base grounded. As expected the response is similar to the 1N604 diode and shows excess charge carrier generation initially and a change of junction capacitance after termination of the radiation pulse. The exponential decay exists for approximately 5 milliseconds.

Additional experiments are planned in order to obtain qualitative data and to resolve what may be small interference during the X-ray pulse. For this purpose new equipment is on order and should enable acquisition of data up to a 50 megacycle signal input to the bridge.

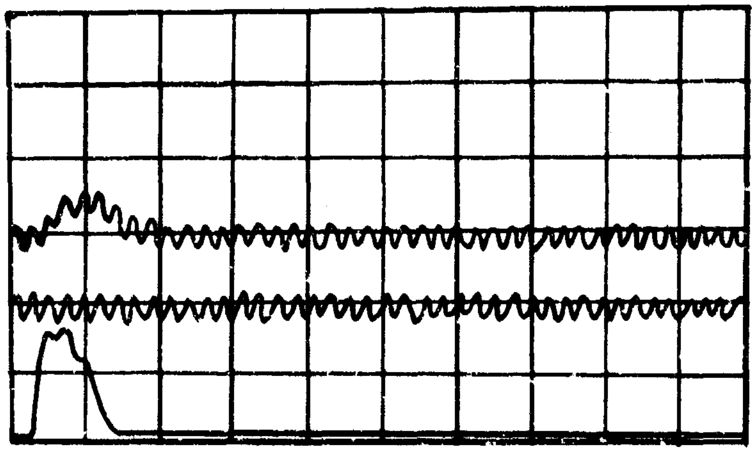

Figure 67

Response of a 20 $\mu\mu f$ Disk Capacitor to X-Ray Pulse

Lower Trace:	X-Ray Monitor Output $\approx 0.6 \times 10^7$ r/sec
Upper Trace:	Output from Bridge
Center Trace:	Bridge Null Before X-Ray Pulse
Sweep:	0.2 μsec/division
Vertical Deflection:	(Center and Upper Trace) 0.5 millivolt/division

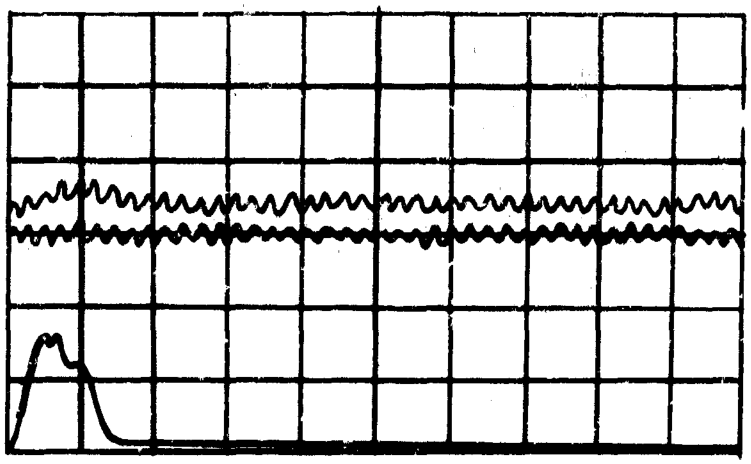

Figure 68

Response of a 50 $\mu\mu f$ Mica Capacitor to X-Ray Pulse

Lower Trace:	X-Ray Monitor Output $\approx 0.6 \times 10^7$ r/sec
Upper Trace:	Output from Bridge
Center Trace:	Bridge Null Before X-Ray Pulse
Sweep:	0.2 μsec/division
Vertical Deflection:	(Center and Upper Trace) 0.5 millivolt/division

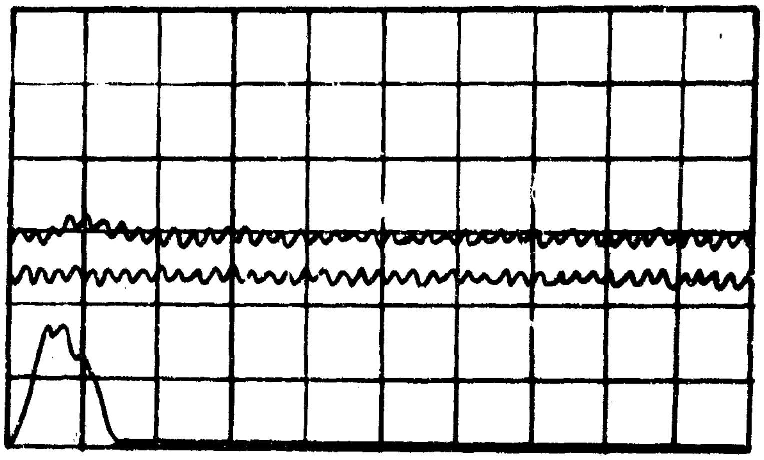

Figure 69

Response of a 100 μμf Mica Capacitor to X-Ray Pulse
Lower Trace: X-Ray Monitor Output ≈ 0.6 x 10^7 r/sec
Upper Trace: Output from Bridge
Center Trace: Bridge Null Before X-Ray Pulse
Sweep: 0.2 μsec/division
Vertical Deflection: (Center and Upper Trace) 0.5 millivolt/division

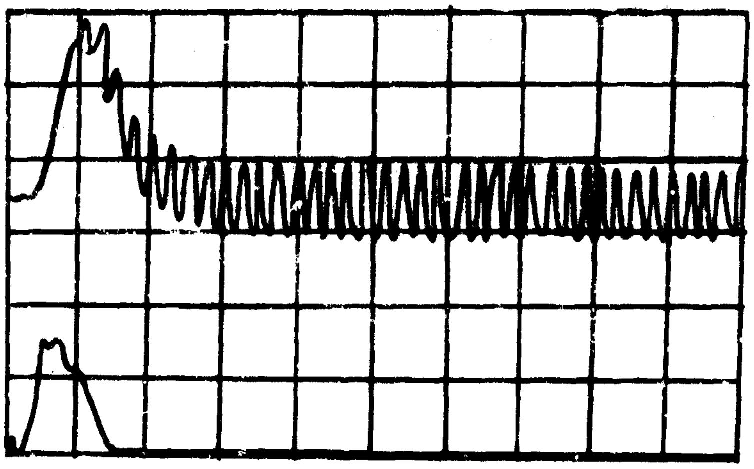

Figure 70

Response of a TI IN604 Silicon Diode to X-Ray Pulse
Lower Trace: X-Ray Monitor Output ≈ 0.6 x 10^7 r/sec
Upper Trace: Output from Bridge
Sweep: 0.2 μsec/division
Vertical Deflection: 0.5 millivolt/division

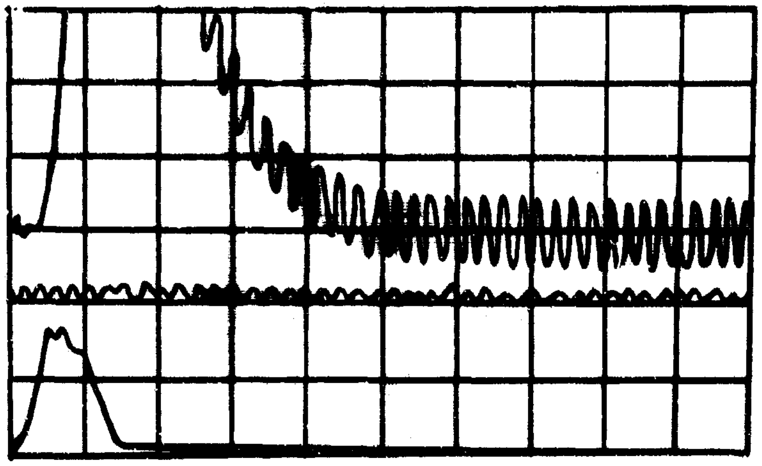

Figure 71

Base-Collector Junction Response
of a Type TO-51 TRW Transistor

Lower Trace:	X-Ray Monitor Output $\approx .65 \times 10^7$ r/sec
Upper Trace:	Output from Bridge
Center Trace:	Bridge Null Before X-Ray Pulse
Sweep:	0.2 μsec/division
Vertical Deflection:	(Center and Upper Trace) 0.5 millivolt/division

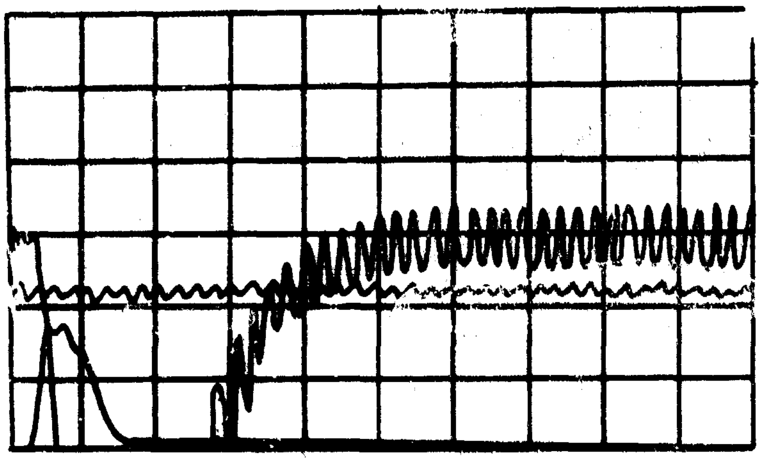

Figure 72

Collector-Base Junction Response
of a Type TO-51 TRW Transistor

Lower Trace:	X-Ray Monitor Output $\approx 0.6 \times 10^7$ r/sec
Upper Trace:	Output from Bridge
Center Trace:	Bridge Null Before X-Ray Pulse
Sweep:	0.2 μsec/division
Vertical Deflection:	(Center and Upper Trace) 0.5 millivolt/division

SECTION VII

A MONTE CARLO CODE FOR TRANSIENT RADIATION EFFECTS

By Wm. J. Byatt and Dale Sparks

1. Introduction

The prompt gamma pulse from a nuclear explosion acts as a source for the generation of Compton and photoelectric electrons within and around the components of electronic circuits. The conductivity of both resistors and capacitors suffers transient changes in rated values because of the release of electrons. It is, in part, our purpose to study the time-dependent changes in conductivity.

A Monte Carlo code has therefore been constructed which will give not only the time-dependenc absorption and scattering of gamma rays, but also the number of electrons generated as a function of energy. The subsequent time-dependent behavior of the electrons can then be discussed by available multiple scattering theories; or crude estimates of the time-dependent behavior of the electrons can be obtained from a knowledge of recombination times within a given material. If the time-dependent behavior of the number of electrons is known, then the conductivity is given by

$$\sigma(t) = \frac{n_e(t)e^2\ell(v)}{mv} \tag{143}$$

where $n_e(t)$ is the number of free electrons per unit volume of charge, e; and of (effective) mass, m; and velocity, v; and whose mean free path is $\ell(v)$. But equation (143) can also be approximated by

$$\sigma(t) \approx n_e(t)\ \tau \tag{144}$$

where τ is a recombination time. If the pulse of gamma rays has passed through the material so that there is no longer any generation of electrons, then it can be crudely estimated that the time

dependent behavior of electrons is given by

$$n_e(t) = n_o e^{-t/\tau} \tag{145}$$

with τ the recombination time. But by equation (144) this means that after the pulse has passed, $\sigma(t)$ should decay according to

$$\sigma(t) = \sigma_0 e^{-t/\tau} \tag{146}$$

if there is single recombination time. If there are several competing processes,

$$\sigma(t) = \sigma_o \Sigma A_i e^{-t/\tau} \tag{147}$$

Again, it is to be stressed that equations (146) and (147) will hold only after the gamma-ray pulse has passed and there is no longer any generation of electrons by Compton scattering or photoelectric absorption of photons. It will be observed that a relation such as equation (147) has been used by workers in the field of transient radiation effects to fit observed conductivity-time behavior (Reference 42).

The above introductory remarks serve to illustrate the importance of having an accurate knowledge of the time-dependent number density of free electrons.

2. <u>Summary</u>

A Monte Carlo code has been constructed which will be used to calculate quantities of importance in transient radiation effects. It is constructed so that the following can be found:

a. The time spreading of the prompt gamma-ray pulse from a weapon; since transient radiation effects are dose-rate dependent, the spreading is of interest.

b. The number of free electrons generated by the prompt pulse; since the free electrons contribute to changes in conductivity, an accurate knowledge of the free electron density is of importance.

In the next few months, the code will be used to accomplish the above program. In this short report, the results of two

problems have been included: one in plane geometry, and the other in spherical geometry, for which some knowledge of the solutions is available. Comparison shows that the code is working properly.

3. The Transport Equation

A code will be described which has been constructed to find $n_e(t)$ by solving the equation

$$\frac{1}{c}\frac{\partial I}{\partial t} + \ell \cdot \nabla I + \sigma_T I = S + \int_{\lambda-2}^{\lambda} k(\lambda' \to \lambda) d\lambda' \int_{\Omega} \delta(1-\lambda + \lambda' - \mu_1) \, I d\Omega' \tag{148}$$

where I is the intensity of photons of speed c in the wavelength range $(\lambda, \lambda + d\lambda)$ at the space-time point (x, t) traveling in a direction whose cosine is denoted by μ; i.e., $I = I(x, t, \mu, \lambda)$. The quantity $\ell \cdot \nabla I$ is geometry dependent, being given by

$$\ell \cdot \nabla I = \mu \frac{\partial I}{\partial x} \tag{149}$$

in plane geometry, and by

$$\ell \cdot \nabla I = \mu \frac{\partial I}{\partial x} + \frac{(1 - \mu^2)}{x} \frac{\partial I}{\partial \mu} \tag{150}$$

in spherical geometry. The notation σ_T stands for the total of absorption (σ_a) plus scattering (σ_s) cross sections; that is, $\sigma_T = \sigma_a + \sigma_s$, where each is to be multiplied by an appropriate density if σ is given in units of cm^2/gm if x is expressed in centimeters. The quantity $k(\lambda' \to \lambda)$ is the Klein-Nishina cross section with λ expressed in units of h/mc. It, too, has dimensions of reciprocal length if x has dimensions of length. The presence of the delta function in the integral on the right-hand side of equation (148) insures that the Compton condition is fulfilled (i.e., that energy is conserved in a scattering event). The source S must have the dimensions of intensity per unit length if ct and x are expressed in units of length.

Whether problems are to be solved in plane or in spherical geometry, one writes

$$\frac{1}{c}\frac{\partial I}{\partial t} + \vec{l} \cdot \nabla I = \frac{dI}{ds} \tag{151}$$

The introduction of (151) requires that the independent variables x, t, μ (and hence λ) are functions of s. The parametric curves x(s), μ(s), and so forth, are known as the characteristics. The characteristics, which change direction on scattering, or terminate with photon absorption are the paths along which the radiation flows.

Since

$$\frac{dI}{ds} = \frac{\partial I}{\partial t}\frac{dt}{ds} + \frac{\partial I}{\partial x}\frac{dx}{ds} + \frac{\partial I}{\partial \mu}\frac{d\mu}{ds} \tag{152}$$

one has, in plane geometry

$$\frac{dt}{ds} = \frac{1}{c}\,;\ \frac{dx}{ds} = \mu;\ \frac{d\mu}{ds} = 0 \tag{153}$$

with the solutions

$$t(s) = t(s_0) + \frac{(s - s_0)}{c}$$

$$x(s) = x(s_0) + \mu(s - s_0) \tag{154}$$

and

$\mu = \mu_0$, a constant

In spherical geometry, the differential equations for the characteristics are

$$\frac{dt}{ds} = \frac{1}{c}\,;\ \frac{dx}{ds} = \mu;\ \frac{d\mu}{ds} = \frac{(1 - \mu^2)}{x} \tag{155}$$

with solutions

$$t(s) = t(s_o) + \frac{(s - s_0)}{c}$$

$$x^2(s) = x^2(s_0) + (s - s_0)^2 + 2x(s_0)\,\mu(s_0)(s - s_0)$$

and

$$x(s)\,\mu\,(s) = x(s_0) + (s - s_0) \qquad (156)$$

With the introduction of the characteristics, the transport equation can now be written

$$\frac{dI}{ds} + \sigma_T I = S + TI \qquad (157)$$

where

$$TI = \int_{\lambda-2}^{\lambda} k(\lambda' \to \lambda)d\lambda' \int_{\Omega} \delta(1 - \lambda + \lambda' - \mu_1)\, I d\,\Omega'$$

The "solution" can then be written as

$$I(s) = I(s_0)e^{-\sigma_T(s-s_0)} + \int_{s_0}^{s} e^{-\sigma_T\,(s-s')} \cdot \left[S(s') + TI(s')\right] ds' \qquad (158)$$

The Monte Carlo code must be constructed so as to provide a direct simulation of equation (158).

4. Description of the Monte Carlo Code

The physical simulation will be described by fixing attention on a problem in plane geometry. The extension to spherical geometry will be clear.

Assume the situation pictured in Figure 73. A source of photons is incident normally on the face $x = o(s = s_o)$ of a slab of material of thickness ℓ.

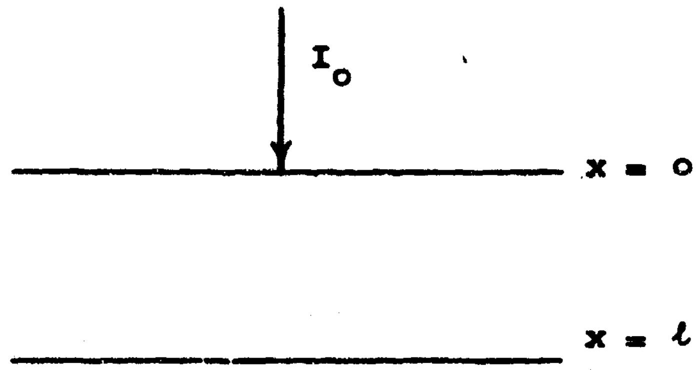

Figure 73. The Geometry for the Scattering and Absorption of Photons in a Slab of Thickness ℓ.

After traveling a distance s into the material, the photon will either suffer a collision or be absorbed. The first task is to find the point s at which such an event takes place. If the wave-length (or energy) of the photon is known, σ_τ can be found from the tables of G. W. Grodstein (Reference 43). On writing

$$\frac{I(s)}{I(s_0)} = e^{-\sigma_\tau(s - s_0)} \tag{159}$$

and solving for $(s - s_0)$, one has

$$(s - s_0) = \frac{-1}{\sigma_\tau} \ln \frac{I(s)}{I(s_0)} \tag{160}$$

If a random number $R = \frac{I(s)}{I(s_0)}$, uniform in the interval $o \le R \le 1$, is now cast, $(s - s_0)$ is determined. The point at which the photon undergoes its first interaction with the material is thereby determined. Knowing $(s - s_0)$ one can then, for either plane or spherical geometry, calculate the time at which the event has occurred and the position $x(s)$ at which it has occurred. If the position is outside the material, the energy is recorded and another photon history is begun. If the event occurred within matter, its nature

must now be determined. It is already assumed that one has either a Compton scattering or a photoelectric absorption. The relative probability of scattering is given by the number

$$\frac{\sigma_s}{\sigma_T} = \frac{\sigma_s}{\sigma_a + \sigma_s} = R_1 \tag{161}$$

while the probability of absorption is $1 - R_1$. Another random number R, uniform in $0 \le R \le 1$, can then be cast such that if $R > R_1$, an absorption has occurred. If the event is an absorption, the energy of the ejected electron is given by

$$E - E_b \tag{162}$$

where E is the original photon energy and E_b is the binding energy of the electron. The energy (162) is recorded as an electron energy. The initial position of the electron is known and the directional distribution as a function of energy is given in Davisson and Evans (Reference 44). On sampling from the distribution, one has the photoelectron direction relative to the direction of the incoming photon.

If the event is a Compton scattering, the new direction of the photon and its new wavelength must be calculated. The two quantities are related by the requirement that

$$\lambda - \lambda = 1 - \mu_1 \tag{163}$$

so that $\lambda = \lambda + \mu_1 - 1$ will be between $\lambda - 2$ (for $\mu_1 = -1$) and λ (for no deflection). It is seen then that if a random number R is cast, uniform in the interval $0 \le R \le 1$, and if

$$R = \frac{\int_{\lambda-2}^{\lambda} k(\lambda' \to \lambda)d\lambda'}{\int_{\lambda-2}^{\lambda} k(\lambda' \to \lambda)d\lambda'} \tag{164}$$

one must determine λ_1, the upper limit of the integral in the numerator, so that equation (164) is satisfied. Then equation (163) can be employed to find μ_1. Since

$$\mu_1 = \mu\mu' + \sqrt{1-\mu^2}\ \sqrt{1-\mu'^2}\ \cos(\varphi - \varphi') \tag{165}$$

with μ' the cosine of the angle before the scattering, and μ its new cosine, one can solve for μ. It is necessary, in view of azimuthal symmetry, to cast a random number in $0 \le \varphi - \varphi' \le 2\pi$ and compute its cosine to find μ uniquely. Since the change in energy of the photon is known, the energy given to the (Compton) scattered electron is also known. With the energy of the electron known, its direction can be found (Reference 45).

With the new energy and direction of the photon given, the new total cross section can be found and the cycle given above repeated until the photon either escapes from the material or is absorbed.

5. Flow Charts and Numerical Results

The Monte Carlo Code has been applied to a variety of problems. Two are discussed here. Since the code can be developed in steps by means of subroutines, the problems have been chosen so as to determine whether a given subroutine, or combination thereof, was operating properly. The coding was done in Fortran language and a separate program listing is, as a consequence, given for each problem. Table XIV is a listing for the first problem discussed below. The flow charts given in this section are for the following situation: Photons of an initial energy of 1 mev are incident normally on the face of a carbon slab of two mean free paths' thickness. It is required to find both the unscattered and the scattered photon intensities which are transmitted through the material. A printout was also requested of the number of electrons ejected within the material as a function of energy and the quantity EN(E), the energy distribution of the electrons. No record of the spatial distribution of electrons was called for, nor was the time dependence called for.

Table XIV. Program Listing for the Monte Carlo Calculations of the Scattering of Photons in a Slab

```
*0808
      DIMENSION LIST (100)
      DIMENSION EE(101), N(101), TIG(100), TIGA(100)
      COMMON EE, N
   23 FORMAT (//,32HANGULAR DISTRIBUTION OF PHOTONS)
   26 FORMAT (/, 3X,12HCOSING THETA, 3X, 14HNO. OF PHOTONS)
   27 FORMAT (1F10.7,10X.115)
    3 FORMAT (1X, 14, 10X, 14  , 10XF10.2
    4 FORMAT (4F6.2)
    5 FORMAT (214,3E16.8)
    6 FORMAT (//,3H J , 10X, 18HNUMBER OF ELECTRON, 10X,6HENERGY)
    7 FORMAT (214,14H PHOTOELECTRIC)
   18 FORMAT (214, 15HPHOTON ABSORBED)
      I=0
   24 CONTINUE
      READ 4, (TIG(K), TIGA(K), K=1,100
      DO 2 J=1,100
      LIST(J)=0
      EE(J) = 0.0
    2 N(J) = 0
   20 READ 4, E4, COS , D , CONV
      J = E4*100.0
      LI = J
      SIG = (TIG(J) + TIGA(J)) * CONV
      SIGA = TIGA(J) * CONV
      WLE = 0.50903/E4
      DO 8 J=1, 100
      WLEN=WLE
      E1=E4
      COSP=COS
      K=0
      DX=0.0
   13 CALL RAND (I,R)
      I=I+1
      S=-(LOGF(R))/SIG
      DX=DX+COSP*S
      IF (DX-D) 14,10,10
   14 IF (DX) 10,10,9
   10 IF (COSP) 30,30,31
   31 L=(COSP + 0.05) *20.0
      LIST(L) = LIST(L) + 1
   30 IF (SENSE SWITCH 3) 25,8
   25 PUNCH 5, J,K, COSP, WLEN
      GO TO 8
    9 CALL RAND (I,R)
```

Table XIV (cont'd)

```
      IF (R-SIGA/SIG) 11,11,12
   11 PUNCH 7, J,K
      GO TO 8
   12 CONTINUE
      CALL COMP (WLEN,ADM,R)
      K=K+1
      COST=1.0+WLEN-ADM
      WLEN=ADM
      CALL SCORE ( E1, WLEN,M)
      IF (E1-0.01) 17,17,16
   17 IF (SENSE SWITCH 3) 19,8
   19 PUNCH 18, J,K
      GO TO 8
   16 SIG = (TIG(M) + TIGA(M) * CONV
      SIGA = (TIGA(M)) * CONV
      CALL RAND (I,R)
      R=R*6.2831853
      COSP=COST*COSP-COSF(R)*SQRTF((1.0-COST**2)*(1.0-COSP**2))
      IF (SENSE SWITCH 1) 15,13
   15 PUNCH 5, I K, COSP
      GO TO 13
    8 CONTINUE
      PUNCH 6
      DO 1 J=1, LI
    1 PUNCH 3 , J , N(J) , EE(J)
      PUNCH 23
      PUNCH 26
      DO 28 M=1,21
      THETA = M
      THETA = THETA*0.05 - 0.05
   28 PUNCH 27, THETA,LIST(M)
      IF( SENSE SWITCH 9) 21,20
   21 PAUSE
   22 IF ( SENSE SWITCH 2) 24,20
      END
```

If one has the above in mind, the flow charts as given in Figures 74 - 77 are appropriate. Figure 78 gives the angular distribution of photons which emerge at the back face of the material when 500 photons were incident. Note that in region 1 on Figure 78 the number of unscattered photons is also given. There are 63 of these. If x is expressed in units of mean free path, then

$$500\, e^{-2} \cong 68$$

should be the number of photons traversing the material suffering neither scattering nor absorption. The ramainder of Figure 78, the angular distribution of scattered photons, is roughly Gaussian. Such a result is to be expected on the basis of the analytical work of L. L. Foldy or I. Ogievetskii (Reference 46). The above two checks on the performance of the code are comforting. One may inquire, finally, as to the connection between Figure 78 and equation (158). The latter is

$$I(s) = I(s_o)e^{-\sigma_T(s-s_o)} + \int_{s_o}^{s} \left[S + TI\right] e^{-\sigma(s-s')} ds'$$

In the problem under consideration, the volume source of photons which could be generated by electron absorption was not calculated. Thus, S = 0 in the present case. The connection between equation (158) and Figure 78 is now clear. For $\mu > 0$, Figure 78 is the Monte Carlo solution to (158). The photons in region 1 are equivalent to the term

$$I(s_o)e^{-\sigma_T(s-s_o)}$$

while the given distribution of scattered photons is the physical simulation of the second term on the right-hand side of (158). It will be observed that the intensity is greater than one would expect on the basis of a "good geometry" experiment; and this, in turn, leads to the concept of a build-up factor.

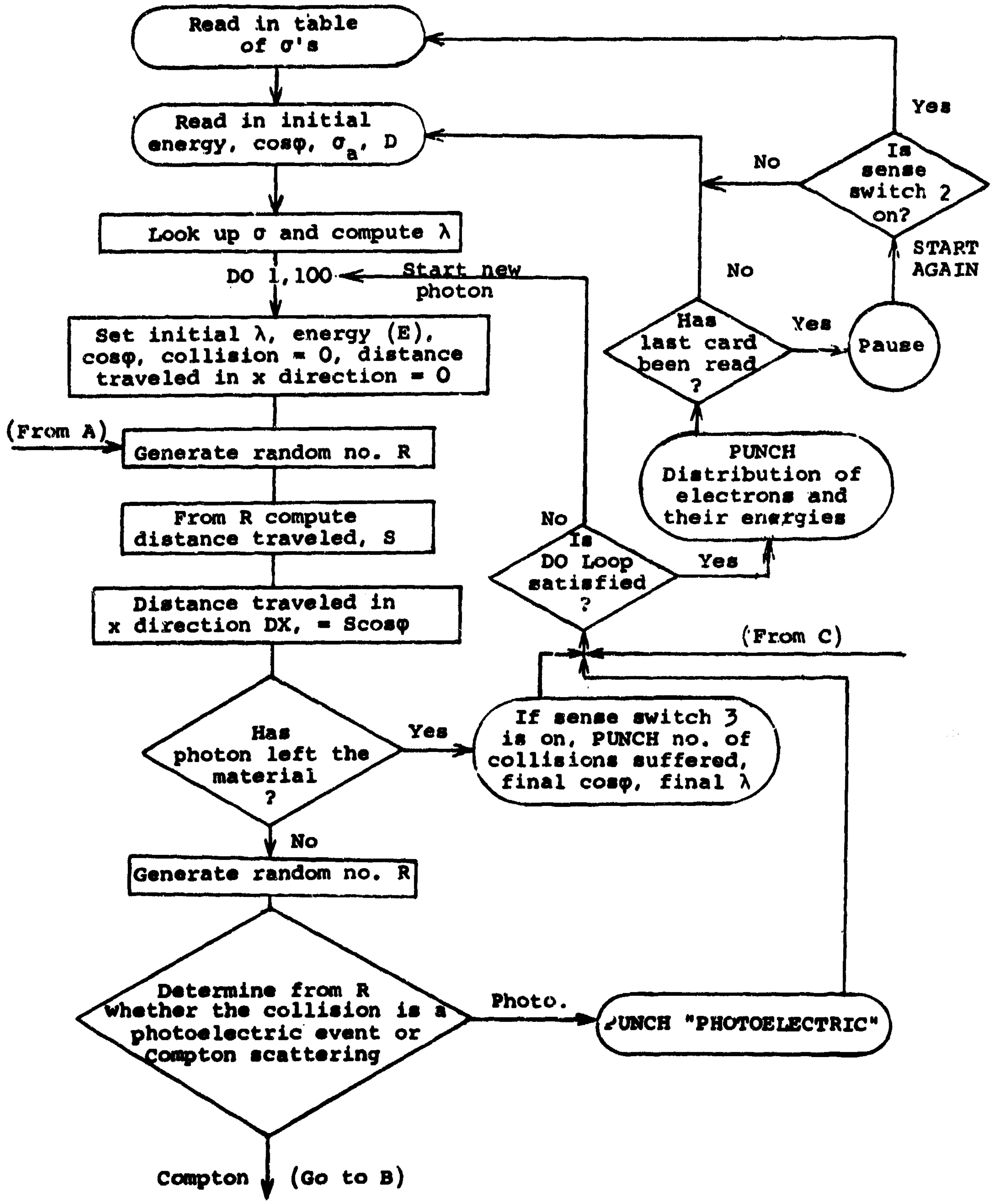

Figure 74. Flow Chart of Main Program

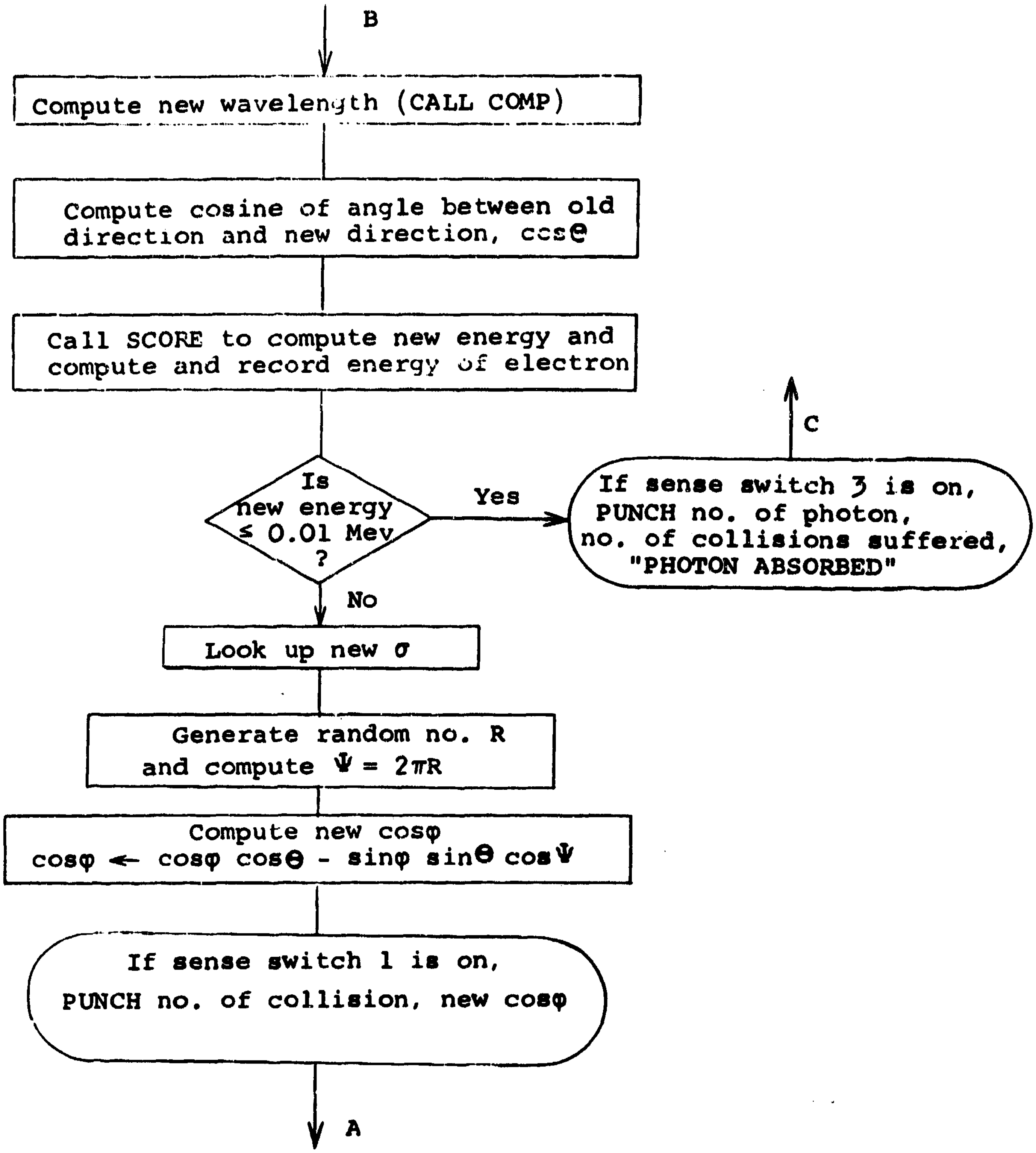

Continuation of Figure 74

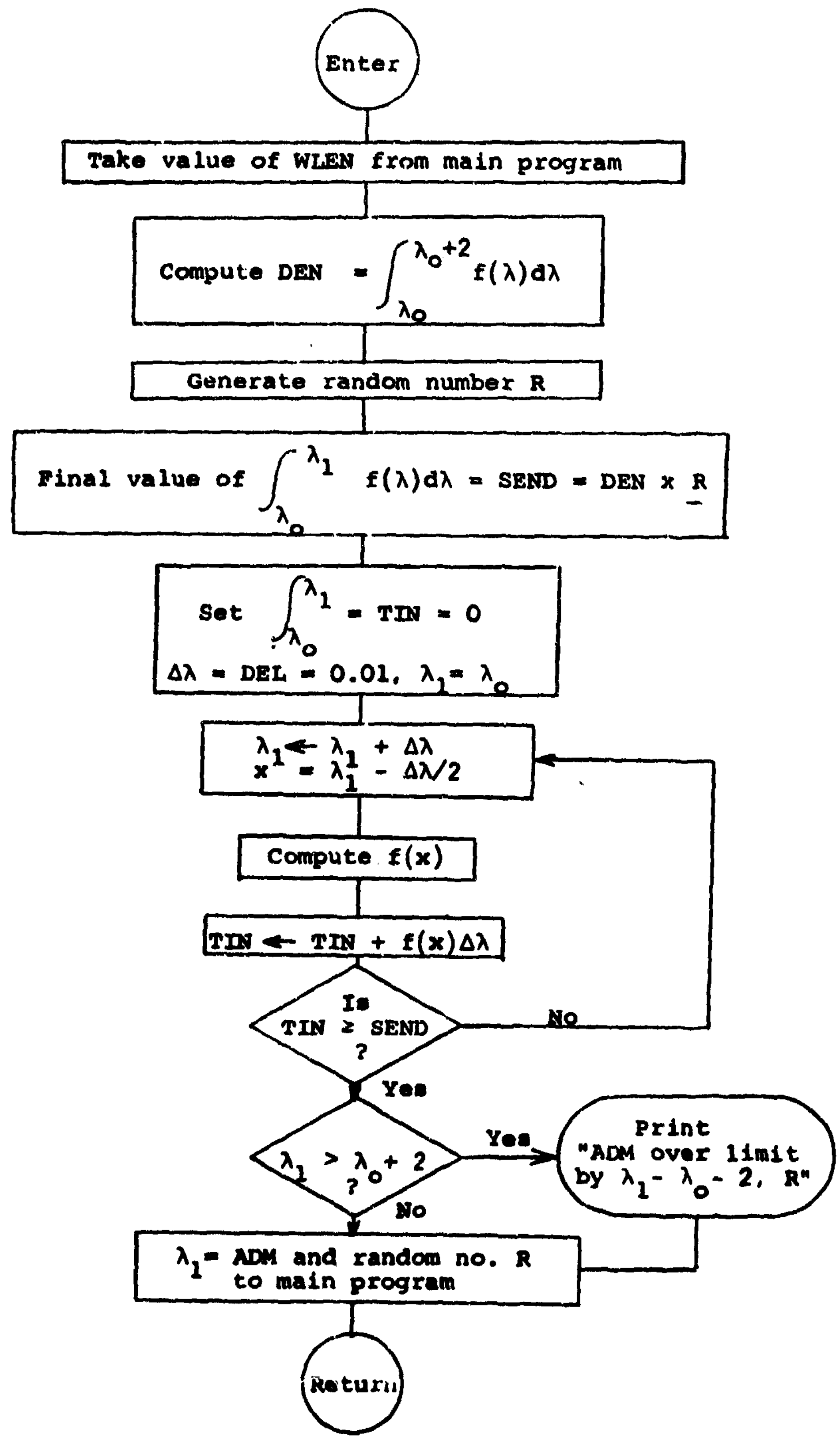

Figure 75. Subroutine for the Calculation of the Wavelength of a Compton Scattered Photon

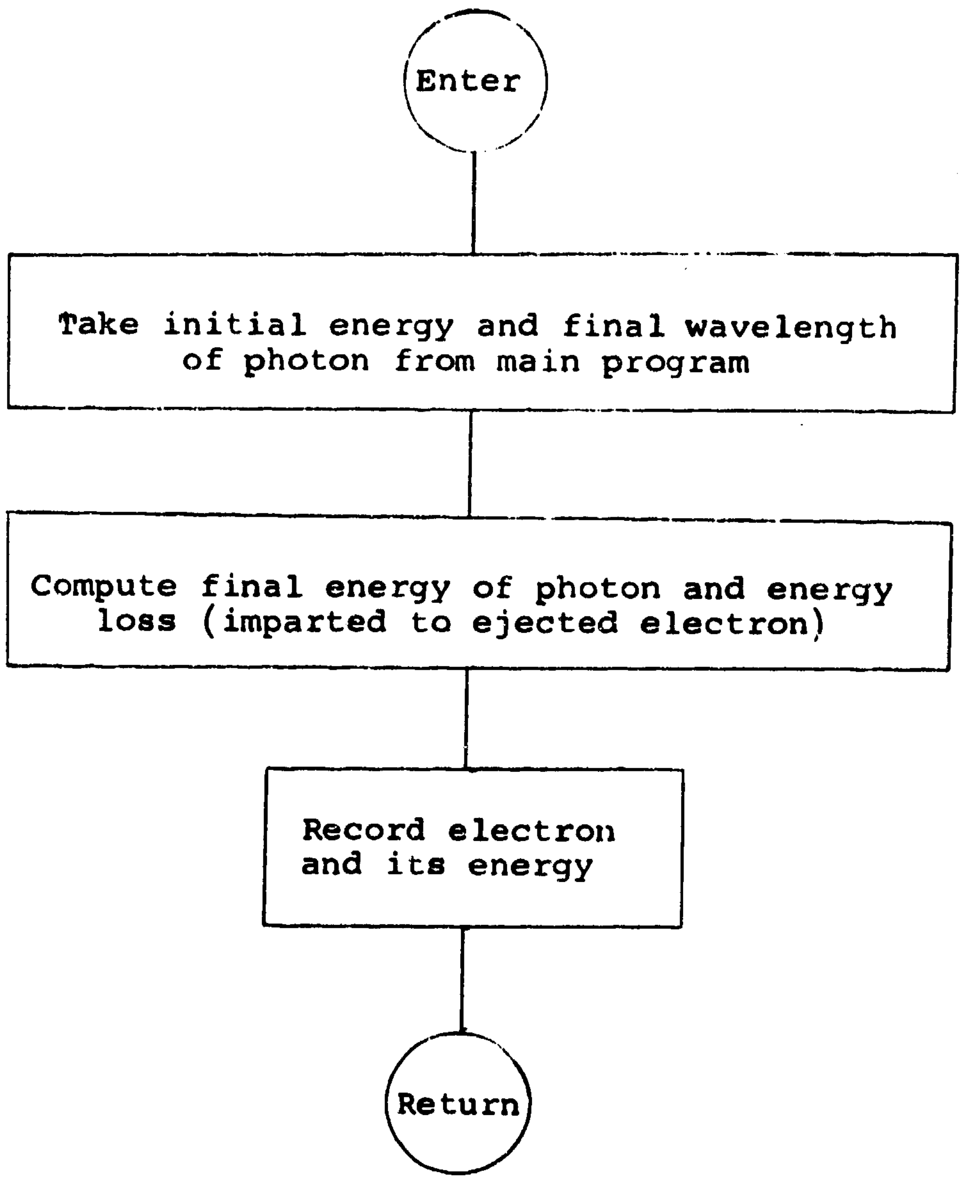

Figure 76. Subroutine for Calculation of Electron Energies

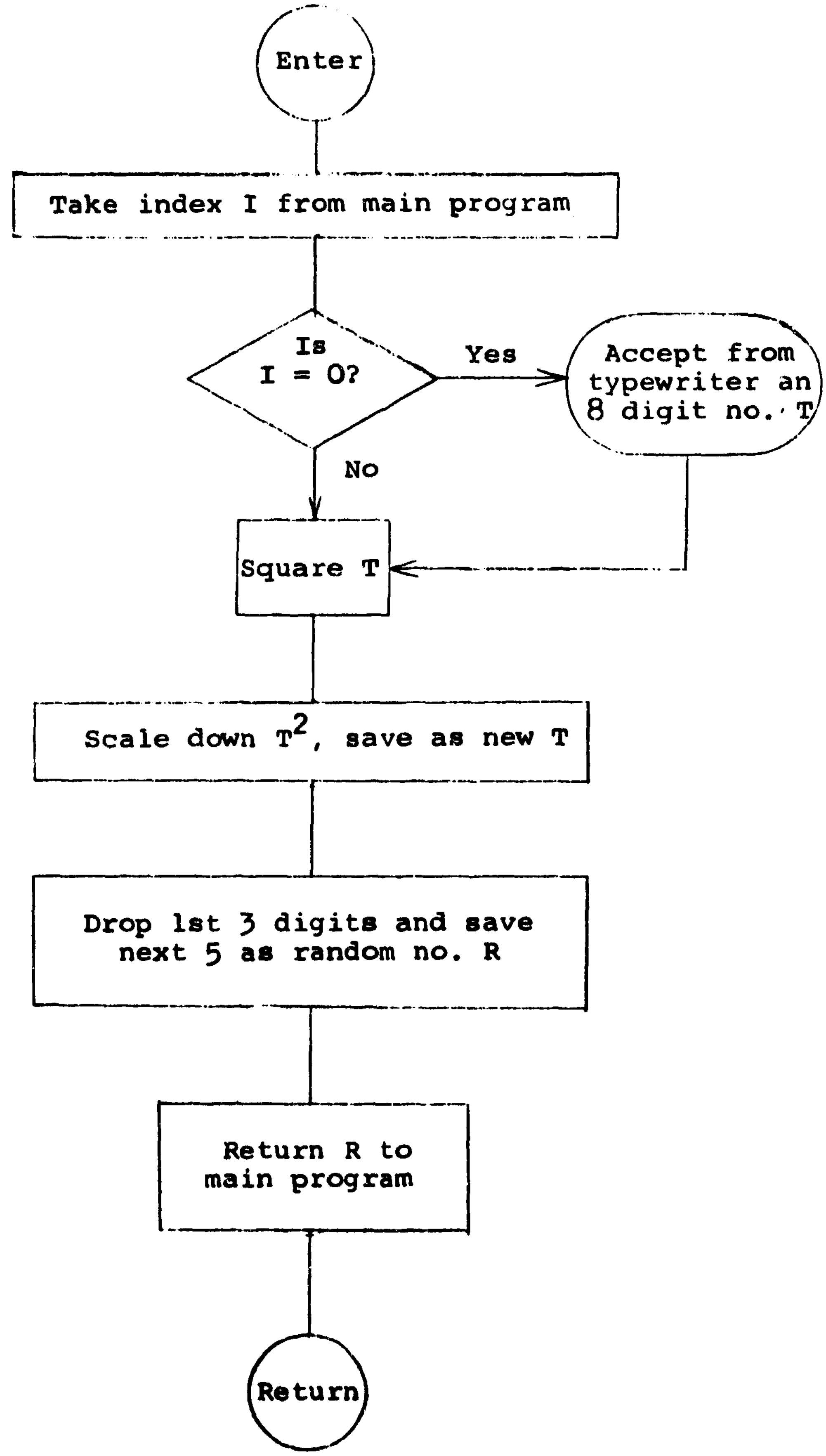

Figure 77. Randon Number Generator Subroutine

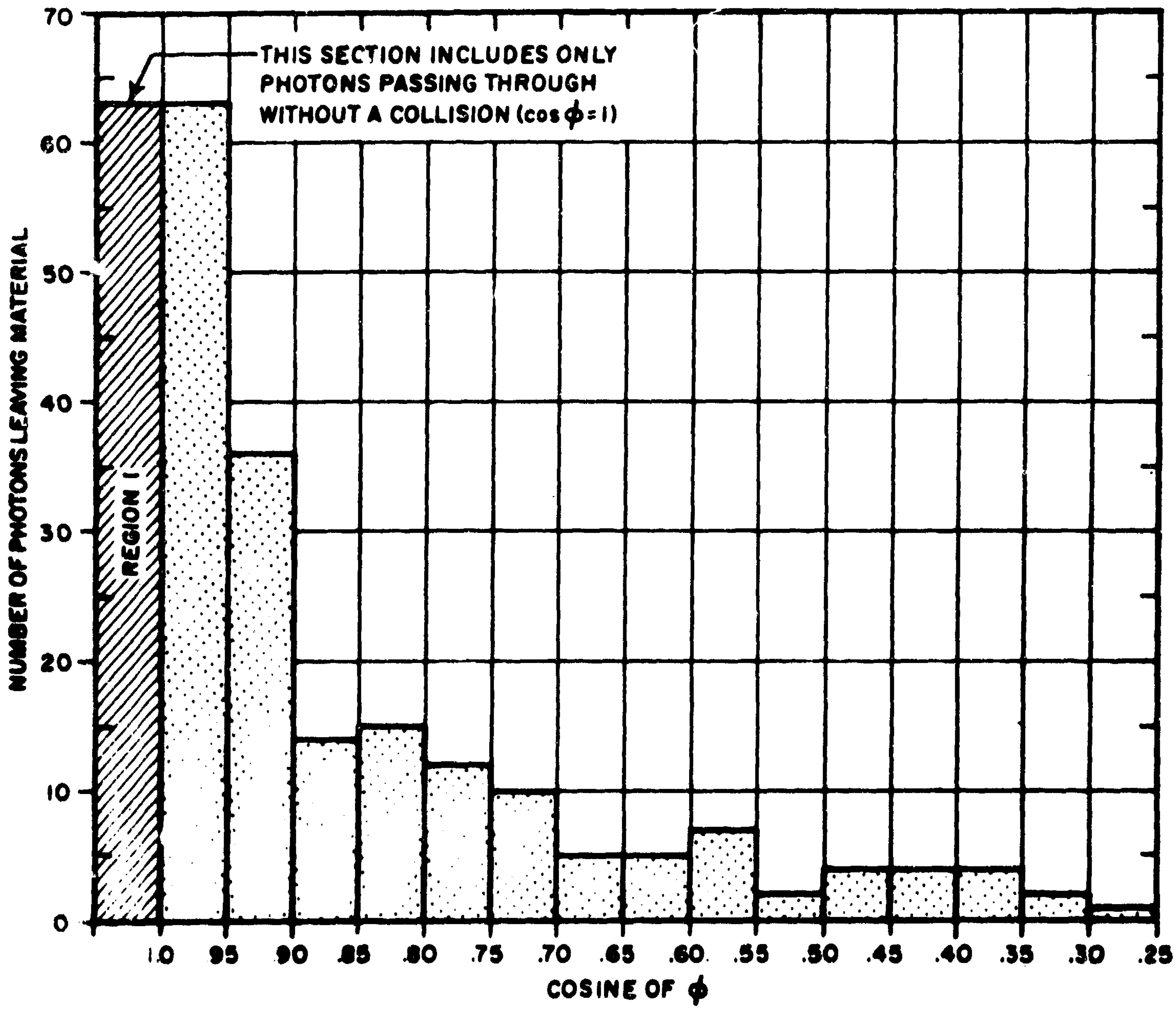

Figure 78. Angular Distribution of Photons Traversing Two Mean Free Paths of Carbon

The second problem discussed herein is done in spherical coordinates. Let a point source emit photons of 1-mev energy radially. If scattering is absent, it develops that the transport equation can be solved exactly for the case at hand. The analytical solution for the photon intensity is

$$I(r,t) = \frac{I_o e^{-\sigma r}}{4\pi r^2} f(t - \frac{r}{c}) H(r) \qquad t \geq \frac{r}{c} \tag{166}$$

and $I(r,t) = 0$ for $t < \frac{r}{c}$. The quantity $f(t - \frac{r}{c})$ is the time dependence of the source which is arbitrary, while $H(r)$ is the Heaviside unit function.

A Monte Carlo simulation of the above absorption problem was done to check the coding in the spherical case. The results are shown in Figure 79. Included therein is the intensity with absorption removed, and with both absorption and spherical spreading removed. If in equation (166) both sides are multiplied by $e^{\sigma r}$, the result is

$$e^{\sigma r} I = \frac{I_o}{4\pi r^2} f(t - \frac{r}{c}) H(r) \tag{167}$$

In the absence of scattering $f(t - \frac{r}{c})$ does not change shape. The spatial dependence of $e^{\sigma r} I$ should then be proportional to r^{-2}. The close agreement between the slope of the $e^{\sigma r} I$ curve (absorption removed) and a curve with a slope of -2 on log-log paper is evident in Figure 79. Finally, if both sides of equation (167) are multiplied by $4\pi r^2$, the right-hand side of (167) is a constant. This fact is indicated in Figure 79 in which it is shown that the curve labeled "absorption and spreading removed" is a constant.

From the above, it can be inferred that problems in spherical geometry can be successfully undertaken: i.e., the coding is such that the Monte Carlo simulation is correctly done.

Parenthetically, it is added that the first of the two problems discussed herein was done on the UNM IBM 1620 computer for

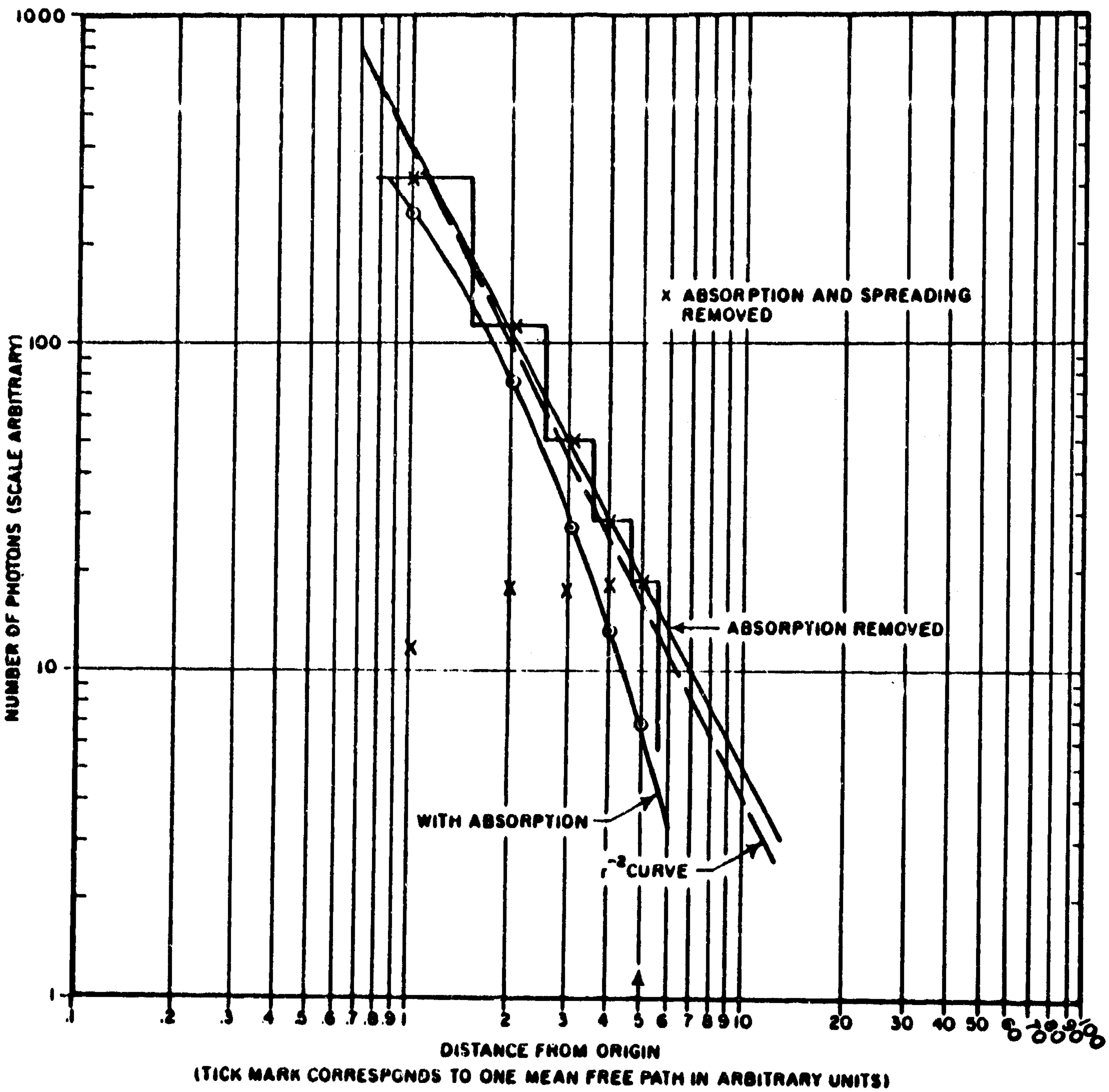

Figure 79. 4,000 Photon Histories - Pure Absorption

500 photon histories and consumed about 1 1/2 hours of computing time. Including "debugging" on the Kirtland AFB CDC 1604, the second problem discussed took about 18 minutes for 4,000 photon histories.

SECTION VIII

GENERAL CONCLUSIONS AND RECOMMENDATIONS

By W. W. Grannemann

The experiments on Carbon composition resistors and the air effects surrounding them show that the radiation effects on this combination increase until a pressure of about 150 mm Hg is reached. Then the radiation effects decrease until a pressure of 1 mm of Hg is reached; the magnitude then remains essentially constant with decreased pressure. In the pressure range 10 to 100 mm Hg the theory indicates that the time dependent behavior of the number of free electrons plays the dominant role in the air conductivity around the resistor. The value of resistance changes as a function of dose rate, and the percentage change of resistance is related to the original value of the resistance. The major transient resistance changes under gamma radiation are due mostly to air ionization effects. This further emphasizes the importance of potting resistors and any open circuit wires, as well as the importance of designing circuits with as low an impedance as possible for the job they are designed to do.

The thin film Hall effect devices were found to be highly radiation resistant to transient gamma pulses. The theory developed indicates that the type of circuit used for the Hall effect device can make considerable difference in the radiation tolerance of it. Experimentally, no measurable change in Hall voltage was observed for dose rates of 10^7 r/sec. From theoretical calculation it appears that the thin film Hall effect devices will operate well in radiation dose rates of 10^9 to 10^{10} with failure occurring somewhere near 10^{11} r/sec. It was also found that displacement voltage effects under irradiation can appear to add to the transient Hall effect voltage so that for a radiation resistant Hall effect device the alignment of the Hall probe is extremely critical. It appears that thin film Hall effect devices can be recommended for use in a transient gamma radiation environment up to 10^9 r/sec and with special circuit configurations this value

might be raised one or two orders of magnitude, but it is recommended that the Hall effect devices be checked on higher dose rate machines to verify the theoretical predictions.

Titanium dioxide diodes have been found to be highly radiation resistant both to neutrons and to gamma pulses. No transient radiation effects were observed for gamma pulses of 10^7 r/sec. From experimental data it appears that the titanium dioxide diodes would go considerably beyond the two orders of magnitude improvement over the normal junction diode. It is recommended that titanium dioxide diodes also be investigated further at higher radiation intensities to determine accurately the magnitude and shape of the transient current pulse resulting from the radiation pulse; and further development and improvement of electrical characteristics of titanium dioxide diodes is recommended. These thin film devices using TiO_2 diodes hold considerable promise for radiation resistant diodes.

The absorption method for obtaining X-ray spectrums has been satisfactorily used on the 600 KV flash X-ray machine. The present method requires knowing the efficiency of the energy absorbed in the detector and the reproducibility of the X-ray pulse from one pulse to the next. The accuracy of the computation is dependent on the $\frac{d\mu}{dE}$. For this reason the method may require some modification to be useful on the super flash X-ray machines. It is recommended that this method of spectrum determination be considered when the need arises for spectrum measurements on super flash X-ray, even though it may be desirable to obtain a complete spectrum from one individual pulse.

Measurements have been made on dielectric materials showing it is now possible to make Hall effect and magnetoresistance measurements on some of the usual dielectric materials such as mylar, polyethylene, and similar dielectric materials used in capacitors. This makes possible a measurement of mobilities of the charge carriers which are predominantly holes in these cases. It is also possible to calculate the resistivity as a function of dose rate from these measurements. The largest bulk effect was the radiation induced conductivity change.

A Schering Bridge was used to measure the effective capacity change of diode junctions under irradiation. The bridge arrangement gives a transient picture of the effect of charge redistribution in the diode. It is planned to use this method of measurement on transistor elements and diode elements in microcircuits in the coming project.

A Monte-Carlo code for transient radiation effects has been developed. The code predicts the number of electrons produced as a function of energy for a transient gamma radiation pulse incident on a material. Included in this code is information on the time dependent absorption and scattering of the gamma rays. Once the number of electrons produced in the material is known as a function of time, the change in conductivity as a function of time can then be calculated. The code can also be used to determine gamma dose after the gamma rays have passed through some intermediate material before striking an electronic device.

This page intentionally left blank.

APPENDIX I

AFWL 600 KV FLASH X-RAY FACILITY

By LeRoy Meyer and W. W. Grannemann

1. AFWL 600 KV Flash X-Ray Facility

The AFWL flash X-ray system consists of a 600 KV Fexitron unit manufactured by Field Emission Corporation. The characteristics of the unit are summarized in Table XV. A double walled rf shield room houses the experimental measuring equipment. By this means the rf noise level is reduced by 120 db. The X-ray beam is fired through a special window in the shielded room. This window is shown in Figure 80. The beam area and dose rates are shown in Figure 81. The room layout is shown in Figure 82. The energy spectrum of the system is shown in Figure 83 for 400 KV X-rays. A graph showing the conversion of gamma flux equivalent to 1 roentgen-hour as a function of gamma energy is shown in Figure 84.

Table XV. Operating Characteristics of the 600 KV Fexitron Flash X-Ray System

Output voltage	600 KV
Output current at peak output voltage	2000 amp
Pulse width	0.2 μ sec
Pulse rise time	50 nanosec
Dose rate maximum	$\approx 2 \times 10^7$ r/sec

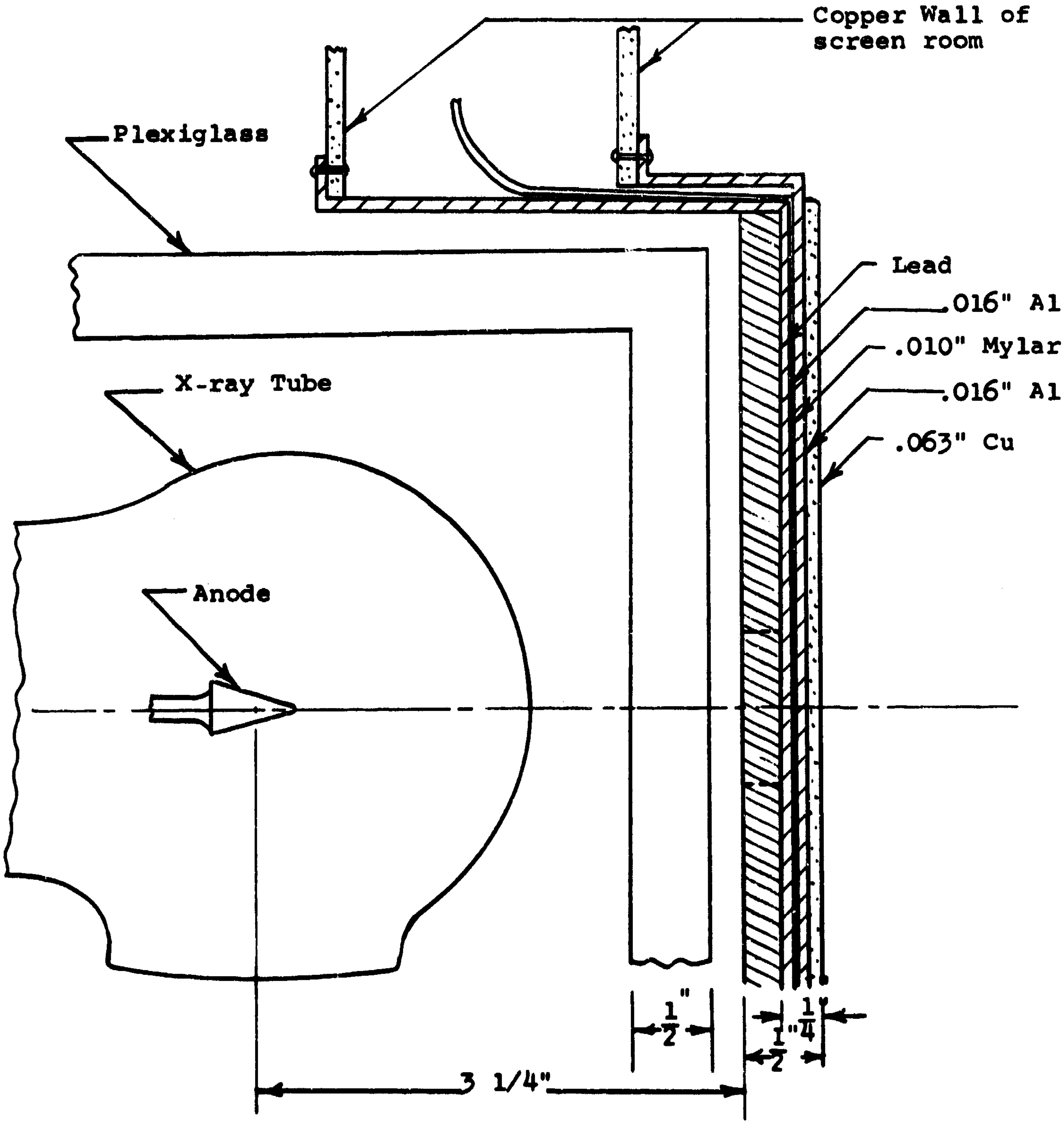

Figure 80. X-Ray Tube and Window in the Screen Room.

Scale: 0.5cm = 1 inch

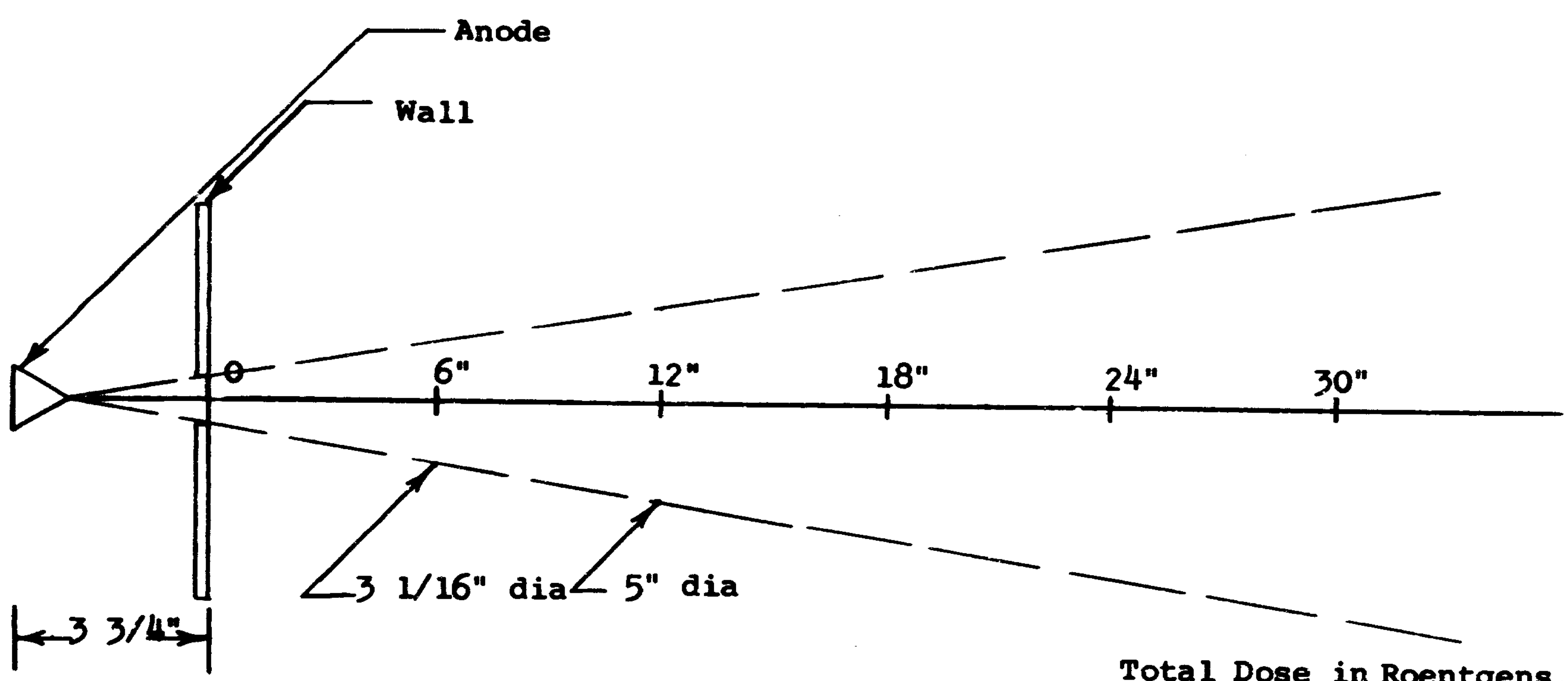

Total Dose in Roentgens,
6" from the Wall

300 kv - 0.13
400 kv - 0.30
500 kv - 0.49

Figure 81. Radiation Beam of AFWL 600 KV Flash X-Ray System.

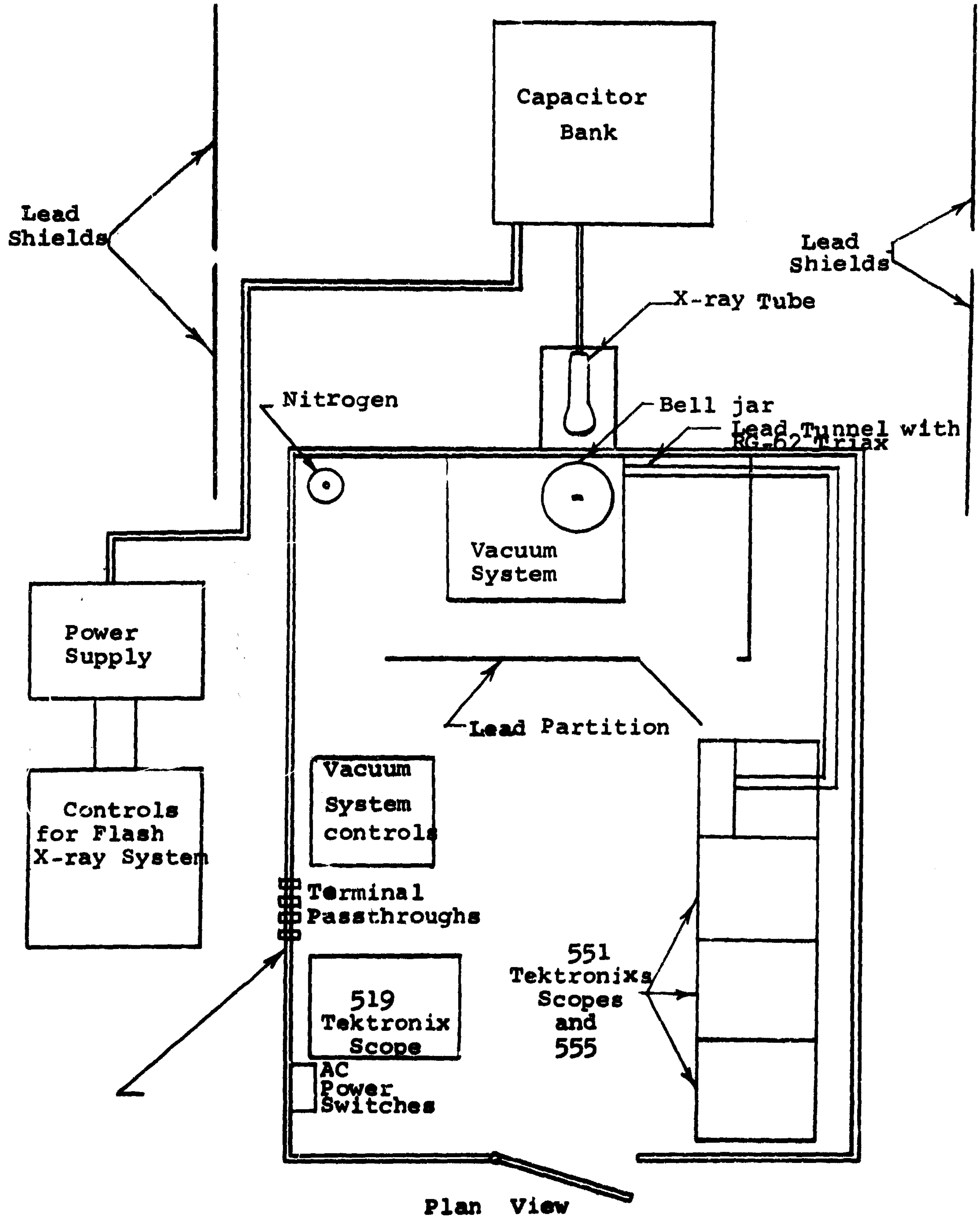

Figure 82, AFWL 600 KV Flash X-Ray Facility

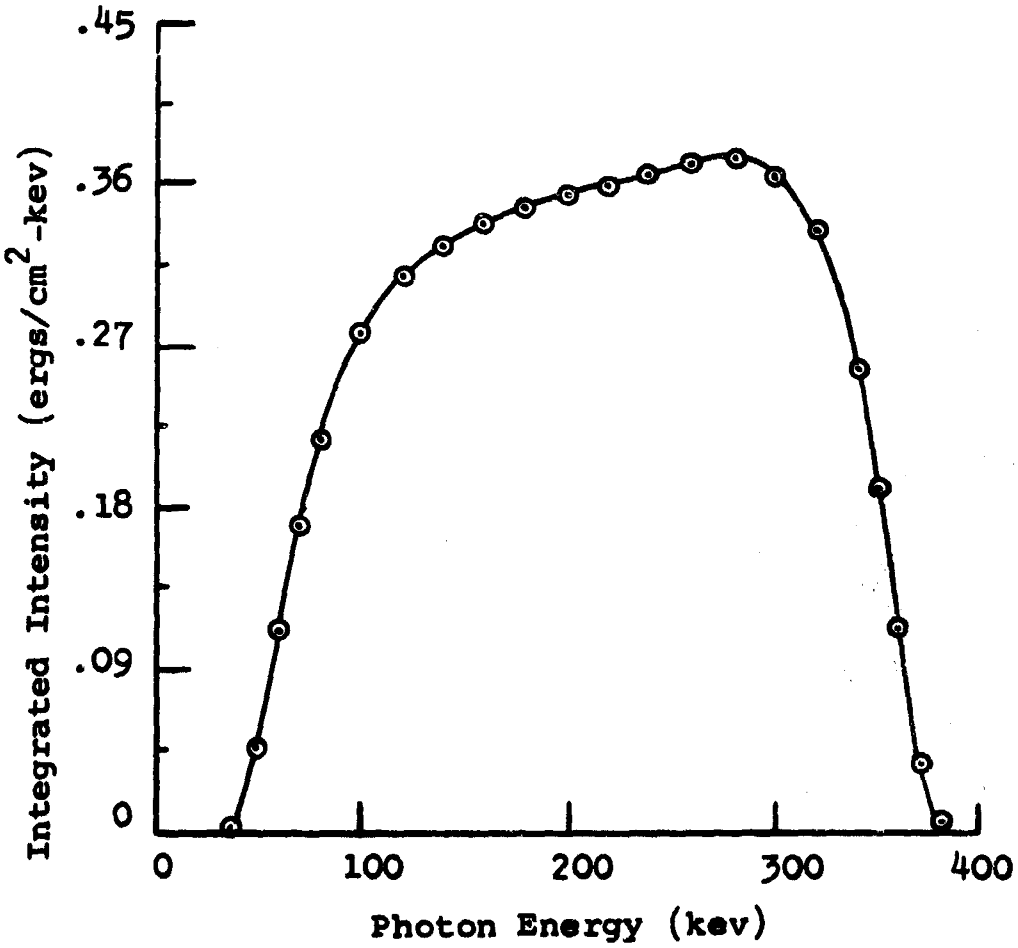

Figure 83. Energy Spectrum of a 400 kvp X-Ray Pulse

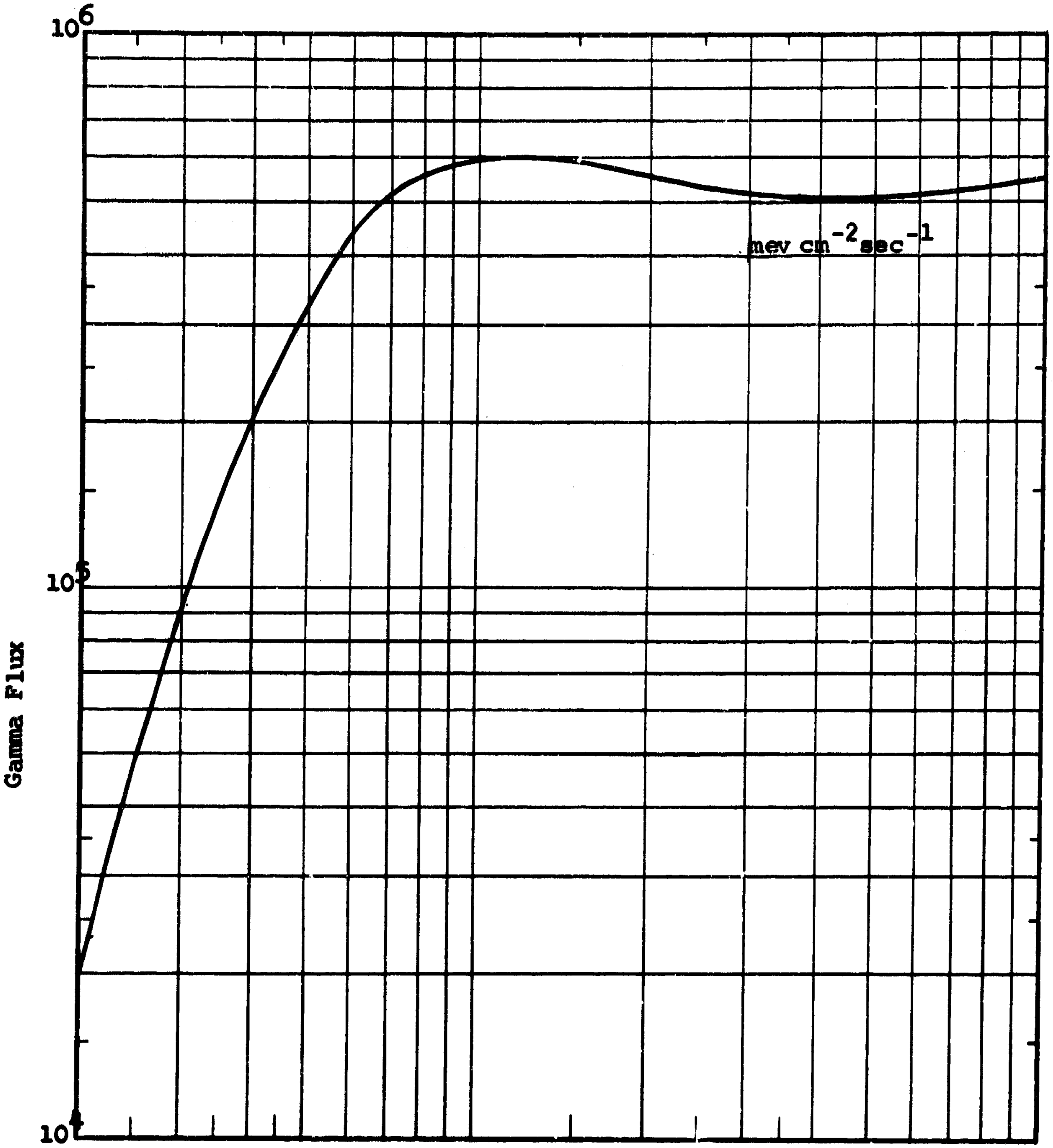

Figure 84. Gamma Flux Equivalent to 1 Roentgen-Hour as a Function of Gamma Energy (Reference 47).

APPENDIX II

TEST EQUIPMENT

By LeRoy Meyer and W. W. Grannemann

The test equipment that was used in the experiments is described below. The major items are:

1. The vacuum system
2. DC micro-volt-ammeter
3. Amplifier
4. NJE High voltage power supply
5. Harrison labs power supply, model 809A
6. Harrison labs power supply, model 855B
7. Atomic Laboratory Electromagnet

1. Vacuum System

A special vacuum system, No. 1308, built by Consolidated Vacuum Corporation of Palo Alto, California, is capable of reaching the 10^{-8} torr range using liquid nitrogen coolant in the baffle. The controls are pneumatically operated from the control panel located outside the lead shielding enclosure. Heating capabilities and a variable leak valve are also built into the system.

Two vacuum gauges are used. They are the magnevac-type GMA-140 and a CVC ionization gauge type GIC-110A. The magnevac gauge has a range of from 1 micron to 500 mm and the ionization gauge has a range of from 1×10^{-3} torr to 2×10^{-9} torr.

The bell jar guard has a window for the X-ray beam to pass through. A covering of aluminum foil is also used over the bell jar for electrostatic shielding.

2. DC Micro-Volt-Ammeter Model MV-07C

The model MV-07C is an extremely stable, sensitive, wide range multiplier and amplifier with full-scale range as low as 10 microvolts and 10 micro-micro-amperes and as high as 1 KV and 1 ma.

Available from Millivac Instruments Inc., 110 Altamont Ave., Schenectady, New York.

3. Amplifier

The 1121 Tektronix amplifier has an overall gain of 100 with a maximum input of ± 10 mv. The input signal can be attenuated from 1 x to 500 x in 9 calibrated steps. The band pass of the amplifier is 5 cps to 17 mc. The noise level is ≈ 50 μvolts.

4. NJE High Voltage Power Supply

Model S-327

500-5000 VDC, 0-10 ma.

5. Harrison Labs Power Supply, Model 809A

The 809A is a constant voltage/constant current, transistor power supply which has an output of 0 to 36 volts and 0 to 10 amps. It is equipped with a continuously adjustable current limit control which allows the maximum output current to be set at any value up to the maximum current rating.

6. Harrison Labs Power Supply, Model 855B

The 855B is a constant voltage/constant current transistor power supply which has an output of 0 to 18 volts and 0 to 1.5 amps. It has a continuously adjustable current limit control with less than 30 millivolts drift for 8 hours.

7. Atomic Laboratory Electromagnet

Cat. No. 79641

Available Atomic Labs. Inc.
3086 Claremont Ave.
Berkely 5, California

This electromagnet can produce a variable magnetic field from 0 to 3 kilogauss in a 1/2" air gap. It also has available hollow pole pieces which were used in the radiation experiments.

APPENDIX III

THEORY OF THE SCHERING BRIDGE

By L. T. Boatwright

Among the numerous bridge network schemes available, the one suggested by H. Schering is one of the better methods for evaluating small capacitors at low and high voltages (Reference 48). The effective capacitance and the equivalent series loss resistance of an imperfect capacitor can be measured with high precision. Furthermore, the sensitivity of the Schering network is much greater for changes in capacitance than for changes in effective resistance as shown below. In transient radiation studies, instrumentation techniques are required for recovery of low level signals in the presence of considerable interference. It appears that an alternating current bridge operating at frequencies above 10 megacycles may offer some advantages over the usual method of viewing the phenomena directly on an oscilloscope.

The Schering Bridge Network has been described extensively in the literature (References 48-53); however, bridge utilization for the observation of transient radiation phenomena is comparatively recent (Reference 54). The basic Schering Bridge circuit is shown in Figure 85. C_1 and R_1 are the effective capacitance and series loss resistance respectively of the capacitor to be tested; C_N is a loss-free standard capacitor; R_2 and R_3 are non-reactive resistances, and C_3 is a variable air capacitor. In addition to C_3, other components in the bridge arms may be variable in order to obtain balance. Bridge balance occurs when there is no detector current, or the potential at C and D is the same. In practice, exact balance may not be possible and a null is obtained for minimum current through the detector. Z_5 and Z_6 are the detector and signal source impedances respectively. The analysis below assumes sine wave excitation of the bridge. Let:

$$z_1 = R_1 + \frac{1}{j\omega C_1} \qquad (168)$$

$$z_2 = R_2 \qquad (169)$$

$$z_3 = \frac{1}{1/R_3 + j\omega C_3} \tag{170}$$

(171)

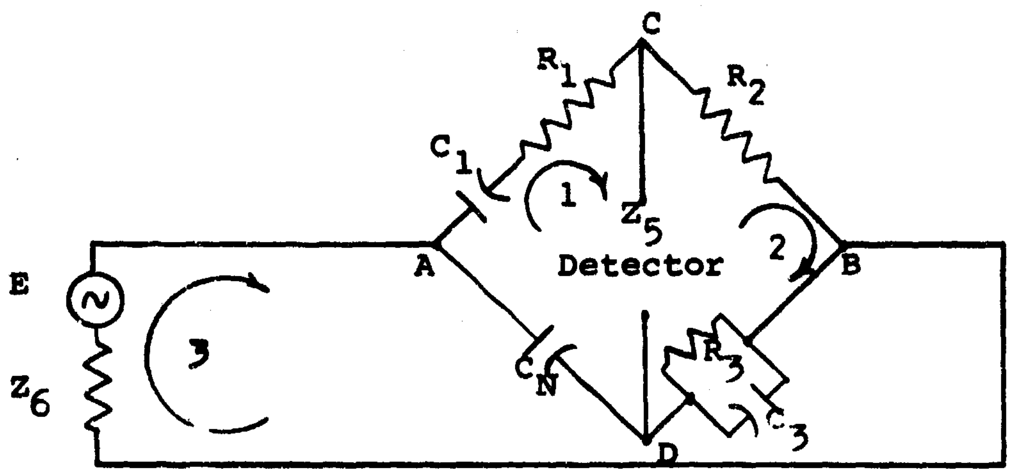

Figure 85. Schering Bridge

Loop equations are written for the circuit of Figure 85 and are solved for the detector current:

$$0 = (z_1 + z_4 + z_5)I_1 = z_5 I_2 - z_4 I_3 \tag{172}$$

$$0 = -z_5 I_1 + (z_2 + z_3 + z_5)I_2 - z_3 I_3 \tag{173}$$

$$E = -z_4 I_1 - z_3 I_2 + (z_3 + z_4 + z_6)I_3 \tag{174}$$

If equations (172)(173) and (174) are solved utilizing determinants,

$$I_1 = \frac{\begin{vmatrix} 0 & -z_5 & -z_4 \\ 0 & z_2 + z_3 + z_5 & -z_3 \\ E & -z_3 & z_3 + z_4 + z_6 \end{vmatrix}}{\Delta}$$

$$I_1 = \frac{E\left[z_3 z_5 + z_4(z_2 + z_3 + z_5)\right]}{\Delta} \tag{175}$$

and equation (177) for the detector current becomes

$$I_D \approx \left[\frac{z_1 z_3 - z_2 z_4}{z_1 z_4(z_2 + z_3 + z_5)}\right] E \tag{180}$$

$$I_D \approx \frac{\left[\omega(c_N c_3 R_3 - c_1{}^2 R_1 R_2) + j(c_N R_3 - c_1 R_2)\right] \omega E}{R_2 + R_3 + R_5 + j(x_5 - \omega c_3 R_3{}^2)} \tag{181}$$

or

$$I_D \approx \frac{a}{\Delta} \omega E \tag{182}$$

If transient radiation of a capacitor, for example, causes an increase in the detector current (normally zero at balance), this can be ascribed to a change in capacitance, conductance, or dielectric constant, of which the latter can be related to the loss angle θ (θ + $\tan^{-1} \omega R_1 c_1$). Equations (181) or (182) reveal that the detector current is directly proportional to both the frequency and the applied voltage. If these are held constant the rate of change of current with respect to any parameter "p" is

$$\frac{\partial I_D}{\partial p} \approx \frac{\Delta_1 \frac{\partial a}{\partial p} - a \frac{\partial \Delta}{\partial p}}{\Delta^2} \omega E \tag{183}$$

When the bridge is balanced, $z_1 z_3 = z_2 z_4$ or $c_1 R_2 = c_4 R_3$, $R_1 c_4 = c_3 R_2$ and $\tan \theta = \omega c_1 R_1 = \omega c_3 R_3$. Consequently, near balance $a \to 0$ and

$$\frac{\partial I_D}{\partial p} \approx \left[\frac{1}{\Delta} \frac{\partial a}{\partial p}\right] \omega E \tag{184}$$

If all other factors are considered constant except those of the test item (c_1, R_1) and $p = c_1$ and $p = R_1$ then

$$\frac{\partial I_D}{\partial R_1} \approx \frac{1}{\Delta} \frac{\partial a}{\partial c_1} \omega E$$

$$I_2 = \frac{\begin{vmatrix} z_1 + z_4 + z_5 & 0 & -z_4 \\ -z_5 & 0 & -z_3 \\ -z_4 & E & z_3 + z_4 + z_6 \end{vmatrix}}{\Delta}$$

$$I_2 = \frac{-E\left[-z_3(z_1 + z_4 + z_5) - z_4 z_5\right]}{\Delta} \tag{176}$$

The detector current $I_o = I_2 - I_1$

$$I_o = \left[\frac{z_1 z_3 - z_2 z_4}{\Delta}\right] E \tag{177}$$

where:

$$\Delta = \begin{matrix} z_1 + z_4 + z_5 & -z_5 & -z_4 \\ -z_5 & z_2 + z_3 + z_5 & -z_3 \\ -z_4 & -z_3 & z_3 + z_4 + z_6 \end{matrix} \tag{178}$$

If equation (178) is expanded

$$\Delta = z_5 z_6\left[z_1 + z_2 + z_3 + z_4\right] + z_5\left[(z_1 + z_2)(z_3 + z_4)\right]$$
$$+ z_6\left[(z_1 + z_4)(z_2 + z_3)\right] + \left[z_1 z_2(z_3 + z_4) + z_3 z_4(z_1 + z_2)\right]$$

If the bridge is to be arranged for greatest sensitivity to a given out-of-balance condition, z_1 and z_4 are required to be much larger than z_2 and z_3 (Reference 52). If this is the case, Δ can be simplified to:

$$\Delta \approx z_1 z_4(z_2 + z_3 + z_5) \tag{179}$$

APPENDIX IV

CABLE STUDY

By Arthur Golubiewski and W. W. Grannemann

Many studies of the effects of nuclear radiation on coaxial cables have been carried out (References 55-63, for example). Nearly all transient radiation studies have been performed with pulsed reactors on linear accelerators on cables whose electrical length is short compared to duration of the radiation pulse.

The purpose of this study is to determine the effects of a flash X-ray pulse on a cable whose electrical length is long compared to the duration of the pulse. A mathematical model is proposed which relates the expected output pulse to gamma induced photoconductivity. It is assumed that the cable has received a sufficient radiation dose to eliminate initial effects.

It is assumed that before irradiation the cable can be considered "lossless". The incremental equivalent circuit is then an L-C circuit:

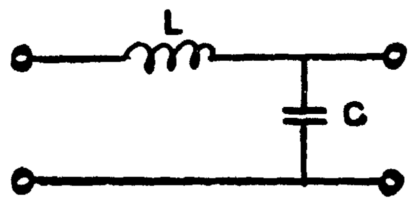

Figure 86

Upon irradiation, gamma photoconductivity alters the incremental equivalent circuit so that there is a conductance in parallel with the capacitance:

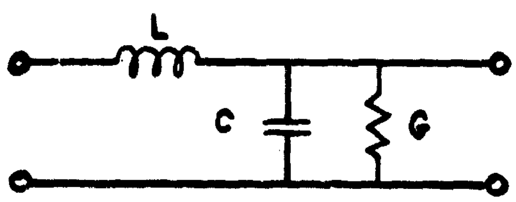

Figure 87

Assuming that the radiation pulse is square, one can take the conductance, G, to be zero until the gamma rays strike the cable, whereupon it increases to a constant value for the duration of the pulse, decreasing again to zero at the end of the pulse.

Mathematical Analysis

By taking the Laplace transform of the general transmission line equations

$$\frac{\partial^2 I(x,s)}{\partial x^2} - (Ls + R)(Cs + G)\, I(x,s)$$
$$= C\,\frac{\partial E(lc,0)}{\partial x} - L(Cs + G)\left[I\ (x,0)\right] \qquad (190)$$

$$\frac{\partial^2 E(x,s)}{\partial x^2} - (Ls + R)(Cs + G)\, E(x,s)$$
$$= L\,\frac{\partial_I (x,0)}{\partial x} - C(Ls + R)\, E(x,0) \qquad (191)$$

where

x = distance along the line
s = the transform variable with respect to time
E = voltage across the line
I = current
L = inductance per unit length
C = capacitance per unit length
R = resistance per unit length
G = leakage conductance per unit length

By using the circuit below, the following initial conditions can be established.

Figure 88

$$\frac{\partial E\ (x,0)}{\partial x} = 0 \qquad (192)$$

$$\frac{\partial_I\ (x,0)}{\partial x} = 0 \qquad (193)$$

$$I(x,0) = \frac{E_o}{Z_L} = I_i \tag{194}$$

$$E(x,0) = E_o \tag{195}$$

Boundary condition is:

$$E(0,s) = \frac{E_o}{s} \tag{196}$$

if $Z_L = Z_o$ is used to simplify the analysis. In addition, to simplify the analysis the resistance, R, in the incremental equivalent circuit should be taken to be zero. The propagation constant, γ, simplifies to $\sqrt{Ls\ (Cs + G)}$, and the characteristic impedance to

$$\sqrt{\frac{Ls}{Cs + G}} = \frac{Ls}{\gamma}$$

Inserting the initial conditions, simplifying, and solving the general line equations gives

$$\frac{\partial^2 E\ (x,s)}{\partial x^2} - LS(Cs + G)E(x,s) = -CLsE_o \tag{197}$$

$$\frac{\partial^2 I(x,s)}{\partial x^2} - LS(Cs + G)I(x,s) = -L(Cs + G)\ I_i \tag{198}$$

$$E(x,s) = A_1 e^{\gamma x} + B_1 e^{-\gamma x} + \frac{CE_o}{Cs + G} \tag{199}$$

$$I(x,s) = A_2 e^{\gamma x} + B_2 e^{-\gamma x} + \frac{I_i}{s} \tag{200}$$

Using the first boundary condition in equation (199)

$$E(o,s) = \frac{E_o}{s} = A_1 + B_1 + \frac{CE_o}{Cs + G} \tag{201}$$

$$E_o\left(\frac{1}{s} - \frac{C}{Cs + G}\right) = A_1 + B_1 \tag{202}$$

Taking a basic line relation and simplifying yields

$$L\left[sI\ (x,s) - I_i\right] = -\frac{\partial E\ (x,s)}{\partial x} \tag{203}$$

Applying equation (203) to equations (199) and (200) yields

$$LS(A_2e^{\gamma x} + B_2e^{-\gamma x}) + LI_i - LI_i = -A_i\gamma e^{\gamma x} + B_1\gamma e^{-\gamma x} \tag{204}$$

Equating coefficients of like exponents one gets

$$LsA_2 = -\gamma A_1. \tag{205}$$

$$LsB_2 = \gamma B_1 \tag{206}$$

$$A_2 = -A_1 \frac{\gamma}{Ls} \tag{207}$$

$$B_2 = B_1 \frac{\gamma}{Ls} \tag{208}$$

If it is remembered that $Z_oI(\ell,s) = E(\ell,s)$, equations (199) and (200) can be combined to yield:

$$\frac{Ls}{\gamma}(A_2e^{\gamma\ell} + B_2e^{-\gamma\ell} + \frac{I_i}{s}) = A_1e^{\gamma\ell} + B_1e^{-\gamma\ell} + \frac{CE_o}{Cs + G} \tag{209}$$

Multiplying through and substituting equations (207) and (208) one obtains

$$B_1e^{-\gamma\ell} - A_1e^{\gamma\ell} + \frac{LI_i}{\gamma} = A_1e^{\gamma\ell} + B_1e^{-\gamma\ell} + \frac{CE_o}{Cs + G} \tag{210}$$

By solving for A_1

$$\frac{LI_i}{\gamma} - \frac{CE_o}{Cs + G} = 2A_1e^{\gamma\ell}$$

$$A_1 = \frac{1}{2}\left[\frac{LI_i}{\gamma} - \frac{CE_o}{Cs + G}\right]e^{-\gamma\ell} \tag{211}$$

And substituting (211) in (202), and solving for B_1

$$B_1 = E_o\left(\frac{1}{s} - \frac{C}{Cs + G}\right) - \frac{1}{2}\left[\frac{LI_i}{\gamma} - \frac{CE_o}{Cs + G}\right] e^{-\gamma \ell} \qquad (212)$$

Rearranging, one gets

$$B_1 = E_o\left[\frac{1}{s} - \frac{C}{Cs + G} - \frac{L}{2}\,\frac{e^{-\gamma\ell}}{Z_L\gamma} + \frac{CE^{-\gamma\ell}}{2(Cs + G)}\right] \qquad (213)$$

Substituting the expressions for A_1 and B_1 in equation (199) one obtains the equation for voltage in the cable during irradiation:

$$E(x,s) = \frac{1}{2}\left[\frac{LI_i}{\gamma} - \frac{CE_o}{Cs + G}\right]e^{-\gamma(\ell - x)} + E_o\left[\left(\frac{1}{s} - \frac{C}{Cs + G}\right)e^{-\gamma x}\right.$$

$$\left. + \frac{1}{2}\left(\frac{C}{Cs + G} - \frac{L}{2Z_L\gamma}\right)e^{-\gamma(\ell + x)}\right] + \frac{E_o}{s + \frac{G}{C}} \qquad (214)$$

Since the signal fed to the oscilloscope is taken off the load resistor, Z_L, one can fix $x = \ell$ and simplify equation (214) somewhat:

$$E(\ell,s) = \frac{LE_o}{2Z_L\gamma} - \frac{CE_o}{2(Cs + G)} + E_o\left[\left(\frac{1}{s} - \frac{C}{Cs + G}\right)e^{-\gamma\ell}\right.$$

$$\left. + \frac{1}{2}\left(\frac{C}{Cs + G} - \frac{L}{2Z_L\gamma}\right)e^{-2\gamma\ell}\right] + \frac{CE_o}{Cs + G} \qquad (215)$$

To facilitate transformation of equation (215) into the time domain, $E(\ell,s)$ is broken up into two parts

$$E(\ell,s) = E_1(\ell,s) + E_2(\ell,s) \qquad (216)$$

where

$$E_1(\ell,s) = \frac{LE_o}{2Z_L\gamma} + \frac{CE_o}{2(Cs + G)} \qquad (217)$$

$$= \frac{LE_o}{2Z_L\sqrt{LS(Cs + G)}} + \frac{CE_o}{2(Cs + G)}$$

$$= \frac{E_o}{2} \left[\sqrt{\frac{L}{C}} \frac{1}{Z_L} \frac{1}{\sqrt{s}\sqrt{s + G/C}} + \frac{1}{s + \frac{G}{C}} \right] \tag{218}$$

E_1 gives the voltage at the load from the inception of irradiation until the reflected pulse given by E_2 arrives at the load. When the reflected signal arrives at the load, the output is the sum of E_1 and E_2. When the radiation ceases, both relations no longer apply. By consulting tables (Reference 64) to find the inverse transform

$$L^{-1} \frac{1}{\sqrt{s}\sqrt{s + a}} = e^{-\frac{a}{2}t} I_o(\tfrac{a}{2})t \tag{219}$$

and letting a in equation (219) $= \frac{G}{C}$ one obtains

$$e_1(\ell,t) = \frac{E_o}{2} \left[\sqrt{L/C} \frac{1}{Z_L} e^{-\frac{G}{2C}t} I_o(\tfrac{G}{2C} t) + e^{-\frac{G}{C}t} \right] \tag{220}$$

Returning to $E_2(\ell,s)$

$$E_2(\ell,s) = E_o \left[\left(\frac{1}{s} - \frac{C}{Cs + G}\right) e^{-\gamma\ell} + \left(\frac{C}{2(Cs + G)} - \frac{L}{2Z_L\gamma}\right) e^{-2\gamma\ell} \right] \tag{221}$$

By multiplying through and expressing γ in terms of circuit constants

$$E_2(\ell,s) = E_o \left[\frac{e^{-\sqrt{Ls(Cs + G)}\,\ell}}{s} - \frac{e^{-\sqrt{Ls(Cs + G)}\,\ell}}{s + \frac{G}{C}} + \frac{e^{-2\sqrt{Ls(Cs + G)}\,\ell}}{2(s + \frac{G}{C})} - \frac{L}{2} \frac{e^{-2\sqrt{Ls(Cs + G)}\,\ell}}{Z_L \sqrt{Ls(Cs + G)}} \right] \tag{222}$$

The exponential factors have the general form (Reference 64).

$$e^{-\left(\frac{x}{v}\right)\sqrt{s^2 + 2s\rho + \rho^2 - \sigma^2}} \qquad (223)$$

which has the inverse transform:

$$e^{-(\rho x/v)}\ \delta\left(t - \frac{x}{v}\right) + \frac{\sigma x}{vz}\ e^{-\rho t} I_1(\sigma z) \qquad (224)$$

where

$$\frac{1}{v} = \sqrt{LC}$$

$$\rho = \frac{R}{2L} + \frac{G}{2C} = \frac{G}{2C} \text{ since } R = 0$$

$$\sigma = \frac{R}{2L} + \frac{G}{2C} + - \frac{G}{2C} \text{ since } R = 0$$

$$z = \sqrt{t^2 - \left(\frac{x}{v}\right)^2}\ t > \frac{x}{v}$$

$$I_1(\sigma z) = -i\ J_1\ (i\sigma z)$$

$e_2(\ell, t)$ can be represented in terms of convolution integrals which cannot, in turn, be expressed in closed form. One then has, finally,

$$e_2(\ell,t) = E_o \int_0^t u(t-\tau) \Big[e^{-\frac{G}{C}\frac{\ell}{2}\sqrt{LC}} \delta(\tau - \ell\sqrt{LC}$$

$$- \frac{G\ell}{2C} e^{-\frac{G}{2C}\tau} \frac{I_1(-\frac{G}{2C})(\tau^2 - \ell^2 LC)^{1/2}}{(\tau^2 - \ell^2\, LC)^{1/2}} \Big] d\tau$$

$$- \int_0^t e^{-\frac{G}{C}(t-\tau)} \Big[e^{-\frac{G}{C}\frac{\ell}{2}\sqrt{LC}} \delta(\tau - \ell\sqrt{LC}) - \frac{G\ell}{2C} e^{-\frac{G\tau}{2C}}$$

$$\frac{I_1(-\frac{G}{2C})(\tau^2 - \ell^2 LC)^{1/2}}{(\tau^2 - \ell^2\, LC)^{1/2}} \Big] d\tau + \frac{1}{2} \int_0^t e^{-\frac{G}{2C}(t-\tau)}$$

$$\Big[e^{-\frac{G}{C}\ell\sqrt{LC}} \delta(\tau - 2\ell\sqrt{LC}) - \frac{G\ell}{C} e^{-\frac{G}{2C}\tau} \frac{I_1(-\frac{G}{2C})(\tau^2 - 4\ell^2 LC)^{1/2}}{(\tau^2 - 4\ell^2 LC)^{1/2}} \Big] d\tau$$

$$- \int_0^t \Big[\frac{L}{2} \frac{e^{-\frac{G}{2C}(t-\tau)}}{Z_L\sqrt{LC}} \Big] I_o \Big[\frac{G}{2C}(t-\tau) \Big] + e^{-\frac{G}{C}(t-\tau)}$$

$$\Big[e^{-\frac{G}{C}\ell\sqrt{LC}} \delta(\tau - 2\ell\sqrt{LC} - \frac{G\ell}{C} e^{-\frac{G}{2C}\tau}$$

$$\frac{I_1(-\frac{G}{2C})(\tau^2 - 4\ell^2 LC)^{1/2}}{(\tau^2 - 4\ell^2 LC)^{1/2}} \Big] d\tau$$

It should be noted that the convolution integrals in equation (275) do not have to be solved if the electrical length of the cable is longer than the gamma ray pulse, since the reflected signals will no longer be given by equation (275).

For a pulse width of 0.2 μsec and a signal velocity of 658 x 10^6 ft/sec, a cable at least 111 feet long should be used to avoid $e_2(\ell, t)$.

<u>Experimental Setup</u>

Seventy-two and 1/2 feet of RG58 C/U coaxial cable was spiral wound on a plywood board. This was hung so that the plane of the board was perpendicular to the axis of the beam from the flash X-ray tube and was positioned to achieve uniform radiation. The cable was terminated with a 51 ohm resistor in series with a 1 microfarad blocking capacitor. Bias was applied to the cable by means of a battery connected to the other end of the cable. The signal was amplified by a Tektronix 1121 A amplifier and then displayed on a Tektronix 551 dual beam oscilloscope. The trace was photographed by a Polaroid camera mounted on the oscilloscope.

<u>Results</u>

Because of the high level of pulser generated r-f noise pickup in the cable, gamma induced effects could not be determined. With the pulser and X-ray tube in a screen room, it is felt certain that r-f noise will be reduced to a level far below gamma-induced signals in the cable.

This page intentionally left blank.

APPENDIX V

DIRECTIONAL RADIATION STUDY

By Goebel Davis and W. W. Grannemann

1.0 Introduction

Recent interest has developed in orientational effects associated with the transient response of electronic components when exposed to gamma or X-rays.

These effects are concerned with:

a) the response for omnidirectional versus mono-directional radiation, and

b) the response for different orientations of components relative to the incident radiation.

Preliminary, crude calculations using deposited energy as the response criteria indicate that these effects can be a factor of significance.

2. Analysis

For this analysis, a rectangle of material (Figure 89) with dimensions a, b, and c respectively in the x, y, and z directions, is exposed, respectively, to X-ray radiations in the x, y, and z directions. The intensities of these incident radiations are $I_x(0)$, $I_y(0)$, and $I_z(0)$ respectively, and are assumed to be all of the same value, I_o (energy per cm^2 per unit of time).

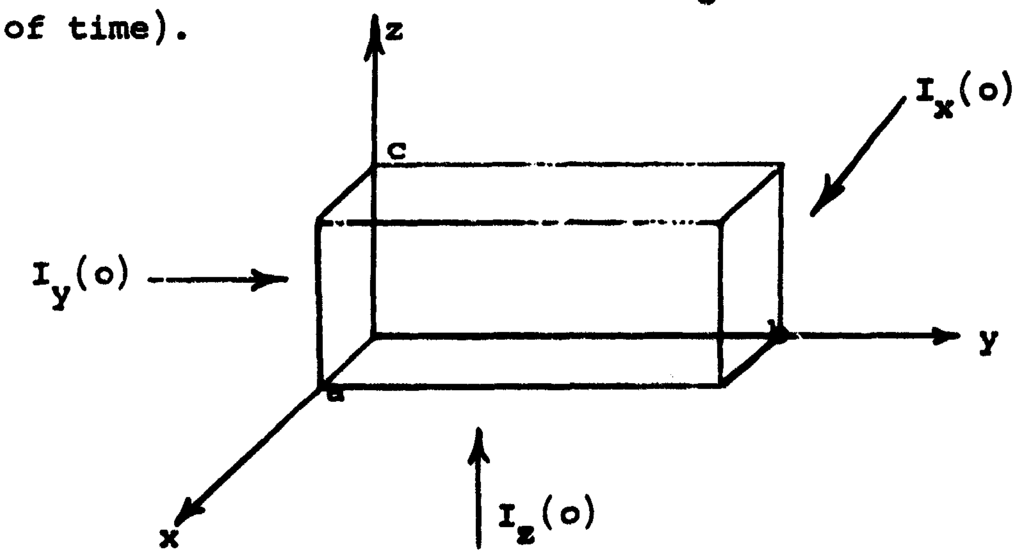

Figure 89.

If one approximates the spectrum of the X-ray source by a single frequency source, then the approximate intensities of the emerging X-rays are:

$$I_x(a) = I_x(0)e^{-\mu a} = I_o e^{-\mu a},$$

$$I_y(b) = I_y(0)e^{-\mu b} = I_o e^{-\mu b}, \text{ and}$$

$$I_z(c) = I_z(0)e^{-\mu c} = I_o e^{-\mu c},$$

where

μ/ρ = mass absorption coefficient (cm^2/g), and

ρ = density of the material (g/cm^3)

respectively.

The energies deposited are proportional to the respective frontal areas and the change in intensities of the incident radiations in passing through the material. Let these deposited energies be E_x, E_y, and E_z respectively. Then, approximately,

$$E_x \sim I_o bc(1 - e^{-\mu a}),$$

$$E_y \sim I_o ac(1 - e^{-\mu b}), \text{ and}$$

$$E_z \sim I_o ab(1 - e^{-\mu c}),$$

From the form of the above equations, it can be seen that usually E_x, E_y and E_z would not be of the same value. This implies a different response for different orientations of the components. Also, these equations show that the response to tridirectional radiation of intensity I_o (in each direction) is different from the response to monodirectional radiation of intensity $3I_o$. Hence, the response to omnidirectional radiation is different from that for monodirectional radiation, even though the total incident radiation levels are the same.

3. Numerical Example

As a sample numerical calculation, it is assumed that $a = 10^{-3}$, $b = 10^{-1}$, $c = 10^{-2}$ cm, and that the X-ray energy is all at 0.3 mev, and the material is silicon. Then $\mu/\rho = 0.107$ cm^2/g, as $\rho = 2.42$ g/cm^3, $\mu = 0.107$ cm^2/g x 2.42 g/cm$^3 \doteq 0.259$ cm^{-1} (Reference 29). If these values are used,

$$E_x \sim 2.60 \times 10^{-7}$$

$$E_y \sim 1.60 \times 10^{-7}, \text{ and}$$

$$E_z \sim 2.59 \times 10^{-7}$$

where the units on E_x, E_y and E_z are arbitrary. It should be noted that the relative values of these energies are consistent with the conclusions of the previous section.

4. Experimental Test

One experimental test of the response of a 1N491 diode was made using the TREES flash X-ray. During the test the transient response output of the diode in a balanced bridge arrangement was displayed on an oscilloscope. The diode was first exposed to radiation straight to the side (exposing the maximum area) and then progressively exposed at tilt angles of 30°, 60°, and 90°. The peak of the transient output tended to follow the relation $A + B \cos \theta$, where A and B are constants and θ is the angle in tilt.

It is not known at present whether part of the response is due to stray ionization around the diode case or due to the diode itself.

5. Limitations and Future Studies

A more sophisticated future study should include:

a) The effect of energy not dissipated locally within the material.

b) The use of a general X-ray energy spectrum.
c) The derivation of energy deposited as a function of a general angle of incidence for the impinging radiation.
d) Possible configurations other than just a rectangle.
e) Additional experimental verification.

REFERENCES

1. D. B. Ebeoglu et al., Transient Radiation Effect in Electronic Materials, Report No. 6, Final Report, Atomics International Report AI-8901, Fort Monmouth, New Jersey,(1 Feb., 1962 to 30 Aug., 1963).

2. Some Effects of Pulsed Radiation of Electronic Components - III, IBM Federal Systems Division, Oswego, New York. Report No. 59-816-916.

3. V. A. J. van Lint et al., Transient Radiation Effects on Electronic Parts, General Atomics Report No. GA-4190, Report #4 of Contract DA 36-039-SC-89196 (Jan. 1, 1963 to March 31, 1963).

4. Transient Radiation Effects on Electronic Parts, General Atomics Report No. GA-4720, Report #6 of Contract DA 36-039 SC 89196 (July 1, 1963 to Sept. 30, 1963).

5. S. E. Harrison, Gamma-Ray Photoconductivity Decay in Organic Dielectric Materials, Sandia Corporation CP63-1143.

6. S. E. Harrison,and P. F. Proulx, Measured Behavior of Gamma-Ray Photoconductivity in Organic Dielectrics, SCR-526,(June, 1962).

7. S. E. Harrison, F. N. Coppage, and O. W. Snyder, Gamma-Ray and Neutron-Induced Conductivity in Insulating Materials, CPA-63-5156,(June, 1963).

8. Battelle Memorial Institute TREES Handbook, ed. D. C. Jones, Prepared for DASA,(July 5, 1963).

9. The Effect of Nuclear Radiation on Semiconductor Devices, REIC #10, AD 240433, Battelle Memorial Institute,(April 30, 1960)

10. Gordon F. Brewster, "Mass Absorption Coefficient of Rutile," Jour. Am. Cer. Soc., Vol. 35, (1952), 35.

11. H. Barnett, R. Bechtel, J. C. Connell, G. Davis, Jr., W. W. Grannemann, Reduced TiO_2 Semiconductor Applications, The University of New Mexico Engineering Experiment Station, 1960.

12. Goebel Davis, Jr., and W. W. Grannemann, "Point Contact Diodes Utilizing Single Crystal Reduced Rutile Titanium Dioxide," Journal of Applied Physics, Vol. 34, No. 1, (Jan, 1963), 228-230.

13. R. Bechtel, G. Davis, Jr., H. Barnett, W. W. Grannemann Surface Studies on Reduced Titanium Dioxide Involving Injection Reagents and Contact Forming, The University of New Mexico Engineering Experiment Station,(1961).

14. W. W. Grannemann, R. Bechtel, G. Davis, Jr., Semiconductor Properties of Titanium Dioxide, The University of New Mexico Engineering Experiment Station,(1960).

15. H. Barnett, R. Bechtel, W. W. Grannemann, Quarterly Progress Report, Semiconductor Properties of Titanium Dioxide, The University of New Mexico Engineering Experiment Station,(1961).

16. R. Bechtel, G. Davis, Jr., W. W. Grannemann, Titanium Dioxide as a Semiconductor, The University of New Mexico Engineering Experiment Station,(1959).

17. American Institute of Physics Handbook, Second Edition, McGraw-Hill,(1963), pp. 9-74

18. H. K. Henisch, Rectifying Semi-Conductor Contacts, Oxford Press,(1957), p. 117.

19. William Shockley, Electrons and Holes in Semiconductors, D. Van Nostrand Company, Inc.,(1963), p. 300.

20. A. Schottky, Physics, Vol. 113, (1939), 367; Vol. 118 (1942), 539.

21. H. A. Bethe, Theory of the Boundary Layer of Crystal Rectifiers, M.I.T. Report 43-12,(1942).

22. L. Silberstein, Philosophical Magazine, Vol. 15,(1933), 375.

23. G. E. Bell, British Journal of Radiology, Vol. 9, (1933), 680.

24. C. R. Emigh, and L. R. Megill, Non-Destructive Testing, Vol. 11, No. 3,(1953), 30.

25. A. Greenfield, R. D. Specht, F. M. Kratz, and K. Hand, AEC-UCL 107,(January, 1951).

26. J. R. Greening, British Journal of Radiology, Vol. 20, (1947), 71.

27. D.E.A. Jones, British Journal of Radiology, Vol. 13, (1940), 95.

28. W. B. Snow, Argonne National Laboratory, Personal Communication, (1963).

29. Gladys White Grodstein, X-Ray Attenuation Coefficients from 10 Kev to 100 Mev, NBS Circular 583,(April, 1957),p. 37.

30. Brophy and Buttrey, Organic Semiconductors, MacMillan Co., (New York, 1962).

31. E. E. Conrad, and S. M. Marcus, Gamma Induced Photoconductivity in a Polyethylene Terephthalate Capacitor, USAELRDL Technical Report 2306, Diamond Ordinance Fuse Lab.,(May, 1962), 344.

32. W. F. Busse, "Review of Two Decades of High-Polymer Physics, A Survey and Forecast," Physics Today, Vol. 17, No. 9, (Sept., 1964), 32-41.

33. J. Rogers, and C. L. Craig, Degradation of Electrical Insulation from Reactor Irradiation, Sperry Gyroscope Co.,(1962),

34. V.A.J. van Lint, Mechanisms of Transient Radiation Effects, GA-4320 General Atomics,(1963).

35. J. F. Fowler, X-Ray Induced Conductivity in Insulating Materials, Ph.D. Thesis, Univ. of London,(1955).

36. P. H. Geil, "Chapter II" Polymer Single Crystals,(New York, 1963).

37. G. T. Cheney, D.M.J. Compton, and R.A. Poll, Radiation Induced Conductivity in Plastic Films at High Dose Rates, GA-5480 General Atomics.

38. S. E. Harrison, F. N. Coppage, and A. W. Snyder, Gamma-Ray and Neutron Induced Conductivity in Insulating Materials, CPA-63-5156, Sandia Corporation.

39. Transient Radiation Effects on Electronic Parts, General Atomics, Reports 1-6 (1962-63). Contract DA 36-639 SC-89196.

40. Transient Radiation Effects on Passive Parts, Hughes Aircraft Company, Reports 1-6 (1962-63). Contract DA 36-039 SC-89112.

41. Measurement of Continuous X-Ray Spectra Using an Absorption Method, The University of New Mexico, WLTDR 64-36 (1964)

42. W. W. Grannemann, et al., Laboratory Testing and Theoretical Studies Supporting the AFSWC Transient Radiation Effects on Electronics (TREES) Program, Report EE-103, UNM Experiment Station,(December, 1963), Or, Reference 5 above.

43. G. W. Grodstein, NBS Circular 583,(1957).

44. C. M. Davisson and R. D. Evans, Review of Modern Physics Vol. 24, (1952), 79. See particularly Figure 22 p.91.

45. C. M. Davisson and R. D. Evans, op cit., Eqation 12, p.80.

46. L. L. Foldy, Physical Review, Vol. 81, (1951) 395-400, or I. Ogievetskii, JETP Vol. 2, No. 2, (1956), 312.

47. Drawing in Radiological Health Handbook, U.S. Department of Health, Education and Welfare, PBIL1784,(1957), p.140.

48. H. Schering, "Die Empfindlichkeit einer Wechselstrom Brucke," Elekt. Zeits, Vol. 52 (1931), 1133-34.

49. J. C. Balsbaugh, et al., "Generalized Bridge h.w. for Dielectric Measurements," Trans. AIEE, Vol. 59 (1940) 950-56.

50. H. W. Bousman, "A Bridge for Capacitance and Low Power-Factor Measurements," General Elec. Review, Vol. 35 (1932), 295-98.

51. A. H. Foley, "A Direct Reading High-Voltage Capacitance Bridge," Trans. AIEE, Vol. 69 (1950), 692-98.

52. B. Hague, Alternating Current Bridge Methods, (Fifth Edition). Sir Isaac Pitman and Sons, Ltd., London, England.

53. G. Hauffe, "Zu Theoric den Scheringschen Brucke," Arch. & Elekt., Vol. 17 (1926), 422-23.

54. Final Report on Some Effects of Pulsed Neutron Radiation on Electronic Components, WADC TR-60-71,(January, 1960).

55. Final Report on Some Effects of Pulsed Neutron Radiation on Electronic Components, IBM Federal Systems Division Report No. 60-911-5,(1960),FXR #IBM-4.

56. FXR #SC-18

57. G. R. Hopkins, A.L.A. Weiman, and D. E. Willis, Transient Radiation Effects on Coaxial Cables, General Atomic Div. of General Dynamics, Report No. GA-3616,(1962),FXR #GA-14.

58. G. R. Hopkins, A.L.A. Weiman, and D. E. Willis, Transient Radiation Effects on Electronic Parts, General Atomic Div. of General Dynamics Corporation, Report No. GA-3858,(1962), FXR #GA-16.

59. G. R. Hopkins, A.L.A. Weiman, and D. E. Willis, Transient Radiation Effects on Electronic Parts, General Atomic Div. of General Dynamics Corporation, Report No. GA-4190,(1963,), FXR #GA-17.

60. Kurt Ikrath, Randolph Constantine, Nuclear Pulse Effects in Cables, United States Army Electronics Research and Development Laboratory, USAERADL Technical Report No. 2292, (1962), FXR #SC-11.

61. C. W. Perkins, R. E. Bailey and C. C. Berggren, Transient Radiation Effects on Passive Parts, Hughes Aircraft Co. Report No. FR 63-17-292, (1963), FXR #HAC-25.

62. Radiation Effects on Microwave Devices, General Electric Company, (1960), FXR #GE-4B.

63. V. A. J. van Lint, Transient Radiation Effects in Electronic Cables State of the Art, General Atomic Div. of General Dynamics, (1962), FXR #GA-13-B.

64. Y. H. Ku, Transient Circuit Analysis, D. Van Nostrand Co., Inc., Princeton, (1961), p. 432.

DISTRIBUTION

No. cys	
	HEADQUARTERS USAF
	Hq USAF, Wash, DC 20330
1	(AFCOA)
1	(AFXOPXOZ)
1	(AFRDP)
1	(AFORQ)
1	(AFNIN)
1	(AFTAC)
1	(AFRSTG)
	MAJOR AIR COMMANDS
	AFSC, Andrews AFB, Wash, DC 20331
1	(SCLT)
1	(SCTR)
1	(SCSSN)
1	(SCSE)
	TAC, Langley AFB, Va 23365
1	(DORQ-M)
1	(TPL-RWD-M)
1	(OA)
	SAC, Offutt AFB, Nebr 68113
1	(OA)
1	(DICC)
1	(OAWS)
1	(DPLBC)
1	AFLC (MCMTC, Lt Col J. E. Thome), Wright-Patterson AFB, Ohio 45433
	ADC, Ent AFB, Colo 80912
1	(ADOOP)
1	(ADLPD)
1	AUL, Maxwell AFB, Ala 36112
1	USAFIT, Wright-Patterson AFB, Ohio 45433
1	USAFA, Colo 80840

DISTRIBUTION (cont'd)

No. cys	
	AFSC ORGANIZATIONS
1	AF Materials Laboratory, Wright-Patterson AFB, Ohio 45433
1	AF Avionics Laboratory (AVNE), Wright-Patterson AFB, Ohio 45433
1	AF Aero-Propulsion Laboratory, Wright-Patterson AFB, Ohio 45433
1	AFSC Scientific and Technical Liaison Office (RTSUM, Capt W. J. Delaney), 68 Albany Street, Cambridge, Mass 02139
	ASD, Wright-Patterson AFB, Ohio 45433
1	(ASAPR)
1	(ASZSI)
1	(SEPIT)
	RTD, Bolling AFB, Wash, DC 20332
1	(RTN-W, Lt Col Munyon)
1	(RTS)
	RTD, Wright-Patterson AFB, Ohio 45433
1	(SENPO, H. R. Shows)
1	(SENS, P. E. Gray)
1	AF Msl Dev Cen (RRRT), Holloman AFB, NM 88330
1	AFMTC (MU-135, Tech Library), Patrick AFB, Fla 32925
1	Hq EAME Comm Area (LGMS, M. V. Swiercz), APO 633, NY 09633
	BSD, Norton AFB, Calif 92409
1	(BST)
1	(BSQ)
1	(BSY)
5	(BSRGA)
	SSD, Los Angeles AFS, AFUPO, Los Angeles, Calif 90045
1	(SSTS)
1	(SSTAS, Lt Col J. W. Gunvordahl)
1	(SSZM, Lt Col T. O. Wear)
1	(SSTRS, Maj D. L. Evans)
1	(SSTRT)
1	(SSTDS, Lt V. Bouquet)

DISTRIBUTION (cont'd)

No. cys	
	ESD, L. G. Hanscom Fld, Bedford, Mass 01731
1	(ESTI)
1	(ESAT)
1	AF Rocket Propulsion Laboratory, Edwards AFB, Calif 93523
1	APGC (PGOZF), Eglin AFB, Fla 32542
	RADC, Griffiss AFB, NY 13442
1	(EMLL, Document Library)
1	(EMEAM, P. B. Richards)
1	(EMEAS, A. W. Desens)
1	(EMERM, J. Forgione)
	KIRTLAND AFB ORGANIZATIONS
	AFSWC, Kirtland AFB, NM 87117
1	(SWEH)
1	(SWT)
1	ADC (ADSWO), Special Weapons Office, Kirtland AFB, NM 87117
	AFWL, Kirtland AFB, MN 87117
20	(WLIL)
1	(WLA)
1	(WLAX-2, Capt Weis)
1	(WLD)
4	(WLDA)
1	(WLDE, Lt Flaherty)
1	(WLR)
1	(WLRJ)
1	(WLRM)
1	(WLRP)
1	(WLRPE)
1	(WLREX)
1	(WLX)
1	(WLF)

DISTRIBUTION (cont'd)

No. cys	
	Director, USAF Project RAND, via: Air Force Liaison Office, The RAND Corporation, 1700 Main Street, Santa Monica, Calif 90406
1	(RAND Physics Div)
1	(RAND Library)
1	Hq OAR (RRN), Bldg T-D, Wash, DC 20333
1	AFOSR (SREC), Bldg T-D, Wash, DC 20333
1	AFCRL, L. G. Hanscom Fld, Bedford, Mass 01731
1	6570 AMRL (RRLO), Wright-Patterson AFB, Ohio 45433
	ARMY ACTIVITIES
	Chief of Research and Development, Department of the Army, Wash, DC 20310
1	(Special Weapons and Air Defense Division)
1	(Atomic Division, Lt Col D. Baker)
	Commanding General, US Army Material Command, Wash, DC 20315
1	(AMCRD-DN, J. F. Corrigan)
1	(Research Division)
	US Army Materiel Command, Harry Diamond Laboratories, Wash, DC 20438
1	(ORDTL 06.33, Technical Library)
1	(230, Chief, Nuclear Vulnerability Branch)
1	Commanding Officer, US Army Combat Developments Command, Nuclear Group (USACDCNG), ATTN: Top Secret Control Officer, Ft Bliss, Tex 79916
1	Redstone Scientific Information Center, US Army Missile Command, Chief, Document Section, Redstone Arsenal, Ala 35809
1	Director, Ballistic Research Laboratories (Library), Aberdeen Proving Ground, Md 21005
	Commanding Officer, Picatinny Arsenal, Samuel Feltman Ammunition Laboratories, Dover, NJ 07801
1	(SMUPA-TY, Chief, Weapons Vulnerability)
1	(SMUPA-VC1, R. Kesselman)
1	(Nike-Zeus Project Officer)
1	(SMUPA-VA6, Tech Info Br)

DISTRIBUTION (cont'd)

No. cys	
	Commanding Officer, US Army Electronics Research and Development Laboratory, Ft Monmouth, NJ 07703
1	(Commanding Officer)
3	(AMSELRDP)
1	(AMSELRDXS, Dr. Kronenberg)
1	(SMVPA-VAG)
1	(AMSELRDNE-5)
1	(AMSELRDNP-1)
1	(AMSELRDNP-8)
1	(AMSELRDPE)
1	(AMSELRDPEE)
1	US Army Tank Automotive Center, ATTN: Mr. Bill Riggle, Warren, Mich
	Commanding General, White Sands Missile Range, White Sands, NM 88002
1	(STEWS-AMTED-E, Mr. Glenn Elder)
1	(Test and Evaluation Directorate)
1	Commanding Officer, Frankford Arsenal, Bridge and Tacony Streets, Philadelphia, Pa 19137
	NAVY ACTIVITIES
	Office of the Chief of Naval Operations, Department of the Navy, Wash, DC 20350
1	(OP-75, ATTN: Director, Atomic Energy Division)
1	(OP-754)
	Chief of Naval Research, Department of the Navy, Wash, DC 20390
1	(Code 418)
1	(Code 427)
	Chief, Bureau of Naval Weapons, Department of the Navy, Wash 25, DC
1	(RRNU)
1	(RMGA-8, J. Lee)
	Commanding Officer, Naval Research Laboratory, Wash, DC 20390
1	(Commanding Officer)
1	(Code 4010, Mr. Lambert)

DISTRIBUTION (cont'd)

No. cys	
1	Commanding Officer and Director, US Naval Radiological Defense Laboratory, ATTN: Mr. H. A. Zagorites, San Francisco, Calif 94135
1	Commanding Officer and Director, Navy Electronics Laboratory (Code 4223), San Diego, Calif 92152
1	Commanding Officer and Director, Naval Applied Science Laboratory, Brooklyn, NY
	Commander, Naval Ordnance Laboratory, White Oak, Silver Spring, Md 20910
1	(Dr. Rudlin)
1	(Mr. N. Taslitt)
1	(Mr. Grantham)
1	Commanding Officer, US Naval Weapons Evaluation Facility (NWEF, Code 404), Kirtland AFB, NM 87117
1	Commanding Officer, US Naval Avionics Facility (RE-01, B. O. Tague), Indianapolis, Ind 46218
1	Commanding Officer, Naval Air Development Center, Johnsville, Pa
1	Commanding Officer, Naval Aviation Material Center, Philadelphia, Pa
1	Commanding Officer, Naval Ordnance Laboratory, ATTN: Dr. Bryant, Corona, Calif
	OTHER DOD ACTIVITIES
	Director, Defense Atomic Support Agency, Wash, DC 20301
1	(Document Library Branch)
1	(RANU, Maj P. K. Mitchell)
1	Commander, Field Command, Defense Atomic Support Agency, Sandia Base, NM 87115
1	(FCAG3, Special Weapons Publication Distribution)
1	(FCTG)
1	(FCWT)
1	Director, Weapon Systems Evaluation Group, Rm 1D847, The Pentagon, Wash, DC 20330
1	Director of Defense Research and Engineering, ATTN: Col R. A. Duffy, Wash, DC 20301

DISTRIBUTION (cont'd)

No. cys	
1	Director, Advanced Research Projects Agency, Department of Defense, The Pentagon, Wash, DC 20301
1	(Maj G. L. Sherwood)
1	(Lt Col R. W. McNamee)
1	Director, Defense Intelligence Agency (DIAAP-IK2), Wash, DC 22212
1	Military Secretary, Joint Chiefs of Staff, Director, Communications-Electronics, J6, Wash, DC 20330
20	DDC (TIAAS), Cameron Station, Alexandria, Va 22314
	AEC ACTIVITIES
1	US Atomic Energy Commission (Headquarters Library, Reports Section), Mail Station G-017, Wash, DC 20545
	Sandia Corporation, Box 5800, Sandia Base, NM 87115
1	(Information Distribution Division)
1	(Dr. J. W. Easley, Dept 5300)
1	(Dr. C. D. Broyles, Dept 5413)
1	(S. C. Rogers, Dept 5321)
1	(A. W. Snyder, Dept 5313)
	University of California Lawrence Radiation Laboratory, P. O. Box 808, Livermore, Calif 94551
2	(Director's Office, Technical Information Division)
1	(Dr. A. Clark)
1	(Mail No. 116, Mr. D. Dawson)
	Director, Los Alamos Scientific Laboratory, P. O. Box 1663, Los Alamos, NM 87554
1	(Helen Redman, Report Library)
1	(Dr. J. Malik)
1	(Division J-8, Mr. D. Stevenson)
1	(GMX-3, R. W. Mathews)
2	Brookhaven National Laboratory, Associated Universities, Inc., ATTN: Dr. C. H. Vineyard, Upton, Long Island, NY
2	Oak Ridge National Laboratory (Tech Library), Oak Ridge, Tenn 37831
2	Argonne National Laboratory (Tech Library), 9700 S. Cass Avenue, Argonne, Ill 60440

DISTRIBUTION (cont'd)

No. cys

OTHER

No. cys	
1	OTS (CFSTI, Chief, Input Section), Sills Bldg, 5285 Port Royal Rd, Springfield, Va 22151
1	Central Intelligence Agency (OCR), 2430 E Street NW, Wash, DC 20505
	Scientific and Technical Information Facility, NASA Representative, P. O. Box 5700, Bethesda, Md 20014
1	(SAK/DL-988)
1	(SAK/DL-887)
1	Assistant to Secretary of Defense for Atomic Energy, Wash, DC 20330
1	Institute for Defense Analysis, ATTN: TIO, Rm 2B257, The Pentagon, Wash 25, DC Contract SD-50
	THRU: ARPA
1	Institute for Defense Analysis, ATTN: TIO, 1710 H Street NW, Wash, DC Contract SD-50
	THRU: ARPA
1	Institute for Defense Analysis, Research and Engineering Support Division, ATTN: TIO, 1825 Connecticut Avenue NW, Wash 25, DC Contract SD-50
	THRU: ARPA
1	AC Spark Plug Division, General Motors Corporation (Dept 32-29, Scott Manlief), Milwaukee, Wisc 53201
1	Admiral Corporation, Government Electronics Division, ATTN: Mr. Bernard Gerstein, 3800 W. Cortland St, Chicago, Ill 60627
1	Aerojet-General Corporation, ATTN: B. J. Gastineau, 6352 Irwindale Avenue, Azusa, Calif
	Aerospace Corporation, P. O. Box 95085, Los Angeles 45, Calif
1	(Mr. J. Statsinger)
1	(Mr. J. P. Stenbit, Communications Analysis)
	Aerospace Corporation, San Bernardino, Calif
1	(Dr. J. Benveniste, Office of Research)
1	(Dr. S. B. Batdorf, Dir Office of Research)
1	(Mr. T. A. Bergstralh, Dir Nuc Effects Subdivision)
1	(Mr. R. P. Kennel)
1	American Components, Inc., ATTN: Mr. Wellard, 8th Ave at Harry St, Conshohoken, Pa

DISTRIBUTION (cont'd)

No. cys	
1	ARINC Research Corporation, ATTN: Mr. W. Schultz, 1700 K Street NW, Wash 6, DC
1	ARMA Division, American Bosch ARMA Corporation, Garden City, Long Island, NY
1	Atomics International, ATTN: W. E. Perkins, Mgr Research, 8900 DeSoto Street, Canoga Park, Calif
	Autonetics Division, North American Aviation, Inc., 3370 East Anaheim Road, Anaheim, Calif 92803
2	(Technical Library, 502-13-9775, Bldg 250)
1	(Mr. Albert Lucic, D-3342-4, Bldg 250)
1	Autonetics Division, North American Aviation, ATTN: T. C. Getten, 9150 Imperial Highway, Downey, Calif
1	AVCO Corporation, Research and Advanced Development Div, ATTN: J. T. Finnell, Sect F-510, Wilmington, Mass 01887
2	Radiation Effects Information Center, Battelle Memorial Institute, ATTN: E. N. Wyler, 505 King Ave, Columbus, Ohio 43201
1	Bell Telephone Laboratories, Inc., 463 West Street, New York, NY
2	Bell Telephone Laboratories, Inc., ATTN: Mr. W. H. Von Aulock, Whippany Road, Whippany, NJ 07981
2	The Boeing Company, Aerospace Division, ATTN: Dr. Glenn L. Keister, Org 2-5470, P. O. Box 3707, Seattle, Wash 98124
1	Burroughs Corporation, ATTN: A. L. Long, Central Avenue and Route 202, Paoli, Pa
1	DASA Data Center, General Electric TEMPO, 735 State Street, Santa Barbara, Calif
1	Missile and Space Systems Division, Douglas Aircraft Company, Inc., ATTN: Dr. B. Barnett, Chief, Nuclear Effects Section/AMT, 3000 Ocean Park Boulevard, Santa Monica, Calif 90406
1	Garrett Corporation, Airesearch Manufacturing Div., ATTN: W. L. Bowler, Dept 35-80, 402 South 36th Street, Phoenix, Ariz 85034
	General Atomic Division, General Dynamic Corp., 10955 John Jay Hopkins Drive, P. O. Box 608, San Diego, Calif
1	(Dr. V. A. J. Van Lint)
1	(Dr. J. L. Russel)
1	(Technical Library, R. J. Tommey)
2	General Dynamics/Fort Worth, ATTN: Nuclear Library (Y-71) for E. L. Burkhard, Asst Proj Eng, P. O. Box 748, Fort Worth, Tex 76101

DISTRIBUTION (cont'd)

No. cys	
1	General Electric Co., Military Communications Dept, Electronics Park, Syracuse, NY
	General Electric Co., Missile and Soace Division, 3198 Chestnut Street, Philadelphia, Pa 19101
1	(Mr. H. L. Olesen, Rm 6278, Reentry Sys Dept)
1	(Documents Library)
1	General Electric Co., Power Tube Dept, Bldg 269, ATTN: Mr. David Hodges, 1 River Road, Schenectady, NY
1	General Electric Co., Military Communications Dept, Nuclear Effects Products Engineering, ATTN: L. H. Dee, Electronics Park, Bldg 14, Syracuse, NY
1	General Electric Co., Military Communications Dept, Radiation Effects Operation, ATTN: J. R. Bilinski, Bldg 1, 400 NW 39th Street, Oklahoma City, Okla
1	General Electric Co., Receiving Tube Dept, ATTN: Mr. Daniel D. Mickey, 316 East Ninth Street, Owensboro, Ky
1	General Electric Co., ATTN: A. A. Sinisgalli, Development Engineer, Advanced Programs, Adv Space Proj Dept, King of Prussia Park, P. O. Box 8661, Philadelphia, Pa
1	General Precision, Inc., Kearfott Division, ATTN: Dr. William H. Duerig, Clifton, NJ
	General Precision Inc., Aerospace Group, Systems Division, 150 Totowa Road, Wayne, NJ 07470
1	(Vehicle Eng, Dr. S. D. Black)
1	(Systems Eng, Mr. M. S. Goldstein)
1	Georgia Institute of Technology and Engineering Experiment Station, ATTN: Dr. R. B. Belser, 722 Cherry Street NW. Atlanta 13, Ga
1	Honeywell, Inc., Aeronautical Division, ATTN: Mr. E. G. Fritz, Materials Engineering 636, 2600 Ridgeway Rd, Minneapolis Minn 55440
1	Hughes Aircraft Company, ATTN: Dr. C. W. Perkins, Bldg 600, Mail Station E131, P. O. Box 3310, Fullerton, Calif
1	Hughes Aircraft Co., Ground Systems Group, ATTN: Mr. J. E. Bell, P. O. Box 2097, Fullerton, Calif
	IBM, Federal Systems Div, Oswego, NY
2	(W. A. Bohan)
1	(Mr. Arthur Yefsky)
1	(Document Library)

DISTRIBUTION (cont'd)

No. cys	
1	Director, Applied Physics Laboratory, Johns Hopkins University, ATTN: Mr. Robert Frieberg, 8621 Georgia Ave, Silver Spring, Md
1	Kaman Nuclear, ATTN: Dr. J. H. Hrock Von Dalebor & Dr. A. P. Bridges, Garden of the Gods Road, Colo 80907
1	Lockheed Aircraft Corporation, Missile and Space Division, ATTN: Mr. Fred Barline, Dept 5872, 1111 Lockheed Way, Sunnyvale, Calif
1	Lockheed Missile and Space Co., ATTN: Mr. H. D. Warshaw, Dept 55/48, Bldg 151, P. O. Box 504, Sunnyvale, Calif
1	Lockheed Missile and Space Company, ATTN: Mr. Harvey Suncan, Dept 62-72, 1123 North Mathilda Ave, Sunnyvale, Calif
1	Lockheed Missile and Space Co., ATTN: W. L. Hollister, Dept 65-50, Bldg 523, Facility 5, Sunnyvale, Calif 94088
1	Lockheed Missile and Space Company, ATTN: Mr. D. A. Yamada, Dept 81-05, P. O. Box 504, Sunnyvale, Calif
	LTV, Vought Aeronautics Division, P. O. Box 5907, Dallas, Tex
1	(H. E. Reynolds)
1	(R. G. Carlson)
	Martin Company, DATAC, P. O. Box 179, Denver 1, Colo
1	(Research Library, A-52)
1	(Lloyd Thayne, A-209)
1	(Harvey Gates)
1	Martin Company, Nuclear Division, ATTN: S. E. Harrison, Mail No. 717, Baltimore, Md 21203
1	Martin Company, Nuclear Divison, ATTN: Nuclear Library, Baltimore 3, Md
	Massachusetts Institute of Technology, Lincoln Laboratory, P. O. Box 73, Lexington, Mass 02173
1	(Document Library)
1	(E. E. Pike)
1	(O. V. Fortier)
1	Melpar Inc., 3000 Arlington Blvd, Falls Church, Va
1	Motorola, Semiconductor Projects Div., ATTN: J. L. Flood, 505 East McDowell Road, Phoenix, Ariz
1	National Cash Register Co., Military Development Division, ATTN: Mr. Don F. Zimmerle, Proj Mgr, Milrata Study, Dayton 9, Ohio 45409

DISTRIBUTION (cont'd)

No. cys	
1	New York University, ATTN: Dr. K. Kallman, Physics Dept, Washington Square, New York 3, NY
1	North American Aviation Corporation, Atomics International Division, ATTN: Dr. A. J. Saur, 8900 De Soto Street, Canoga Park, Calif
1	North American Aviation, Space and Information Systems Division, ATTN: Mr. S. Falbaum, 5555 Ferguson St, Commerce, Calif
	Northrop Corporation, Ventura Division, 1515 Rancho Conejo Blvd, Newbury Park, Calif 91320
1	(Dr. T. M. Hallman)
2	(TIC)
1	Planning Research Corporation (Document Control, Donna Neuman), Box 24726, Los Angeles, Calif 90024
	Physics International Co., 2229 Fourth Street, Berkeley, Calif 94710
1	(Dr. F. Ford)
1	(Mr. Eugene Teatum)
2	Space Technology Laboratories, ATTN: Dr. B. Sussholz & Mr J. Maxey, 5730 Arbor Vitae Street, Los Angeles, Calif
1	Space General Corporation, ATTN: I. Doshay, El Monte, Calif
1	Sperry Gyroscope Co., ATTN: Eugene C. De Mark, CP-21, Information and Communication Division, Glen Cove Road, Carle Place, NY 11514
1	Sperry Microwave Electronics Co., ATTN: Dr. Gordon R. Harrison, P. O. Box 1828, Clearwater, Florida
1	Sylvania Electric Products, Inc., Emporium, Pa
1	Times Wire and Cable Division, International Silver Company, Transmission Systems Section, ATTN: Allen M. Kushner, Wallingford, Conn
1	TRW Space Technology Laboratories, Inc., One Soace Park, Redondo Beach, Calif
1	Stevens Institute of Technology, ATTN: Dr. E. Hanley, 501 and 711 Hudson Street, Hoboken, NJ
1	Varian Associates, ATTN: Dr. J. Haimson, 611 Hansen Way, Palo Alto, Calif
1	Univac Div of Sperry Rand Corp., Radiation Effects Lab/ADI, ATTN: J. Khambata, St Paul, Minn 55116
1	University of British Columbia, Dept of Physics, ATTN: P. J. Sykes, Jr., Vancouver 8, BC

DISTRIBUTION (cont'd)

No. cys	
1	University of Michigan, Institute of Science and Technology, ATTN: BAMIRAC, Mr. Richard Jamron, Box 618, An Arbor, Mich
20	Bureau of Engineering Research, 101-D Electrical Engineering Bldg, ATTN: Dr. W. W. Grannemann, University of New Mexico, Albuquerque, NM
1	Official Record Copy (Capt D. G. Martin, WLDA-1)

UNCLASSIFIED

Security Classification

DOCUMENT CONTROL DATA - R&D

(Security classification of title, body of abstract and indexing annotation must be entered when the overall report is classified)

1. ORIGINATING ACTIVITY (Corporate author) University of New Mexico Albuquerque, NM	2a. REPORT SECURITY CLASSIFICATION UNCLASSIFIED 2b. GROUP

3. REPORT TITLE

RESEARCH, LABORATORY TESTING AND THEORETICAL STUDIES SUPPORTING AFWL TREES PROGRAM

4. DESCRIPTIVE NOTES (Type of report and inclusive dates)

13 April 1963-17 August 1964

5. AUTHOR(S) (Last name, first name, initial)

Grannemann, W. W.; Southward, Harold; Byatt, William J.; et al.

6. REPORT DATE	7a. TOTAL NO. OF PAGES	7b. NO. OF REFS
January 1965	246	64

8a. CONTRACT OR GRANT NO. AF 29(601)-5976 Modification No. S.A.#2(65-87) b. PROJECT NO. 8812, ARPA Order No. 307-62 c. Project No. 5710, DASA WEB No. 16.015 d.	9a. ORIGINATOR'S REPORT NUMBER(S) WL TR-64-123 9b. OTHER REPORT NO(S) (Any other numbers that may be assigned this report)

10. AVAILABILITY/LIMITATION NOTICES

DDC release to OTS is authorized.

11. SUPPLEMENTARY NOTES	12. SPONSORING MILITARY ACTIVITY
	AFWL (WLDA-1) Kirtland AFB, NM 87117

13. ABSTRACT

Hall effect semiconductor devices and titanium dioxide idodes have been found to be highly resistant to transient X-ray pulses. Transient X-ray radiation effects on air surrounding resistive elements as a function of pressure were measured and a theory developed for the effects. Continuous X-ray spectrums have been calculated from X-ray transmission data in the energy range from 180 kilovolts to 600 kilovolts and this method has proved to be satisfactory for outputs of both the flash X-ray and the DC X-ray machines in this energy range. In addition, basic radiation effects measurements were made on dielectric materials using the Hall effect and magnetoresistance measurements in a steady state gamma flux. Hall effect magnetoresistance effects were observed in polystyrene, polyethylene, and other dielectric materials. A Schering Bridge method was used to determine the changes of capacitance of components during flash X-ray exposure. (This bridge is much less responsive to conductance changes than to capacitance changes.) And a Monte Carlo code has been written which describes time-dependent photon transport within finite pieces of material. The energy of the ejected electrons is recorded and photon histories are traced.

14. KEY WORDS	LINK A		LINK B		LINK C	
	ROLE	WT	ROLE	WT	ROLE	WT
Transient radiation effects						
Radiation induced conductivity						
X-Ray spectrum measurement						
Radiation effects on Dielectric materials						
Radiation effects on Hall devices						
Radiation transport Monte Carlo code						

INSTRUCTIONS

1. ORIGINATING ACTIVITY: Enter the name and address of the contractor, subcontractor, grantee, Department of Defense activity or other organization *(corporate author)* issuing the report.

2a. REPORT SECURITY CLASSIFICATION: Enter the overall security classification of the report. Indicate whether "Restricted Data" is included. Marking is to be in accordance with appropriate security regulations.

2b. GROUP: Automatic downgrading is specified in DoD Directive 5200.10 and Armed Forces Industrial Manual. Enter the group number. Also, when applicable, show that optional markings have been used for Group 3 and Group 4 as authorized.

3. REPORT TITLE: Enter the complete report title in all capital letters. Titles in all cases should be unclassified. If a meaningful title cannot be selected without classification, show title classification in all capitals in parenthesis immediately following the title.

4. DESCRIPTIVE NOTES: If appropriate, enter the type of report, *e.g.*, interim, progress, summary, annual, or final. Give the inclusive dates when a specific reporting period is covered.

5. AUTHOR(S): Enter the name(s) of author(s) as shown on or in the report. Enter last name, first name, middle initial. If military, show rank and branch of service. The name of the principal author is an absolute minimum requirement.

6. REPORT DATE: Enter the date of the report as day, month, year; or month, year. If more than one date appears on the report, use date of publication.

7a. TOTAL NUMBER OF PAGES: The total page count should follow normal pagination procedures, i.e., enter the number of pages containing information.

7b. NUMBER OF REFERENCES: Enter the total number of references cited in the report.

8a. CONTRACT OR GRANT NUMBER: If appropriate, enter the applicable number of the contract or grant under which the report was written.

8b, 8c, & 8d. PROJECT NUMBER: Enter the appropriate military department identification, such as project number, subproject number, system numbers, task number, etc.

9a. ORIGINATOR'S REPORT NUMBER(S): Enter the official report number by which the document will be identified and controlled by the originating activity. This number must be unique to this report.

9b. OTHER REPORT NUMBER(S): If the report has been assigned any other report numbers *(either by the originator or by the sponsor)*, also enter this number(s).

10. AVAILABILITY/LIMITATION NOTICES: Enter any limitations on further dissemination of the report, other than those imposed by security classification, using standard statements such as:

(1) "Qualified requesters may obtain copies of this report from DDC."

(2) "Foreign announcement and dissemination of this report by DDC is not authorized."

(3) "U. S. Government agencies may obtain copies of this report directly from DDC. Other qualified DDC users shall request through
_______________________________."

(4) "U. S. military agencies may obtain copies of this report directly from DDC. Other qualified users shall request through
_______________________________."

(5) "All distribution of this report is controlled. Qualified DDC users shall request through
_______________________________."

If the report has been furnished to the Office of Technical Services, Department of Commerce, for sale to the public, indicate this fact and enter the price, if known.

11. SUPPLEMENTARY NOTES: Use for additional explanatory notes.

12. SPONSORING MILITARY ACTIVITY: Enter the name of the departmental project office or laboratory sponsoring *(paying for)* the research and development. Include address.

13. ABSTRACT: Enter an abstract giving a brief and factual summary of the document indicative of the report, even though it may also appear elsewhere in the body of the technical report. If additional space is required, a continuation sheet shall be attached.

It is highly desirable that the abstract of classified reports be unclassified. Each paragraph of the abstract shall end with an indication of the military security classification of the information in the paragraph, represented as *(TS)*, *(S)*, *(C)*, or *(U)*.

There is no limitation on the length of the abstract. However, the suggested length is from 150 to 225 words.

14. KEY WORDS: Key words are technically meaningful terms or short phrases that characterize a report and may be used as index entries for cataloging the report. Key words must be selected so that no security classification is required. Identifiers, such as equipment model designation, trade name, military project code name, geographic location, may be used as key words but will be followed by an indication of technical context. The assignment of links, rules, and weights is optional.